Rechargeable Lithium-Air Batteries Using Mathematical Modelling

A Thesis Submitted by

Ukrit Sahapatsombut

For the Degree of Doctor of Philosophy

School of Chemical Engineering and Advanced Materials
Newcastle University
Newcastle upon Tyne, United Kingdom

February 2014

Abstract

Throughout the years numerous studies for non-aqueous Li-air or Li-oxygen batteries have been investigated to elucidate their reactions and mechanisms. However, there have been only a few models developed for Li-air batteries. Therefore, the main objective of this work was to develop mathematical models for non-aqueous Li-air battery to increase understanding of the air cathode behaviour as well as predict the battery performance during cycling.

A micro-macro homogeneous mathematical model was developed for a rechargeable Li-air battery using a concentrated binary electrolyte theory, and validated against experimental data. The dynamic behaviour of the porous cathode was determined by a numerical solution of the combined continuity, transport and kinetics equations. The microscopic behaviour included the local mass transfer between lithium peroxide (Li_2O_2) layer inside the cathode and active surface morphology changing with the Li_2O_2 solid precipitate growth. The model predicted that the capacity and discharge potential were sensitive to the solubility of oxygen and also the cathode porosity, the cathode structure and kinetic parameters. In addition, the charging behaviour was simulated by modelling the dissolution of solid Li_2O_2 product. The model suggested that the charging voltage can be decreased depending on capability of electrolyte to dissolve the Li_2O_2 discharge products. To improve the battery performance, the promising structure of a Li-air flow battery system with a electrolyte recycling unit continuously delivered the discharge capacity and provided high power density.

To understand the deterioration of cycle performance and energy efficiency related with non-aqueous rechargeable Li-air batteries, a micro-macro homogeneous model was developed to include the practical feature of Li_2CO_3 formation which occurs by electrolyte degradation during battery cycling. A modelling study of cycling behaviour and battery performance was presented and included the influence of electrolyte solution degradation. The battery cycling simulation and porous-electrode experiment indicated that there was a gradual decrease in discharge capacity in a number of battery cycles due to the effect of the irreversible formation of the Li_2CO_3 discharge product. A good agreement between this cell cycling simulation and porous-electrode experiment

data was obtained, thus creating a more reliable model for a rechargeable Li-air battery in non-aqueous electrolyte. The termination of the discharged battery was not from the pore blockage but by the repeated depositing of discharge products as there are some available pores at the end of each discharge cycle.

A macro-homogeneous model was developed to evaluate the impact of replacing pure oxygen with ambient air on the performance of a rechargeable non-aqueous Li-air battery. The model exhibited a significant reduction in discharge capacity, e.g. from 1240 to 226 mAh g_{carbon}^{-1} at 0.05 mA cm^{-2} when using ambient air rather than pure oxygen. The model correlated the relationship between the performance and electrolyte decomposition and formation of discharge products (such as Li_2O_2 and Li_2CO_3) under ambient air conditions. The model predicted a great benefit of using an oxygen-selective membrane on increasing capacity. The results showed a good agreement between the experimental data and the model.

A macro-homogeneous model was developed to evaluate the impact of replacing a conventional flooded electrode with gas diffusion electrode on the performance of a rechargeable non-aqueous Na-air battery under pure oxygen gas. The model demonstrated a significant improvement in battery performance, providing about a 48% increase in initial discharge capacity (over 1500 mAh g_{carbon}^{-1} at 0.1 mA cm^{-2}) and higher discharge potential when using a gas diffusion electrode rather than a flooded electrode. Overall, the gas diffusion electrode model showed the promising performances for a rechargeable Na-air. The model correlated the relationship between the performance and electrolyte decomposition, which occurs during battery cycling, and formation of discharge products (such as Na_2O_2 and Na_2CO_3).

From the analysis of the different models developed in this thesis, they can potentially be used to accurately describe the main mechanisms inside Li-air batteries as well as optimise the porous cathode structure by varying the battery parameters, leading to improve the battery performance. The developed model can be widely applied to evaluate the performances in other battery systems, which have the similar mechanisms.

ACKNOWLEDGEMENT

More than three years, since I have prepared myself for study abroad and received the opportunity to work with everybody in Newcastle University. I would like to take this acknowledgement to thank the key individuals who gave me this unforgettable opportunity.

First of all, I would like to thank my supervisor, Professor Keith Scott, for giving me the opportunity to work on his project. Over the last three years he has been a great mentor, his support, guidance and encouragement were essential to achieve my objectives. This is my great honour to be his postgraduate student.

I would like to thank Associate Professor Siriluck Nivitchanyong, the Deputy executive director of National Metal and Materials Technology Center (MTEC), for offering me the scholarship in studying Ph.D.

I also would like to thank my boss, Dr. Subongkoj (Lab head of Bio-energy group at MTEC until 2010) and Dr. Nuwong (Lab head of Renewable Energy Lab at MTEC), for helping me in recommendation and useful suggestions before I came to Newcastle.

To my wonderful parents, thank you for enabling me to fulfil my dream and supporting me during the studying.

To my friends and colleagues both at MTEC in Thailand and at Electrochem Lab in U.K., I like to thank for their help, advice, and support me to overcome some difficult times during study.

Finally, I would like to thank Ministry of Science and Technology, and Royal Thai Government for granting a full scholarship.

Table of Contents

List of Figures

List of Tables

Nomenclature

Unites are given is SI system. Boldface systems are vectors. Symbols used to simplify the symbolic representation of equations are not listed.

a	Specific interfacial area ($m^2\ m^{-3}$)
A	Membrane surface area (m^2)
c_i	Concentration of species i (mol m^{-3})
$c_{i,s}$	Concentration of species i at the wall or surface of electrode (mol m^{-3})
Da	Damköhler number (dimensionless)
D_i	Diffusion coefficient of species i ($m^2\ s^{-1}$)
$D_{i,eff}$	Effective diffusion coefficient of species i ($m^2\ s^{-1}$)
$D_{i,film}$	Effective diffusion coefficient of species i across the film layer ($m^2\ s^{-1}$)
D_{ij}	Stefan-Maxwell binary diffusivities ($m^2\ s^{-1}$)
D_{ij}^{eff}	Effective Stefan-Maxwell binary diffusivities ($m^2\ s^{-1}$)
$\widetilde{D}_{ij}$	Symmetric diffusivities ($m2\ s^{-1}$)
E	Electrode potential of cathode at any state (V)
E^0	Electrode potential of cathode at standard state (V)
E_m^0	Theoretical open-circuit potential for reaction, *m* (V)
f	Activity coefficient of $LiPF_6$ or $NaPF_6$ salt
F	Faraday's constant (96,485 C mol^{-1})
$\bar{F}$	Permeation flow rate of gasses (mol s^{-1})
G_f^0	Gibbs free energy of formation (J mol^{-1})
H	Henry's law constant (mol m^{-3} atm^{-1})
i_0	Exchange current density (A m^{-2})
$\boldsymbol{i_1}$	Current density in the electrode phase (A m^{-2})
$\boldsymbol{i_2}$	Current density in the electrolyte phase (A m^{-2})
I	Applied current density (A m^{-2})
j_m	Interfacial or local transfer current density of reaction *m* (A m^{-2})
$\boldsymbol{J_i}$	Diffusion flux (kg $m^{-2}\ s^{-1}$)
k	Reaction rate constant
k_d	Dissolution rate constant for Li_2O_2 during charge (s^{-1})

K	Boltzmann constant (1.38×10^{-23} J K^{-1})
l	Thickness of discharged products film (m)
l_e	Thickness of electrolyte film (m)
l_m	Thickness of membrane (m)
L_A, L_C, L	Thickness of APL, separator, and porous cathode respectively (m)
M_i	Symbol for the chemical formula or molecular weight of species i (mol kg^{-1})
n	Number of electrons transferred in the electrode reaction
$\boldsymbol{N_i}$	Molar flux of species i (mol m^{-2} s^{-1})
$\boldsymbol{N_{i,mass}}$	Mass flux of species i (kg m^{-2} s^{-1})
p	Geometrical factor or pressure inlet
$\bar{p}$	Partial pressure of gases (Pa)
P	Permeability of gasses (mol m^{-2} s^{-1} Pa^{-1})
Q	Constant in Stefan-Maxwell diffusion
r_s	Particle radius in the electrode (m)
r_{diss}	Rate of Li_2O_2 dissolution in non-aqueous electrolyte (mol m^{-3} s^{-1})
r_i	Reaction rate term that accounts for electrochemical and chemical reactions (mol m^{-3} s^{-1})
R	Universal gas constant (8.3143 J mol^{-1} K^{-1})
R_{film}	Electrical resistivity across Li_2O_2 film formation (Ω m^2)
s_i	Stoichiometric coefficient of species i in electrode reaction
S	Electrolyte fraction in the porosity of the electrode
S_{mass}	Source terms (kg m^{-3} s^{-1})
t	Time (s)
t_+	Transference number of cation in electrolyte
T	Temperature (K)
$\boldsymbol{u}$	Darcy velocity (m s^{-1})
U	Equilibrium potential (V)
v_i	Molecular diffusion volumes of species i (m^2)
$\boldsymbol{v}_y$	Superficial velocity in y-axis direction
V	Electrode potential (V)
V_{cell}	Cell voltage (V)
w_i	Mass fraction of species i
x_i	Mole fraction of species i

z_i	Valence of charge number of species i

Greek letters

α	Transfer coefficient
β	Symmetry factor
ε	Porosity or void volume fraction of porous cathode
ε_c	Initial volume fraction of cathode electrode (carbon, catalyst and binder)
ε_g	Volume fraction of gas
ε_l	Volume fraction of liquid electrolyte
ε_s	Volume fraction of solid phase in porous cathode
η	Surface or activated overpotential (V)
κ	Conductivity of electrolyte (S m^{-1})
κ_{eff}	Effective conductivity of electrolyte (S m^{-1})
$\tilde{\kappa}$	Permeability of porous media (m^2)
μ	Viscosity of electrolyte (Pa s or kg m^{-1} s^{-1})
μ_i	Pore-fluid viscosity of gas i in GDE (Pa s or kg m^{-1} s^{-1})
μ_0	Viscosity of pure solvent (Pa s or kg m^{-1} s^{-1})
ν	Number of moles of ions into which a mole of electrolyte dissociates
ν_+	Numbers of moles of cations produced by the dissociation of a mole of electrolyte
ρ	Density of mixture (kg m^{-3})
ρ_i	Density of a solid phase of species i (kg m^{-3})
σ	Conductivity of the electrode (S m^{-1})
σ_{eff}	Effective conductivity of the electrode (S m^{-1})
ϕ_1	Electric potential in the electrode (V)
ϕ_2	Electric potential in the electrolyte (V)
$\Delta\phi_{film}$	Voltage drop across discharge products film formation (V)

Subscripts and Superscripts

o	Initial
1	Electrode phase
2	Electrolyte phase
a	Anodic
c	Cathodic

c_1,c_2,c_3	Reaction for Li_2CO_3 formation from mechanism 1 and 2, and solvent degradation, respectively
$diss$	Dissolution
e	Electrolyte
eff	Effective
g	Gases
m	Electrode reaction, solid species or membrane

Mathematical operators

∇	Differential operator
$\frac{\partial}{\partial t}$	Time derivative
$\sum$	Summation
exp	Exponential function
ln	Natural logarithm function

Chapter 1: Introduction

This Chapter describes basic characteristics of batteries and definition in battery performance. Li-air batteries are introduced in term of the fundamental electrochemical reactions and theoretical energy, and compared to other commercial batteries.

1.1 Introduction

With the growing demand of global energy consumption and diminishing fossil fuels there is need to find renewable energy sources which are more sustainable and environmentally friendly compared to the oil-based energy. The continuous raise in CO_2 levels and the limited natural resources stimulate the search for high energy density and efficient energy storage, especially electrochemical systems such as fuel cells, batteries super capacitors. In particular, battery development is one of the most important factors of many pathways toward sustainable development, including energy sources for both fully electric or hybrid vehicles (EVs) in transportation and for energy storage for renewable energy. At present, the specific capacity of conventional rechargeable lithium ion battery (Li-ion) is limited by the amount of active materials ($LiCoO_2$, $LiMn_2O_2$ or $LiFePO_4$ for positive electrode) which can store only 130-150 mAh g^{-1} of charge compared with 300 mAh g^{-1} of the graphite negative electrode.

Recently, a new type of lithium battery, the lithium-air battery (Li-air), is considered by a number of research groups as the promising technology for the power source in EVs [1, 2]. This battery, which combines the advantages of fuel cells and batteries, is an advanced energy storage and electrochemical technology to replace conventional Li-ion batteries in the near future.

1.2 Li-air batteries, promising energy storage

Research presented in this thesis investigated the rechargeable Li-air batteries, also called lithium-oxygen batteries (Li-O_2). Due to their high theoretical energy densities, Li-air batteries are currently considered as one of the most important battery systems which contribute towards a number of applications, such as small portable electronics to electric vehicles. Moreover, Li-air batteries are different from many primary and secondary batteries in that the active materials are a pure lithium metal as the anode

material and air (or oxygen) is not stored inside the cell, but can be continuously derived from the environment around the cell. The use of ambient air as the active oxidant makes Li-air battery safer than commercial lithium-ion batteries. Li-air batteries have received much attention, because they provide a superior theoretical specific energy (13,000 Wh kg^{-1}, based on Li metal alone), 5-10 times better than conventional rechargeable Li-ion batteries, using $LiCoO_2$ or $LiMn_2O_4$ as the positive electrode [3]. At the same time, the batteries using cathodes with nickel and cobalt present risks to health and have environmental impact. This comes from the production, processing and use of these heavy metals, leading to resource depletion, global warming, and ecological hazards on disposal [4].

However, the practical performance of Li-air batteries is currently limited by the low current density, inadequate cyclability, and low charge/discharge efficiency. All of these problems are mostly due to the interfacial reactions of oxygen with the Li ions and the pore structure in the air electrode. Moreover, the discharge Li-air reaction is affected by the insoluble lithium oxides discharge products that can cover the active surface area of the cathode as well as blocking the pathway for reactive species, preventing further reactions inside the cathode. As a result, many research groups are developing key components in the Li-air cell, such as new materials for the positive electrode, electrolyte and catalyst, to overcome these problems. As experimental studies are very time-consuming and costly. Thus, the mathematical model of Li-air battery could be used as an important tool during the battery design and development.

1.3 Battery configuration

A battery is a device that converts chemical energy into electrical energy and *vice versa*. The chemical energy is stored in the electrochemical active species of the two electrodes inside the battery. The conversion between chemical and electrical energy occur through electrochemical reduction-oxidation (redox reactions) or charge-transfer reactions [5, 6]. The redox reactions take place at the electrode/electrolyte interface in a battery containing two electrodes separated by electrolyte and connected with external electronic wire. An electrode is a material such as metal or other electronic conductor in which only electrons are the mobile species. Generally, the term “battery” is used to describe a device that converts chemical energy directly to electrical energy. Hence, a battery is usually specified during discharging, whereas during charging electrical

energy is required to convert battery back to chemical energy. The basic electrochemical unit inside each battery cell during discharging consists of the three main components connected in series as followed [6]:

1. *The anode or negative electrode* where the oxidation reaction takes place and supplies electrons to an external circuit during the electrochemical reaction. Anions (negative charge ion) migrate to this electrode. Hence, the negative electrode is the anode during discharging.
2. *The cathode or positive electrode* where the reduction reaction takes place and accepts the electrons from the external circuit during the electrochemical reaction. Cations (positive charge ion) migrate to this electrode. Hence, the positive electrode is the cathode during discharging.
3. *The electrolyte or ionic conductor* in which the ions are the mobile species inside the cell between anode and cathode. The two electrodes are separated by an electrolyte such as an ion-conducting separator. The electrolyte used in electrochemical battery systems includes molten salts, dissociated salts in water or solvent solution and solid electrolytes.

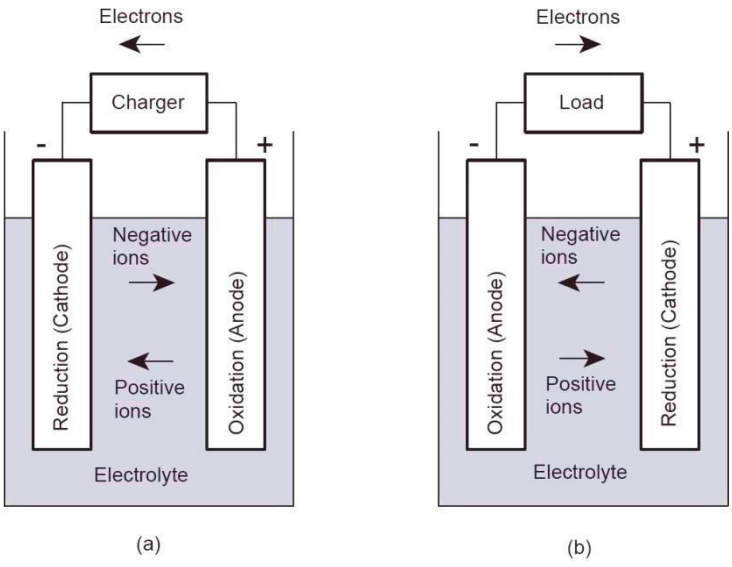

Figure 1-1 Electrochemical operation of a cell during: (a) charging and (b) discharging.

The electrochemical battery during charging and discharging are schematically described in Figure 1-1(a) and (b), respectively. The negative electrode (-) is shown on the left and the positive electrode (+) on the right. Figure 1-1b shows that oxidation occurs at negative electrode during discharging, whereas reduction occurs at the positive electrode. The reverse takes place during charging.

In electrochemical systems, the anode is chosen for cell operation based on properties such as high efficiency as a reducing agent, high specific capacity output (mAh g^{-1}), high conductivity, stability and low cost. Generally, the anode is mainly adopted a metal as active material especially when it has to be small and light weight. Lithium, known as the lightest metal, has a high value of electrochemical equivalence and has presently become a very attractive anode adopted in batteries in suitable and compatible electrolyte.

The cathode is usually a highly oxidizing agent that can withstand contact with the electrolyte. In practical systems, a number of general cathode materials are metallic oxides. However, oxygen, taken directly from the atmosphere, is also used for cathode active materials in electrochemical cell, as in the Al, Mg, Zn or Li/air battery.

The electrolyte must have the following characteristics: good ionic conductivity, non-reactive with the electrode materials, low volatility with temperature, safety in handling, and low cost.

From a thermodynamic background, all batteries are composed of two separated electrode half-cell reactions; one electrode where the reduction reaction occurs can be represented by

$$aA + ne^- \rightleftharpoons cC \tag{1-1}$$

where a molecules of A consume n electrons e^- to from c molecules of C. The second electrode where the oxidation reaction occurs can be represented by

$$bB \rightleftharpoons ne^- + dD \tag{1-2}$$

The overall reaction in the cell is given by combining these two half-cell reactions

$$aA + bB \rightleftharpoons cC + dD \tag{1-3}$$

The theoretical voltage of a reaction is determined by the difference between the Gibbs free energy of reactants and products.

$$\Delta G^0_{reaction} = \Sigma \Delta G^0_{f\,(products)} - G^0_{f\,(reactants)} \tag{1-4}$$

The change in standard free energy ΔG^0 of this reaction is related to the theoretical

voltage by

$$\Delta G^0_{reaction} = -nFE^0 \quad (1\text{-}5)$$

where n = number of electrons transferred in the electrode reaction

F = Faraday's constant (96,485 C mol^{-1})

E^0 = Equilibrium potential or open-circuit voltage, OCV (V)

1.4 The specific capacity and energy

The theoretical specific capacity is the total quantity of charge involved in a reaction defined as coulombs or ampere-hours (Ah). Normally, theoretical specific capacity are normalized by active mass of materials that are involved in the electrochemical reactions and defined in the unit, ampere-hour per kilogram, (Ah kg^{-1}) or mAh g^{-1}.

$$\text{Specific capacity} = (nF \,/\, 3600M) \quad (1\text{-}6)$$

where n is the number of electron transferred in the reaction, F is Faraday's constant which is equal to 96,485 C mol^{-1}, and M is the molecular weight (kg mol^{-1}) of all the active or reacting materials in the system. The theoretical specific energy of batteries, i.e. the energy per unit mass is expressed in Wh kg^{-1} and is given by multiplying the specific capacity by the equilibrium potential or open-circuit voltage, E^0

$$\text{Specific energy} = \text{Specific capacity} \times E^0 \quad (1\text{-}7)$$

For instance, in the case of a Li-air battery, the lithium metal anode is oxidised to lithium ion with one electron transfer in the electrochemical reaction as presented in Eq. (1-8). From Eq. (1-6) and (1-7), ignoring oxygen and the nominal potential of the battery is 3V, the specific capacity and energy can be calculated by

Specific capacity = (1 × 96485 C mol^{-1}) / (3600 C Ah^{-1} × 0.0069 kg mol^{-1})
= 3,884 Ah kg^{-1}

Specific energy = 3,884 Ah kg^{-1} × 3 V
= 11,640 Wh kg^{-1}

Note that the term "energy density" means energy per unit volume. Some authors prefer to use the terms "gravimetric energy density" and "volumetric energy density" instead of "specific energy" and "energy density," respectively.

1.5 Classification of batteries and electrochemical cells

Batteries and electrochemical cells can be classified into primary (non-rechargeable) or secondary (rechargeable), depending on their capability to being electrically recharged. However, there are also another type of classification which uses the different structure and designs such as fuel cell. The definition on each electrochemical cells and batteries are as follow.

1.5.1 Primary cells or batteries

This type of battery is any kind of battery in which the reaction is not electrically reversible or rechargeable. They are commonly known as alkaline batteries, which contain zinc and manganese chemistry, and are currently used as the electrical source of power for various portable electronic devices, torches, toys and memory backup. The major advantage of primary batteries is long periods of storage due to their low self-discharge rates compared to rechargeable batteries. Moreover, they also have a good shelf life and high energy density at low discharge rates. The main structure type of single cell cylindrical and flat button have been adopted in primary battery.

1.5.2 Secondary or rechargeable cells or batteries

This type of battery can be electrically recharged after discharge by applying an electric current which reverses the direction to that of the discharge current. The major applications of secondary batteries are as energy-storage devices that are normally connected to a current source. The energy is discharged through a load when required, for example, lead-acid batteries in various vehicles, uninterrupted power supplies (UPS) for emergency back-up and hybrid electric vehicles. Other rechargeable batteries consist of many dry cells which are enclosed units and are useful in electronic apparatus such as mobile phones, laptops, and tablet computers. This type of dry cell includes nickel-cadmium (NiCd), nickel-zinc (NiZn), nickel metal hydride (NiMH), and lithium-ion (Li-ion) cells.

1.5.3 Reserve batteries

This type of battery is the same as primary cell which cannot recharge, except that the key component is separated from the rest of the battery before being used or activated. Therefore, this can eliminate the chemical self-discharge in the battery. Normally, the

electrolyte is the main part that is separated from the battery system.

1.5.4 Fuel Cells

Fuel cells are similar to batteries in basic electrochemical reaction that convert chemical active reactant into electrical energy in a clean, environmentally friendly way, with no greenhouse carbon dioxide (CO_2) and nitrogen oxide (NO_x) emissions. However, in fuel cells, the active materials or reactants are continuously fed into the system from an external source when power is required, while active materials are not stored inside the cells. Then, the fuel cell has the capacity to produce electrical energy as long as the active materials are still fed to the electrode. Compared to battery, the electrical energy will terminate when limiting reactant is used up. Generally, the anode active materials applied to fuel cell are gaseous or liquid (hydrogen or methanol) and oxygen or air fed into the cathode side is the main reactant. Fuel cells have been developed for more than 150 years as more energy efficiency and less pollutant [7]. The wide ranges of power applications for fuel cells include load levelling, on-site electric generators and electric vehicles.

1.6 The lithium-air battery

The world energy crisis is now a hot topic with the need to discover new efficient energy which is also environment friendly. At present, oil represents 34% of the wolrd's total primary energy source and this accounts for 40% of total CO_2 emission [8]. A major cause of environmental pollutant originates from the various transportation sectors so hybrid electric vehicles (EVs) or fully electric vehicles have been developed. However, the commercialization and popularization of EVs are still rather limited. It is widely acknowledged that the success of EVs hinges upon the performances and prices of energy storage technologies, especially batteries. Currently, there are a number of available battery technologies under on-going investigation and their energy densities are compared in Figure 1-2 [6, 9].

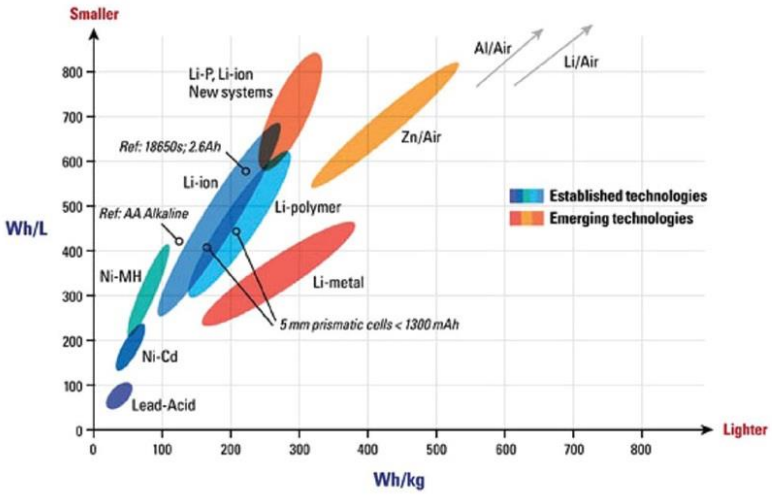

Figure 1-2 Comparing energy densities among current and developing batteries [9].

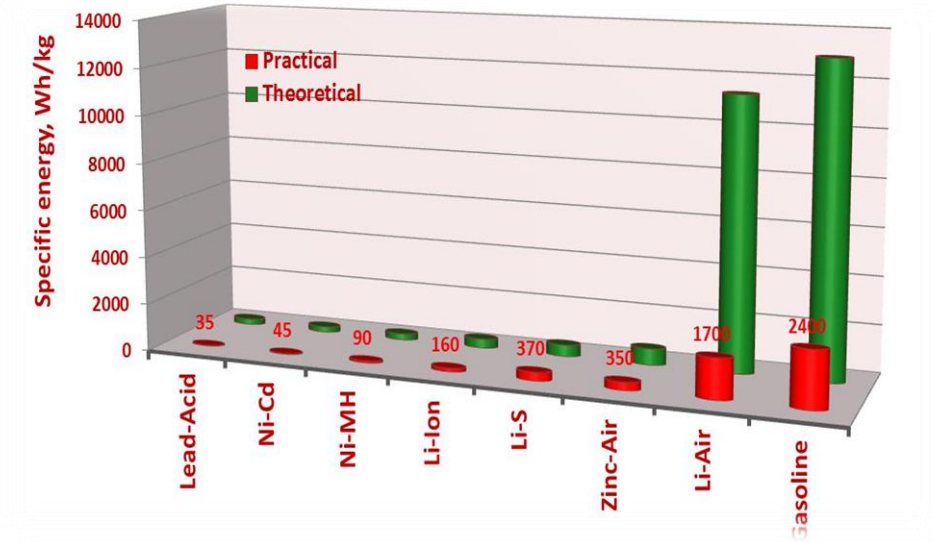

Figure 1-3 The specific energy densities (Wh kg^{-1}) of various commercial rechargeable types of batteries compared to gasoline [8].

Comparing all commercial battery systems, Li-ion batteries are generally considered for efficient energy storage for portable electronic devices, such as mobile phones, laptop computers, digital cameras, music plate, etc., because of their high energy and power density. However, the specific energy density of conventional Li-ion batteries is limited by the amount of active material stored inside the electrode. A proposed solution is replacing the Li-ion cathode with an air/O_2 electrode showing high theoretical energy density beyond current batteries as shown in Figure 1-3. From the calculated energy density in Eq. (1-7), the oxidation of 1 kg of lithium metal delivers 11640 Wh kg^{-1} not much lower than the energy density of gasoline as compared in Figure 1-3. Therefore, metal-oxygen or air batteries, especially for Li-air, have been generating interest as

batteries.

Metal-oxygen or air batteries are different from other batteries in that the active material, oxygen or air, in the cathode is not stored in the battery system but can be supplied from the environmental atmosphere to a porous carbon cathode in the half-cell oxygen reduction electrode [10]. Hence, there is no need to carry the reactant on-board, and access of oxygen is theoretically infinite. Among anode metals (iron, zinc, aluminium, magnesium and calcium), lithium is the predominant active material used in the anode of the metal-air battery because of their merits of high energy density and flexibility for design in battery [11]. Table 1-1 shows standard redox potentials for various redox couples versus a standard hydrogen electrode (SHE)[5]. Lithium metal is considered as the strongest reducing agent with high voltage, high electrochemical equivalence (-3.04 V versus SHE) and also is the lightest metal, that is beneficial for diffusion (equivalent weight M =6.94 g mol^{-1} and specific gravity ρ = 0.53 g cm^{-3}). In the last 15 years, batteries have adopted lithium as the anode active material as metal compounds ($LiMn_2O_4$, $LiCoO_2$ and $LiFePO_4$) [12]. Li-air batteries are now interested by number of research groups as the promising technology for the key component in EVs [3, 13, 14].

Table 1-1 Standard electrode potentials in aqueous solutions at 25ºC in Volt vs. SHE

Electrode reaction	**E^o / V**	**Electrode reaction**	**E^o / V**
$Li^+ + e^- \rightarrow Li$	-3.045	$AgI^+ + e^- \rightarrow Ag + I^-$	-0.152
$K^+ + e^- \rightarrow K$	-2.925	$Sn^{2+} + 2e^- \rightarrow Sn$	-0.136
$Ca^{2+} + 2e^- \rightarrow Ca$	-2.840	$Pb^{2+} + 2e^- \rightarrow Pb$	-0.125
$Na^+ + e^- \rightarrow Na$	-2.714	$2H^+ + 2e^- \rightarrow H_2$	0.00
$Mg^{2+} + 2e^- \rightarrow Mg$	-2.560	$Sn^{4+} + 4e^- \rightarrow Sn^{2+}$	0.150
$Sc^{3+} + 3e^- \rightarrow Sc$	-2.030	$AgCl + e^- \rightarrow Ag + Cl^-$	0.222
$Be^{2+} + 2e^- \rightarrow Be$	-1.970	$0.5O_2 + H_2O + 2e^- \rightarrow 2OH^-$	0.400
$Al^{3+} + 3e^- \rightarrow Al$	-1.670	$Cu^+ + e^- \rightarrow Cu$	0.520
$Ti^{2+} + 2e^- \rightarrow Ti$	-1.630	$Fe^{3+} + e^- \rightarrow Fe^{2+}$	0.771
$Mn^{2+} + 2e^- \rightarrow Mn$	-1.180	$Ag^+ + e^- \rightarrow Ag$	0.799
$Zn^{2+} + 2e^- \rightarrow Zn$	-0.763	$Pd^{2+} + 2e^- \rightarrow Pd$	0.915
$Fe^{2+} + 2e^- \rightarrow Fe$	-0.440	$O_2 + 4H^+ + 4e^- \rightarrow 2H_2O$	1.229

1.6.1 Difference between Li-air and other batteries

Owing to the outstanding properties in high voltage, high capacity, and the capability to use over a wide temperature range, lithium metal is regarded as an excellent material for both primary and secondary cells. The safety issues in using this high reactive metal are mainly considered in rechargeable or secondary cells. During battery operation in a rechargeable lithium cell, lithium at the negative electrode is oxidised to become lithium ion (Li^+) which dissolve into the electrolyte. This process is reversed during the charge cycle and metallic lithium is electroplated back onto the anode surface forming an uneven porous deposit with a large surface area than the original metallic electrode. When the battery is repeatedly charged and discharged, the growing of lithium dendrites from the anode surface can cause short-circuiting in the battery when it forms through the separator and contacts the cathode. This behaviour can lead to battery explosion. However, due to the advantages of lithium metal, new advanced batteries have been still researched based on this metal, including Li-air.

Li-air batteries are considered as highly electrochemical energy density which potentially theoretically provides specific energies of 11,640 Wh kg^{-1} by weight of lithium alone (excluding the weight of oxygen) and specific capacity 3,884 mAh g^{-1} [2, 3, 13-15]. In using oxygen as the cathode, the Li-air battery can potentially provide a specific energy higher than those of commercially rechargeable batteries, as shown in Figure 1-3. Moreover, the energy density of Li-air battery is about 10 times greater than well-known Li-ion battery which is generally between 100-200 Wh kg^{-1}. However, the practical energy of Li-air is still far from its theoretical energy. Then, further research is needed to improve the Li-air battery to achieve better energy efficiency.

Theoretical energies and capacities for the metal-air batteries can be calculated from the Gibbs Free energies of formation data [16], and the results are compared in Table 1-2 [6, 17].

Table 1-2 Theoretical specific energy and capacity comparison for selected metal/oxygen batteries

Metal-air system	OCV (V)	Specific energy (Wh kg^{-1})	Specific capacity (mAh g^{-1})
$2Li + \frac{1}{2}O_2 \rightleftharpoons Li_2O$	2.91	11,302 [a]	3,884
$2Li + O_2 \rightleftharpoons Li_2O_2$	2.96	11,640 [a]	3,884
$2Li + \frac{1}{2}O_2 + H_2SO_4 \rightleftharpoons Li_2SO_4 + H_2O$	4.27	2,046 [a]	479
$2Li + \frac{1}{2}O + H_2O \rightleftharpoons 2LiOH$	3.45	5,789 [a]	1,684
$Al + 0.75O_2 + 1.5H_2O \rightleftharpoons Al(OH)_2$	2.70	4,021 [a]	1,489
$Mg + \frac{1}{2}O_2 + H_2O \rightleftharpoons Mg(OH)_2$	2.76	3,491 [a]	1,267
$Zn + \frac{1}{2}O_2 \rightleftharpoons ZnO$	1.65	1,353 [a]	820
$x6C + LiCoO_2 \rightleftharpoons xLiC_6 + Li_{1-x}CoO_2$	~4.2	420 [b]	139 [b]

[a] The molecular mass of O_2 is not include in the calculation because O_2 is free from the atmosphere and therefore does not have to be stored in the metal-air battery.
[b] Based on $x = 0.5$ in $Li_{1-x}CoO_2$

As can be seen from the table above, the Li-air couples have the most energy because lithium metal battery is the lightest metal with a high voltage, and thus greatest energy density of all metals. For this reason, there are many appearances of the battery design based on lithium metal as anode material. Generally, there are two types of Li-air batteries being developed, namely non-aqueous electrolyte system [13] and aqueous electrolyte system [17]. The possible electrochemical reactions of cathodic mechanism at the cathode and lithium metal oxidation at the anode for the two electrolyte systems could involve the following reactions [18]:

Anode:

$$Li(s) \rightleftharpoons Li^+ + e^- \qquad (E^0 = 0.00\ V_{Li}) \qquad (1\text{-}8)$$

Cathode: (non-aqueous)

$$2Li^+ + O_2(g) + 2e^- \rightleftharpoons Li_2O_2(s) \qquad (E^0 = 2.96\ V_{Li}) \qquad (1\text{-}9)$$

$$4Li^+ + O_2(g) + 4e^- \rightleftharpoons 2Li_2O(s) \qquad (E^0 = 2.91\ V_{Li}) \qquad (1\text{-}10)$$

Cathode: (aqueous)

(Alkaline) $4Li^+ + O_2(g) + 2H_2O + 4e^- \rightleftharpoons 4LiOH \qquad (E^0 = 3.43\ V_{Li})$ (1-11)

(Acid) $4Li^+ + O_2(g) + 2H_2SO_4 + 4e^- \rightleftharpoons 2Li_2SO_4 + 2H_2O \qquad (E^0 = 4.27\ V_{Li})$ (1-12)

All standard reaction potentials shown above are measured with reference to the lithium electrode (V_{Li}). The battery couple with Li-O_2 in aqueous electrolyte solution has a high voltage, ($E_0 = 4.26$ V) in the case of acidic electrolyte and $E_0 = 3.43$ V in case of alkaline electrolyte [19]. However, this type of battery is not considered here because; (1) its theoretical energy density is estimated to be lower than a non-aqueous system when considering that acid and alkaline participate in the reactions [8, 19, 20], (2) the aqueous system faces the problems of electrolyte decomposition and severe corrosion of the lithium anode electrode with aqueous solution contact [21, 22].

To date, the non-aqueous battery system has generated most interest and shows a promising of electrical rechargeable ability. The idea of lithium metal anode combined with an oxygen electrode to achieve a high theoretical energy density was first proposed by Littauer and Tsia in 1976 [23], and the practical Li-air cell using non-aqueous electrolyte was first demonstrated experimentally by Abraham and Jiang in 1996 [13]. Their battery system, comprised a lithium foil anode, a non-aqueous electrolyte, and air electrode, provided a discharge capacity of 1300 mAh g^{-1} based on the weight of carbon, and was cycled several times. Lithium peroxide (Li_2O_2) is the main reduction product at the cathode, although the lithium oxide (Li_2O) formation may be produced at high discharge rate [24]. The reversible cell voltages or equilibrium potential (E^0) of the Li-air battery are referenced vs Li/Li^+ which make the equilibrium potential at the anode equal to zero as shown in Eq. (1-8). However, the other published literatures reported the E^0 for Li_2O_2 as approximately 3.1 V [13, 25], no evidences on the thermodynamic of Gibbs free energy database were provided. Hence, E^0 for Li_2O_2 formation calculated from published Gibbs free energy data for the reaction is 2.96 V [16, 18].

1.6.2 Types of Li-air battery

Currently, four chemical architectures of Li-air batteries are being proposed worldwide, defined on the basis of the electrolyte used, as shown in Figure 1-4 [8]. These can be divided into three versions with liquid electrolytes, namely

i. A fully aprotic/non-aqueous liquid electrolyte.
ii. An aqueous electrolyte.
iii. A mixed/hybrid system between an aqueous electrolyte immersing the cathode and an aprotic electrolyte immersing the anode.

iv. An all-solid-state battery with using a solid electrolyte.

All four types of Li-air batteries use lithium metal as the anode and oxygen gas as the cathode. Although the fundamental electrochemical reaction depends upon the electrolyte around the cathode, all these four Li-air structures need to overcome the challenge of developing a high efficient electrode that maintains access of oxygen and limits its contaminants (e.g., H_2O, CO_2, N_2) [8].

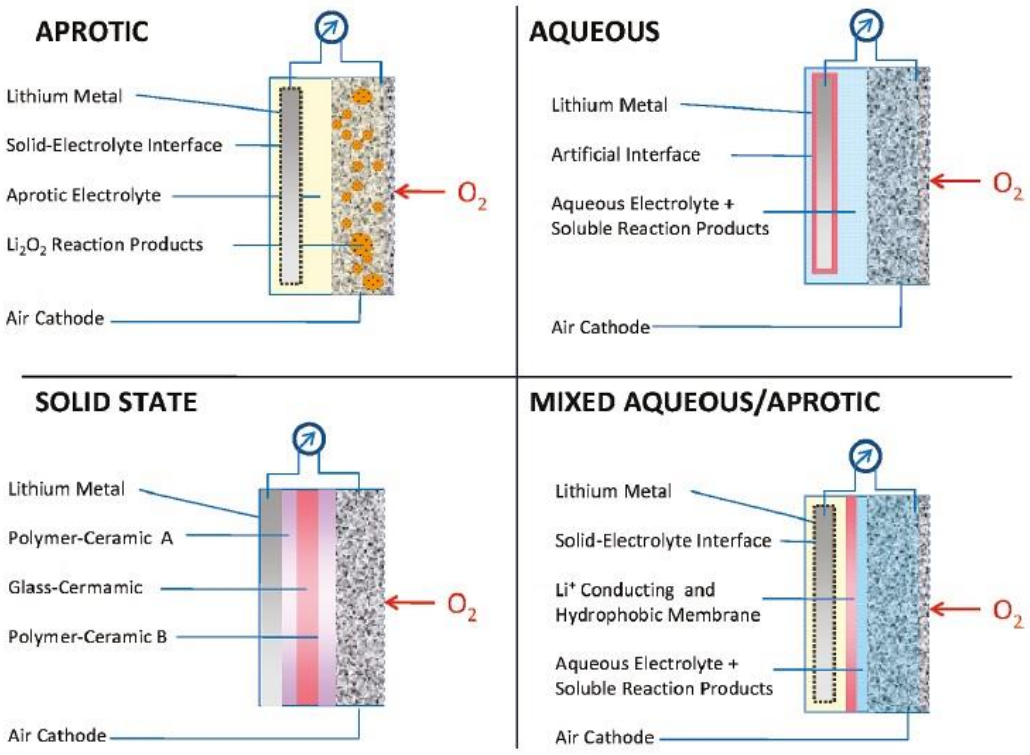

Figure 1-4 Four different architectures of Li-air batteries. The main compartments are as labelled in the figure [8].

A liquid organic electrolyte is used in aprotic/non-aqueous electrolytic structure of Li-air batteries. Lithium salts such as $LiPF_6$, $LiAsF_6$ $LiN(SO_2CF_3)_2$, and $LiSO_3CF_3$ in organic solvent such as organic carbonates, ethers, and ester are normally used electrolytes [26]. In aqueous electrolytic cell, the Li-air battery configuration is similar to that of the aprotic structure except that the electrolyte is based on an aqueous solvent. However, in non-aqueous electrolyte, the Li-air performance of the aprotic structure is limited by the low oxygen solubility and the deposition of lithium oxides within the porous carbon cathode, which affect the transport of oxygen through the air cathode [17]. Li-air battery with aqueous electrolyte does not face the problem of cathode

blockage because the reaction products are soluble in aqueous electrolyte, which continuously maintain the battery performance over time [27]. However, the lithium anode can react violently with water, thus the Li-air battery with aqueous electrolyte structure requires an solid electrolyte interface (SEI) to cover the lithium metal. Usually, a glass or ceramic, which conducts lithium ions, is used as the SEI [27].

The advantages of both aprotic and aqueous structures are applied in the mixed structure of Li-air battery. A lithium anode is placed in the aprotic electrolyte side while the porous carbon cathode is placed in the aqueous electrolyte side. This mixed type of Li-air battery can overcome limitations of either aqueous or aprotic structure. Generally, a lithium ion-conducting ceramic is used as membrane to separate the two electrolytes [27]. In a solid state structure, all electrolytes are solid polymers and are separated by a ceramic membrane [28]. However, the main disadvantage of this Li-air structure is the low ionic conductivity of the polymer electrolytes compared to the liquid electrolytes [29].

1.6.3 Li-air battery challenge

The perfect structure for Li-air battery is a challenging issue as each alternative structure of Li-air batteries has specific advantage. Because only the aprotic system of non-aqueous electrolyte for Li-air batteries has demonstrated a promising result in rechargeability, this system has attracted worldwide attention and is the focus of this thesis.

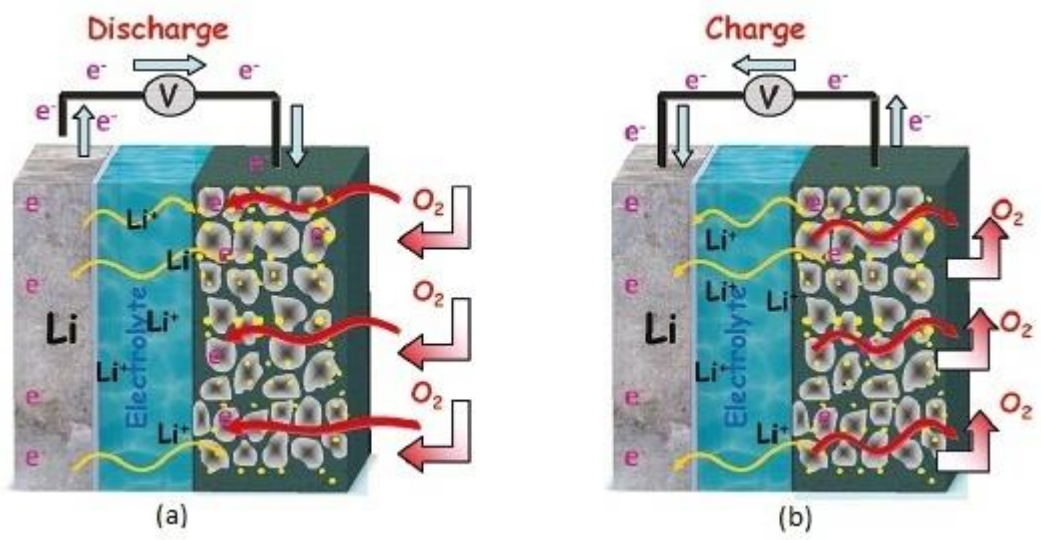

Figure 1-5 Schematic operation of rechargeable Li-air battery: (a) Discharging process, (b) Charging process [8].

Generally, the Li-air cell contains a lithium metal anode, a dissolved lithium salt in a non-aqueous organic electrolyte and a porous air cathode composed of a large surface area of carbon, a catalyst and binder as shown in Figure 1-5 [8]. During battery discharge, lithium is oxidized to form lithium ions (Eq. (1-8)) at the anode and the latter transfer towards the cathode. Electrons from the oxidation reaction flowing through an external circuit then react with lithium ions and oxygen to create Li_2O_2 and Li_2O in the pores of the cathode electrode.

There is the evidence measured by Raman spectroscopy that the main electrochemical product of Li-air cell when discharge is the Li_2O_2 as shown in Eq. (1-8) [13, 30]. The system arrangement of Li-air $\langle Li^{anode}|non-aqueous\ electrolyte|oxygen^{cathode}\rangle$ is the same as the common metal-air $\langle Metal^{anode}|aqueous\ electrolyte|oxygen^{cathode}\rangle$ battery; however, the difference inside the porous cathode of Li-air is that the discharge products (Li_2O_2 and Li_2O) are insoluble in the non-aqueous electrolytes. Then, these products are deposited inside the porous cathode's active surface, block oxygen transport from the atmosphere and prevent further reaction in the cathode. This process is shown in Figure 1-6 [8].

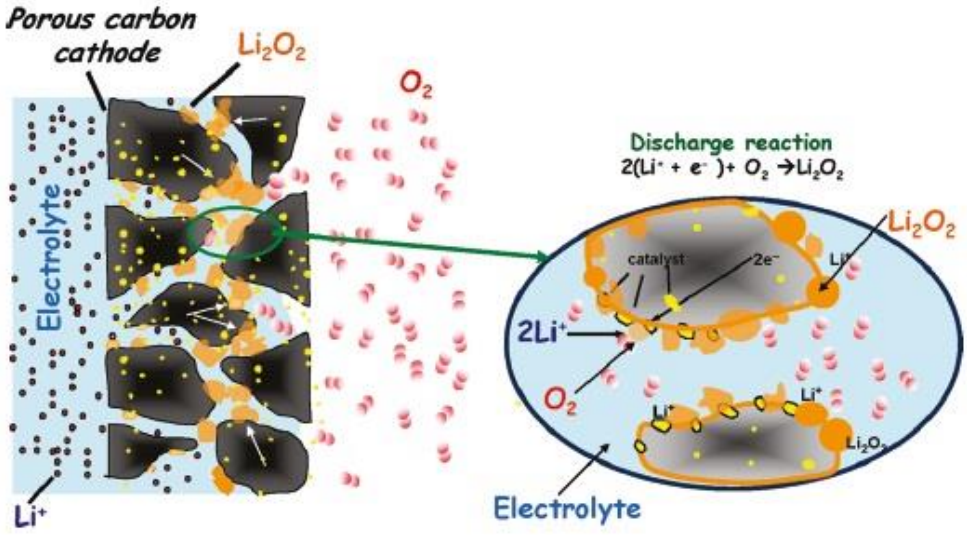

Figure 1-6 The reaction products of Li_2O_2 deposited at the porous carbon cathode [8].

During discharge of the Li-air battery, oxygen from the atmosphere diffuses through the pores of the carbon cathode and is reduced to provide the cell energy capacity expressed as milliampere-hour per gram of carbon (mAh g^{-1}). Many research groups are still improving the Li-air battery key components, such as materials for negative and

positive electrodes, electrolyte, catalyst and separators, to overcome the problems of lithium-air battery.

Li-air batteries are now in the development stage and their practical energy density is still far from the theoretical values. Then, many research groups are still improving the key components, such as develop appropriate pore structure for negative and positive electrode, enhance suitable electrolytes and organic solvents, and synthesize high activity catalyst, to overcome the problem of Li-air battery and yield the best performance close to the theoretical value. Nowadays, battery technology is just changing from nickel metal hydride to commercial lithium-ion batteries and this required about 35 years in research and development. Therefore, the switching to high energy Li-air batteries technology should be considered in the same time range cycle of the lithium-ion battery.

1.7 Objectives of this research

The objective of this research focused on the mathematical modelling for the Li-air battery to increase understanding of the porous carbon cathode behaviour. The operation of the electrode depends on the transport of external dissolved oxygen through the pore of cathode, diffusion across the electrolyte, and reaction with the lithium ion to form the discharge products on the active surface of the porous cathode. The mathematical model to accurately describe the behaviour of Li-air batteries should provide suitable mass transport of both the lithium ion and oxygen inside the porous carbon and also consider the main mechanisms inside the Li-air batteries during operation.

The aim of the research was the development of a time dependent computational model which could predict the behaviour of a Li-air battery using non-aqueous electrolyte during the battery operation including the cycling behaviour.

The research programme was comprised of the following targets:

1. Study the impact of lithium oxide formation in the pores of the cathode as well as the other products formation from electrolyte degradation.
2. Develop a dynamic mathematical model of the Li-air battery system aimed at the porous cathode structure to predict the battery performance. The developed model could be implemented in other similar battery systems.

3. Develop a one-dimensional macro-homogeneous model to describe the Li-air battery behaviour during discharge and charge process. The model includes the dynamic change of the microscopic physical phenomena such as porosity, active area, and film thickness.
4. Develop a one-dimensional macro-homogeneous model to investigate electrolyte degradation and to predict battery performance.
5. Develop a one-dimensional macro-homogeneous model for the Na-air battery to study the impact of using a gas diffusion electrode as the cathode.

A transient one-dimensional mathematical model was developed and used to study the performance of the Li-air cell during discharge. The model considers the negative (lithium metal) electrode, separator and positive (porous carbon) electrode, and predicts the electrochemical reactions in the electrode and mass transfer limitations. The model equation for Li-air batteries are presented in Chapter3.

This thesis has been divided into 8 chapters

Chapter 1 An overview of a basic principle of battery device and a focus on Li-air battery are presented.

Chapter 2 The review in more details of each compartments of Li-air battery composed of anode, separator, electrolyte, catalyst and porous cathode is presented.

Chapter 3 This Chapter describes the battery model that forms the core of this thesis. All basic governing equations of a micro-macro homogeneous mathematical model are explained. These include the combined continuity, transport and kinetics equations for the Li-air battery with a non-aqueous electrolyte. Those who want to have a thorough understanding of the background and construction of the models should read this Chapter.

Chapter 4 A micro-macro homogeneous mathematical model is developed for a rechargeable Li-air battery using a concentrated binary electrolyte theory. The dynamic behaviour of the porous cathode is determined. The developed model is used to predict the effect of various parameters on battery performance including cell capacity and discharge-charge potential.

Chapter 5 To understand the deterioration of cycle performance and energy efficiency

related with non-aqueous rechargeable Li-air batteries, a micro-macro homogeneous model has been developed to include the practical feature of Li_2CO_3 formation which occurs by electrolyte degradation during battery cycling. The discharge products can limit the cyclability and passivate the porous-cathode surface. A modelling study of cycling behaviour and cell performance for Li-air batteries in a non-aqueous electrolyte is presented which includes the influence of electrolyte solution degradation.

Chapter 6 A macro-homogeneous model has been developed to evaluate the impact of replacing pure oxygen with ambient air on the performance of a rechargeable non-aqueous Li-air battery. The Li-air model is also integrated with an oxygen-selective membrane to improve the battery performance when using air as feeding.

Chapter 7 The gas diffusion electrode model has been developed to evaluate the performance of rechargeable non-aqueous Na-air battery under pure oxygen gas. The model includes the loss from electrolyte degradation during battery cycling and is used to simulate the influence of operating condition, cell parameters and performance on the battery capacity.

Chapter 8 Conclusions of the study are presented and future research directions are recommended.

1.8 References

1. Bruce, P.G., S.A. Freunberger, L.J. Hardwick and J.M. Tarascon, *Li-O_2 and Li-S batteries with high energy storage.* Nature Materials, 2012. 11(1): p. 19-29.
2. Armand, M. and J.M. Tarascon, *Building better batteries.* Nature, 2008. 451(7179): p. 652-657.
3. Ogasawara, T., A. Débart, M. Holzapfel, P. Novák and P.G. Bruce, *Rechargeable Li_2O_2 electrode for lithium batteries.* Journal of the American Chemical Society, 2006. 128(4): p. 1390-1393.
4. Yu, Y., X. Wang, D. Wang, K. Huang, L. Wang, L. Bao and F. Wu, *Environmental characteristics comparison of Li-ion batteries and Ni–MH batteries under the uncertainty of cycle performance.* Journal of Hazardous Materials, 2012. 229–230(0): p. 455-460.
5. Bard, A.J. and L.R. Faulkner, *Electrochemical Methods Fundamentals and*

Applications. 2 ed2001, New York: John Wiley & Sons.

6. Linder, D. and T.B. Reddy, *Handbook of Batteries*. 3rd ed2002, New York: McGraw Hill.
7. Devanathan, R., *Recent developments in proton exchange membranes for fuel cells.* Energy & Environmental Science, 2008. 1(1).
8. Girishkumar, G., B. McCloskey, A.C. Luntz, S. Swanson and W. Wilcke, *Lithium-air battery: Promise and challenges.* Journal of Physical Chemistry Letters, 2010. 1(14): p. 2193-2203.
9. Zhang, L.-L., Z.-L. Wang, D. Xu, X.-B. Zhang and L.-M. Wang, *The development and challenges of rechargeable non-aqueous lithium-air batteries.* International Journal of Smart and Nano Materials, 2012: p. 1-20.
10. Sandhu, S., G. Brutchen and J. Fellner, *Lithium/air cell: Preliminary mathematical formulation and analysis.* Journal of Power Sources, 2007. 170(1): p. 196-209.
11. Patil, A., V. Patil, D. Wook Shin, J.W. Choi, D.S. Paik and S.J. Yoon, *Issue and challenges facing rechargeable thin film lithium batteries.* Materials Research Bulletin, 2008. 43(8-9): p. 1913-1942.
12. Broussely, M. and G. Archdale, *Li-ion batteries and portable power source prospects for the next* 5-10 *years.* Journal of Power Sources, 2004. 136(2 SPEC. ISS.): p. 386-394.
13. Abraham, K.M. and Z. Jiang, *A polymer electrolyte-based rechargeable lithium/oxygen battery.* Journal of the Electrochemical Society, 1996. 143(1): p. 1-5.
14. Debart, A., J. Bao, G. Armstrong and P.G. Bruce, *An O_2 cathode for rechargeable lithium batteries: The effect of a catalyst.* Journal of Power Sources, 2007. 174(2): p. 1177-1182.
15. Bruce, P.G., *Energy storage beyond the horizon: Rechargeable lithium batteries.* Solid State Ionics, 2008. 179(21-26): p. 752-760.
16. Chase Jr, M.W., J. Phys. Chem. Ref. Data, 1998. **Monograph** 9: p. 1510.
17. Kowalczk, I., J. Read and M. Salomon, *Li-air batteries: A classic example of limitations owing to solubilities.* Pure and Applied Chemistry, 2007. 79(5): p. 851-860.
18. Lu, Y.C., H.A. Gasteiger, M.C. Parent, V. Chiloyan and Y. Shao-Horn, *The influence of catalysts on discharge and charge voltages of rechargeable Li-oxygen batteries.* Electrochemical and Solid-State Letters, 2010. 13(6): p. A69-

A72.

19. Zheng, J.P., R.Y. Liang, M. Hendrickson and E.J. Plichta, *Theoretical energy density of Li-air batteries.* Journal of the Electrochemical Society, 2008. 155(6).
20. Zheng, J.P., P. Andrei, M. Hendrickson and E.J. Plichta, *The Theoretical Energy Densities of Dual-Electrolytes Rechargeable Li-Air and Li-Air Flow Batteries.* Journal of the Electrochemical Society, 2011. 158(1): p. A43-A46.
21. Littauer, E.L. and K.C. Tsai, *Anodic Behavior of Lithium in Aqueous Electrolytes - 1. Transient Passivation.* Journal of the Electrochemical Society, 1976. 123(6): p. 771-776.
22. Littauer, E.L. and K.C. Tsai, *Corrosion of Lithium in Alkaline Solution.* Journal of the Electrochemical Society, 1977. 124(6): p. 850-855.
23. Littauer, E.L. and K.C. Tsai, *Anodic Behavior of Lithium in Aqueous Electrolytes: I . Transient Passivation.* Journal of the Electrochemical Society, 1976. 123(6): p. 771-776.
24. Read, J., *Characterization of the lithium/oxygen organic electrolyte battery.* Journal of the Electrochemical Society, 2002. 149(9): p. A1190-A1195.
25. Zhang, S.S., D. Foster and J. Read, *Discharge characteristic of a non-aqueous electrolyte Li/O_2battery.* Journal of Power Sources, 2010. 195(4): p. 1235-1240.
26. Xu, K., *Nonaqueous liquid electrolytes for lithium-based rechargeable batteries.* Chemical Reviews, 2004. 104(10): p. 4303-4417.
27. He, P., Y. Wang and H. Zhou, *A Li-air fuel cell with recycle aqueous electrolyte for improved stability.* Electrochemistry Communications, 2010. 12(12): p. 1686-1689.
28. Kumar, B., J. Kumar, R. Leese, J.P. Fellner, S.J. Rodrigues and K.M. Abraham, *A solid-state, rechargeable, long cycle life lithium-air battery.* Journal of the Electrochemical Society, 2010. 157(1): p. A50-A54.
29. Kumar, B. and J. Kumar, *Cathodes for solid-state lithium-oxygen cells: Roles of nasicon glass-ceramics.* Journal of the Electrochemical Society, 2010. 157(5): p. A611-A616.
30. Debart, A., A.J. Paterson, J. Bao and P.G. Bruce, *a-MnO_2 nanowires: A catalyst for the O_2 electrode in rechargeable lithium batteries.* Angewandte Chemie - International Edition, 2008. 47(24): p. 4521-4524.

Chapter 2: Li-air Battery Review

This Chapter provides a brief review of the most important issues in the Li-air battery. The main attention will be aimed at the significant material components of the battery regarding recent research and development. Moreover, Li-air battery modelling, which is used to simulate the influence of operating conditions and to predict the cell performance on various parameters, is also reviewed.

2.1 Introduction

Despite many promising results on specific energy provided by the Li-air battery, its development is still in an early research stage and significant effort is necessary to overcome technical challenges for understanding the complex electrochemical reactions of Li-O_2 during charge and discharge, optimising the appropriate electrolyte, and designing the cathode materials. Before Li-air batteries are ready for commercial markets many problems need to be solved to assure proper cyclability and rechargeability, particularly those related to the cathode:

i. The incomplete discharge due to the blockage in the porous cathode, by lithium oxides.
ii. The higher charge overpotential in comparison to the discharge overpotential, leading to low cycle efficiency.
iii. The development of catalyst to increase cycle efficiency.
iv. The decomposition of the carbonate-based and ether electrolytes during discharge [1].
v. The protection of the cathode from moisture and CO_2 by using an oxygen-selective membrane [2].
vi. The improvement in the rechargeability and long life cycle of the battery.
vii. The carbon corrosion problem at the cathode during battery charging.

In recent years, there has been an increasing amount of literature on the Li-air battery. Different authors proposed their mechanisms for the discharge product formation during discharging of the Li-air battery. The possible cathode reactions during discharge to form the discharge products could involve the following reactions that are generally proposed as oxygen reduction reaction (ORR)

$$O_2 + Li^+ + e^- \longrightarrow LiO_2 \qquad E^0 = 3V\ vs\ Li/Li^+ \qquad (2\text{-}1)$$

$$2LiO_2 \longrightarrow Li_2O_2 + O_2 \qquad (2\text{-}2)$$

$$LiO_2 + Li^+ + e^- \longrightarrow Li_2O_2 \qquad E^0 = 3.1V\ vs\ Li/Li^+ \qquad (2\text{-}3)$$

For charging, the electrochemical decomposition of Li_2O_2 directly to lithium and oxygen has been reported by Ogasawara et al. [3], and the charging reaction is referred to as the oxygen evolution reaction (OER) as follows:

$$Li_2O_2 \longrightarrow 2Li^+ + 2e^- + O_2 \qquad (2\text{-}4)$$

An in situ spectroscopic study by Peng et al. found that the pathway for ORR in aprotic electrolyte includes the lithium superoxide (LiO_2) as an intermediate species during oxygen reduction before it disproportionates to the final product Li_2O_2 [4]:

oxygen reduction	$O_2 + e^- \longrightarrow O_2^-$	
intermediate species	$O_2^- + Li^+ \longrightarrow LiO_2$	(2-5)
disproportionate	$2LiO_2 \longrightarrow Li_2O_2 + O_2$	

However, for the OER or charging process, Li_2O_2 decomposes directly in a one-step reaction to evolve oxygen following the oxidation reaction of Eq. (2-4), and does not pass through the same route of LiO_2 as an intermediate product in ORR [4]. It has been reported that the formation of the discharge products (Li_2O_2 and LiO_2) are influenced by the kinetics of ORR, which are affected by the presence of the various catalyst [5] and the types of electrolytes and solvents applied in the Li-air battery [6]. Since the Li-air battery is currently progressing in its early stage of development, there are several scientific obstacles that need to be overcome in order to produce an effectively rechargeable Li-air battery. In the following sections, the recent development of rechargeable Li-air, including porous cathodes, catalysts, electrolytes, and lithium metal anodes is summarised to provide a better understanding of this technology.

2.2 Development and challenges

The Li-air battery is considered the most promising technology for the energy storage system and was preliminary studied in 1996 by Abraham and Jiang [7]. In this research, a Li-air cell had been proven to have the capability of a rechargeable

behaviour in a few cycles with good Coulombic efficiency. The cell system consists of a Li^+ conductive medium organic polymer electrolyte (non-aqueous) placed between a lithium metal anode and a thin porous carbon electrode catalysed with cobalt phthalocyanine. The Li-air cell provided an OCV of 3 V. The obtained capacity and specific energy were about 1410 mAh g^{-1}_{carbon} and 250-350 Wh kg^{-1} at a discharge current density of 0.1 mA cm^{-2}, respectively. The electrochemical reactions are the same as Eq. (1-8)-(1-10) shown in Chapter 1 with the Li_2O_2 detected as the main reduction product at the discharged carbon electrode without an evidence of Li_2O.

Afterwards Abraham and Jiang reported a novel Li-air battery [7], and the advantages of using a non-aqueous electrolyte to decrease the corrosion at the anode and substantially increase the capacity higher than conventional Li-ion batteries, Li-air batteries have now become an attraction for many research groups [2, 7-12], especially after the Bruce group demonstrated the rechargeability in 2006 [3, 9]. Consequently, IBM and theirs partners have initiated the Battery 500 project to estimate the Li-air potential as batteries for automotive application.

As there are many compartments (e.g. porous cathode, catalyst, electrolyte and anode) in Li-air batteries, in the following section, the details will focus on the significant development for the porous cathode compartment by referring to only non-aqueous electrolyte systems. Next, the recent finding in electrolytes behaviour and new catalysts activity will be discussed.

2.2.1 Porous carbon-based air cathode

Because an air or oxygen electrode plays an important component connected to the performance of a Li-air battery, most of the previous work [2-6, 8-11] tried to improve the cathode based on carbon, of which the characteristics, such as porosity, surface area and morphology can affect the charge and discharge behaviour of the battery. In an operating cell, oxygen is dissolved in both gas phase and electrolyte solution, while the electrons move inside the conductive electrode material. During discharge, the oxygen molecules receive electrons from the cathode and interact with lithium ions to form lithium oxide products on the half-cell reduction. The intrinsic kinetics for this reaction at Li-air cathode are quite slow and affects the overall performance of the battery resulting in low discharge voltage and discharge rate. A porous carbon

structure, which allows air/oxygen to access to the gas transport channel and provides the storage for the discharge products of lithium oxides, is normally used as the air electrode in non-aqueous Li-air systems.

In an aprotic solvent, both Li_2O_2 and Li_2O are not soluble in non-aqueous electrolyte and deposit on the active surface of the cathode, leading to the blockage of the oxygen-diffusing pathway. Previous studies have reported that the decrease in battery capacity at high current density may be due to the direct results from the blockage of the pores by the discharge products, which cannot be completely removed by the oxidation reaction during the subsequent charge process [13, 14]. This significantly limits the oxygen reduction reaction and causes a lower specific capacity than the theoretical value. Hence, it seems that the porous carbon with high active area and better morphology structure is a key factor to improve the performance of Li-air batteries in terms of increasing capacity and cyclability, reducing the charge overpotential, and assuring a long cycle life.

Up to now, in the air electrode, many research groups have focused on both various commercially available and synthesised meso-porous carbons. These carbons have appropriate surface area and pore volume to act as the cathode in the Li-air battery. The various types of carbon include activated carbon (AC), Super P, Vulcan XC-72, Ketjen black (KB), carbon nanotubes (CNTs), etc. [3, 15-20], their properties are summarised in Table 2-1.

It can be seen from the data in Table 2-1 that the surface area of AC is highest among such carbons (2500 m^2 g^{-1}) but its specific capacity is the lowest (414 mAh g^{-1}) because of its very small pore size of only 2 nm in diameter. Comparing this to the case of Super P carbon, although it has low surface area only 62 m^2 g^{-1}, relative to AC, the specific capacity showed the highest (1736 mAh g^{-1}) [21]. This is due to its larger pore diameter (50 nm), which provides a better access for diffusion of reactants and the deposition of discharge products. This thus supports the results that porous carbons with high surface area and small pores, such as AC, provide the lower specific capacity and are less desirable than other carbons, which may have lower measured surface area but have suitable mesopores for lithium oxide deposition.

Table 2-1 Specific capacity (at discharge rate of 0.1 mA cm^{-2}, the cutoff voltage at 2.0 V), surface area and pore diameter of some carbon materials [21]

Carbon material	**Surface area (m^2 g^{-1})**	**Pore diameter (nm)**	**Capacity (mAh g^{-1})**
Super P	62	50	1736
Vulcan XC-72	250	2	76
AC [a]	2500	2	414
CNT [b]	40	10	583
Graphite	6	-	560
Ball-milled graphite	480	-	136
MCF-C [c]	824	30	2500

[a] activated carbon; [b] carbon nanotube; [c] mesocellular carbon foam.

Due to the fact that Li-air performance is strongly dependent on the carbon structure, new carbon materials with different morphologies, surface area, porosity and pore volume have been proposed and studied. Yang et al. [21] demonstrated that meso-cellular carbon foam (MCF-C) prepared by a nanocasting technology can provide much better discharge capacity (2500 mAh g^{-1}) than other commercial carbons owning to its appropriate particle size (824 m^2 g^{-1}) and large mesopores structure (pore diameter 30 nm), as shown in Table 2-1.

The compared performance on the other types of porous carbon had been studied by Park et al. [22] as shown in Table 2-2. The Li-air cell was fabricated from 0.4 g of various carbons on the circular disk (1.962 cm^2). The electrolyte was 1 M $LiPF_6$ in a carbonated solvent mixture. It can be seen that among all commercial carbon materials, Ketjen black EC600JD, with the largest surface area of 1325 m^2 g^{-1} and pore volume of 2.47 cm^3 g^{-1}, provides the highest specific capacity (2600 mAh g^{-1}).

The same commercial carbon materials used for the air electrode are also studied by Solomon et al. [23], and the results show that fabricated composite cathode using carbon with high surface area and high micro and macrospores volume (Ketjen black EC600JD) exhibits mechanically stable and high porosity structure. The high pore volume of carbon powder allow oxygen and electrolyte solution to diffuse through the active site of electrode.

Table 2-2 Specific capacity (at discharge rate of 0.1 mA cm^{-2}, the cutoff voltage at 1.5 V), surface area and pore diameter of some commercial carbon materials [22]

Carbon material	Surface area (m^2 g^{-1})	Pore volume (cm^3 g^{-1})	Capacity (mAh g^{-1})
Ketjen black EC600JD	1325	2.47	2600
Super P	62	0.32	2150
Ketjen black EC300JD	890	1.98	956
Denka black	60	0.23	757
Ensaco 250G	62	0.18	579

Figure 2-1 demonstrates the idea of how the discharge lithium oxide products could form and be accommodated inside the different cathode morphology [13]. In case of the carbon with a majority of micro-pores, the pore entrance would be blocked by the lithium oxides, and thus the inside pore surface becomes inaccessible. On the other hand, the larger pores provide more space for the discharge products and allow the access of the electrolyte and oxygen at the same time. This information on lithium oxide product formation supports the results that the porous carbons with high surface area and small pores, such as AC, as presented in Table 2-1 provide the lower specific capacity than the other carbon, and vice versa.

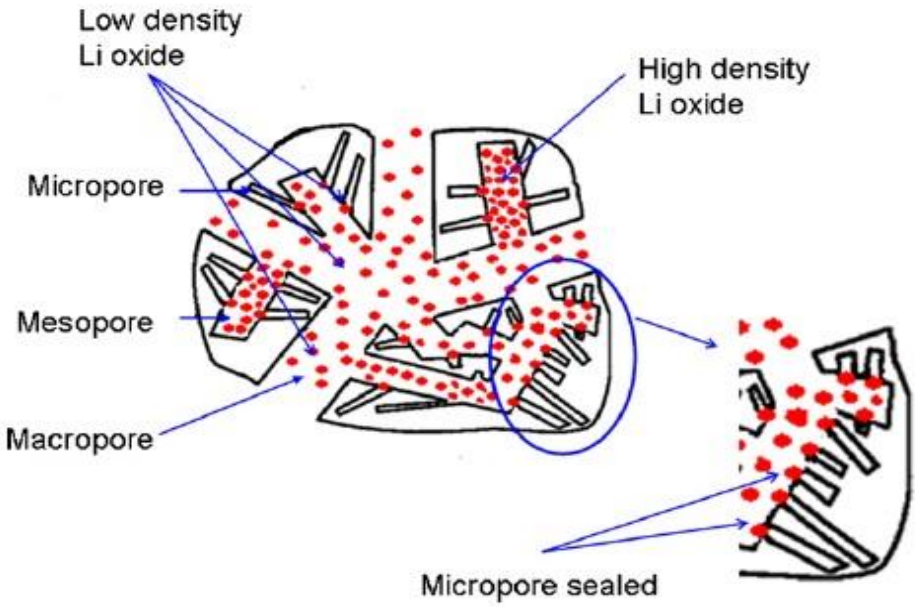

Figure 2-1 Accommodation of lithium oxide products in various pore sizes of carbon electrode [13].

Recently, a unique carbon structure of graphene nanosheets (GNSs) has been synthesised [24, 25] and used as an active cathode with high electrocatalytic activity for the oxygen reduction reaction (ORR). When used in the non-aqueous Li-air battery this GNS based cathode delivered a discharge capacity of 8705.9 mAh g^{-1}, which is the highest capacity of any carbon-based electrode in Li-air batteries ever reported [26]. This might be due to the specific morphology of GNSs, which provides the ideal three-phase (solid-liquid-gas interface) electrochemical interface areas for electrolyte wetting and the oxygen diffusion, thus increasing the discharge capacity significantly. The presence of a three-phase interface, where the lithium ions in liquid electrolyte, the oxygen from the atmosphere and the active carbon or insoluble solid products coexist, is highly desirable for non-aqueous Li-air batteries [13].

Moreover, in order to optimise the cell performance, the amount of carbon loading could be considered during the electrode preparation. An amount of porous carbon loading on the air cathode should be appropriate to maintain the porosity structure, electronic conductivity, transport of electrolyte and diffusion of oxygen [15, 27]. Too low in carbon loading and the electrode cannot provide enough space for depositing the insoluble discharge products, and thus the Li-air performance will decrease. On the other hand, too high in carbon loading will compress the pore volumes together and then hinder the accessing of oxygen from outside the electrode [22, 28]. It is worth noting that different carbon materials have different optimal amounts of loading depending on their unique characteristics.

2.2.2 Electrocatalysts

The standard potential (E^0) for a general organic Li-air battery based on thermodynamic data of Li_2O_2 reduction product is $2.96\ V$ (Equation 1-9). However, for the real Li-air battery investigated nowadays, the discharge potential for the oxygen reduction reaction (ORR) and charge potential for the oxygen evolution reaction (OER) are normally different from the theoretical value; approximately around 2.5-2.7 V and above 4.0 V, respectively [29, 30]. These differences (overpotential) from standard potential, severely reduce the electrical energy efficiency during battery discharge and charge cycle (only 62.5% charge/discharge efficiency). Electrocatalysts can improve the round-trip efficiency of the Li-air battery, by reducing the cell overpotential and thus can potentially maintain the cycle

performance for long cycle life.

Two types of catalysts have been the focus of research, namely metal oxide and noble metal catalysts (Pd, Pt, Au and Ru). These catalysts are used with different electrolytes and show reasonable but not as yet suitable cycling ability.

- *Metal oxide catalysts*

A number of studies have investigated the use of manganese oxides in differently structural forms as the catalysts for Li-air battery as they are inexpensive, easy to prepare, and have high catalytic activity [3, 18, 31-37]. Debart et al. studied the effect of electrolytic manganese dioxide (EMD) on the cycle performance of Li-air battery as demonstrated in Figure 2-2 [38]. A Li-O_2 cell in which the porous cathode consists of only carbon, has been discharged at a potential of around 2.6 V with subsequent charging occurring at around 4.8 V. After the EMD have been incorporated into the porous cathode, this has a significant increase in discharge capacity to around 1000 mAh g^{-1} and shifts the charging potential to a lower voltage of 4.3 V.

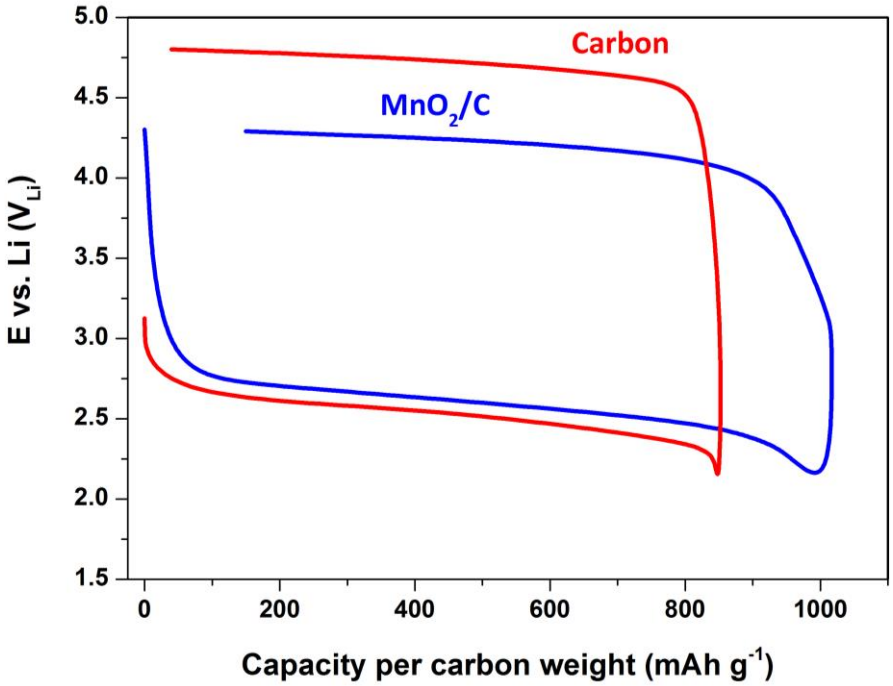

Figure 2-2 The Li-O_2 cell discharge/charge profiles of carbon (Super S, at a rate 70 mA g^{-1}_{carbon}) and MnO_2/C (blue, 70 mA g^{-1}_{carbon}) catalyst (adapted from [38]).

Consequently, several studies on the Li-air performance by using different structural forms of MnO_x catalysts have been systematically investigated by Bruce and co-workers [3, 33]. These catalysts include commercial Mn_2O_3, Mn_3O_4, bulk MnO_2 (α, β,

γ and λ), α-MnO_2 nanowires, and β-MnO_2 nanowires. The α-MnO_2 nanowires were reported to be the best effective catalysts for rechargeable Li-air batteries giving a specific capacity up to 3000 mAh g^{-1} due to their special crystal structure and high surface area, showing the high BET surface area of 22 m^2 g^{-1} compared to 12 m^2 g^{-1} from β-MnO_2 nanowires. Zhang et al. also applied α-MnO_2 nanorods as cathode catalyst into a composite paper air electrode mixed with carbon nano-tubes (CNTs) and carbon nano-fibres (CNFs) and studied their performance in Li-air batteries with/without α-MnO_2 nanorods as cathode catalysts [36]. It was reported that the catalysts did not improve the discharge capacity but increased the charge capacity and cyclability. Zhang et al. [36] concluded that α-MnO_2 enhanced the charge behaviour due to its reaction with the discharge products Li_2O to form Li_2MnO_3 during discharge process. Thereafter, Li_2MnO_3 could be converted back to Li_2O and α-MnO_2 during charge process.

Besides manganese as a based metal catalyst in Li-air batteries, other transition metal oxides such as Fe, Co, Ni and Cu, as well as binary oxides combining these two transition metals, have also been studied [38]. Among them, Fe_2O_3 demonstrates the highest initial capacity of 2,700 mAh g^{-1} at a constant current of 70 mA g^{-1}, while Fe_3O_4, CuO and $CoFe_2O_4$ show the better capacity retention capability (6.67% per cycle), i.e. Fe_3O_4 provides the discharge capacity of 1,200 mAh g^{-1} on 1st cycle and maintains the capacity of 800 mAh g^{-1} on 10th cycle [38].

Hence, these studies showed that a good catalyst is the key on the performance of oxygen electrode in that of its initial energy capacity, capacity retention and lower charging voltage. It should be noted that although manganese oxides are very promising for the Li-air catalysts, the real role of catalytic mechanism which affects the battery performance during discharge and charge is still not clear and requires more research in the future.

- *Noble metal catalysts*

As the ORR in the Li-air cathode is similar to the reaction inside the fuel cell, then the noble metal catalysts applied in the fuel cell have been studied in the Li-air system to reduce the overpotential between discharge and charge cycle. Lu et al. revealed that the 40% loading of gold catalyst (Au) on carbon can improve the ORR during discharging and the same loading of platinum (Pt) has the strong influence on OER

during charging [39]. They continuously studied the combination of these two noble metals on a carbon cathode and created a bi-functional catalyst as shown in Figure 2-3, which gave a higher discharge voltage than pure Vulcan XC-72 carbon by 150-360 mV, and the average charge potential of PtAu/C is reduced to 3.6 V (900 mV lower than that of pure carbon). Their system can account for a round-trip efficiency of approximately 77% [16].

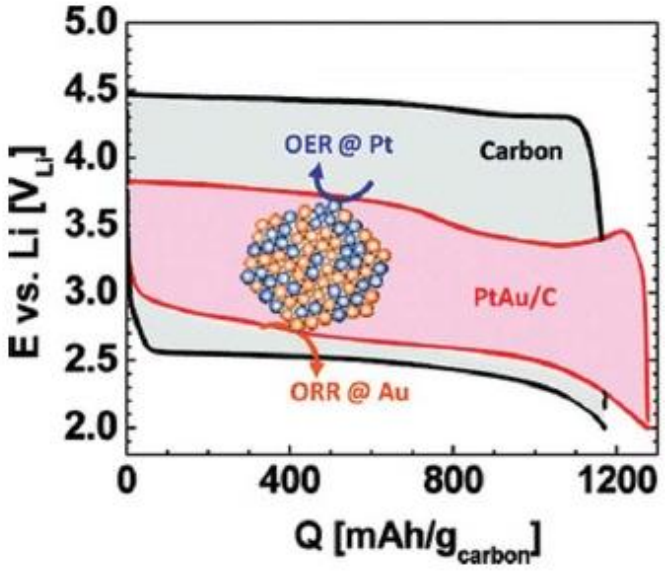

Figure 2-3 The Li-O_2 cell discharge/charge profiles of carbon (black, at a rate 85 mA g^{-1}_{carbon}) and bi-functional PtAu/C (red, 100 mA g^{-1}_{carbon}) catalyst at a rate of 0.04 mA cm^{-2} [16].

Thapa et al. developed the carbon free cathode for Li-air batteries by adding a small amount of Pd to mesoporous α-MnO_2 [40, 41]. The charge-discharge performance for the Li-air battery using mesoporous α-MnO_2 supported Pd electrode at a low current density of 0.025 mA cm^{-2} in pure oxygen demonstrated an initial discharge capacity of 365 mAh $g^{-1}_{catalyst}$ (corresponded to 3650 mAh g^{-1}_{carbon}). The discharge plateau increases to 2.7-2.9 V, while the charge voltage reduces to 3.6 V, providing a system efficiency of 82%. The further charge-discharge of the Li-air battery showed the rechargeable ability up to 7 cycles with 97 % capacity retention.

It should be noted that although the electrocatalysts of the cathode in Li-air batteries can significantly improve the both ORR and OER together with reducing the overpotential and increasing the round-trip efficiency, the catalytic mechanism of these catalysts during the cycling of the battery is still unclear.

2.2.3 Electrolyte

Over the past few years, most of the research work in Li-air batteries have mainly focused on the development of new catalysts and cathode materials as previously described above, while some progress has been made for the Li-air electrolyte which is the key factor to obtain the high efficiency from these devices [2, 11, 12, 42]. Moreover, the basic properties of the electrolyte such as ionic conductivity, reactants and products solubility, viscosity, and volatility influence the Li-air battery performance in terms of specific capacity and cell voltage [27, 43-45]. In some cases, it has been demonstrated that heterogeneous electrocatalysts in non-aqueous organic for Li-air battery promote the electrolyte solvent decomposition rather than the desired ORR at the cathode, and the catalyst for Li-air battery may be unnecessary [46]. A recent study by Freunberger et al. reported the same aspect that the electrolytes degradation to form lithium formate (HCO_2Li), lithium acetate (CH_3CO_2Li), and lithium carbonate (Li_2CO_3), rather than the desired Li_2O_2 product, was the dominant process being catalysed by the α-MnO2 nanowires [47]. In the cases above, the catalyst seems to favour the electrolyte decomposition instead of the electrochemical process. Hence, the real role of catalyst in non-aqueous electrolytes needs to be researched more in the future.

In general, electrolytes with high solubility as well as high diffusivity of oxygen must be considered to ensure the maximum concentration of dissolved oxygen throughout the entire cathode pores and to improve the Li-air performance [42]. Another factor affecting the cell capacity of a Li-air battery is the electrolyte quantity that fills the void space of the porous carbon network. As shown in Figure 2-4, Xu et al. demonstrated that the highest discharge capacity can be obtained at an optimum electrolyte quantity (the amount in millilitre of 1 M LiTFSI in PC:EC) presented in the void space of the Li-air battery [48]. When the electrolyte is below the optimum point, an increase in electrolyte amount shows the better cell capacity due to the more capability in dissolution of oxygen and transportation of Li^+ ions. Above the maximum amount of electrolyte, the cell performance decreases significantly as a result of the flooding inside the pores and decreasing three-phase regions (gas/liquid/solid interface) in electrode.

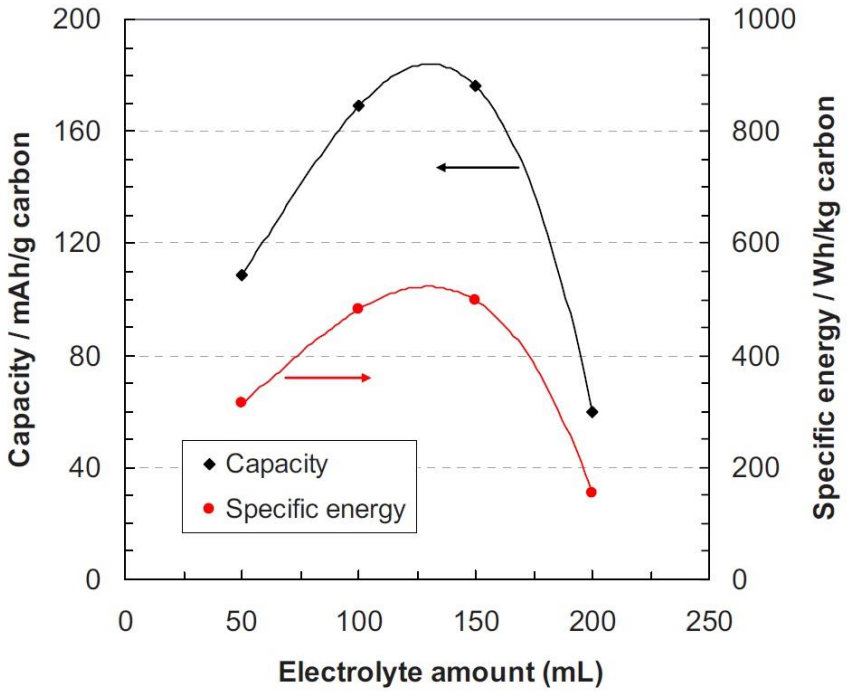

Figure 2-4 The influence of electrolyte quantity (mL) on the discharge capacity of Li-air batteries. The electrolyte formulation is 1.0 M LiTFSI in PC:EC (1:1 by weight) [48].

Generally, as described in the first Chapter, the Li-air or Li-O_2 batteries can be operated on two types of electrolytes, namely non-aqueous and aqueous electrolyte. Although in both systems the discharge process involves mainly the oxygen reduction reaction, electrochemical mechanisms of non-aqueous and aqueous electrolyte are totally different inside the porous cathode resulting in completely distinct products. In a non-aqueous system, the discharge products are insoluble in the electrolyte, and they normally form a solid passivation on the active area of the carbon surface and possibly fill the available pores, leading to block the diffusivity of oxygen to the reaction sites. For these reasons, the practical specific capacity or energy of Li-air batteries is still far from the theoretical aspects.

As shown in Figure 2-5, two models of the catalytic ORR zones in both non-aqueous and aqueous systems has been proposed by Zhang and Foster [49]. In the aqueous system, the active area can be divided into three parts, namely liquid (electrolyte), solid (catalyst), and gas phase (O_2) called “a three-phase reaction zone”, while the non-aqueous may be described by a two-phase reaction zone in the presence of both liquid electrolyte and solid carbon/catalyst. Comparing both advantages and

disadvantages of the two systems, the aqueous electrolytes shows the formation of soluble discharge products resulting in no pore clogging, but the lithium anode may be severely damaged from water corrosion, leading to more difficult cell fabrication. On the other hand, the non-aqueous electrolyte can demonstrate higher specific capacity and better rechargeability than the aqueous cells. In the following section, both electrolytes will be reviewed.

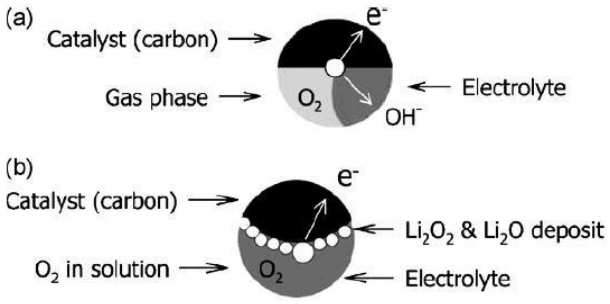

Figure 2-5 Models of the reaction zones for catalytic ORR. (a) aqueous electrolyte-based cells: "three phase reaction zone"; (b) non-aqueous electrolyte-based cell: "two phase reaction zone" [49].

- *Non-aqueous electrolytes*

Besides the carbon and catalyst, significant research has also been carried out with appropriate non-aqueous electrolytes based on three different classes, namely i) organic liquid carbonates and other solvents, ii) hydrophobic ionic liquids and iii) polymer (gel) electrolyte. In general the solvent should ideally enable relatively high oxygen solubility and stability, have low volatility so that they are not lost by evaporation during charging and facilitate good ionic conductivity and be stable under charge and discharge conditions.

The organic carbonate-based electrolytes have been widely used and proven in the conventional Li-ion battery because of their low volatility, compatibility with lithium anode, high ionic conductivity and oxidation stability with respect to the Li/Li^+ couple. In the case of the Li-air battery, organic carbonate-based electrolytes (e.g., $LiPF_6$ in propylene carbonate, (PC) or ethylene carbonate (EC)) have been widely used [3, 15, 27, 34, 43, 50, 51]. Also different co-solvents, such as ethylene carbonate, ethers or glymes, are also used in combination with these carbonate electrolytes in order to increase the oxygen solubility, decrease viscosity and increase ionic conductivity, and the polarity [44, 52]. Xu et al. investigated the Li-air and found that both discharge

capacity and energy density depended on the lithium salts in the cell, e.g. the cells with lithium bis(trifluoromethanesulfonyl)imide (LiTFSI) showed higher O_2 solubility (5.8 mg litre^{-1}) and lower viscosity (7 mPa.s) than both lithium hexfluorophosphat ($LiPF_6$) and lithium perchlorate ($LiClO_4$)-based electrolyte [44]. Moreover, the Li-air batteries with organic carbonated electrolytes demonstrated a much higher discharge capacity than those using ether- or glyme-based electrolytes (a discharge capacity of 167.5 mAh g^{-1} in the 1.0 M LiTFSI in PC:EC (1:1 by weight), whereas 21-27 mAh g^{-1} in ether-based solvents) [44]. This was because ethers and glymes-based electrolyte have higher accessibility to the carbon porous structure, leading to easy blocking of oxygen pathways [44].

However, all the previously mentioned carbonate-based electrolytes suffer from a serious limitation that they decompose to by-products during discharge, as shown by detailed spectroscopic studies (FTIR, Raman, differential electrochemical mass spectrometry, *in situ* GC/MS) [51, 53, 54] and are not good prospects as electrolytes for Li-air or Li-O_2 batteries. In using the carbonate-based solvents, the intermediate species, superoxide, formed during the battery discharging can undergo the nucleophilic reaction. As a result of this, a solvent degradation occurs to generate H_2O, CO_2, Li_2CO_3, as well as other lithium alkyl carbonates, such as HCO_2Li, CH_3CO_2Li, $C_3H_6(OCO_2Li)_2$, at the porous cathode [51, 53, 54]. The charging process then involves the oxidation of these carbonated by-products with the evolution of H_2O and CO_2. The proposed mechanism for the reaction schemes are suggested in the previous reports [51, 55] and presented in Chapter 5.

Freunberger et al. analysed spectroscopic studies on Li-O_2 cells with alkyl carbonate electrolyte and showed that the large formation of Li_2CO_3 together with lithium formate and lithium acetate by-products generated from the electrolyte degradation prefer to accumulate on the cathode surface [51]. This behaviour leads to a failing battery mechanism involving the electrolyte consumption and the fast capacity fading on the consecutive battery cycling. Therefore, the currently reversible Li-air batteries in an organic carbonate-based electrolytes is not a sustainable system, because, in reality, the formation of the carbonate by-products through the reductive decomposition of carbonate solvent are oxidized to form H_2O and CO_2 in the subsequent charging which is different reaction route comparing to discharge process. Hence, a more stable electrolyte, that can ensure the formation of desired Li_2O_2 on air

electrode and does not undergo to an irreversible by-products formation during discharging, is required for genuinely rechargeable Li-air batteries.

To eliminate the electrolyte degradation effects on carbonate solvent, ether-based electrolytes were chosen for candidate in Li-air batteries because of good stability, excellent rate capacity and high oxygen solubility [14]. With viscosity is lower than carbonated-base electrolyte, ether-based solvents seem to be a promising. Read studied the ether-based solvent with different salts and confirmed that once a certain level of oxygen solubility is reached, viscosity becomes the key factor to determining the optimum cell capacity [56]. Hence, further work on ether-based electrolyte try to reduce the electrolyte viscosity to improve the cell performance. It has been suggested that using the crown ethers as an additive into the electrolytes could improve the capability to coordinate with lithium ions and thus increase the ionic conductivity of the electrolyte [57-59].

Xu et al. examined several crown ethers as additives into the carbonate-based electrolyte and demonstrated that the appropriate content of crown ether (15 wt% in the electrolyte) can significantly improve the Li-air battery capacity (about 28%) [60]. However, a recent study from Freunberger et al. found that although ether-based electrolytes are more stable than organic carbonates, they also experience decomposition during operation [47]. The first discharge for Li-O_2 cell using ether-based electrolytes confirms the formation of Li_2O_2, but on the subsequent cycling the Li_2O_2 disappears as the discharge product and the electrolyte decomposes to form a mixture of Li_2CO_3, HCO_2Li, CH_3CO_2Li, polyethers/esters, CO_2 and H_2O. For these reasons, even the ether-based solvents would not be suitable as the electrolyte for Li-air battery systems. Therefore, finding suitable electrolytes that can ascertain the formation of desired lithium oxide products on the air electrodes and reduce other by-products during cycling process remains a major challenge.

Another factor in the Li-air battery relates to the solubility of lithium oxides, the discharge products of the cathode reaction, which are normally insoluble in an organic solvent. Certain additives or co-solvents added to the battery electrolytes can partially increase the dissolution of lithium oxides and thus enhance the Li-air battery performance. Tris(pentafluorophenyl)borane (TPFPB) additive can help to partially dissolve lithium oxide products (Li_2O_2 and Li_2O) which can increase the surface of

carbon exposed for further ORR [48].

The vaporisation of organic electrolyte can also limit the Li-air performance in term of discharge capacity and cyclability. As a result, hydrophobic ionic liquids (ILs) were also investigated for the Li-air battery owing to no vapour pressure and their compatibility with the lithium anode. This type of electrolyte has been mostly applied in the conventional Li-ion batteries [61]. The first study of an ionic liquid composing of 1-alkyl-3methyllimidazolium tetrafluoroborate as the electrolyte was undertaken by Kuboki et al. to examine the discharge behaviour of the air electrode [62]. The cell with ILs demonstrated a high discharge capacity of 5360 mAh g^{-1} for more than 56 days at very low current density of 0.01 mA cm^{-2} in an air environment at 60% humidity without electrolyte vaporisation and hydrolysis of the anode. ILs were also prepared as components in polyvinylidene fluoride (PVDE) base gel electrolytes. Zhang et al. have synthesised a propylimidazolinium-TFSI-silica-PVdF-HFP gel as a Li-air electrolyte, which can stabilise the anode/electrolyte interface and thus reduce lithium anode corrosion [63]. The cell gave a discharge capacity about 2800 mAh g^{-1}, better than the case of a pure ionic liquid system (1500 mAh g^{-1}). Hence, the hydrophobic ILs are good candidates for long-term use in practical system of rechargeable Li-air batteries.

- *Aqueous electrolytes*

Unlike the non-aqueous electrolytes, the aqueous electrolytes are restricted to weak or strong acid or basic solutions. As previously mentioned, lithium oxide discharge products are insoluble in organic electrolyte; however, these products are generally soluble in the aqueous solutions when applied as electrolyte in Li-air battery. This is regarded as the main advantage of the aqueous Li-air system and the porous cathode does not suffer from the blockage or passivation of the solid products, leading to lower cell performance. The typical aqueous solutions is the mixture LiOH-LiCl-H_2O [17, 64], and many other systems are also considered, such as LiOH, HCl/$LiClO_4$, HNO_3/$LiNO_3$ etc. [65].

However, in the case of aqueous electrolyte, an anode-protecting layer with high Li^+ conductivity is required to prevent the lithium metal corrosion, and this makes the cell system more complicated than that of the non-aqueous electrolytes. Hence, the Li-air battery using an aqueous electrolyte still needs a good structural design to maintain its

performance. In this study, the aqueous Li-air battery is not include here because its theoretical energy density is estimated to be lower than a non-aqueous battery system. This aqueous Li-air batteries are still facing the most challenging problem in the anode, which needs to be protected from the highly-reacting Lithium metal [8, 66]. Moreover, due to the similarity in the fundamental reactions at the cathode of the battery with aqueous electrolyte system, the successfully developed technology from the Zn-air battery or fuel cell systems can be used in the aqueous Li-air batteries.

2.2.4 Separators

Besides a cathode electrode and the electrolytes compartments of a Li-air battery, an ideal separator should be considered for gases prevention, good penetrator for Li^+, high storage for electrolyte, suitable mechanical properties, etc. Up to date, there are three types of separators: inorganic ceramic membranes [1, 64, 67-70], polymer-ceramic (PC) compound separators [71] and polymer separators [7, 72].

The inorganic ceramic separator is the recent development of a fast ionic conducting ceramic such as LISICON and LIPON which prevent gas access in the cell and show high ionic conductivity. However, the disadvantages of this separator limiting for practical Li-air cell are its fragile behaviour and high cost issue. Hence, PC separators have been used to enhance the mechanical strength and reduce the cost simultaneously. Generally, polymer separators applied in conventional Li-ion batteries, such as Celgard porous polyolefin separators and glass fibre, have been used in Li-air batteries owing to their high ionic conductivity, low resistance and low cost. The first organic Li-air battery developed by Abraham and Jiang was prepared by using a non-aqueous thin solid polymer electrolyte membrane as the separator [7]. However, these separators cannot completely block the gases to the anode and could result in electrode corrosion. As such, a better separator is urgently required to increase the Li-air performance.

2.2.5 Anode electrode

Owing to its extremely high energy density compared to common lithium-intercalated carbon anodes, lithium metal is regarded as a good anode compartment of Li-air batteries. However, it still faces the most challenging issue due to its stability loss for the long-term operation, mainly in the case of practical application in ambient

atmosphere. This is different from the current laboratory tests so far, which are conducted on the Li-air cell using mostly pure O_2 as the active material. There are some exceptional cases that operate the Li-air batteries by using ambient air [17, 24, 73]. The Li-air battery with air operation is presented in Chapter 6. In fact, lithium metal is highly reactive with moisture and CO_2, which both come from the air and/or electrolyte decomposition. Moreover, lithium metal as an anode electrode in organic electrolyte faces a problem with dendrite formation after many charge-discharge cycles, which finally may lead to short circuits between the anode and cathode due to the prolonged deposition/dissolution of lithium [74]. These effects reduce cycle life and safety of rechargeable Li-air batteries with lithium metal as an anode electrode.

At present, the solution for this problem is the separation of a lithium anode from contact with the liquid electrolyte. The proposed method includes interfacial or protective layers coated on the metallic lithium, such as polymer, ceramics, or glasses which provide conductivity for lithium ions [75]. Another approach to prevent moisture and electrolyte decomposition products in the air electrode has been proposed by Crowther et al. [18]. They developed a silicone rubber oxygen-selective membrane to protect the outer surface of cathodes from moisture as well as to increase the oxygen permeation. This silicone rubber blocks the water transport from the atmosphere into the Li-air battery and also prevents the solvent loss from the cell into atmosphere. The Li-air battery with a cathode protected with the thin 83 μm silicone rubber delivered a discharge capacity of 570 mAh g^{-1} at a discharge rate 0.2 mA cm^{-2}, whereas the unprotected cathode showed a capacity only 151 mAh g^{-1}.

Generally, there are a number of studies which have been investigated on the effects of catalyst to improve the discharge potential [16, 41], battery capacity, and lowering the charge potential [15, 76]. Although those studies are usually focused on the performance of the cathode air electrode or non-aqueous electrolyte in Li-air batteries, usage of lithium metal is another factor for achieving high energy density. Effects of lithium amount used for anode electrode on the discharge capacity were recently studied [77]. It has been demonstrated that the discharge capacity of a Li-air battery decreased from 1760 to 370 mAh g^{-1} when the amount of lithium on the anode reduced from 14 to 0.9 mg, respectively. Moreover, the cyclability of the cells also decreased with increasing the usage of lithium because there are more dendrite formation and porous structure of the deposited lithium after 10th cycle [77].

2.3 Modelling of lithium air battery

Recently, many research groups have developed and improved the key components, such as new materials for negative and positive electrode, electrolyte, catalysts, and separators, to overcome the problems of Li-air battery and yield the best performance. Besides experimental works, battery mathematical modelling on electrochemical and chemical reactions has been previously applied to understand and support many research groups for optimising many conventional batteries including metal-air batteries [78-84]. A mathematical model is essential for the battery development process, because a battery model after validation with experiment data can be used to identify battery-limiting mechanisms and predict battery performance for design, scale-up, and optimisation with adjusting parameters. Owing to a current application of high-performance computers, modelling and simulation have been applied in the study of many batteries, such as lead-acid [85, 86], nickel-metal hydride [87], and Li-ion [88], and fuel-cells as proton-exchange-membrane [89, 90]. Up to date, there has been an increasing amount of mathematical simulations used to investigate metal-air batteries.

Recently, Zn-air batteries have been considered as promising power sources and energy storage devices because of their high specific energy (more than 100 Wh kg^{-1}), and inexpensive and environmental materials. A one-dimensional numerical model of electrically rechargeable Zn-air battery had been developed and used to validate with the galvanostatic experiments [91]. The model included diffusion and migration of the dissolved species in the electrolyte of the porous Zn electrode and the separator. The electrochemical and chemical reactions occurring in both the porous Zn electrode and oxygen electrode, which were assumed to be flat electrodes, were considered in the model. The model can be fitted well with experimental data, such as cell voltage, the Zn electrode potential and O_2 potential with Zn as reference electrode. The simulation model showed the concentration profiles of participated species, current source density, and partial current source density profile during discharging and charging of the Zn-air battery. The cyclability of battery performance from the simulation model demonstrated up to 40 cycles and predicted that hydroxide (OH^-) depletion was a limiting factor for high-current discharge. This model proved to be beneficial for optimising Zn-air battery [91].

The context of the various reaction mechanisms in many batteries can be found in current battery systems, which include intercalation batteries (e.g. nickel-metal hydride battery, $C_6/LiCoO_2$, and other Li-ion couples), plating or stripping batteries (e.g. Li and Zn metal), alloying batteries (e.g. Li-Si alloys), and solution-precipitation batteries (e.g. Pb/PbO_2, Zn/O_2 and, some Li/S) [92]. However, a non-aqueous electrolyte system like Li-air battery is different from those batteries previously mentioned above. In Li-air battery, the discharge products of lithium oxides (Li_2O_2 and Li_2O) seem to be completely insoluble in non-aqueous electrolyte unlike the conventional intercalation Li-ion batteries or the solution-precipitation lead-acid batteries. With these differences and complicated mechanisms of Li-air battery, mathematical modelling is required for design and optimisation. Because the study on Li-air battery is still in an early stage and also lacks the physical understanding in complex reaction mechanisms of a non-aqueous system, the current mathematical model is only a starting point of physical equations which aim to improve the system performances.

Zheng et al. carried out the model predicting the theoretical energy density of the Li-air batteries based on the thermodynamic equations [93]. The calculation of specific energy and energy density based on the weight of the electrode and volume of air electrode were estimated in both aqueous and non-aqueous electrolytes. The battery performance was calculated including weight of the electrolyte, carbon cathode with 70% porosity and lithium, but excluding construction materials-current collector and housing. It was determined that the energies of Li-air cell are extremely dependent on the porosity of the air electrode. In alkaline aqueous electrolyte, the maximal Li-air cell specific energy and energy density were estimated at 1300 Wh kg^{-1} and 1520 Wh L^{-1}, respectively, and 1400 Wh kg^{-1} and 1680 Wh L^{-1} in acidic electrolyte. For the non-aqueous electrolyte, the assumption was made that the discharge terminated if all pore volume of the air cathode was filled or plugged with lithium oxide. The specific energy and energy density in this case were 2790 Wh kg^{-1} and 2800 Wh L^{-1}, respectively.

Recently, a diffusion-limited transient mathematical model with air cathode flooded with an organic electrolyte had been developed by Sandhu et al. [79]. The one-dimensional model was simulated by assuming that the cathode structure was the

number of cylindrical open-ended pores each of which had mean pore radius, $\bar{r}_p$. The electrochemical reaction and the Li_2O_2 formation took place inside these cylindrical pores. The simulation profiles presented the distribution of the Li_2O_2 product in the cathode during battery discharging in the assumption that the lithium ion concentration in the electrolyte solution was high enough to consider as a constant value, and the electrochemical cathode reaction was assumed to be pseudo first-order with respect to the dissolved oxygen concentration. The specific capacities of the Li-air battery, as a function of oxygen partial pressure and current density, were also predicted and compared with literature experiment results. Moreover, the model showed that the battery performance as measured in terms of specific capacity increased when the cathode thickness was reduced.

Similarly, the model of the air electrode with cylindrical pores structure had been designed to increase power rate operation of Li-air batteries [94]. Several methods were proposed to improve the power performance, such as a single pore system, dual pore system materials and dual pore systems with multiple time-release catalysts. The simulated results demonstrated that the dual pore system, which consists of two interconnected porosity systems: one that is catalysed and one that is not catalysed, increased the oxygen transport into the area of air cathode. However, this system alone can only offer high power for a short period. Then, the time-release catalysts technique coupled together with the dual pore configuration was proposed to prevent the decline of power output during discharge process.

The recent study of Li-air model using the theory of concentrated binary electrolyte solution was carried out by Andrei et al. [95]. This model was similar to the previous intercalation models for Li-ion batteries [78, 96, 97]. However, the model also included the oxygen transport diffusion and reaction inside the porous cathode. Unlike the kinetic reaction from Sandhu et al. [79], the electrochemical oxygen reduction reaction depended on the Li^+ and oxygen concentrations. Once again this model also assumed the structure of the cathode as many open-ended cylindrical pores as shown in Figure 2-6. It has been demonstrated that the discharge product of Li_2O_2 is deposited uniformly on the inner surface of the pores. The Li-air discharge capacity was largely dependent on the oxygen diffusivity in the electrolyte and the discharge current density. Therefore, several methods in order to increase the specific capacity and energy density of the Li-air battery were proposed, for example using a uniformly

distributed catalyst and a non-uniform catalyst. The former increased only the current and power density of the system while the latter improved only the specific capacity and energy density. In addition, the solvents with high oxygen solubility and diffusivity demonstrated the enhancement of the energy density.

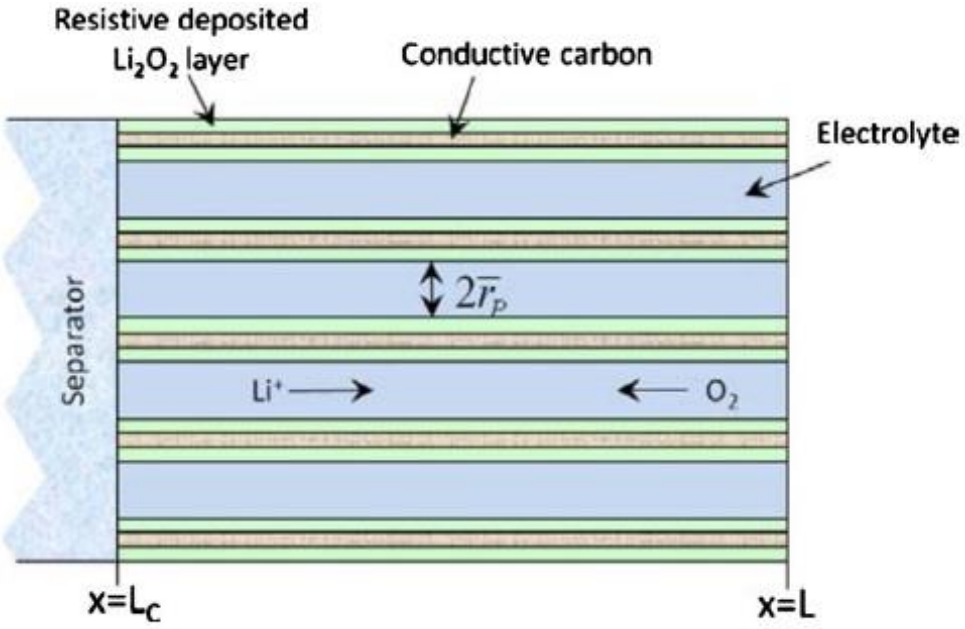

Figure 2-6 Schematic diagram of the Li-air model with cylindrical pores for oxygen diffusion and Li_2O_2 formation inside the porous carbon cathode [95].

However, the micrograph from Scanning Electron Microscopy (SEM) revealed that the Li-air cathode structure was formed as the porous carbon matrix with high tortuosity, as shown in Figure 2-7, rather than straight pores which are assumed in the previously mentioned models [79, 94, 95]. Hence, the more exact detailed structure of the porous cathode model has been proposed by using a macro-homogeneous model theory which simulates the battery using a volume-averaging technique and accounts for the essential features of an actual electrode (porosity, volume fraction and active surface area) without going into exact geometric details of porous carbon electrode as described in the next section.

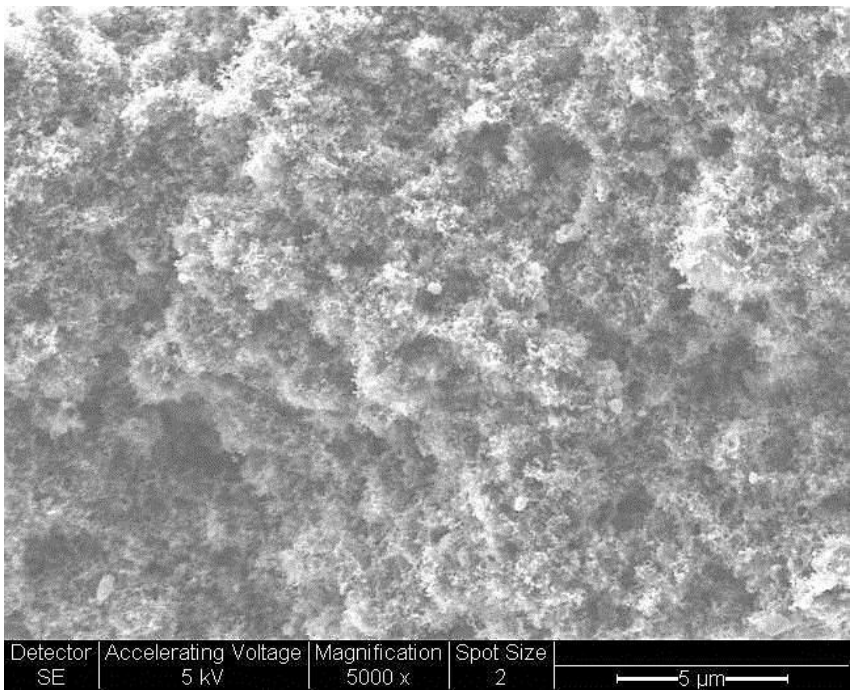

Figure 2-7 The SEM micrograph of a cross-section of pristine porous carbon electrode with 45 µm thick prepared by casting a mixture of carbon powder and binder on a thin open aluminium mesh.

2.4 Li-air battery with macroscopic model

The cathode structure in Li-air batteries could be considered as the porous electrode (as shown in Figure 2-7), which consists of porous matrices of a single electronic conduction (carbon powder) or mixtures of solids together with essentially nonconducting, reactive materials in addition to electronic conductors. Therefore, the Li-air model in this study is based on porous electrode theory, which was first carried out by Newman and Tiedemann [98, 99]. This theory considers the porous electrode as the macroscopic description, which consists of porous matrices of an active electronic conductor or a mixture of solids. Moreover, the void spaces of the porous matrices are served as a host for penetration of electrolyte solution, and also served as a reaction site for any chemical and electrochemical processes. At any given time, these reactions rates vary depending on the electrode physical structure, conductivity of porous matrices, electrolyte properties and individual parameters on each electrode reactions. After discharging, the void space of the porous cathode is filled with the insoluble discharge products depending on the electrochemical reactions occurring inside the battery and the applied electrolytes as displayed in Figure 2-8. Unlike the pristine electrode as shown in Figure 2-7, it is apparent from the micrograph that the morphology of the discharged electrode is filled with the solid products throughout the

entire porosity.

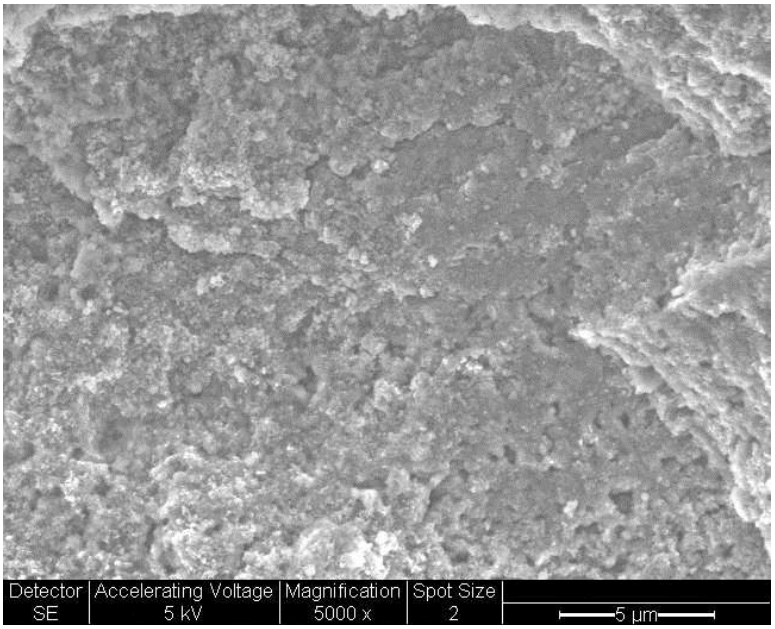

Figure 2-8 The SEM micrograph of a cross-section of porous carbon electrode form the discharged Li-air battery.

Therefore, the macro-homogeneous model, which is a useful tool for a theoretical analysis in this complicated porous electrode, is applied in this Li-air model study. To simplify such a complex structure, the model accounts for only the essential structure of an actual electrode without considering the exact geometric detail of a porous electrode. This model assumes that the porous electrode is an average of solid electrode and the electrolyte, which involves the averaging of various variables over the overall dimensions of the electrode. Moreover, the model should be predicted by the parameters which can be obtained by simple physical measurements [98, 99]. For example, a complex porous structure can be described by its porosity or void fraction inside the electrode and its average surface area per unit volume.

There are numerous mathematical macro-homogeneous models applied on the previous batteries simulation, especially for lithium-ion batteries and fuel cell modelling. Mathematical modelling of lithium-ion batteries involving the macro-homogeneous model of dependant variables, such as electrolyte phase potential, solid phase potential and solution concentrations, was developed by Doyle et al. [78, 88, 98, 100]. The models for lithium-ion intercalation consisting of a porous electrode, separator and a current collector were based on actual physical parameters of the battery system and specify for boundary and initial conditions. This model also used a

theory of concentrated solution due to the high concentration of electrolyte [99]. Moreover, this effort on lithium-ion model development can be applied further for similar electrochemical battery systems, e.g. modelling of nickel/metal hydride (Ni-MH) and silver-zinc batteries [80, 87].

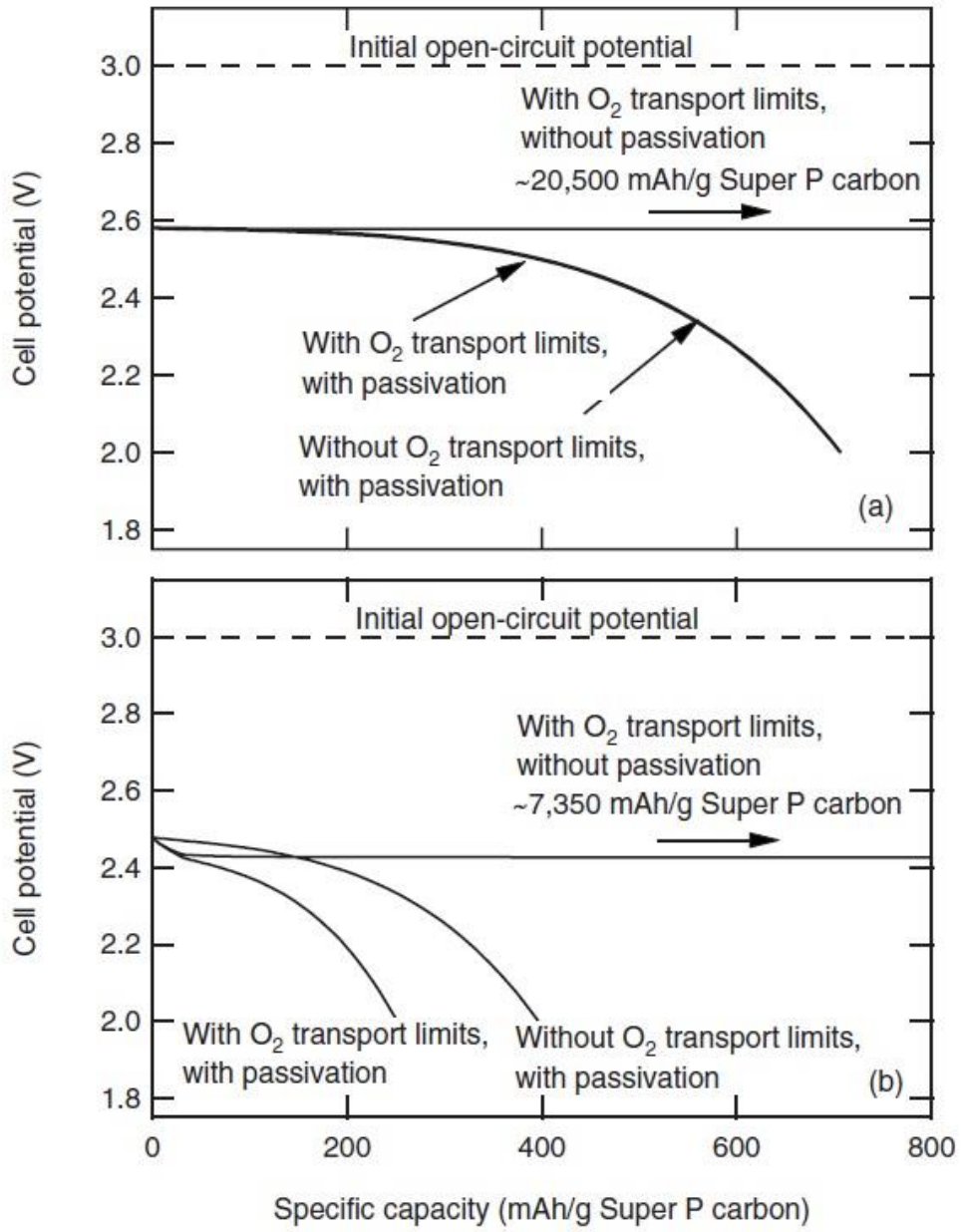

Figure 2-9 Simulation results demonstrating the relative impacts of eliminating oxygen transport limitations and eliminating the electronic resistance of the discharge products: (a) 0.08 and (b) 0.47 mA cm^{-2} [82].

The difference from aqueous system, the Li-air discharge products being solid and an insulator in non-aqueous system causes the Li-air battery model to be much more

complicated and it is difficult to identify the limiting factors that contribute to the cell overpotential (i.e., the factors may come from the oxygen mass transport limit or the products passivation limit). Albertus et al. recently developed the macro-homogeneous modelling work and experimental results to determine the principal factor limiting the Li-air battery capacity [82]. As shown in Figure 2-9, they concluded that the passivation of the cathode surface by the non-conducting discharge products, such as Li_2CO_3 and lithium alkyl carbonate, is the critical limitation in non-aqueous Li-air system [82]. At low discharge rate (Figure 2-9a), removing oxygen transport limitation (by setting diffusion coefficient of oxygen to infinity) had little effect on the discharge potential and capacity. However, when removing the passivation of the solid products (by setting the electronic resistivity of solid products to zero), the battery discharge capacity dramatically increased to 20,500 mAh g^{-1} higher than the case with passivation resistivity provided only 720 mAh g^{-1}. The similar results were obtained at high discharge current density as demonstrated in Figure 2-9b. Albertus et al. points out that passivation resistivity is the crucial role to be overcome for a non-aqueous Li-air battery with a high practical specific energy and capacity [82].

2.5 Conclusions

In this review, the fundamentals and recent progress in the field of Li-air batteries have been summarised. Nevertheless, the research on Li-air batteries is still at an early stage. There are still many challenges facing the design of rechargeable Li-air batteries such as optimizing cathode structure, blockage of the porous carbon cathode, decomposition of the electrolyte during charge and discharge, and the highly reactive Li anode with atmospheric moisture. The mathematical modelling can describe the mechanism inside the Li-air battery. Hence, the previous and present models are developed based on the starting point of these review information. When more details of physical and electrochemical information for Li-air battery are available, the model can be improved to meet those of practical Li-air behaviours and can be used as a tool to develop the Li-air battery.

2.6 References

1. Zhang, T., N. Imanishi, Y. Shimonishi, A. Hirano, Y. Takeda, O. Yamamoto, and N. Sammes, *A novel high energy density rechargeable lithium/air battery*. Chemical Communications, 2010. **46**(10): p. 1661-1663.

2. Kraytsberg, A. and Y. Ein-Eli, *Review on Li-air batteries - Opportunities, limitations and perspective.* Journal of Power Sources, 2011. **196**(3): p. 886-893.
3. Ogasawara, T., A. Débart, M. Holzapfel, P. Novák, and P.G. Bruce, *Rechargeable Li_2O_2 electrode for lithium batteries.* Journal of the American Chemical Society, 2006. **128**(4): p. 1390-1393.
4. Peng, Z., et al., *Oxygen reactions in a non-aqueous Li^+ electrolyte.* Angewandte Chemie - International Edition, 2011. **50**(28): p. 6351-6355.
5. Cheng, H. and K. Scott, *Selection of oxygen reduction catalysts for rechargeable lithium-air batteries-Metal or oxide?* Applied Catalysis B: Environmental, 2011. **108-109**: p. 140-151.
6. Laoire, C.O., S. Mukerjee, K.M. Abraham, E.J. Plichta, and M.A. Hendrickson, *Influence of nonaqueous solvents on the electrochemistry of oxygen in the rechargeable lithium-air battery.* Journal of Physical Chemistry C, 2010. **114**(19): p. 9178-9186.
7. Abraham, K.M. and Z. Jiang, *A polymer electrolyte-based rechargeable lithium/oxygen battery.* Journal of the Electrochemical Society, 1996. **143**(1): p. 1-5.
8. Armand, M. and J.M. Tarascon, *Building better batteries.* Nature, 2008. **451**(7179): p. 652-657.
9. Bruce, P.G., *Energy storage beyond the horizon: Rechargeable lithium batteries.* Solid State Ionics, 2008. **179**(21-26): p. 752-760.
10. Ellis, B.L., K.T. Lee, and L.F. Nazar, *Positive electrode materials for Li-Ion and Li-batteries.* Chemistry of Materials, 2010. **22**(3): p. 691-714.
11. Girishkumar, G., B. McCloskey, A.C. Luntz, S. Swanson, and W. Wilcke, *Lithium-air battery: Promise and challenges.* Journal of Physical Chemistry Letters, 2010. **1**(14): p. 2193-2203.
12. Padbury, R. and X. Zhang, *Lithium-oxygen batteries - Limiting factors that affect performance.* Journal of Power Sources, 2011. **196**(10): p. 4436-4444.
13. Tran, C., X.Q. Yang, and D. Qu, *Investigation of the gas-diffusion-electrode used as lithium/air cathode in non-aqueous electrolyte and the importance of carbon material porosity.* Journal of Power Sources, 2010. **195**(7): p. 2057-2063.
14. Lu, Y.C., D.G. Kwabi, K.P.C. Yao, J.R. Harding, J. Zhou, L. Zuin, and Y. Shao-Horn, *The discharge rate capability of rechargeable Li-O_2 batteries.* Energy and Environmental Science, 2011. **4**(8): p. 2999-3007.

15. Beattie, S.D., D.M. Manolescu, and S.L. Blair, *High-capacity lithium-air cathodes.* Journal of the Electrochemical Society, 2009. **156**(1): p. A44-A47.
16. Lu, Y.C., Z. Xu, H.A. Gasteiger, S. Chen, K. Hamad-Schifferli, and Y. Shao-Horn, *Platinum-gold nanoparticles: A highly active bifunctional electrocatalyst for rechargeable lithium-air batteries.* Journal of the American Chemical Society, 2010. **132**(35): p. 12170-12171.
17. Zhang, J.G., D. Wang, W. Xu, J. Xiao, and R.E. Williford, *Ambient operation of Li/Air batteries.* Journal of Power Sources, 2010. **195**(13): p. 4332-4337.
18. Crowther, O., B. Meyer, M. Morgan, and M. Salomon, *Primary Li-air cell development.* Journal of Power Sources, 2011. **196**(3): p. 1498-1502.
19. Li, Y., J. Wang, X. Li, J. Liu, D. Geng, J. Yang, R. Li, and X. Sun, *Nitrogen-doped carbon nanotubes as cathode for lithium-air batteries.* Electrochemistry Communications, 2011. **13**(7): p. 668-672.
20. Ren, X., S.S. Zhang, D.T. Tran, and J. Read, *Oxygen reduction reaction catalyst on lithium/air battery discharge performance.* Journal of Materials Chemistry, 2011. **21**(27): p. 10118-10125.
21. Yang, X.h., P. He, and Y.y. Xia, *Preparation of mesocellular carbon foam and its application for lithium/oxygen battery.* Electrochemistry Communications, 2009. **11**(6): p. 1127-1130.
22. Park, C.K., S.B. Park, S.Y. Lee, H. Lee, H. Jang, and W.I. Cho, *Electrochemical performances of lithium-air cell with carbon materials.* Bulletin of the Korean Chemical Society, 2010. **31**(11): p. 3221-3224.
23. Crowther, O., B. Meyer, M. Morgan, and M. Salomon, *Primary Li-air cell development.* Journal of Power Sources, 2010.
24. Wang, Y. and H. Zhou, *To draw an air electrode of a Li-air battery by pencil.* Energy and Environmental Science, 2011. **4**(5): p. 1704-1707.
25. Yoo, E. and H. Zhou, *Li-air rechargeable battery based on metal-free graphene nanosheet catalysts.* ACS Nano, 2011. **5**(4): p. 3020-3026.
26. Li, Y., J. Wang, X. Li, D. Geng, R. Li, and X. Sun, *Superior energy capacity of graphene nanosheets for a nonaqueous lithium-oxygen battery.* Chemical Communications, 2011. **47**(33): p. 9438-9440.
27. Read, J., *Characterization of the lithium/oxygen organic electrolyte battery.* Journal of the Electrochemical Society, 2002. **149**(9): p. A1190-A1195.
28. Xiao, J., D. Wang, W. Xu, R.E. Williford, J. Liu, and J.G. Zhang, *Optimization of air electrode for Li/air batteries.* Journal of the Electrochemical Society,

2010. **157**(4): p. A487-A492.

29. Débart, A., J. Bao, G. Armstrong, and P.G. Bruce, *An O_2 cathode for rechargeable lithium batteries: The effect of a catalyst.* Journal of Power Sources, 2007. **174**(2): p. 1177-1182.
30. Zhang, D., Z. Fu, Z. Wei, T. Huang, and A. Yu, *Polarization of oxygen electrode in rechargeable lithium oxygen batteries.* Journal of the Electrochemical Society, 2010. **157**(3): p. A362-A365.
31. Dobley, A., C. Morein, and K.M. Abraham. *Cathode optimization for lithium-air batteries*. in *Meeting Abstracts*. 2005. Los Angeles, CA.
32. Tran, C., J. Kafle, X.Q. Yang, and D. Qu, *Increased discharge capacity of a Li-air activated carbon cathode produced by preventing carbon surface passivation.* Carbon, 2011. **49**(4): p. 1266-1271.
33. Débart, A., A.J. Paterson, J. Bao, and P.G. Bruce, *α-MnO2 nanowires: A catalyst for the O_2 electrode in rechargeable lithium batteries.* Angewandte Chemie - International Edition, 2008. **47**(24): p. 4521-4524.
34. Cheng, H. and K. Scott, *Carbon-supported manganese oxide nanocatalysts for rechargeable lithium-air batteries.* Journal of Power Sources, 2010. **195**(5): p. 1370-1374.
35. Scrosati, B. and J. Garche, *Lithium batteries: Status, prospects and future.* Journal of Power Sources, 2010. **195**(9): p. 2419-2430.
36. Zhang, G.Q., J.P. Zheng, R. Liang, C. Zhang, B. Wang, M. Au, M. Hendrickson, and E.J. Plichta, *α-MnO 2/Carbon nanotube/Carbon nanofiber composite catalytic air electrodes for rechargeable lithium-air batteries.* Journal of the Electrochemical Society, 2011. **158**(7): p. A822-A827.
37. Trahey, L., C.S. Johnson, J.T. Vaughey, S.H. Kang, L.J. Hardwick, S.A. Freunberger, P.G. Bruce, and M.M. Thackeray, *Activated lithium-metal-oxides as catalytic electrodes for Li-O_2 cells.* Electrochemical and Solid-State Letters, 2011. **14**(5): p. A64-A66.
38. Debart, A., J. Bao, G. Armstrong, and P.G. Bruce, *An O_2 cathode for rechargeable lithium batteries: The effect of a catalyst.* Journal of Power Sources, 2007. **174**(2): p. 1177-1182.
39. Lu, Y.C., H.A. Gasteiger, M.C. Parent, V. Chiloyan, and Y. Shao-Horn, *The influence of catalysts on discharge and charge voltages of rechargeable Li-oxygen batteries.* Electrochemical and Solid-State Letters, 2010. **13**(6): p. A69-A72.

40. Thapa, A.K., K. Saimen, and T. Ishihara, *Pd/ MnO_2 air electrode catalyst for rechargeable lithium/air battery.* Electrochemical and Solid-State Letters, 2010. **13**(11): p. A165-A167.
41. Thapa, A.K. and T. Ishihara, *Mesoporous α-MnO_2/Pd catalyst air electrode for rechargeable lithium-air battery.* Journal of Power Sources, 2011. **196**(16): p. 7016-7020.
42. Bruce, P.G., S.A. Freunberger, L.J. Hardwick, and J.M. Tarascon, *Li-O_2 and Li-S batteries with high energy storage.* Nature Materials, 2012. **11**(1): p. 19-29.
43. Read, J., K. Mutolo, M. Ervin, W. Behl, J. Wolfenstine, A. Driedger, and D. Foster, *Oxygen Transport Properties of Organic Electrolytes and Performance of Lithium/Oxygen Battery.* Journal of the Electrochemical Society, 2003. **150**(10): p. A1351-A1356.
44. Xu, W., J. Xiao, J. Zhang, D. Wang, and J.G. Zhang, *Optimization of nonaqueous electrolytes for primary lithium/air batteries operated in ambient environment.* Journal of the Electrochemical Society, 2009. **156**(10): p. A773-A779.
45. Kowalczk, I., J. Read, and M. Salomon, *Li-air batteries: A classic example of limitations owing to solubilities.* Pure and Applied Chemistry, 2007. **79**(5): p. 851-860.
46. McCloskey, B.D., R. Scheffler, A. Speidel, D.S. Bethune, R.M. Shelby, and A.C. Luntz, *On the efficacy of electrocatalysis in nonaqueous Li-O_2 batteries.* Journal of the American Chemical Society, 2011. **133**(45): p. 18038-18041.
47. Freunberger, S.A., Y. Chen, N.E. Drewett, L.J. Hardwick, F. Bardé, and P.G. Bruce, *The lithium-oxygen battery with ether-based electrolytes.* Angewandte Chemie - International Edition, 2011. **50**(37): p. 8609-8613.
48. Xu, W., J. Xiao, D. Wang, J. Zhang, and J.G. Zhang, *Effects of nonaqueous electrolytes on the performance of lithium/air batteries.* Journal of the Electrochemical Society, 2010. **157**(2): p. A219-A224.
49. Zhang, S.S., D. Foster, and J. Read, *Discharge characteristic of a non-aqueous electrolyte Li/O_2 battery.* Journal of Power Sources, 2010. **195**(4): p. 1235-1240.
50. Debart, A., A.J. Paterson, J. Bao, and P.G. Bruce, *a-MnO_2 nanowires: A catalyst for the O_2 electrode in rechargeable lithium batteries.* Angewandte Chemie - International Edition, 2008. **47**(24): p. 4521-4524.
51. Freunberger, S.A., Y. Chen, Z. Peng, J.M. Griffin, L.J. Hardwick, F. Bardé, P. Novák, and P.G. Bruce, *Reactions in the rechargeable lithium-O_2 battery with*

alkyl carbonate electrolytes. Journal of the American Chemical Society, 2011. **133**(20): p. 8040-8047.

52. Crowther, O., D. Keeny, D.M. Moureau, B. Meyer, M. Salomon, and M. Hendrickson, *Electrolyte optimization for the primary lithium metal air battery using an oxygen selective membrane.* Journal of Power Sources, 2012. **202**: p. 347-351.
53. Xu, W., V.V. Viswanathan, D. Wang, S.A. Towne, J. Xiao, Z. Nie, D. Hu, and J.G. Zhang, *Investigation on the charging process of Li_2O_2-based air electrodes in Li-O_2 batteries with organic carbonate electrolytes.* Journal of Power Sources, 2011. **196**(8): p. 3894-3899.
54. Xu, W., et al., *Reaction mechanisms for the limited reversibility of Li-O_2 chemistry in organic carbonate electrolytes.* Journal of Power Sources, 2011. **196**(22): p. 9631-9639.
55. Bryantsev, V.S., V. Giordani, W. Walker, M. Blanco, S. Zecevic, K. Sasaki, J. Uddin, D. Addison, and G.V. Chase, *Predicting solvent stability in aprotic electrolyte Li-air batteries: Nucleophilic substitution by the superoxide anion radical (O2 •-).* Journal of Physical Chemistry A, 2011. **115**(44): p. 12399-12409.
56. Read, J., *Ether-based electrolytes for the lithium/oxygen organic electrolyte battery.* Journal of the Electrochemical Society, 2006. **153**(1): p. A96-A100.
57. Morita, M., H. Hayashida, and Y. Matsuda, *Effect of crown cther addition to oraganic electrolytes on the cycling behaviour of the TiS_2.* Journal of the Electrochemical Society, 1987. **l34**(9): p. 2107-2111.
58. Nagasubramanian, G. and S. Di Stefano, *12-Crown-4 ether-assisted enhancement of ionic conductivity and interfacial kinetics in polyethylene oxide electrolytes.* Journal of the Electrochemical Society, 1990. **137**(12): p. 3830-3835.
59. Nagasubramanian, G., A.I. Attia, and G. Halpert, *Effects of 12-crown-4 ether on the electrochemical performance of CoO_2 and TiS_2 cathodes in Li polymer electrolyte cells.* Journal of the Electrochemical Society, 1992. **139**(11): p. 3043-3046.
60. Xu, W., J. Xiao, D. Wang, J. Zhang, and J.G. Zhang, *Crown ethers in nonaqueous electrolytes for lithium/air batteries.* Electrochemical and Solid-State Letters, 2010. **13**(4): p. A48-A51.
61. Quartarone, E. and P. Mustarelli, *Electrolytes for solid-state lithium*

rechargeable batteries: Recent advances and perspectives. Chemical Society Reviews, 2011. **40**(5): p. 2525-2540.

62. Kuboki, T., T. Okuyama, T. Ohsaki, and N. Takami, *Lithium-air batteries using hydrophobic room temperature ionic liquid electrolyte.* Journal of Power Sources, 2005. **146**(1-2): p. 766-769.
63. Zhang, D., R. Li, T. Huang, and A. Yu, *Novel composite polymer electrolyte for lithium air batteries.* Journal of Power Sources, 2010. **195**(4): p. 1202-1206.
64. He, P., Y. Wang, and H. Zhou, *A Li-air fuel cell with recycle aqueous electrolyte for improved stability.* Electrochemistry Communications, 2010. **12**(12): p. 1686-1689.
65. Zheng, J.P., P. Andrei, M. Hendrickson, and E.J. Plichta, *The theoretical energy densities of dual-electrolytes rechargeable Li-air and Li-air flow batteries.* Journal of the Electrochemical Society, 2011. **158**(1): p. A43-A46.
66. Imanishi, N., S. Hasegawa, T. Zhang, A. Hirano, Y. Takeda, and O. Yamamoto, *Lithium anode for lithium-air secondary batteries.* Journal of Power Sources, 2008. **185**(2): p. 1392-1397.
67. Wang, Y. and H. Zhou, *A lithium-air battery with a potential to continuously reduce O_2 from air for delivering energy.* Journal of Power Sources, 2010. **195**(1): p. 358-361.
68. Hasegawa, S., N. Imanishi, T. Zhang, J. Xie, A. Hirano, Y. Takeda, and O. Yamamoto, *Study on lithium/air secondary batteries-Stability of NASICON-type lithium ion conducting glass-ceramics with water.* Journal of Power Sources, 2009. **189**(1): p. 371-377.
69. Kumar, B. and J. Kumar, *Cathodes for solid-state lithium-oxygen cells: Roles of nasicon glass-ceramics.* Journal of the Electrochemical Society, 2010. **157**(5): p. A611-A616.
70. Shimonishi, Y., T. Zhang, P. Johnson, N. Imanishi, A. Hirano, Y. Takeda, O. Yamamoto, and N. Sammes, *A study on lithium/air secondary batteries-Stability of NASICON-type glass ceramics in acid solutions.* Journal of Power Sources, 2010. **195**(18): p. 6187-6191.
71. Kumar, B., J. Kumar, R. Leese, J.P. Fellner, S.J. Rodrigues, and K.M. Abraham, *A solid-state, rechargeable, long cycle life lithium-air battery.* Journal of the Electrochemical Society, 2010. **157**(1): p. A50-A54.
72. Wang, D., J. Xiao, W. Xu, and J.G. Zhang, *High capacity pouch-type Li-air batteries.* Journal of the Electrochemical Society, 2010. **157**(7): p. A760-A764.

73. Stevens, P., G. Toussaint, G. Caillon, P. Viaud, P. Vinatier, C. Cantau, O. Fichet, C. Sarrazin, and M. Mallouki, *Development of a lithium air rechargeable battery*. ECS Transactions, 2010. **28**(32): p. 1-12.
74. Schalkwijk, W.A.v. and B. Scrosati, *Advances in Lithium-Ion Batteries*2002, New York: Kluwer Academic/Plenum Publishers.
75. Zhang, T., N. Imanishi, S. Hasegawa, A. Hirano, J. Xie, Y. Takeda, O. Yamamoto, and N. Sammes, *Water-stable lithium anode with the three-layer construction for aqueous lithium-air secondary batteries.* Electrochemical and Solid-State Letters, 2009. **12**(7): p. A132-A135.
76. Thapa, A.K., Y. Hidaka, H. Hagiwara, S. Ida, and T. Ishihara, *Mesoporous β-MnO_2 air electrode modified with pd for rechargeability in lithium-air battery.* Journal of the Electrochemical Society, 2011. **158**(12): p. A1483-A1489.
77. Jang, I.C., Y. Hidaka, and T. Ishihara, *Li metal utilization in lithium air rechargeable batteries.* Journal of Power Sources, 2013. **244**: p. 606-609.
78. Doyle, M., T. Fuller, and J. Newman, *Modeling of galvanostatic charge and discharge of the lithium/ polymer/insertion cell.* Journal of the Electrochemical Society, 1993. **140**(6): p. 1526-1533.
79. Sandhu, S., J. Fellner, and G. Brutchen, *Diffusion-limited model for a lithium/air battery with an organic electrolyte.* Journal of Power Sources, 2007. **164**(1): p. 365-371.
80. Venkatraman, M. and J.W. Van Zee, *A model for the silver-zinc battery during high rates of discharge.* Journal of Power Sources, 2007. **166**(2): p. 537-548.
81. Boovaragavan, V., R.N. Methakar, V. Ramadesigan, and V.R. Subramanian, *A Mathematical Model of the Lead-Acid Battery to Address the Effect of Corrosion.* Journal of the Electrochemical Society, 2009. **156**(11): p. A854-A862.
82. Albertus, P., G. Girishkumar, B. McCloskey, R.S. Sánchez-Carrera, B. Kozinsky, J. Christensen, and A.C. Luntz, *Identifying capacity limitations in the Li/oxygen battery using experiments and modeling.* Journal of the Electrochemical Society, 2011. **158**(3): p. A343-A351.
83. Danilov, D., R.A.H. Niessen, and P.H.L. Notten, *Modeling all-solid-state Li-ion batteries.* Journal of the Electrochemical Society, 2011. **158**(3): p. A215-A222.
84. Wang, Y., *Modeling discharge deposit formation and its effect on lithium-air battery performance.* Electrochimica Acta, 2012. **75**(0): p. 239-246.
85. Gu, H., T.V. Nguyen, and R.E. White, *Mathematical model of a lead-acid cell:*

discharge, rest, and charge. Journal of the Electrochemical Society, 1987. **134**(12): p. 2953-2960.

86. Gu, W.B., C.Y. Wang, and B.Y. Liaw, *Numerical modeling of coupled electrochemical and transport processes in lead-acid batteries.* Journal of the Electrochemical Society, 1997. **144**(6): p. 2053-2061.
87. Paxton, B. and J. Newman, *Modeling of nickel/metal hydride batteries.* Journal of the Electrochemical Society, 1997. **144**(11): p. 3818-3831.
88. Fuller, T.F., M. Doyle, and J. Newman, *Simulation and optimization of the dual lithium ion insertion cell.* Journal of the Electrochemical Society, 1994. **141**(1): p. 1-10.
89. Scott, K., S. Pilditch, and M. Mamlouk, *Modelling and experimental validation of a high temperature polymer electrolyte fuel cell.* Journal of Applied Electrochemistry, 2007. **37**(11): p. 1245-1259.
90. Sousa, T., M. Mamlouk, and K. Scott, *An isothermal model of a laboratory intermediate temperature fuel cell using PBI doped phosphoric acid membranes.* Chemical Engineering Science, 2010. **65**(8): p. 2513-2530.
91. Deiss, E., F. Holzer, and O. Haas, *Modeling of an electrically rechargeable alkaline Zn-air battery.* Electrochimica Acta, 2002. **47**(25): p. 3995-4010.
92. Newman, J. and K.E. Thomas-Alyea, *Electrochemical Systems*. 3 ed2004, New York: John Wiley & Sons.
93. Zheng, J.P., R.Y. Liang, M. Hendrickson, and E.J. Plichta, *Theoretical energy density of Li-air batteries.* Journal of the Electrochemical Society, 2008. **155**(6).
94. Williford, R.E. and J.G. Zhang, *Air electrode design for sustained high power operation of Li/air batteries.* Journal of Power Sources, 2009. **194**(2): p. 1164-1170.
95. Andrei, P., J.P. Zheng, M. Hendrickson, and E.J. Plichta, *Some possible approaches for improving the energy density of Li-air batteries.* Journal of the Electrochemical Society, 2010. **157**(12).
96. Subramanian, V.R., V. Boovaragavan, and V.D. Diwakar, *Toward real-time simulation of physics based lithium-ion battery models.* Electrochemical and Solid-State Letters, 2007. **10**(11): p. 255-260.
97. Botte, G.G., V.R. Subramanian, and R.E. White, *Mathematical modeling of secondary lithium batteries.* Electrochimica Acta, 2000. **45**(15-16): p. 2595-2609.
98. Newman, J.S. and C.W. Tobias, *Theoretical Analysis of Current Distribution in*

Porous Electrodes. Journal of the Electrochemical Society, 1962. **109**(12): p. 1183-1191.

99. Newman, J. and W. Tiedemann, *Porous-electrode theory with battery applications.* AIChE Journal, 1975. **21**(1): p. 25-41.
100. Fuller, T.F., M. Doyle, and J. Newman, *Relaxation phenomena in lithium-ion-insertion cells.* Journal of the Electrochemical Society, 1994. **141**(4): p. 982-990.

Chapter 3: Li-air Model

This chapter describes the basic governing equations of a micro-macro homogeneous mathematical model. These include the combined continuity, transport and kinetics equations as well as the model parameters for the Li-air batteries with a non-aqueous electrolyte. The model was used to describe and predict the Li-air behaviour as presented in Chapters 4, 5, 6 and 7.

3.1 Introduction

Electrochemical energy devices, such as lead-acid and lithium batteries, as well as fuel cells, are widely used in consumer applications and electric vehicles. These devices and modern metal-air batteries such as Zn, Al, Na, and Li are now increasingly in demand for the purpose of developing more advanced energy storage with higher energy density, higher capacity, and longer cycle life. Mathematical modelling is extremely an indispensable tool during the process of battery design and development. Once a battery model has been validated with experiments, it plays an important role to identify cell-limiting mechanisms and predict cell performance for design, scale-up, and optimisation. Modelling and simulations consume less time, effort and cost than an experimental process. Therefore, owing to high-performance computers and useful numerical equations, modelling and simulation of battery and fuel cell system has been rapidly studied together with the experimental field.

3.2 Governing equations

A mathematical description of a prismatic cell of Li-air battery has been developed involving conservation of mass and current, species transport, and reaction kinetics in the cathode and separator to clarify the mechanism inside the battery. The model used in this study is applied to a Li-air cell consisting of a thin lithium anode electrode, an anode protective layer (APL), a separator, and a porous carbon oxygen/air cathode filled with an organic electrolyte as shown in Figure 3-1. As the porous cathode is flooded with an organic electrolyte, no gas phase occurs in the porosity of the air cathode. Current collectors are placed at the back of each electrode. The equations are presented with time-dependent to describe the dynamic behaviour of Li-air batteries during

discharge and charge processes. In this section a general form of the governing equations used in Chapters 4, 5, 6 and 7 is presented.

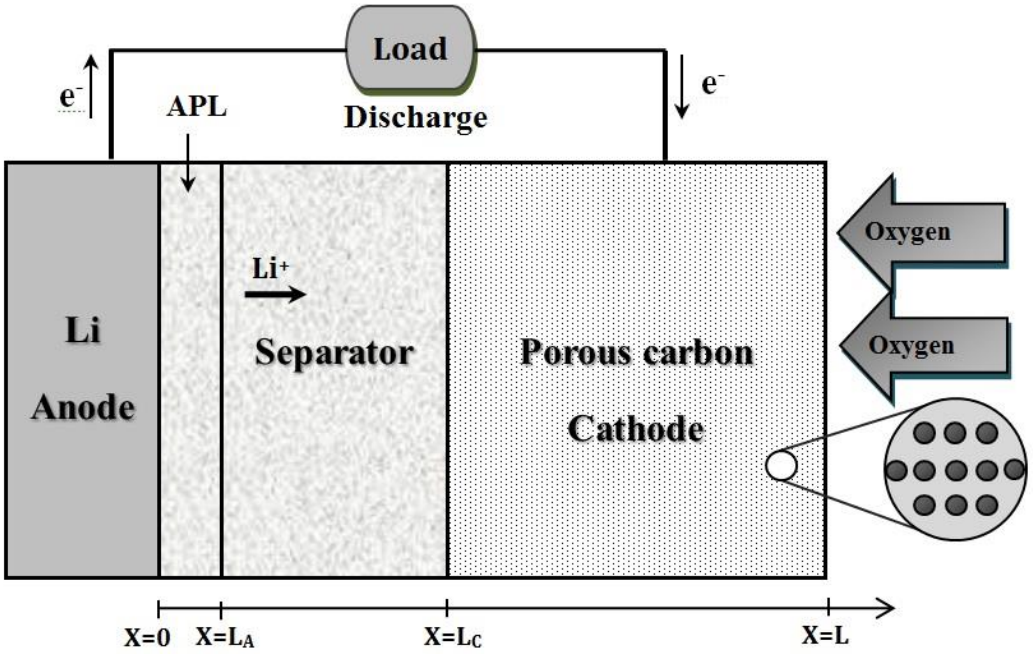

Figure 3-1: Schematic diagram of the computation domain for a Li-air battery during discharge. The inset demonstrates the porous carbon cathode.

3.2.1 Transport of species

The mass balance of a species i was obtained by applying the law of conservation of mass of species i to the volume element fixed in space, where the species was moving through. The mass balance for a system with the reactions is as follows:

$$\begin{Bmatrix} time\ rate \\ of\ change \\ of\ species\ i \end{Bmatrix} = \begin{Bmatrix} rate\ of \\ mass\ i \\ in \end{Bmatrix} - \begin{Bmatrix} rate\ of \\ mass\ i \\ out \end{Bmatrix} + \begin{Bmatrix} rate\ of\ production \\ or\ consumption \\ of\ species\ i\ by\ reaction \end{Bmatrix} \tag{3-1}$$

As the model was based on the macroscopic theory of porous electrode which considers the solution and solid matrix phases to be a superimposed continuum [1, 2]. Based on this approach, a material balance equation in term of the concentration for species i transport in the liquid electrolyte can be expressed as:

$$\frac{\partial(\varepsilon c_i)}{\partial t} = -\nabla \cdot \boldsymbol{N}_i + r_i \tag{3-2}$$

where c_i is the bulk concentration of species i in the solution phase which is averaged

over the volume of the solution in the pores, ε is the porosity of the electrode which is the electrolyte space in the matrix phase, $\boldsymbol{N_i}$ is the molar flux of species i in the porous solution averaged over the cross sectional area of the electrode, and r_i is the volumetric production rate of species i from the solid phase (electrode material) to solution phase (electrolyte in the porous) within the porous electrode.

As the lithium salts are always used as the electrolyte in a Li-air battery, the concentration of ionic species in the electrolyte is the same as the concentration of lithium ions (Li^+) due to the binary electrolyte assumption (an electrolyte dissociates into one positive ion and one negative ion). This takes into account the fact that ionic species were transported by diffusion and by migration while other species were moved by diffusion only. The convection term was negligible in the model because the porosity of electrode was filled with the electrolyte, i.e. flooded electrode. Hence, the molar flux in Eq. (3-2) for mass transfers for both Li^+ and species in the battery can be expressed respectively as:

$$\boldsymbol{N_{Li}} = -D_{Li,eff}\nabla c_{Li} + \frac{\boldsymbol{i}_2 t_+}{F} \tag{3-3}$$

$$\boldsymbol{N_i} = -D_{i,eff}\nabla c_i \tag{3-4}$$

where $D_{Li,eff}$ and $D_{i,eff}$ are the effective diffusion coefficients of Li^+ and species i, respectively, t_+ is the transference number of Li^+, F is Faraday's constant which is equal to 96,485 C mol^{-1}, and $\boldsymbol{i}_2$ is the current density in the solution phase or electrolyte current density which can be defined by the gradient of the potential in concentrated electrolyte solution as [1, 3]:

$$\nabla\phi_2 = -\frac{\boldsymbol{i}_2}{\kappa_{eff}} - \frac{\nu RT}{F}\left(\frac{s_+}{n\nu_+} + \frac{t_+}{z_+\nu_+} - \frac{s_0 c}{n c_0}\right)\left(1 + \frac{\partial lnf}{\partial lnc}\right)\nabla lnc \tag{3-5}$$

where n, s_+, s_0, ν_+, and ν represent the number of electrons transferred, the stoichiometric coefficients for cation and solvent, the number of cations, and the number of moles of ions into which a mole of electrolyte dissociates, respectively. c and c_0 are the molar concentrations of the electrolyte and solvent in the electrolyte phase, respectively. For Li-air battery, a 1:1 binary electrolyte is applied in the cell. Then, s_0 = 0, s_+ = -1, ν_+= n = 1, and ν = 2. The Eq. (3-5) can be rearranged into the current density in electrolyte as:

$$\boldsymbol{i}_2 = -\kappa_{eff}\nabla\phi_2 - \frac{2RT\kappa_{eff}}{F}(t_+ - 1)\left(1 + \frac{\partial lnf}{\partial lnc_{Li}}\right)\nabla lnc_{Li} \quad (3\text{-}6)$$

where κ_{eff} is the effective conductivity of the electrolyte, ϕ_2 is the electrolyte potential (electric potential of Li^+), R is the universal gas constant which is 8.3143 J mol^{-1} K^{-1}, T is the cell temperature in Kelvin, and f is the activity coefficient of $LiPF_6$ salt.

In the solid matrix phase, the movement of electrons is governed by Ohm's law which evaluates the electric potential variation or potential of electron, ϕ_1, as follows:

$$\boldsymbol{i}_1 = -\sigma_{eff}\nabla\phi_1 \quad (3\text{-}7)$$

where σ_{eff} is the effective conductivity of the electron in the electrode. This parameter is affected by the volume fraction of solid electrode inside the porous cathode. Moreover, the effective parameters of $D_{i,eff}$, κ_{eff} and σ_{eff} in the above equations also depend on the tortuosity of individual phases in the porous cathode (through porosity or volume fraction). These parameters are applied only for the porous cathode region and are corrected to account for the porosity effect using the Bruggeman correlation [4]:

$$D_{Li,eff} = \varepsilon^{1.5} D_{Li} \quad (3\text{-}8)$$

$$D_{i,eff} = \varepsilon^{1.5} D_i \quad (3\text{-}9)$$

$$\kappa_{eff} = \varepsilon^{1.5}\kappa \quad (3\text{-}10)$$

$$\sigma_{eff} = (1-\varepsilon)^{1.5}\sigma \quad (3\text{-}11)$$

where D_{Li}, D_i, κ and σ are the diffusion coefficient of the Li^+ and each specie in electrolyte and the conductivity of electrolyte and electron in the cathode, respectively.

3.2.2 Conservation of charge

For the porous electrode theory, the charge conservation for the matrix and solution phases would require the divergence of the total current density to be zero as defined by:

$$\nabla \cdot \boldsymbol{i}_1 + \nabla \cdot \boldsymbol{i}_2 = 0 \quad (3\text{-}12)$$

During battery discharging or charging, the electrochemical reactions occurring at the electrode/electrolyte interface (charges transfer reaction) are expressed for individual reactions according to the conventionally general formula which takes the form:

$$\sum s_i M_i^{z_i} \rightarrow ne^- \tag{3-13}$$

The charge transfer from solid phase to electrolyte phase per unit volume of electrode ($\nabla \cdot \boldsymbol{i}_2$) is related to the all local charge transfer current density (j_m) of electrochemical reactions, m, occurring at the cathode given by:

$$\nabla \cdot \boldsymbol{i}_2 = \sum_m a j_m \tag{3-14}$$

This equation states that the transfer current per unit electrode volume is equivalent to the electrode chemical reaction rate where the M_i is a species symbol participating in the electrochemical reaction, z_i and s_i are the charge number and the stoichiometric coefficient of the species i, n is the number of electron transferred in the reaction, a is the specific interfacial area of the pore per unit volume of the total electrode, and j_m is local transfer current density between electrode and electrolyte interface of each reaction at the cathode. The values of s_i, z_i, and n can be defined by matching with an individual electrode reaction using the general form of Eq. (3-13). For example, in the Li_2O_2 formation reaction in Eq. (3-15), the values of s_{Li}, z_{Li}, and n of Li^+ are -2, 1, and 2, respectively:

$$2Li^+ + O_2 + 2e^- \rightleftharpoons (Li_2O_2)_{solid} \tag{3-15}$$

Once the charge transfer from solid phase to electrolyte phase in the porous electrode is determined in Eq. (3-14), the superficial production or consumption rate of each species (referred to Eq. (3-2)) from solid phase to pore solution in the individual reactions *m* is given by Faraday's law:

$$r_i = -\frac{s_i}{nF} \nabla \cdot \boldsymbol{i}_2 = -\sum_m \frac{a s_{i,m}}{nF} j_m \tag{3-16}$$

3.2.3 Rate expressions at cathode

For Li-air battery, the porous cathode is regarded as the main contributor to the battery's performance as its thickness and surface area cover almost the entire Li-air compartments. Hence, the reactions and chemical mechanisms for the charge/discharge products mainly occur in this area.

Li_2O_2 formation:

The actual reaction paths and mechanisms for the discharge products are not available

and are quite complex involving various intermediates [5, 6]. Hence, to describe the electrochemical kinetic expression for the porous cathode, the model adopts the kinetic expression based on Eq. (3-15) for Li_2O_2 formation. For electrochemical reaction of Li_2O_2 at the cathode, a modified version of the Butler-Volmer equation is applied to the model using two rate coefficients. The reaction for Li_2O_2 formation depends on the concentration of (Li^+) and oxygen in a non-aqueous electrolyte for discharge and the concentration of Li_2O_2 during charge as in the following equation:

$$\frac{j_c}{2F} = k_a\left(c_{Li_2O_2}\right)exp\left[\frac{(1-\beta)nF}{RT}\eta_m\right] - k_c(c_{Li,s})^2\left(c_{O_2,s}\right)exp\left[\frac{-\beta nF}{RT}\eta_m\right] \tag{3-17}$$

$$\eta_m = \phi_1 - \phi_2 - \Delta\phi_{film} - E_m^0 \tag{3-18}$$

$$\Delta\phi_{film} = j_m R_{film}\varepsilon_s \tag{3-19}$$

where j_c is local transfer current density between electrode and electrolyte interface for Li_2O_2 reaction, $c_{i,s}$ is the molar concentration of species i at the wall or surface of electrode and can be determined in Eq. (3-26), k_a and k_c are the anodic and cathodic rate constant, respectively, β is the symmetry factor equal to 0.5, η_m is surface or activated overpotential for individual reaction, m, at the cathode, $\Delta\phi_{film}$ and R_{film} are the voltage drop and the electrical resistivity across Li_2O_2 film formation, respectively, ε_s is the volume fraction of solid Li_2O_2, and E_m^0 is the theoretical open-circuit potential for each reaction. The subscript m defined in the Eq. (3-17) to Eq. (3-19) is presented in case there is more than one electrochemical reaction at a porous cathode.

3.2.4 Rate expressions at anode

The electrochemical reaction rate for the anode is the oxidation of lithium metal to soluble Li^+ into the electrolyte. This anode electrode was used as the reference electrode in Li-air battery model and its standard reference potential was equal to 0 V. The electrochemical reaction is described by a general Butler-Volmer equation as follows:

$$j_a = i_0\left[exp\left(\frac{(1-\beta)nF}{RT}\eta_a\right) - exp\left(\frac{-\beta nF}{RT}\eta_a\right)\right] \tag{3-20}$$

where i_0 is exchange current density for anode electrode, η_a is surface or activated overpotential for reaction at anode, and the other parameter are as described above.

3.2.5 Specific interfacial area

The specific area, a of the electrode/electrolyte interface in Eq. (3-14) and Eq. (3-16) is decreased by the morphology and dynamic change of the porosity due to the solid discharge products. These discharge products can be any lithium oxides, lithium carbonates as well as lithium alkyl carbonates as described in Chapter 2. However, only Li_2O_2 and Li_2CO_3 were considered as the model for the discharge products in this study. These products are insoluble in several non-aqueous electrolytes and cover the active surface area during battery discharging. The variation of effective local surface area per unit volume of electrode can be commonly written by a geometric relation [7, 8] as follows:

$$a = a_o \left[1 - \left(\frac{\varepsilon_s}{\varepsilon^o}\right)^p\right] \tag{3-21}$$

where ε_s and ε^o are the volume fraction of solid discharge products, and initial electrode porosity, respectively. This empirical equation is used to describe the dynamic change in the interfacial area for electrochemical reactions that occur during discharge because of the fast passivation of Li_2O_2 and Li_2CO_3 covering a portion of the active sites for electrochemical reaction over the carbon surface [9]. The magnitude of exponent p is a geometrical factor indicating the morphology shape of the solid peroxide that covers the active area. Small values of p indicate that the flat, plate-like precipitate of Li_2O_2, conversely, large values of p reflects the needle-like solid which cover small active area. In Chapter 2, the SEM micrograph of a cross-section of porous carbon electrode from the discharged Li-air battery shows that the morphology of the discharged products look like flat-plated shape, therefore the value of $p = 0.4$ has been applied in this model.

3.2.6 Dynamic porosity change

The porosity volume change of the carbon electrode will be decreased due to the formation of insoluble solid products covering the catalyst and active particles as described in Eq. (3-22). Thus, the effective diffusivity for all species inside the cell and the effective ionic conductivity are influenced by the porosity change due to the Li_2O_2 and Li_2CO_3 formation. These parameters can be corrected by the Bruggeman relationship (referred to Eq. (3-8)-Eq. (3-11)). Because the solid distributions in the model are Li_2O_2 and Li_2CO_3, we use the properties of these solids for the build-up of discharge products inside the porous electrode as expressed in the following

relationship:

$$\frac{\partial \varepsilon}{\partial t} = \sum_{solid\ phase\ m} a j_m \frac{M_m}{nF\rho_m} \tag{3-22}$$

where M_m and ρ_m are the molecular weight and the mass density of solid discharged products, respectively. The volume fraction of the discharged solid formation can be determined from the cathode volume balance as shown in Figure 3-2 and Eq. (3-23)

$$\varepsilon_s = 1 - \varepsilon - \varepsilon_c \tag{3-23}$$

where ε_c is the initial volume fraction of solid phase of cathode electrode (active carbon, catalyst and binder).

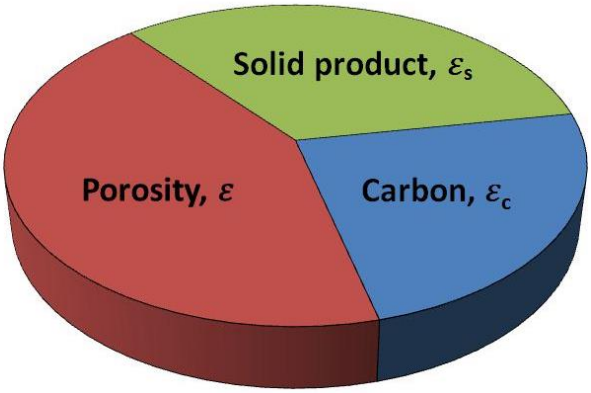

Figure 3-2: Schematic diagram of volume fraction in the porous cathode electrode

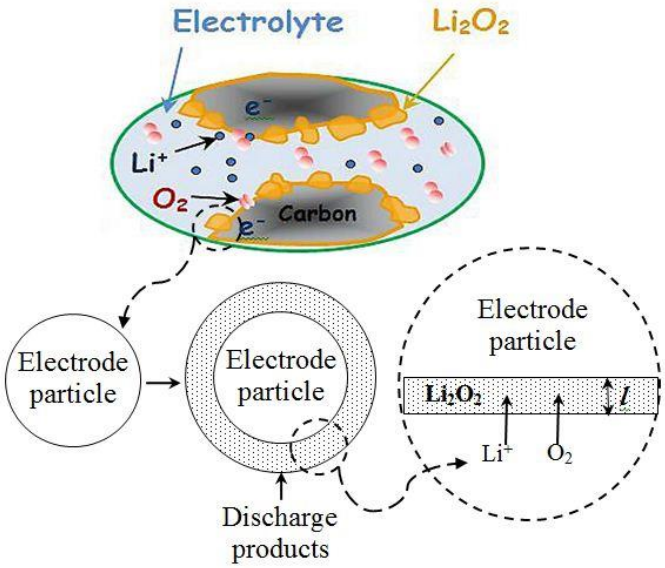

Figure 3-3: Schematic diagram of reactant transport inside the porous electrode and the growth of discharge products on the surface of spherical electrode particle. The inset shows the enlargement of diffusion transport through the barrier of discharge product layer, l.

3.2.7 Transport through discharge products layer

In practice, the electrode surface may not be uniformly covered during the battery discharge and its cover may grow while discharging. However, to simplify the calculation, the build-up of the solid products is assumed to uniformly cover the electrode surface of the previous deposit. During discharge in a short period of time, a thin discharge products layer (Li_2O_2 or Li_2CO_3) could be formed continuously, covering the active carbon surface. This implies that the discharge products form a spherical shell on the surface of spherical active particles, as illustrated in Figure 3-3. Hence, the diffusion of Li^+ and oxygen species from the porous media has the additional transport resistance through these layers. In other words, the transport of active reactants comprises two types of diffusion regimes. The first one is diffusion of Li^+ and oxygen reactants along the porous media and the other is their pass through the discharge product film layer. The latter transport can be derived according to Fick's law as presented in Eq. (3-24), which is proportional to the concentration gradient between the bulk and active surface, corresponding with the electrochemical reaction in which each species is consumed at the active electrode surface (Eq. (3-16)).

To determine the species concentrations at the active electrode surface, Fick's law for diffusion was used as follows:

$$\boldsymbol{N_i} = -D_{i,film}\frac{\partial c_i}{\partial x} \tag{3-24}$$

where $\boldsymbol{N_i}$ is the reactants molar flux across the discharge product layer, $D_{i,film}$ is the effective diffusion coefficient of species i across the film layer. The molar flux of reactant can be obtained from the local charge transfer current density at cathode (j_c) in the following relationship:

$$\boldsymbol{N_i} = \frac{s_i}{nF}j_c \tag{3-25}$$

Combining Eq. (3-24) and Eq. (3-25) together with the assumption that the film layer is very thin, the molar concentration of species i at the surface of electrode can be obtained as:

$$-\frac{s_i}{nF}j_c = \frac{D_{i,film}(c_i - c_{i,s})}{l} \tag{3-26}$$

$$l = \left(\frac{\varepsilon_s + \varepsilon_c}{\varepsilon_c}\right)^{1/3} r_s - r_s \tag{3-27}$$

where l is the thickness of the film calculated from the volume fraction of the solid discharge products by assuming the spherical electrode particles and uniform covering of solid products as shown in Figure 3-3 and Eq. (3-27), and r_s refers to the particle radius in the electrode.

3.2.8 Charging process

The rate expression for a Li-air cathode presented in the previous section includes two rate constants, k_a for anodic current and k_c for cathodic current. During discharge, the second term on the right hand side of Eq. (3-17) is predominant due to the negative overpotential (η_m). However, it is other way around during the charging process due to the positive overpotential. The model assumes one-step charging reaction to form Li^+ and oxygen, and depends on the Li_2O_2 concentration in organic electrolyte as in the following reaction:

$$Li_2O_2 \longrightarrow 2Li^+ + O_2 + 2e^- \tag{3-28}$$

It is known that the Li_2O_2 is insoluble in most organic solvents and deposits on the active surface of carbon. However, there are limited concentrations (saturated concentration) that Li_2O_2 can dissolve into the non-aqueous electrolyte. Tasaki et al. (2009) reported the solubility of various lithium salts, such as lithium carbonate (Li_2CO_3), lithium fluoride (LiF), lithium hydroxide (LiOH) and Li_2O, in organic solvents and found that Li_2O is the lowest solubility (less than 9×10^{-5} mol dm^{-3}) in carbonate-based solvent [10].

For battery on charge, the provided solid Li_2O_2 volume fraction ($\varepsilon_{Li_2O_2}$) has been produced. There will be a finite Li_2O_2 concentration ($c_{Li_2O_2}$) dissolved in solution (saturation concentration), and the rate of oxidation reaction (Eq. (3-28)) would be constant and will only decrease when the solid is consumed or $c_{Li_2O_2}$ goes below the solubility limit. Therefore, the model assumption applied on charge is that the dissolution rate (r_{diss}) of solid peroxide is quick compared to the electrochemical reaction and can be written in Eq. (3-29). The dissolution rate equation is included for $c_{Li_2O_2}$ species balance in Eq. (3-2) during battery on charge and the driving force term for this reaction is when the $c_{Li_2O_2}$ decreases below its solubility in the

electrolyte (c_{max}).

$$r_{diss} = k_d \varepsilon_{Li_2O_2}(c_{max} - c_{Li_2O_2}) \quad (3\text{-}29)$$

where k_d is the dissolution rate constant for Li_2O_2 during charge which assumed very fast ($k_d = 4$ s^{-1}), and c_{max} is the solubility limit of Li_2O_2 dissolved in organic electrolyte ($c_{max} = 9\times10^{-5}$ mol dm^{-3}). The dissolution rate in Eq. (3-29) is coupled with the electrochemical oxidation reaction (Eq. (3-17)) during charging battery.

3.3 Constitutive relations and model parameters

To solve the governing equations listed and described in Section 3.2, all of the parameters for reactants and materials and physical properties were carefully selected from the published literature available so that they could be applied in the model. These input parameters could strongly influence the results of battery behaviour, therefore it was important to estimate and/or select them rigorously. In this section, a detailed description of how these parameters and properties were obtained is presented. The other parameters, which were not described in this section, are summarised in Table 3-4 of Section 3.4.

3.3.1 Cell design geometry

The thickness of each region in the model of the Li-air battery was set by following the experimental cell construction. The separator and porous cathode electrode are completely flooded with non-aqueous electrolyte so that there is no gas phase in the battery model. The model also neglects the carbon particle size distribution in the positive electrode, i.e. only one single size of carbon particle is considered in the model. This particle size is used to determine the specific surface area presented in Section 3.3.4. The model also assumes that all the carbon particles are well connected to the current collector (nickel or copper mesh), then the contact resistances are zero.

When the lithium metal anode of Li-air battery is in contact with the organic electrolyte or solvent, it reacts instantly to form a thin Li-ion conductive film on its surface [10, 11]. As the reaction between lithium anode and electrolyte continues, a multilayer deposition of lithium salts is created. This passivation layer is known as an anode protective layer (APL) or solid electrolyte interface (SEI) and is shown in Figure 3-4. The composition of SEI depends on the electrolyte and the type of active material on

which the SEI is formed [12]. The SEI barrier inhibits the reaction between the lithium anode and organic electrolyte, and also prevents the corrosion of lithium metal from the moisture [13]. Initially, SEI formation protects the anode electrode, but, as the battery repeats charge/discharge cycles, it affects battery performance such as the self-discharge, the safety problem due to lithium dendrite formation, and the irreversible capacity [10, 13, 14]. However, these SEI effects are not considered in this Li-air model. The SEI thickness has been reported at more than 5 nm [12] and its thickness continues to grow over time during the battery's cycles [15, 16]. The SEI in the lithium battery containing $LiPF_6$ in carbonate-based solvent has been identified by transmission electron microscopy (TEM) and was reported as 50 nm thick [17]. This value was applied as SEI thickness in our Li-air model.

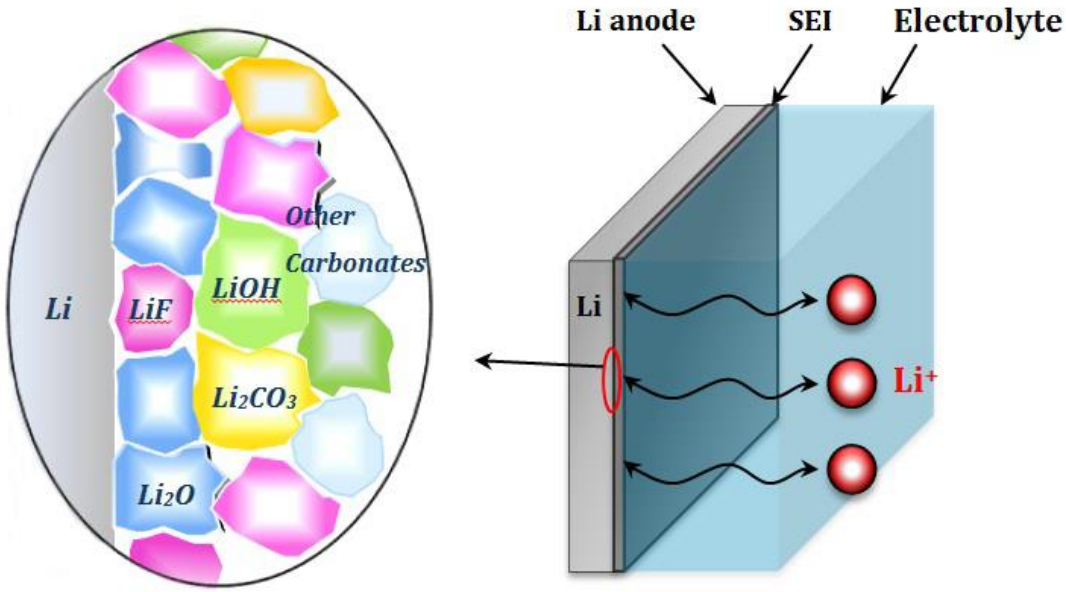

Figure 3-4: Schematic drawing of the solid electrolyte interface (SEI) on the lithium metal anode. SEI formed by reduction of the organic electrolyte.

Glass-fibre filter paper GF/C or Celgard 5500 membrane is normally used as a separator between the anode and cathode compartment in a Li-air battery [18-20]. The separators have a wide range of thickness (15 – 110 μm) depending on the material types and manufacturers [21]. The separator of 50 μm thickness was applied in the model.

For the cathode thickness, this region is considered the crucial part because many reactions and products perform in this area to obtain the high battery performance.

Similar to the separator, many research groups reported different cathode thicknesses depending on their electrode preparation. Zhang et al. (2010) produced the porous cathode with the thickness of carbon film at around 700-800 μm [18]. Read (2002) prepared the air cathode from Super P carbon black and the finished electrode had a thickness of 800 μm [22]. Hence, the average cathode thickness of 750 μm was applied in our Li-air model. It is worth noting that the thickness of the APL and the separator are much smaller than the thickness of cathode. Hence the exact values in these regions insignificantly affect the results of the model simulation in term of battery behaviour and performance.

3.3.2 The transport properties of lithium salt in non-aqueous electrolyte

The transport properties of lithium salt in electrolyte solution, such as diffusion coefficient (D_{Li}), transference number (t_+), activity coefficient ($f_\pm$), and conductivity (κ) depend on both the dissolved lithium salt concentration in non-aqueous electrolyte and the various type of organic solvent. In practice, lithium hexafluorophosphate ($LiPF_6$) is normally used as electrolyte of choice for a Li-air battery because it has been widely adopted in Li-ion batteries in previous decades [23]. Hence, the model assumed that the $LiPF_6$ dissolved in acetonitrile solvent was used as the electrolyte solution in a Li-air battery and the transport properties of $LiPF_6$ had little change in different solvents. The acetonitrile solvent was chosen due to the formation of Li_2O_2 when using this solvent [5]. However, due to the unavailable information of some transport properties for acetonitrile solvent, the other transport properties of the other solvents were applied to the model instead. In summary, the diffusion coefficient of $LiPF_6$ in acetonitrile was applied in the model, whereas the other transport properties of electrolyte, such as t_+, $f_\pm$ and κ , were used from the mixture solvent of ethylene carbonate and ethyl methyl carbonate (EC:EMC) as reported below.

The other solvents, especially carbonate-based electrolytes, are not stable and decompose to form the Li_2CO_3 by-product [24-26]. The model with the electrolyte degradation effect is presented in Chapter 5.

Diffusion coefficient:

The measurement of diffusion coefficient of $LiPF_6$ in various solvents for lithium batteries was reported by Stewart and Newman [27]. The diffusion coefficient of $LiPF_6$

solutions in acetonitrile (ACN) and in a 1:1 mixture by weight of ethylene carbonate and diethyl carbonate (EC:DEC) were measured at room temperature. It has been shown that the diffusion coefficient decreases with electrolyte concentration as a result of an increase in the viscosity of concentrated electrolyte [27]. The relationship between diffusion coefficient and concentration can be determined according to the following equations:

$LiPF_6$ in acetonitrile $$D_{Li} = 3.018 \times 10^{-5} \exp(-0.357 c_{LiPF_6}) \quad (3\text{-}30)$$

$LiPF_6$ in 1:1 (EC:DEC) $$D_{Li} = 2.582 \times 10^{-5} \exp(-2.856 c_{LiPF_6}) \quad (3\text{-}31)$$

where D_{Li} is in $cm^2\ s^{-1}$ and c_{Li} is the concentration in mol dm^{-3}. Figure 3-5 shows the variation of diffusion coefficient with concentration for solution of $LiPF_6$ in ACN and in a 1:1 mixture by weight of EC:DEC. It can be seen that at 1 molar concentration the diffusion coefficient of $LiPF_6$ dissolved in ACN is higher about one order of magnitude than the diffusion coefficient in EC:DEC.

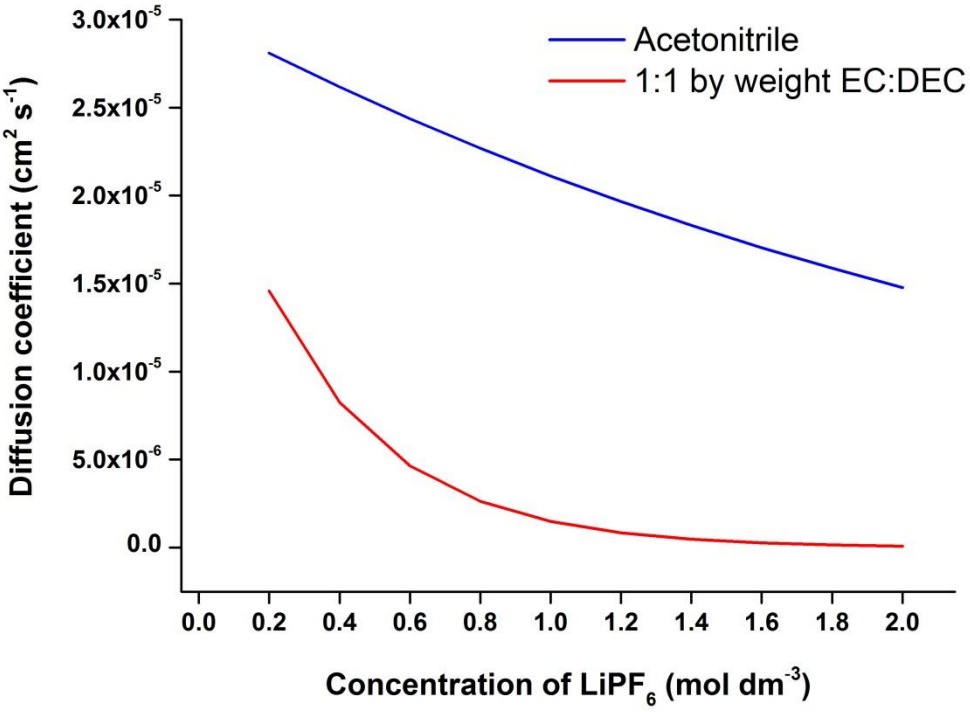

Figure 3-5: Diffusion coefficient as a function of the $LiPF_6$ concentration dissolved in ACN and in a 1:1 ratio mixture by weight of EC:DEC at room temperature, Eq. (3-30) and Eq. (3-31) respectively. The diffusion coefficient decreases with an increase in $LiPF_6$ concentration [27].

Transference number:

Another electrolyte parameter used to describe the charge transport in the battery model is transference number (or transport number). This parameter describes the charge transport of the specific ions of electrolyte, i.e. the fractions of current carried by cation and anion [28]. In the $LiPF_6$ solution, t_+ is the transference number for Li^+ and t_- assigns for PF_6^-. An analogous expression is clearly described as:

$$t_+ + t_- = 1 \tag{3-32}$$

For and electrolyte containing many ions, i

$$\sum_i t_i = 1 \tag{3-33}$$

Generally, liquid electrolytes show both cation and anion transference number depending on how many ions can carry the charge, whereas solid electrolytes have one mobile ion (cation t_+ = 1 or anion t_- = 1). In lithium batteries, electrolytes with low lithium ion transference numbers and salt diffusion coefficients result in large concentration polarisations during the operation of the battery. This leads to deterioration in battery performance and cycling stability [29].

The lithium ion (Li^+) transference number for $LiPF_6$ in a 3:7 mixture by weight of ethylene carbonate and ethyl methyl carbonate (EC:EMC) was reported for concentrations between 0.2 and 2.0 mol dm^{-3} at room temperature by Nyman et al. (2008) as shown in the following relationship [29]:

$$t_+ = 0.4492 - 0.4717c_{LiPF_6} + 0.4106c_{LiPF_6}^2 - 0.1287c_{LiPF_6}^3 \tag{3-34}$$

The Li^+ transference number as a function of the $LiPF_6$ concentration in EC:EMC solvents is presented in Figure 3-6. This expression for transference number in Eq. (3-34) was applied in the model to describe the Li^+ transport, which was changing during the battery operation.

Activity coefficient:

The activity coefficient ($f_\pm$) is one of the thermodynamic properties that describe the transport phenomena in an electrolyte. Nyman et al. (2008) reported the transport properties and thermodynamic properties for $LiPF_6$ in 3:7 (EC:EMC) by using experiments which combined a mathematical description [29]. The polynomial equation

of the concentration-dependent activity coefficient for $LIPF_6$ was fitted to the experimental results and presented in the equation below [29]:

$$\left(1+\frac{\partial ln f_{\pm}}{\partial ln c_{LiPF_6}}\right)=\frac{0.28687c_{LiPF_6}^2-0.74678c_{LiPF_6}+0.44103}{0.1287c_{LiPF_6}^3-0.4106c_{LiPF_6}^2+0.4717c_{LiPF_6}+0.5508} \quad (3\text{-}35)$$

The activity coefficient as a function of the $LiPF_6$ concentration in 3:7 (EC:EMC) solvent is plotted in Figure 3-7.

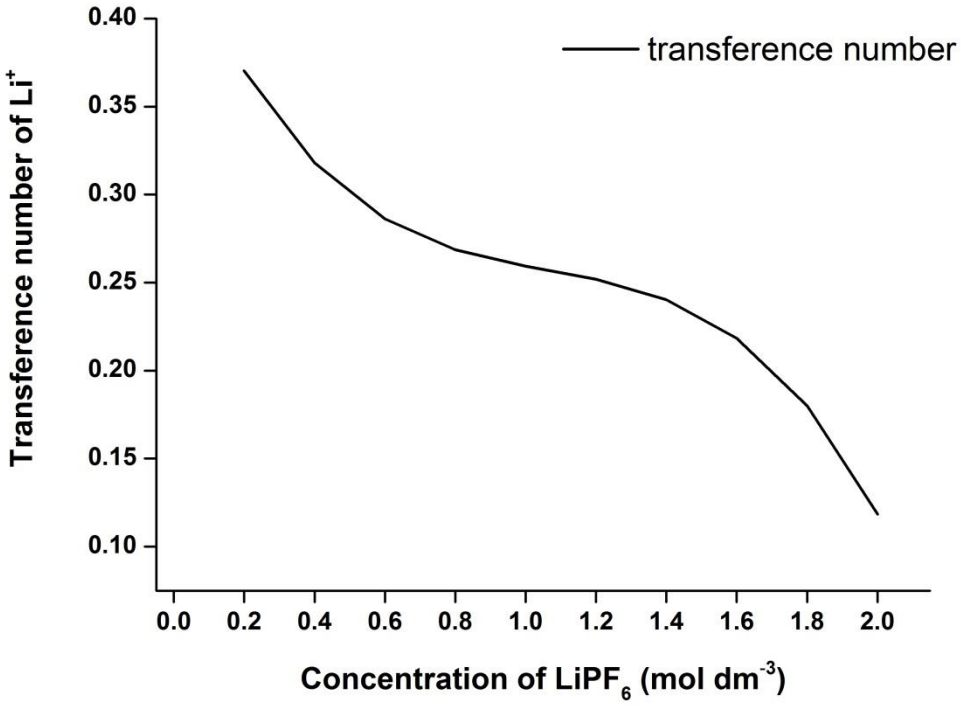

Figure 3-6: The lithium ion transference number as a function of the $LiPF_6$ concentration dissolved in a 3:7 ratio mixture by weight of EC:DEC at room temperature, Eq.(3-34) [29].

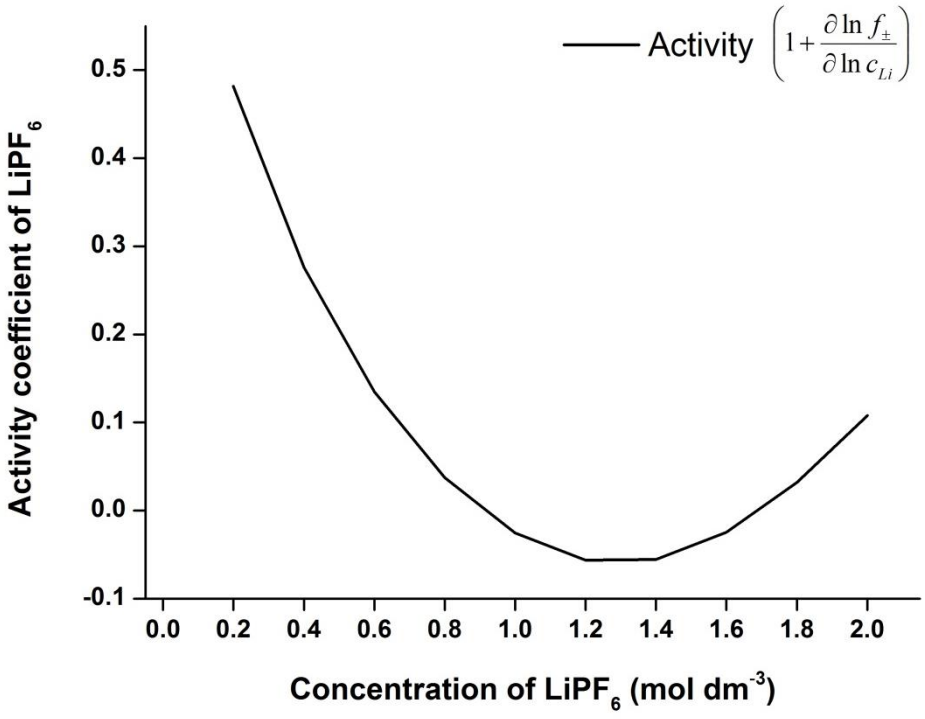

Figure 3-7: The activity coefficient as a function of the $LiPF_6$ concentration dissolved in a 3:7 ratio mixture by weight of EC:DEC at room temperature, Eq.(3-35) [29].

Conductivity:

Electrolyte conductivity (κ) is a measure of the ability of an electrolyte solution to conduct an electric current. The higher its conductivity, the more ions there are in the electrolyte solution. In the porous cathode electrode, the $LiPF_6$ solution in non-aqueous solvent is responsible for the movement of ions in the solution. The conductivity of $LIPF_6$ electrolyte in a 3:7 ratio mixture by weight of EC:DEC at various concentrations was reported in the following relationship [29]:

$$\kappa = A_1 c_{LiPF_6}^3 + A_2 c_{LiPF_6}^{1.5} + A_3 c_{LiPF_6} \tag{3-36}$$

where A_1, A_2 and A_3 are the coefficient values which are summarised in Table 3-1. The conductivity as a function of the $LiPF_6$ concentration in 3:7 (EC:EMC) solvent is plotted in Figure 3-8. As can be seen from the graph, the maximum conductivity is obtained at 1 molar of $LiPF_6$. Hence, the initial electrolyte concentration applied in the Li-air model was operated based on this concentration. At the low concentration regions, the conductivity increases with the $LiPF_6$ concentration until it reaches the highest conductivity at 1 molar because of the increasing ions which become dissociated from the electrolyte. However, at high concentration regions, the electrolyte viscosity is increasing as well as the $LiPF_6$ in the solution leading to decreasing in its

conductivity as described previously by [30].

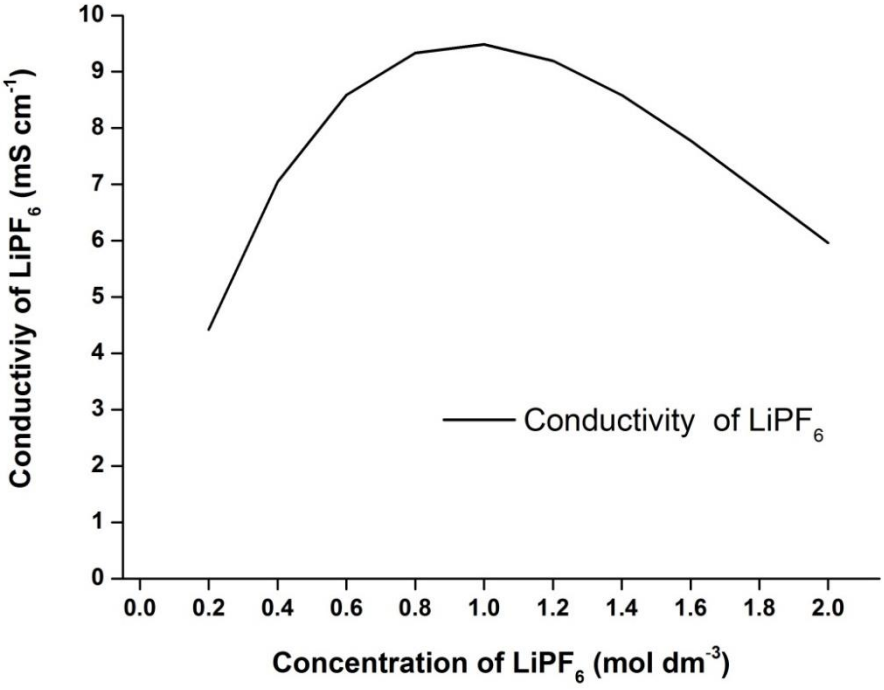

Figure 3-8: The conductivity as a function of the $LiPF_6$ concentration dissolved in a 3:7 ratio mixture by weight of EC:DEC measured at room temperature, Eq. (3-36) [29].

Table 3-1: coefficient values for the $LiPF_6$ conductivity in Eq. (3-36)

A_1 (10^{-2} S dm^8 mol^{-3})	A_2 (10^{-2} S $dm^{3.5}$ mol^{-2})	A_1 (10^{-2} S dm^2 mol^{-1})
1.297±0.059	-25.1±0.44	33.29±0.39

Density:

The density of the electrolyte solutions ($LiPF_6$ in various solvents) have been reported by the manufacturer [31] within the range of 1.20-1.22 g cm^{-3} at 25ºC as summarised in Table 3-2. The electrolyte density of 1.20 g cm^{-3} was used in the model for all simulations.

Table 3-2: Density and conductivity of $LiPF_6$ electrolyte in various solvents

Solvents mixture by weight	Density (g cm^{-3}) at 25ºC	Conductivity (mS cm^{-1})
EC:DEC (1:1)	1.21	7.50
EC:EMC (1:1)	1.20	9.50
EC:DMC:EMC (1:1:1)	1.22	11.0
EC:DEC:EMC (1:1:1)	1.22	10.5

3.3.3 Porosity of porous carbon electrode

In the case of porous cathode electrodes, the total surface area of a carbon material can be determined by the sum of the surface areas of all pore sizes, containing micro pores to macro pores. For an electrode with the same mass, the surface area of the material is inversely related to the size of the pores, i.e. material with the high distribution of small pores has a greater surface area than material with a high distribution of large pores. In practice, the carbon powders (primary particles) will combine or aggregate together during the cathode preparation due to the addition of binding material (PTFE or PVDF) or the mechanical pressure to form the aggregated particles or secondary particles [32]. Thus, there are two types of pores created during the cathode formation process. The first type of pore is formed between the primary carbon particles inside the aggregated particles and the second type of pore is the space between the aggregated particles as shown in Figure 3-9.

A detailed study of the correlation between the average pore diameter of carbon cathode and discharge capacity of Li-air battery by Tran et al. (2010) reported that the discharge capacity increases linearly with the increase of average pore diameter [32]. They also concluded that the discharged products are preferentially formed in macro-pores and meso-pores, while the micro-pores size is inaccessible of the discharge products. Thus, in the model, the porosity of the cathode electrode is assumed to be the uniform contribution of average pore sizes, in which the electrochemical reactions can occur. The initial cathode porosity (ε^0) of 0.73 is applied in this model study. This value represents the porosity of pristine electrodes including the PTFE or PVDF binding materials (lower than the porosity of pristine electrode without binder, ~ 0.85) [22, 33]. This porosity is served as the space for electrolyte and the accommodation for discharge products. The specific interfacial area is presented in the next section.

3.3.4 Specific interfacial area

The specific interfacial area (a) is the active surface area of the electrolyte/electrode interface where the charge transfer reaction occurred per unit volume of the total electrode. This parameter is an important piece in the battery modelling especially in the battery performance, and provides the information regarding the microscopic geometry of electrode interface. To determine the specific interfacial area, it should provide the average interfacial area of the electrode without going to the actual

geometric detail of the pores. The specific interfacial area in the Li-air battery varies in relation to changes in the electrode morphology and dynamic mechanism due to the solid particles precipitation inside the porous electrode.

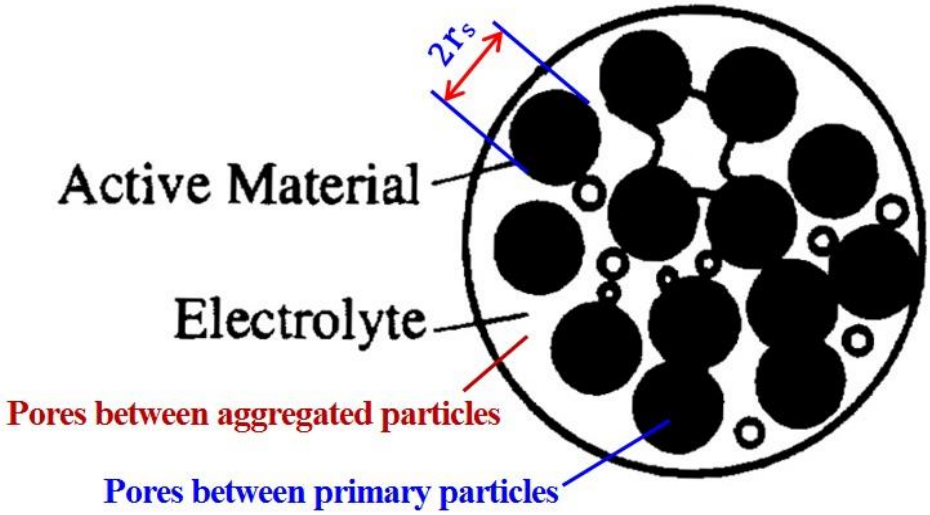

Figure 3-9: Schematic illustration of the spherical particles of radius r_s in the porous cathode.

Assuming that the spherical particles of radius r_s inside the electrode as shown in Figure 3-9, the specific area can be calculated by [8]:

$$a_0 = \frac{3\varepsilon_c}{r_s} = \frac{3(1-\varepsilon^0)}{r_s} \tag{3-37}$$

where ε^0 is the initial porosity of the electrode, which is $\varepsilon^0 = 0.73$ in our model. A particle of radius r_s can be estimated by the scanning electron microscope (SEM) image of the porous carbon morphology from our research group as shown in Figure 3-10. It can be seen from the figure that the diameter of spherical particle is around 0.5 μm, ($r_s = 0.25$ μm). Input these values into Eq. (3-37) to determine the specific interfacial area of the cathode electrode for the model is 3.24×10^6 m^2 m^{-3}.

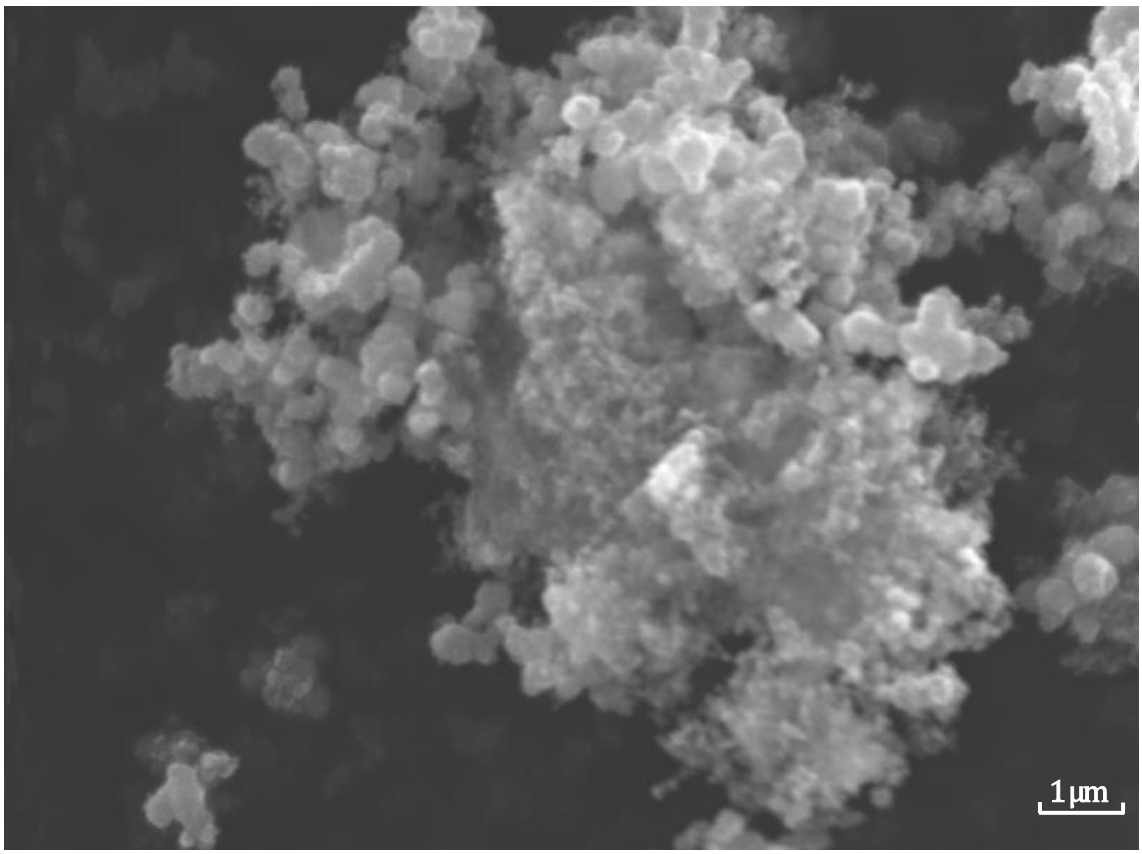

Figure 3-10: SEM image of the pristine porous carbon electrode.

3.3.5 Kinetic parameters

In Section 3.2.3, the rate expressions for the Li_2O_2 formation were introduced without proper explanation as to why this kinetic model was based on the two reaction rate constants (Eq. (3-17)) instead of the general Butler-Volmer equation. Let us consider the simplest possible redox electrode reaction, where O is the oxidised species and R is the reduced species:

$$O + ne^- \rightleftharpoons R \tag{3-38}$$

If only one reaction occurs at the electrode, then the reactions, which depend on the surface overpotential and reactant concentrations, in cathodic and anodic direction can be expressed as:

$$r = \frac{i}{nF} = k_a c_R exp\left[\frac{(1-\beta)nF}{RT}V\right] - k_c c_O exp\left[\frac{-\beta nF}{RT}V\right] \tag{3-39}$$

where k_a and k_c are rate constants for the anodic and cathodic reaction, respectively, and c_R and c_O are the concentration of the anodic and cathodic reactants, respectively.

At the equilibrium potential (U), the net rate of reaction is zero and then the rate of the

forward reaction equals to the rate of the backward reaction. Then Eq. (3-39) becomes:

$$k_a c_R exp\left[\frac{(1-\beta)nF}{RT}U\right] = k_c c_O exp\left[\frac{-\beta nF}{RT}U\right] \tag{3-40}$$

Rearrangement of the Eq. (3-40) yields the equilibrium potential (U) as:

$$U = \frac{RT}{nF}\ln\left(\frac{k_c c_O}{k_a c_R}\right) \tag{3-41}$$

The surface overpotential η is defined as the difference between the actual potential and the equilibrium potential as:

$$\eta = V - U \tag{3-42}$$

Substituting the Eq. (3-41) and Eq. (3-42) into Eq. (3-40) yields:

$$\begin{aligned} r = \frac{i}{nF} = k_a c_R exp\left[\frac{(1-\beta)nF}{RT}\eta + (1-\beta)\ln\left(\frac{k_c c_O}{k_a c_R}\right)\right] \\ - k_c c_O exp\left[\frac{-\beta nF}{RT}\eta - \beta\ln\left(\frac{k_c c_O}{k_a c_R}\right)\right] \end{aligned} \tag{3-43}$$

Rearrange the Eq. (3-43) into the general Butler Volmer equation given by:

$$i = i_0\left\{exp\left[\frac{(1-\beta)nF}{RT}\eta_s\right] - exp\left[\frac{-\beta nF}{RT}\eta_s\right]\right\} \tag{3-44}$$

where the exchange current density (i_0) is defined by:

$$i_0 = nF(k_a)^{\beta}(k_c)^{1-\beta}(c_O)^{1-\beta}(c_R)^{\beta} \tag{3-45}$$

This equation is known as the Butler-Volmer equation, which is normally used as the kinetic equation for battery and fuel cell modelling.

However, in practice, the reaction of Li_2O_2 formation ($2Li^+ + O_2 + 2e^- \rightleftharpoons Li_2O_2$) is not a completely reversible reaction, which consists of many elementary reactions [5, 6, 34]. Hence, the assumption of reversible reaction (where the rate of the forward reaction equals the rate of the backward reaction) in Eq. (3-40) may not be applicable to using the general Butler-Volmer equation in the Li-air battery model.

Therefore, the kinetic model was based on the two reaction rate constants as described in Eq. (3-39) and can be expressed in the Li_2O_2 formation reaction as presented in Eq.

(3-17). A problem with this kinetic expression is that it does not consider the standard potential for the reaction in terms of the Nernst behaviour as shown in Eq. (3-47), i.e. surface overpotential (η) is expressed in terms of the standard potential as present in Eq. (3-42):

$$2Li^+ + O_2 + 2e^- \rightleftharpoons Li_2O_2 \qquad E^0 = 2.96\ V_{Li} \tag{3-46}$$

$$E = E^0 + \frac{RT}{nF} ln \left[\frac{c_{O_2} c_{Li}^2}{c_{Li_2O_2}}\right] \tag{3-47}$$

The Nernst equation describes that the standard potential (E^0) is varied as a function of the concentrations of species, which is involved in electrochemical reaction. As the assumption of reversibility for Eq. (3-46) may not be valid to use the general Butler-Volmer equation, thus the kinetic reaction for Li_2O_2 formation have to consider the two rate constants of anodic (k_a) and cathodic (k_c) as separate values. These values are optimised to fit with the experimental results of the discharge and charge behaviour of Li-air battery. The values of $k_a = 1.11 \times 10^{-15}$ m s^{-1} and $k_c = 3.4 \times 10^{17}$ m^7 s^{-1} mol^{-2} are fitted well with the experiment.

3.3.6 Electrical resistivity across Li_2O_2 film

In Eq. (3-18), the surface overpotential for the cathode kinetic reaction includes the voltage drop from the electrical resistivity across the discharges products Li_2O_2, which is defined as expression ($\Delta\phi_{film} = j_m R_{film} \varepsilon_s$) in Eq. (3-19). To determine the electrical resistivity (R_{film}), Li et al. (2001) measured the interface resistance with a value of less than 50 Ω cm^2 between a lithium metal electrode and a polymer electrolyte and found that the interface resistance depends on the lithium salts formed on the surface [35]. This interface resistance is sometimes called solid electrolyte interface (SEI) which is normally formed on the electrode in lithium-ion batteries during the first few cycles [10]. SEI films consist of many insoluble materials including lithium oxides (LiO_x), lithium carbonate (Li_2CO_3), lithium fluoride (LiF), lithium hydroxide (LIOH), etc [10, 36]. Hence, the solid discharge products (Li_2O_2 and Li_2CO_3), formed on the active surface of the Li-air batteries, are similar in chemical and physical properties to those of SEI layer. Therefore, the model used the electrical resistivity of SEI to define the electrical resistivity of Li_2O_2 (R_{film}). The electrical resistivity of Li_2O_2 from the study of Li et al. (2001) is constant value as 50 Ω cm^2 [35].

However, to develop a model which is close to the practical behaviour of a Li-air battery, the electrical resistivity of Li_2O_2 could be dynamical changed with Li_2O_2 build up during the battery discharging process. Thus, the electrical resistivity of Li_2O_2 is modified so that it is dynamically changed with the Li_2O_2 layer (l) expressed in Eq. (3-48) [37] as follows:

$$R_{film} = l\ exp[c_1(l - c_2)] \tag{3-48}$$

where l is the thickness of the discharged product film as defined in Eq. (3-27), c_1 and c_2 are the film resistivity constant with the value of 4.9×10^7 and 3.6×10^{-7}, respectively.

It is worth noting that the constant value of R_{film}= 50 Ω cm^2 was used only in the Li-air model in Chapter 4, and the dynamic value of R_{film} in Eq. (3-48) was applied thereafter.

3.3.7 Oxygen solubility and diffusion in organic electrolyte

Finding the appropriate electrolyte is currently one of the greatest challenges to achieving high performance in Li-air batteries [38]. It was found that electrolyte formulation has a substantial effect on both cell performance and on the type of deposited product formed during discharging [22, 24, 34, 39]. The electrolyte with high oxygen solubility and diffusivity can provide a superior battery performance with high discharge capacity. Hence, the transport of the oxygen through the porous electrode, in which the electrolyte is filled all the void space, is an important set of parameters applied in the Li-air battery model.

Read et al. (2003) studies the oxygen transport properties of several organic electrolytes by using the measurements of oxygen solubility and electrolyte viscosity [39]. The oxygen diffusion coefficients were also calculated from the Stokes-Einstein relationship. The oxygen solubility was measured in term of the Bunsen coefficient, which is defined as the volume of gas (oxygen) absorbed by unit volume of solvent. Read et al. (2003) calculated and reported the Bunsen coefficient in unit of "cm^3 O_2/cm^3 liquid" at 1 atm and 25 ºC for $LiPF_6$ salt dissolved in various solvents as presented in Table 3-3 [39].

Table 3-3: Bunsen coefficient of oxygen in various electrolytes

Electrolyte [a]	**Bunsen coefficient (cm^3 O_2/cm^3 liquid)**	**Concentration calculated from ideal gas law (mol dm^{-3})**
1 M $LiPF_6$ PC:EC (1:1)	0.0482	0.00197
1 M $LiPF_6$ PC	0.0516	0.00211
1 M $LiPF_6$ PC:DME (1:1)	0.0722	0.00295
1 M $LiPF_6$ PC: DMC (1:1)	0.0729	0.00298
1 M $LiPF_6$ PC:DEC (1:1)	0.0787	0.00322
1 M $LiPF_6$ PC:DME (1:2)	0.0998	0.00408
0.5 M $LiPF_6$ PC:DME (1:2)	0.1218	0.00498

[a] Propylene carbonate (PC), Ethylene carbonate (EC), 1,2-dimethoxyethane (DME), Dimethyl carbonate (DMC), Diethyl carbonate (DEC)

From the Bunsen coefficient, the saturated oxygen concentration which is dissolved in the electrolyte and applied in the model can be calculated from the ideal gas law expressed as:

$$PV = nRT \tag{3-49}$$

where P is pressure from the experiment (1 atm), V is the volume of oxygen dissolved in electrolyte, n is the number of moles, R is the universal gas constant equal to 82.06 cm^3 atm K^{-1} mol^{-1}, and T is the temperature form the experiment (298.15 K). As the Bunsen coefficient is reported in terms of units of cm^3 O_2/cm^3 electrolyte, the saturated oxygen concentration is calculated from the ideal gas law and presented in Table 3-3. It can be seen that the type of electrolyte influences on the oxygen concentration leads to different battery performances.

Because the oxygen concentrations vary depending on the electrolyte applied to the Li-air battery, the model was adopted according to the moderate concentration of oxygen (0.00322 mol dm^{-3} from 1 M $LiPF_6$ PC:DEC) to represent the dissolved oxygen concentration. Moreover, this electrolyte was also used to represent the transport properties of lithium salt described in Section 3.3.2.

Knowing the electrolyte viscosity, the diffusion coefficient of oxygen (D_{O_2}) in organic electrolyte was determined by the Stoke-Einstein relation as shown in the following

equation [39]:

$$D_{O_2} = \frac{KT}{6\pi\mu a} \tag{3-50}$$

where a is the effective hydrodynamic radius of oxygen (121 pm), K is the Boltzmann constant (1.38×10^{-23} J K^{-1}), and μ is the electrolyte viscosity. The diffusion coefficient of oxygen calculated by Read et al. (2003) using Eq. (3-50) is 7×10^{-6} cm^2 s^{-1} [39], which is lower than the diffusion coefficient of lithium ion.

3.4 Summarised parameters

The parameters described in this chapter are summarised in Table 3-4. The other parameters that were not mentioned before were also included. These basic parameters are applied in the Li-air model used in all chapters unless other values are specified.

3.5 Numerical solution

The solution of the governing equations coupled with the initial condition was obtained through a numerical method which is called the finite element method (FEM). In any system, the derivation of the governing equations to describe the behaviours inside the particular system requires a good understanding of the physical and/or chemical process along with mathematical models. However, it is extremely difficult to obtain an exact solution for these models, which include a set of coupled differential and algebraic equations. This problem can be overcome by using an approximate solution through numerical methods such as FEM. The finite element method is a computational technique that subdivides an object of interest into very small finite-size elements, called finite elements. Each element is assigned a set of characteristic equations (physical and/or chemical properties and boundary conditions), which are then solved simultaneously to predict the object's behaviour following the assigned physical and chemical equations [40, 41].

As the finite element method can divide the domain of an object into a set of simple sub domains or finite elements, then it is not limited solely to use in a domain with complex geometries. The basic steps of the finite element analysis of a problem are [41] as follows:

Table 3-4: Parameters used in the Li-air model (SI unit)

Parameter	Value	Unit	symbol	Ref.
Cell properties				
Thickness of APL	5×10^{-8}	m	L_A	[18]
Thickness of separator	5×10^{-5}	m	L_C	[18]
Thickness of porous positive electrode	7.5×10^{-4}	m	L	[18]
Conductivity of positive electrode	10	S m^{-1}	σ	[42]
Porosity	0.73	-	ε^o	[43]
Specific interfacial area of cathode	3.24×10^{6}	m^2 m^{-3}	a	Calculated
Electrical resistivity across Li_2O_2 film formation	50	Ω m^2	R_{film}	[35]
Electrolyte properties				
Electrolyte concentration	1000	mol m^{-3}	$c_{Li,0}$	[22]
Solubility factor of oxygen	0.34	-	S_{O_2}	[42]
External oxygen concentration in air at 1 atm	9.46	mol m^{-3}	$c_{O_2,ext}$	[42]
Oxygen concentration at x=L ($S_{O_2} * c_{O_2,ext}$)	3.22	mol m^{-3}	$c_{O_2,0}$	[39]
Solubility limit of Li_2O_2 dissolved in electrolyte	0.09	mol m^{-3}	c_{max}	[10]
Li^+ diffusion coefficient [a]	2.11×10^{-9}	m^2 s^{-1}	D_{Li}	[27]
Oxygen diffusion coefficient	7×10^{-10}	m^2 s^{-1}	D_{O_2}	[39]
Conductivity of Li^+ in electrolyte [a]	0.9487	S m^{-1}	κ	[29]
Transference number of Li^+ [a]	0.2594	-	t_+	[29]
$\partial lnf/(\partial lnc_{Li})$ [a]	-1.03	-	-	[29]
Kinetic parameters				
Reaction rate coefficient anodic current	1.11×10^{-15}	m s^{-1}	k_a	Fitted
Reaction rate coefficient cathodic current	3.4×10^{-17}	m^7 s^{-1} mol^{-2}	k_c	Fitted
Dissolution rate coefficient of Li_2O_2	4.0	s^{-1}	k_d	Fitted
Exchange current density for anode	1	A m^{-2}	i_0	Fitted
Symmetry factor	0.5	-	β	[42]
General parameter				
Mass density of Lithium peroxide (Li_2O_2)	2140	kg m^{-3}	$\rho_{Li_2O_2}$	[44]
Mass density of electrolyte solution ($LiPF_6$)	1200	kg m^{-3}	ρ_{LiPF_6}	[44]
Mass density of carbon	2260	kg m^{-3}	ρ_c	[44]
Particle radius in the electrode	25×10^{-8}	m	r_s	[19]
Operating temperature	298.15	K	T	

[a] vary with concentration

i. Discretization of the given domain into a collection of finite elements.
ii. Derivation of element equations for all elements in the mesh.
iii. Assembly of element equations to obtain the equations of the whole problem.
iv. Imposition of the boundary conditions of the problem.
v. Solution of the assemble equations.
vi. Post-processing of the results.

The first three steps are the major features of the finite element method and they are closely related. The discretization of the domain represents the complex geometries which are subdivided into geometric simple domains called elements. The shape of each element depends on the complexity and dimension of the geometry. For 1D the domain is simply divided into smaller intervals (used in this work); for 2D the domain can be divided into triangular or quadrilateral mesh elements; finally, in 3D the domain separation is done by tetrahedral, hexahedral, or prism mesh elements. The approximation functions used over each mesh element are in general algebraic polynomials which are derived using interpolation theory. These functions are dependent on several aspects, such as, geometry, number and location of nodes (which are selected points used to express the polynomial approximation), and quantities to be interpolated. The assembly of elements is based on the idea that the solution is continuous at the inter-element boundaries. The final system of algebraic equations is a numerical analogy of the original mathematical model [41, 45-47].

3.6 Building and solving a Li-air model using COMSOL

In this work, the conservation equations and the boundary conditions described above were discretized using a finite element method and solved in a one-dimensional battery system using a commercial software package COMSOL multiphysics (version 4.3) [40]. The COMSOL software is designed to solve a set of coupled differential and algebraic equations. The battery simulation model was performed on a 32 bit Windows platform with 4 GB RAM, and Intel Core 2 Duo 2.93 GHz processor. The different transport equations and the electrochemical reactions were solved as time dependent until the cell voltage reached the stop condition during discharge and charge. The general steps to build the model are explained below:

i. Build the Li-air battery geometry. Due to the one-dimension model, the

geometry of a Li-air battery was created as the straight line containing 3 different domains following the thickness as demonstrated in Figure 3-1 (APL, separator and porous cathode). Each domain can be assigned with governing equations which represent the physical behaviour in that domain.

ii. Add the COMSOL module. The COMSOL software not only capable to solve a set of coupled differential and algebraic equations, but also has the optional modules for specific application [40]. These modules provide the built-in physic interfaces in the particular discipline. In this work, "Batteries & Fuel Cell Module", had been applied to the Li-air model. This module provides customised physics interfaces for modelling of batteries and fuel cells. These physics interface have tools for building detailed models of the configuration of the electrodes and electrolyte in electrochemical cells. They include descriptions of the electrochemical reactions and the transport properties that influence the performance of batteries, i.e. transportation for concentrated binary electrolyte, porous electrodes and user-defined equations (modified Butler-Volmer equation, dynamic porosity change, specific interfacial area and electrical resistivity across Li_2O_2 interface).

iii. Specify the governing equations. The model equations which describe the physical phenomena on the domains were assigned for each domain using the set of governing equation in Section 3.2. Note that this governing equations were described the physics in the form of porous cathode domain. The other domains also use the same governing equations without the porosity variable (ε).

iv. Define the initial value. To solve the governing equations, the initial values for all variables, such as electrolyte concentrations, porosity, specific surface area and cell potential, must be specified to model. The initial values were chosen base on the experiments and the micrograph from the Scanning Electron Microscopy (SEM). The initial concentration of 1 molar was used due to the highest electrolyte conductivity as described in Section 3.3.2. The initial porosity of 0.73 was chosen from the literature which measures the pore volume by BET technique as shown in Section 3.3.3. The specific surface area was calculated from the micrograph of electrode prepared by our group (Section 3.3.4). The initial cell potential was chosen as 2.96 V vs Li/Li^+ due to the standard cell potential for Li_2O_2 formation.

v. Build the mesh for 1D model. The meshing technique is one of the processes to solve the problem in the finite element method described in Section 3.5. The

mesh feature enables the discretisation of the geometry model into smaller unites of simple shapes (or mesh elements). This mesh generation divides a complex problem into small elements to solve accurately solution. In this work, the geometry for a Li-air model was divided in 5027 mesh elements (all in intervals). The software can create a mesh for the simulation domain. There are different levels of size that the user can select to mesh the domain (Extremely fine, Extra Fine, Finer, Fine, Normal, Coarse, Coarser, Extra coarse, Extremely coarse). These mesh sizes do not affect much on the results obtained from simply 1D model. However, they significantly impact on the simulation time used to converge to solution, i.e. the smaller mesh size on the domain, the more usage time to find the solution. In a Li-air model, the "Extra fine" was used to create a mesh.

vi. Create the study for solving the model. There are many study type provided in COMSOL software to be selected depending on the behaviour of the problem. Two common studies are "stationary study", which is used for a stationary or steady-state situation where all variables are not depend on time, and "time dependent study", which is used for transient simulation using a time dependent solver for computing the solution over time [40]. In a Li-air model, the mechanism and structure always changed with time during discharge and charge so that the time dependent study was chosen. In COMSOL, the solver is a numerical technique for finding approximate solution to boundary value problems for differential equations. For the time dependent problem, the Newton's method (also known as the Newton-Raphson method) was selected to solve the model equation [40]. The maximum number of iterations was set to 25. The solution was considered as a converged solution when the difference between the two results was less than 10^{-4} (relative tolerance) for all variables. The number of 25 was specified because the simulation can find a converged solution. If the number is lower than 25, the solution are not meet the criteria (relative tolerance less than 10-4) and cannot converge to solution.

vii. Specify the stop conditions. These conditions stop the solver when a specified condition is fulfilled. For a Li-air battery, the battery potentials were specified to stop the solver at 2.2 V and 4.2 V for discharge and charge process, respectively. These voltages are the stop voltage for discharge (2.2 V) and charge (4.2 V) process in galvanostatic operation of Li-air battery. If the Li-air battery is discharged lower than 2.2 V, the irreversible products such as Li_2O and Li_2CO_3

occur instead of desired Li_2O_2 which is reversible during charge. Likewise, if the battery is charged higher than 4.2 V, the carbon is corroded to form CO_2 and finally product Li_2CO_3.

viii. Create the results. All data from the simulated models were obtained by the post-processing step.

These are the main steps used to build and to solve the Li-air battery model. The simulation time to obtain the solution was around 20-35 minutes depending on the complication of the models.

3.7 Conclusion

A micro-macro homogeneous mathematical model was developed for a rechargeable Li-air battery using a concentrated binary electrolyte theory. All phenomena in the Li-air battery were described using differential and algebraic equations, which were based on the physical and chemical behaviour of the species and battery processes. All the transport processes were taken into account when considering the main feature which occurred in the Li-air battery.

The main features of this model were the considerations of the time and space dependence of the battery system, the microscopic behaviours of the local mass transport through the discharge products (Li_2O_2) layers and the potential loss from the resistivity of lithium oxides film, and the dynamic change of the active surface area and the porosity with the Li_2O_2 growth. It is also important to note that the majority of the system parameters and species properties were treated as dependent variables. In order to solve these equations, a commercial software package was used to solve and analyse the battery system through the finite element method.

In summary, the developed model, which included the important details of battery feature, can be used to describe the behaviour of Li-air batteries as well as to optimise the performance and structure of these battery electrodes.

3.8 References

1. Newman, J. and K.E. Thomas-Alyea, *Electrochemical Systems*. 3 ed2004, New York: John Wiley & Sons.

2. Newman, J. and W. Tiedemann, *Porous-Electrode Theory with Battery Applications.* AIChE Journal, 1975. **21**(1): p. 25-41.
3. Schalkwijk, W.A.v. and B. Scrosati, *Advances in Lithium-Ion Batteries*2002, New York: Kluwer Academic/Plenum Publishers.
4. Bruggeman, D.A.G., *The calculation of various physical constants of heterogeneous substances.* Ann. Phys. (Leipzig), 1935. **24**: p. 636-679.
5. Peng, Z., et al., *Oxygen reactions in a non-aqueous Li^+ electrolyte.* Angewandte Chemie - International Edition, 2011. **50**(28): p. 6351-6355.
6. Laoire, C.O., S. Mukerjee, K.M. Abraham, E.J. Plichta and M.A. Hendrickson, *Elucidating the mechanism of oxygen reduction for lithium-air battery applications.* Journal of Physical Chemistry C, 2009. **113**(46): p. 20127-20134.
7. LaFollette, R.M. and D.N. Bennion, *Design fundamentals of high power density, pulsed discharge, lead-acid batteries. II. Modeling.* Journal of the Electrochemical Society, 1990. **137**(12): p. 3701-3707.
8. Wang, C.Y., W.B. Gu and B.Y. Liaw, *Micro-macroscopic coupled modeling of batteries and fuel cells: I. Model development.* Journal of the Electrochemical Society, 1998. **145**(10): p. 3407-3417.
9. Ren, X., S.S. Zhang, D.T. Tran and J. Read, *Oxygen reduction reaction catalyst on lithium/air battery discharge performance.* Journal of Materials Chemistry, 2011. **21**(27): p. 10118-10125.
10. Tasaki, K., A. Goldberg, J.J. Lian, M. Walker, A. Timmons and S.J. Harris, *Solubility of lithium salts formed on the lithium-ion battery negative electrode surface in organic solvents.* Journal of the Electrochemical Society, 2009. **156**(12): p. A1019-A1027.
11. Girishkumar, G., B. McCloskey, A.C. Luntz, S. Swanson and W. Wilcke, *Lithium-air battery: Promise and challenges.* Journal of Physical Chemistry Letters, 2010. **1**(14): p. 2193-2203.
12. Chagnes, A. and J. Swiatowska, *Electrolyte and Solid-Electrolyte Interphase Layer in Lithium-Ion Batteries*, in *Lithium Ion Batteries - New Developments*, D.I. Belharouak, Editor 2012, InTech.
13. Aurbach, D., *Review of selected electrode-solution interactions which determine the performance of Li and Li ion batteries.* Journal of Power Sources, 2000. **89**(2): p. 206-218.
14. Pinsona, M.B. and M.Z. Bazant, *Theory of SEI formation in rechargeable batteries: Capacity fade, accelerated aging and lifetime prediction.* Journal of the

Electrochemical Society, 2013. **160**(2): p. A243-A250.

15. Pinson, M.B. and M.Z. Bazant, *Theory of SEI Formation in Rechargeable Batteries: Capacity Fade, Accelerated Aging and Lifetime Prediction.* Journal of the Electrochemical Society, 2013. **160**(2): p. A243-A250.
16. McArthur, M.A., S. Trussler and J.R. Dahn, *In situ investigations of SEI layer growth on electrode materials for lithium-ion batteries using spectroscopic ellipsometry.* Journal of the Electrochemical Society, 2012. **159**(3): p. A198-A207.
17. Nie, M., D. Chalasani, D.P. Abraham, Y. Chen, A. Bose and B.L. Lucht, *Lithium ion battery graphite solid electrolyte interphase revealed by microscopy and spectroscopy.* Journal of Physical Chemistry C, 2013. **117**(3): p. 1257-1267.
18. Zhang, J.G., D. Wang, W. Xu, J. Xiao and R.E. Williford, *Ambient operation of Li/Air batteries.* Journal of Power Sources, 2010. **195**(13): p. 4332-4337.
19. Cheng, H. and K. Scott, *Carbon-supported manganese oxide nanocatalysts for rechargeable lithium-air batteries.* Journal of Power Sources, 2010. **195**(5): p. 1370-1374.
20. Debart, A., J. Bao, G. Armstrong and P.G. Bruce, *An O_2 cathode for rechargeable lithium batteries: The effect of a catalyst.* Journal of Power Sources, 2007. **174**(2): p. 1177-1182.
21. *Celgard® High Performance Battery Separators*. 2009 [cited 14 October 2013]; Available from: http://www.celgard.com/pdf/library/Celgard_Product_Comparison_10002.pdf.
22. Read, J., *Characterization of the lithium/oxygen organic electrolyte battery.* Journal of the Electrochemical Society, 2002. **149**(9): p. A1190-A1195.
23. Shao, Y., F. Ding, J. Xiao, J. Zhang, W. Xu, S. Park, J.G. Zhang, Y. Wang and J. Liu, *Making Li-air batteries rechargeable: Material challenges.* Advanced Functional Materials, 2013. **23**(8): p. 987-1004.
24. Freunberger, S.A., Y. Chen, Z. Peng, J.M. Griffin, L.J. Hardwick, F. Bardé, P. Novák and P.G. Bruce, *Reactions in the rechargeable lithium-O_2 battery with alkyl carbonate electrolytes.* Journal of the American Chemical Society, 2011. **133**(20): p. 8040-8047.
25. Xu, W., et al., *Reaction mechanisms for the limited reversibility of Li-O_2 chemistry in organic carbonate electrolytes.* Journal of Power Sources, 2011. **196**(22): p. 9631-9639.
26. Xu, W., et al., *The stability of organic solvents and carbon electrode in*

nonaqueous Li-O_2 batteries. Journal of Power Sources, 2012. **215**: p. 240-247.

27. Stewart, S.G. and J. Newman, *The Use of UV/vis absorption to measure diffusion coefficients in $LiPF_6$ electrolytic solutions.* Journal of the Electrochemical Society, 2008. **155**(1): p. F13-F16.
28. Bard, A.J. and L.R. Faulkner, *Electrochemical Methods Fundamentals and Applications*. 2 ed2001, New York: John Wiley & Sons.
29. Nyman, A., M. Behm and G. Lindbergh, *Electrochemical characterisation and modelling of the mass transport phenomena in $LiPF_6$-EC-EMC electrolyte.* Electrochimica Acta, 2008. **53**(22): p. 6356-6365.
30. Ding, M.S., K. Xu, S.S. Zhang, K. Amine, G.L. Henriksen and T.R. Jow, *Change of Conductivity with Salt Content, Solvent Composition, and Temperature for Electrolytes of LiPF6 in Ethylene Carbonate-Ethyl Methyl Carbonate.* Journal of The Electrochemical Society, 2001. **148**(10): p. A1196-A1204.
31. Sahapatsombut, U., H. Cheng and K. Scott, *Modelling of operation of a lithium-air battery with ambient air and oxygen-selective membrane.* Journal of Power Sources, 2014. **249**(0): p. 418-430.
32. Tran, C., X.Q. Yang and D. Qu, *Investigation of the gas-diffusion-electrode used as lithium/air cathode in non-aqueous electrolyte and the importance of carbon material porosity.* Journal of Power Sources, 2010. **195**(7): p. 2057-2063.
33. Lu, Y.C., D.G. Kwabi, K.P.C. Yao, J.R. Harding, J. Zhou, L. Zuin and Y. Shao-Horn, *The discharge rate capability of rechargeable Li-O_2 batteries.* Energy and Environmental Science, 2011. **4**(8): p. 2999-3007.
34. Freunberger, S.A., Y. Chen, N.E. Drewett, L.J. Hardwick, F. Bardé and P.G. Bruce, *The Lithium–Oxygen Battery with Ether-Based Electrolytes.* Angewandte Chemie International Edition, 2011. **50**(37): p. 8609-8613.
35. Li, Q., H.Y. Sun, Y. Takeda, N. Imanishi, J. Yang and O. Yamamoto, *Interface properties between a lithium metal electrode and a poly(ethylene oxide) based composite polymer electrolyte.* Journal of Power Sources, 2001. **94**(2): p. 201-205.
36. Zhang, S., M.S. Ding, K. Xu, J. Allen and T.R. Jow, *Understanding solid electrolyte interface film formation on graphite electrodes.* Electrochemical and Solid-State Letters, 2001. **4**(12): p. A206-A208.
37. Albertus, P., G. Girishkumar, B. McCloskey, R.S. Sánchez-Carrera, B. Kozinsky, J. Christensen and A.C. Luntz, *Identifying capacity limitations in the Li/oxygen battery using experiments and modeling.* Journal of the Electrochemical Society, 2011. **158**(3): p. A343-A351.

38. Rahman, M.A., X. Wang and C. Wen, *A review of high energy density lithium-air battery technology.* Journal of Applied Electrochemistry, 2013: p. 1-18.
39. Read, J., K. Mutolo, M. Ervin, W. Behl, J. Wolfenstine, A. Driedger and D. Foster, *Oxygen Transport Properties of Organic Electrolytes and Performance of Lithium/Oxygen Battery.* Journal of the Electrochemical Society, 2003. **150**(10): p. A1351-A1356.
40. COMSOL, *COMSOL Multiphysics User's Guide, version 4.3.* 2012.
41. Reddy, J.N., *An introduction to the finite element method*. 2nd ed. McGraw-Hill Series in Mechanical Engineering. 1993, New York: McGraw-Hill. xix, 684.
42. Andrei, P., J.P. Zheng, M. Hendrickson and E.J. Plichta, *Some possible approaches for improving the energy density of Li-air batteries.* Journal of the Electrochemical Society, 2010. **157**(12).
43. Lu, Y.-C., D.G. Kwabi, K.P.C. Yao, J.R. Harding, J. Zhou, L. Zuin and Y. Shao-Horn, *The discharge rate capability of rechargeable Li-O_2 batteries.* Energy & Environmental Science, 2011. **4**(8): p. 2999-3007.
44. Lide, D.R., *CRC Handbook of Chemistry and Physics*. 87 ed2007, Boca Raton, Florida: Taylor & Francis.
45. Huebner, K.H., E.A. Thornton and T.G. Byrom, *The finite element method for engineers*. 3 rd ed. 1995, New York: Wiley. xxvi, 627.
46. Lewis, P.E. and J.P. Ward, *The finite element method : principles and applications.*1991, Reading, Mass: Addison-Wesley. ix, 421.
47. Sousa, T., M. Mamlouk and K. Scott, *A non-isothermal model of a laboratory intermediate temperature fuel cell using PBI doped phosphoric acid membranes.* Fuel Cells, 2010. **10**(6): p. 993-1012.

Chapter 4: Modeling the Micro-Macro Homogeneous of a Li-air Battery

In this chapter, a one-dimensional micro-macro homogeneous model for a Li-air battery with a non-aqueous electrolyte is presented. The model incorporates the flooded porous cathode electrode with a concentrated binary electrolyte theory described in Chapter 3. The dynamic behaviour of the porous cathode was determined by a numerical solution of the combined continuity, transport and kinetics equations. This model considered the microscopic behaviour of the local mass transfer between lithium peroxide (Li_2O_2) layer inside the cathode and the active surface morphology changing with the Li_2O_2 growth. The main purpose of this model was to develop the Li-air battery model including the microscopic behaviour and to predict the battery's performances in term of various parameters. Initially, the model in this chapter only considers the Li_2O_2 as the discharge product during Li-air operation. Then, the developed model included the Li_2CO_3 from the electrolyte degradation reactions to create a more realistic Li-air model which is closer to the practical Li-air batteries as presented in the next chapter.

4.1 Introduction

The development of high performance and light-weight energy storage devices has recently focused on the rechargeable lithium-air batteries. Owing to their high energy density, which is theoretically up to 11,640 Wh kg^{-1} (which is about 10 times greater than well-known lithium-ion battery), such batteries are now considered as one of the promising alternatives to lithium-ion batteries with potentially wide applications, from small portable electronics to electric vehicles. The first Li-air system with a non-aqueous electrolyte was presented by Abraham and Jiang in 1996 [1]. After their promising rechargeable ability was demonstrated by the Bruce group [2], Li-air batteries have attracted much more attention among many research groups [2-7].

As shown in Figure 4-1, a Li-air battery contains a metal lithium anode, a solid polymer separator and a porous carbon or catalyst-loaded carbon air electrode filled with an organic electrolyte comprising lithium salt dissolved in an aprotic solvent. The porous carbon electrode provides a site for the electrochemical reduction of oxygen. During the battery's operation, oxygen (coming from the external air) is dissolved in the

electrolyte, penetrates through the pore of the cathode and reacts with the lithium ion (Li^+) at the active site. It is important to understand the oxygen reduction mechanisms, including the intermediate steps (e.g. formation of discharge products).

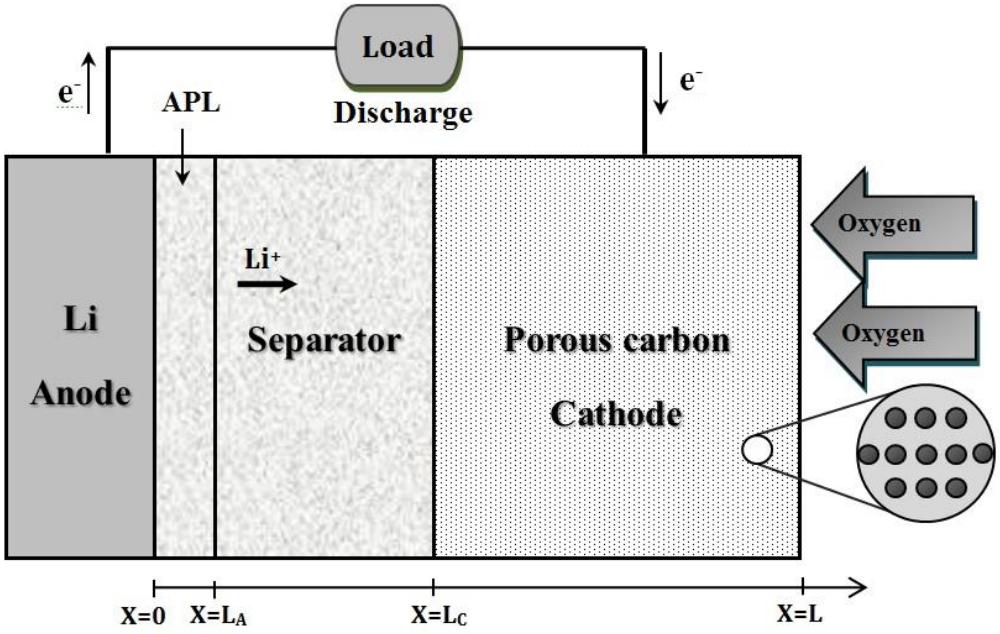

Figure 4-1: Schematic diagram of a computation domain for a Li-air cell during discharge showing 3 sub domains. The inset demonstrates the porous carbon cathode flooded with electrolyte.

Up to now, there have been various mechanisms for oxygen reduction reactions (ORR) depending on the types of electrolytes, catalysts and battery operating conditions. Peng et al. (2011) [8] investigated *in situ* spectroscopic data of oxygen reactions in a non-aqueous electrolyte and found strong evidence that lithium superoxide (LiO_2) is indeed an intermediate species during oxygen reduction before its disproportion in relation to the final Li_2O_2 product. For battery charging, the reaction is simply the oxidation of Li_2O_2 directly into oxygen and Li^+ without passing through the intermediate LiO_2 route. Based on literature [1, 8-10], the model assumes the following battery reactions:

Anode	$Li \rightleftharpoons Li^+ + e^-$	$(E^0 = 0.00\, V_{Li})$	(4-1)
Cathode	$2Li^+ + O_2 + 2e^- \rightleftharpoons Li_2O_2$	$(E^0 = 2.96\, V_{Li})$	(4-2)
	$2Li^+ + Li_2O_2 + 2e^- \rightleftharpoons 2Li_2O$		(4-3)
Combining Eq. (4-2) and Eq. (4-3)	$4Li^+ + O_2 + 4e^- \rightleftharpoons 2Li_2O$	$(E^0 = 2.91\, V_{Li})$	(4-4)

All standard reaction potentials shown above are measured with reference to the lithium electrode (V_{Li}). Li_2O_2 is the main reaction product which is considered in this model because it is insoluble in the organic electrolyte and could cover the active surface area inside the porous cathode as well as block the pathway for reactive species (Li^+ and oxygen). This behaviour prevents further reactions inside the cathode and contributes to the end of the discharging of the battery [10, 11]. Zhang et al. (2010) found that the fraction of the discharged Li_2O_2 can be further converted to Li_2O at a high discharge voltage below 2 V [10]. Therefore, the conversion of Li_2O_2 to Li_2O is not considered (Eq. (4-4)) because, if anything occurs at all, it only occurs at a significantly more negative (lower) potential below 2 V, which is beyond the potential range of the model.

Thus, a micro-macro homogeneous mathematical model, dealing with the entire electrode-electrolyte cell system as two continua (one from the electrode matrix and the other from the solution filling in all the space of the electrode), is developed for the cycling operation of a porous cathode of a rechargeable Li-air battery using a concentrated binary electrolyte theory [12, 13]. The model predicts the time dependence of electrolyte concentration, non-uniform porosity and reaction rate. A more accurate kinetic reaction in a porous cathode is established by including the dependency of the diffusion transport on reactant concentrations and the solubility limit of the product. Important parameters, such as porosity and thickness of electrode, electrolyte transport properties and surface activity, are investigated through this modeling study. The model predicts the direction of improving the Li-air battery performance in terms of the discharge product formation and dynamic model parameters.

In a different way from previous model approaches [14, 15], assuming that the cathode only contains a large number of cylindrical pores without considering the macroscopic aspects, our model considers electrochemical kinetic dependency on both Li^+ and oxygen species and includes local mass transport through the solid Li_2O_2 layer. In addition, variable physical and chemical properties are carefully applied in the model based on available experimental data which has been published. Therefore, this model can be used to describe the behaviour of Li-air batteries as well as to optimise the performance of these batteries.

4.2 Model Development

4.2.1 Model description

A mathematical description for a prismatic Li-air battery has been developed involving the conservation of mass and current, species transport, and kinetic reaction in the cathode and separator to clarify the mechanism inside the cell. The model used in this work is a Li-air cell consisting of a thin lithium sheet negative electrode, an anode protective layer (APL), a separator, and a porous carbon oxygen/air cathode filled with an organic electrolyte as shown in Figure 4-1. Current collectors were placed at the back of each electrode. Therefore, the one-dimensional computational domain was divided into 3 different sub domains: an APL layer, a separator layer and a porous cathode layer.

A concentrated binary electrolyte theory is used to describe the motion for each species in the electrolytic solution. The Li_2O_2 formation inside the porous cathode is presented using a macro-homogeneous porous model, defining the electrode by its porosity which is initially uniform but changes during the battery discharge. The macroscopic theory of porous electrode treats the solution and solid matrix phases as superimposed continuum. The details of governing equations and parameters are described in Chapter 3.

4.2.2 Model assumptions

In addition to the general assumption discussed throughout Chapter 3, the following assumptions were used with this particular model:

i. The Li_2O_2 was the main reaction product (Eq. (4-2)) and was only formed inside the porous cathode.
ii. The electrolytes used in Li-air batteries assumed a binary monovalent electrolyte which consists of a single salt in a homogeneous organic solvent mixture.
iii. The Li^+ diffusion could be simulated by the concentrated solution theory.
iv. The pores within cathode were full of liquid phase electrolyte (flooded electrode).
v. The oxygen was assumed to dissolve in the organic electrolyte with the saturated concentration initially.
vi. The convection for mass transport was negligible inside the Li-air battery.
vii. The Li-air cell was operated in isothermal condition so that the thermal effect is not considered.

4.2.3 Governing equations

Taking into account all assumptions, the governing equations described in Chapter 3 can be summarised in Table 4-1. The definitions and expressions of all parameters are referred to in Chapter 3. It is worth noting that the governing equations in Table 4-1 are derived for the porous cathode sub domain layer. The same governing equations are applied to the other layers except that there is no reaction in those layers.

Table 4-1: Governing equations used in the micro-macro homogeneous model

Equation description		
1. Transport of species		
Species material balance	$\frac{\partial(\varepsilon c_i)}{\partial t} = -\nabla \cdot \boldsymbol{N}_i + r_i$	(4-5)
Molar flux for Li^+	$\boldsymbol{N_{Li}} = -D_{Li,eff}\nabla c_{Li} + \frac{\boldsymbol{i}_2 t_+}{F}$	(4-6)
Molar flux for oxygen	$\boldsymbol{N_{O_2}} = -D_{O_2,eff}\nabla c_{O_2}$	(4-7)
2. Conservation of charge		
Solid-phase current density	$\boldsymbol{i}_1 = -\sigma_{eff}\nabla\phi_1$	(4-8)
Liquid-phase current density	$\boldsymbol{i}_2 = -\kappa_{eff}\nabla\phi_2 - \frac{2RT\kappa_{eff}}{F}(t_+ - 1)\left(1 + \frac{\partial lnf}{\partial lnc_{Li}}\right)\nabla lnc_{Li}$	(4-9)
Charge conservation	$\nabla \cdot \boldsymbol{i}_1 + \nabla \cdot \boldsymbol{i}_2 = 0$	(4-10)
Charge transfer current density	$\nabla \cdot \boldsymbol{i}_2 = aj_c$	(4-11)
3. Rate expression at cathode		
Butler-Volmer equation	$\frac{j_c}{nF} = k_a\left(c_{Li_2O_2,s}\right)exp\left[\frac{(1-\beta)nF}{RT}\eta_c\right] - k_c(c_{Li^+,s})^2\left(c_{O_2,s}\right)exp\left[\frac{-\beta nF}{RT}\eta_c\right]$	(4-12)
4. Rate expression at anode		
Butler-Volmer equation	$j_a = i_0\left[exp\left(\frac{(1-\beta)nF}{RT}\eta_a\right) - exp\left(\frac{-\beta nF}{RT}\eta_a\right)\right]$	(4-13)

4.2.4 Boundary conditions

All materials and species properties were computed using the methodology described in Chapter 3. Boundary conditions (Table 4-2) had to be applied for all variables of interest, in order to solve the governing equations (Eq. (4-5) –Eq. (4-13)). The boundary dimensions discussed in this section are referred to their position in Figure 4-1. To solve the governing equation for the battery cycling process, initial conditions are specified for all the species concentration inside the electrochemical battery, the porosity, the specific interfacial area, and the cell thickness. These initial values applied in the Li-air battery model are adopted from literature and summarised in Table 3-4.

Table 4-2: Boundary conditions used in the micro-macro homogeneous model

Conservation of species	
Boundary condition were imposed for Li^+ and oxygen concentration, and for the solid and electrolyte current density $at\ x = L$:	
$c_{O_2} = S_{O_2} * c_{O_2,ext}$	(4-14)
$N_{Li} = 0$	(4-15)
$i_1 = I$	(4-16)
$i_2 = 0$	(4-17)
Boundary condition $at\ x = L_c$:	
$i_1 = 0$	(4-18)
Boundary condition $at\ x = 0$:	
$N_{O_2} = 0$	(4-19)
$c_{Li} = 1\ mol\ dm^{-3}$	(4-20)
The voltage of the cell was calculated by the difference between the electrode potential at cathode current collector and the electrolyte potential at the anode side	
$V_{cell} = \phi_1(x = L) - \phi_2(x = 0)$	(4-21)

From Figure 4-1, a schematic view of the model cell can be formed consisting of four boundaries and three regions. The constant for oxygen concentration feeding at the right side of the cathode ($x = L$) can be estimated from the oxygen's solubility (S_{O_2}) and the external concentration ($c_{O_2,ext}$) as shown in Table 3-4. At the current collector or the back side of the carbon electrode ($x = L$), the current density in the solid phase is equal to the applied discharge current density (I), the current density in the electrolyte phase equals to zero, and the flux of each species is zero. At the carbon electrode/separator

interface ($x = L_c$) the continuous boundary conditions are specified for the fluxes of all species, i.e. N_i at L_c^- equal to N_i at L_c^+. The current density in the solid phase in this interface becomes zero, and the current density in the electrolyte then equals the applied discharge current density. These boundary conditions are summarised in Table 4-2.

4.2.5 Solution technique

The conservation equations and the boundary conditions described above were discretized using a finite element method and solved in one-dimensional battery system by commercial software package COMSOL multiphysics (version 4.2a). The COMSOL software is designed to solve a set of coupled differential and algebraic equations and the battery simulation model is performed on a 32 bit Windows platform with 4 GB RAM, and Intel Core 2 Duo 2.93 GHz processor. The different transport equations and the electrochemical reactions were solved as time dependent. The solutions were considered as converged solutions when the differences between the two results were less than 10^{-4} (relative tolerance) for all variables.

4.3 Results and Discussion

4.3.1 Effect of applied current density

The simulated voltage-capacity curve of the Li-air battery during discharge and then charge in 1 M $LiPF_6$ dissolved in an organic solvent between 2.4 and 4.2 V vs. Li/Li^+ at 0.1 mA cm^{-2} is shown in Figure 4-2. It can be seen from Figure 4-2 that the simulated results match the experimental voltage well during discharge at 1 atm of oxygen [7]. During discharge, the cell potential fell steeply at the beginning due to the high kinetic resistance for the oxygen reduction reaction [16, 17], from a voltage of 3.4 V to a plateau at around 2.7 V, and decreased continuously to 2.4 V. As the battery starts to operate in discharging phase, saturated oxygen dissolving in the electrolyte solution is consumed. Consequently, the discharge overpotential or activation losses become greater and thus the potential falls at the beginning. The reason for termination of the discharge process was increased polarisation because solid Li_2O_2 were formed and passivated the surface of the pores [18].

In the charge process, the voltage increased sharply to reach plateau at about 4.0 V and recharging occurred at 4.0-4.2 V as shown in Figure 4-2. From the model result, the large charge overpotential can contribute to the limited solubility of solid Li_2O_2 in the

non-aqueous electrolyte, which results in the high polarisation during charge process. In practice, there may be a number of other contributing factors for the large charge overpotential other than the low solubility of Li_2O_2, such as poor electronic conductivity of Li_2O_2 [19], and contaminants of Li_2CO_3 in the discharge products from electrolyte decomposition [20].

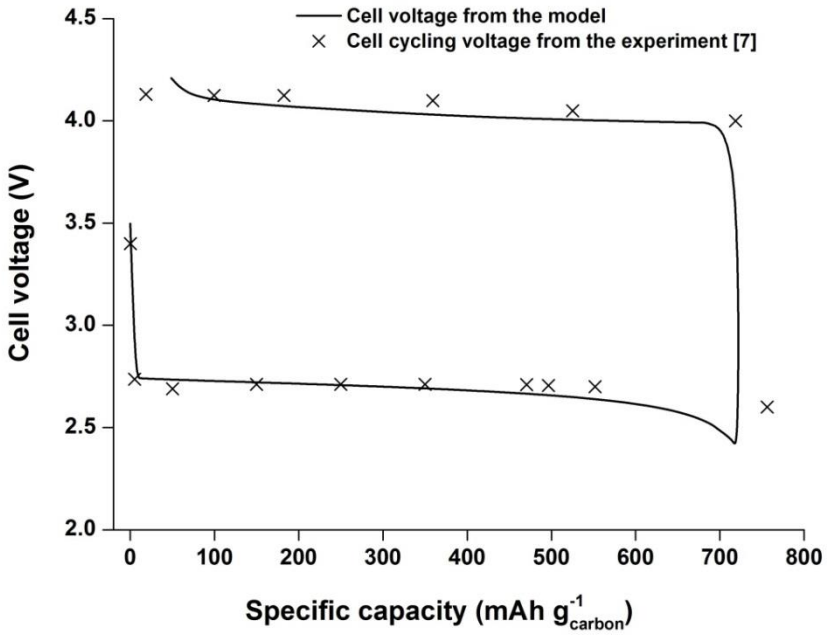

Figure 4-2: Voltage-capacity curve on discharge then charge for a Li-air battery at a rate of 0.1 mA cm^{-2}. The electrolyte contains 1 M $LiPF_6$ dissolved organic solvent. The oxygen solubility factor in the electrolyte is 0.38. The cathode electrode thickness is 750 μm with porosity of 0.73. The cell cycle is simulated between 2.4 and 4.2 V in pure 1 atm of oxygen at operating temperature 298.15 Kelvin. The model compares to the published data [7].

The discharge cell potential at around 2.5-2.7 V was also compared to our group's previous report and showed a good agreement for a similar battery discharged in 1 atm oxygen as shown in Figure 4-3 [21]. Although some of the parameters, such as carbon material and electrolyte solution, applied in the model are different from the experimental data in Figure 4-3, the model results and experimental data showed similarities, suggesting that the model is a promising tool to identify the Li-air cell mechanisms and forecast the cell performance for design and scale-up. The discharge capacity based on weight of carbon for the case with the parameters in Table 3-4 was about 722 mAh g_{carbon}^{-1}. From the model simulation, the potential rise at the end of

charge process results from the deficiency of the Li_2O_2 dissolving in the electrolyte. Therefore, the charging overpotential suddenly increased.

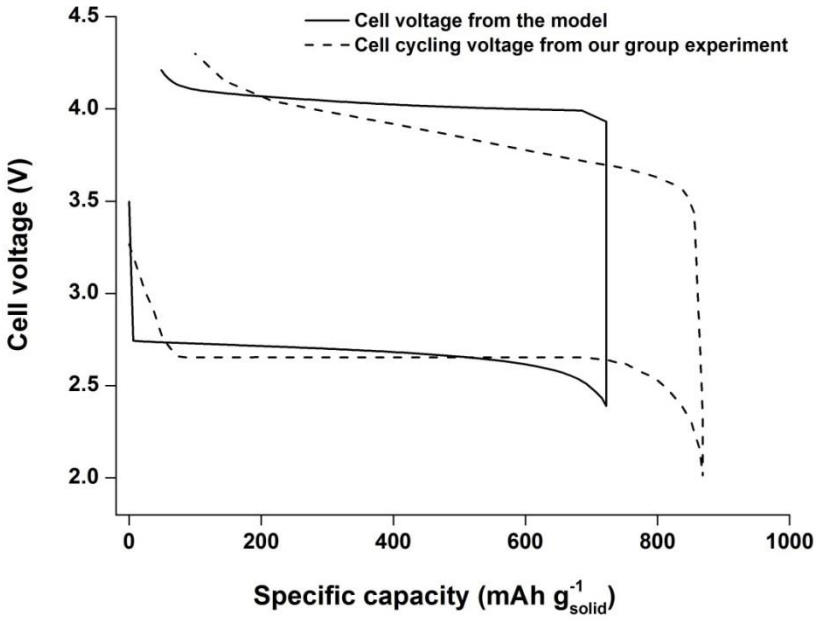

Figure 4-3: Voltage-capacity curve on discharge then charge for a non-aqueous Li-air battery at a rate of 0.1 mA cm^{-2}. The other parameters used in the model are the same as described in Figure 4-2. The model compares to our group's experiment.

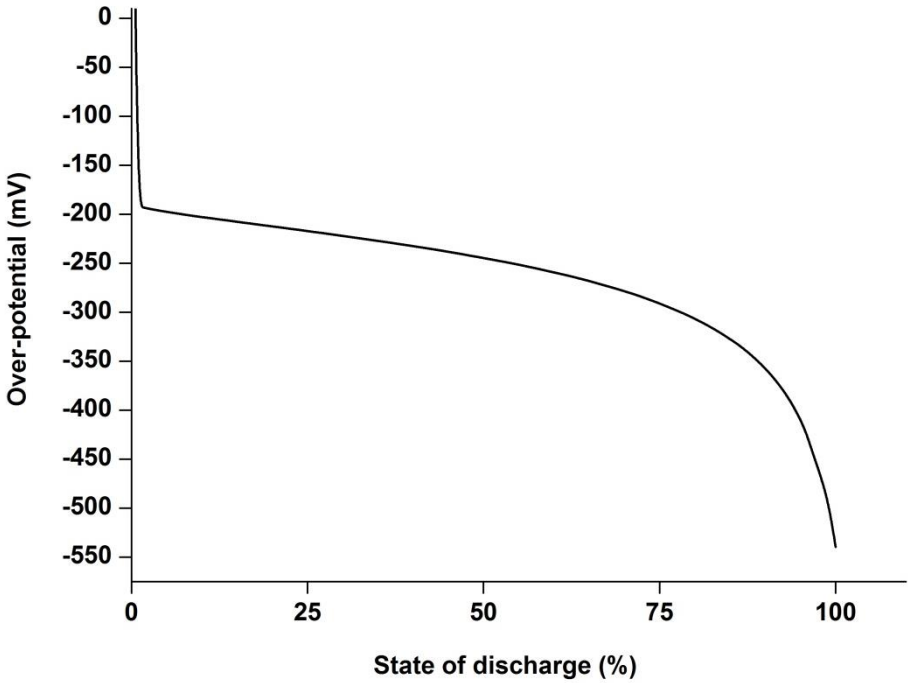

Figure 4-4: Change of positive electrode over-potential during discharge at a rate 0.1 mA cm^{-2} at different discharge state (0% = battery is fully charged).

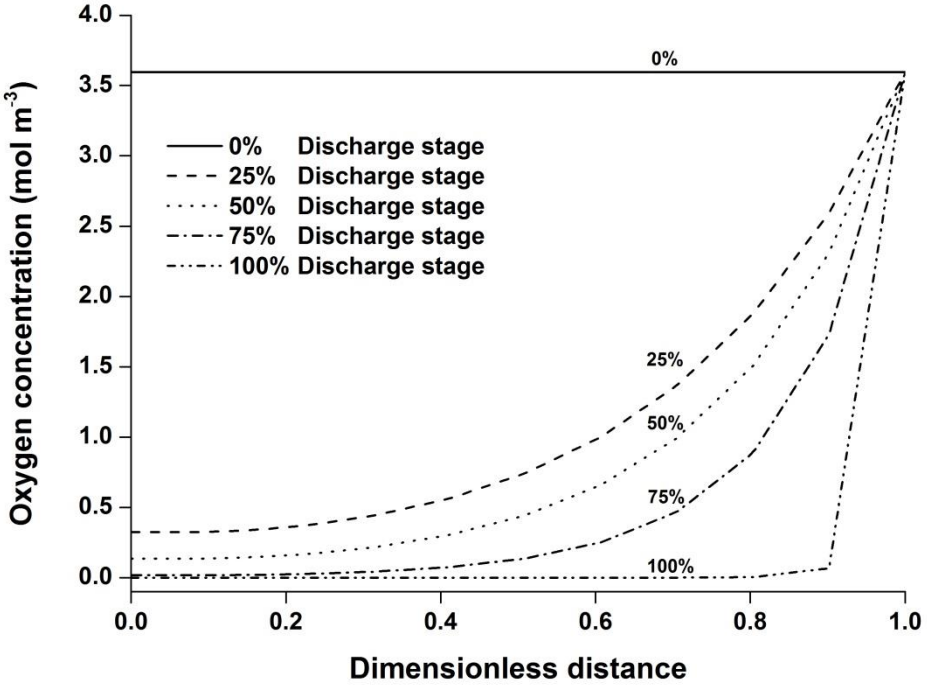

Figure 4-5: Local concentrations of oxygen profile inside the Li-air cell during discharge at a rate 0.1 mA cm^{-2} at different discharge state (0% = battery is fully charged). The other parameters used in the model are the same as described in Figure 4-2.

As shown in Figure 4-4, the discharge process was terminated by a rapid increase in polarisation from 200 mV at the start of battery discharge to 550 mV at the end of discharge (100% discharge state) due to the oxygen concentration limitation resulting from solid Li_2O_2 formation on the cathode surface, inhibiting the flow of reactants (oxygen, Li^+, and electrons) to the active surface as shown in Figure 4-5.

Figure 4-5 presents the oxygen concentration profiles inside the cell during battery discharging at various discharge states. The oxygen concentration decreases at the oxygen feed side of the cathode and oxygen cannot diffuse further inside the electrode because of the continuous growth of Li_2O_2 solid on the active surface of the porous carbon in an electrode. The deposition of this solid product diminishes the available pores for electrolytes resulting in either increasing Li_2O_2 insulated film or pore blocking. Both phenomena lead to the restriction of oxygen transportation and severely limit the cell's capacity. As can be seen from Figure 4-5, the region near the separator/cathode interface (dimensionless near 0-0.1) demonstrates very low oxygen

concentration (0.3 mol m^{-3}) at 25% discharge state and no oxygen is presented at 100% discharge state.

To overcome this problem, the suitable carbon material should be used with a sufficiently large pore size distribution over the entire electrochemically active surface as a cathode to provide enough space for the discharge products. The effect of different initial cathode porosities is presented later in Section 4.3.4. The variation of the cathode porosity as a function of space and time for a discharge current of 0.1 mA cm^{-2} is presented in Figure 4-6. As the diffusion coefficient of oxygen is very low compared to that of Li^+ species in this non-aqueous electrolyte, the porosity falls predominantly at the oxygen feed side of the cathode due to the Li_2O_2 formation. As the extent of discharge increases to 100% discharge state the porosity falls almost to zero and thus blocks the diffusion of oxygen species into the cell, as already presented in Figure 4-5.

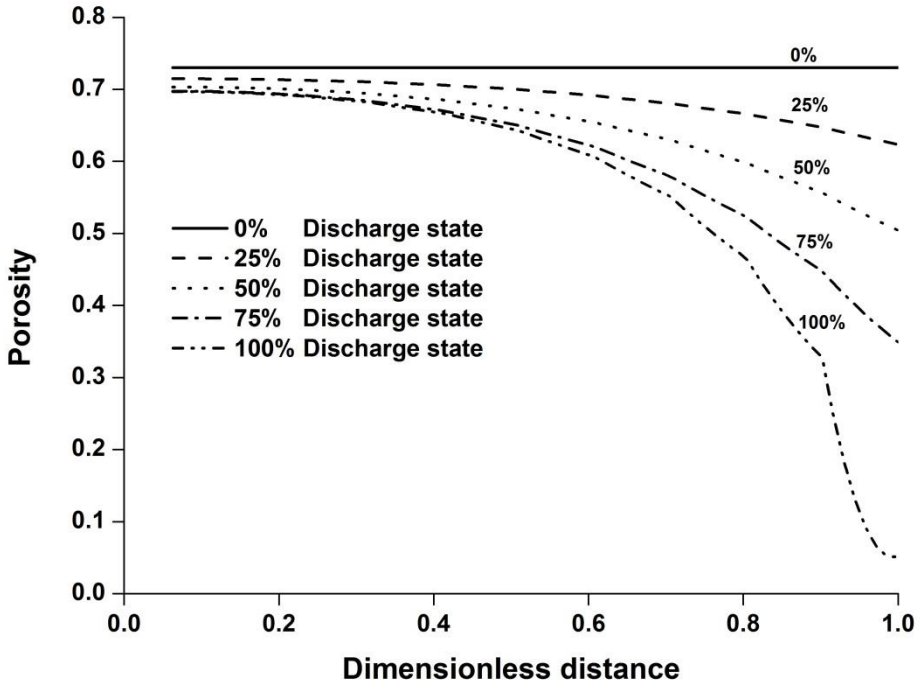

Figure 4-6: Local porosity profile inside the Li-air cell during discharge at a rate 0.1 mA cm^{-2} at different discharge state (0% = battery is fully charged). The other parameters used in the model are the same as described in Figure 4-2.

Figure 4-7 shows the effect of applied current density on the simulated discharge curves for a Li-air battery using the same cathode details as shown in Figure 4-2. The discharge capacity demonstrates a large decrease from 1350 mAh g_{carbon}^{-1} at low current density of

0.05 mA cm^{-2} to 213 mAh g_{carbon}^{-1} at a high current density of 1 mA cm^{-2}. This is consistent with experiments published by Read (2002) [7] and indicates a similar trend to that of previous groups in that the current density has significant effects on the Li-air battery's capacity [22, 23]. Moreover, the discharge voltage plateau is also lower with increasing current density.

The capacity loss at the high discharge rates can be discussed in terms of the transport limitation of oxygen diffusion through the cathode flooded with electrolyte, which cannot maintain the electrochemical reaction (oxygen-diffusion limitation). Thus, oxygen reduction occurs in a small region close to the cathode-current collector interface as the discharge rate increases. Moreover, the rapid porosity reduction due to the deposition of Li_2O_2 on the surface of the active area also limits oxygen transport into the cell and incompletely utilises the full capacity of the electrode porosity.

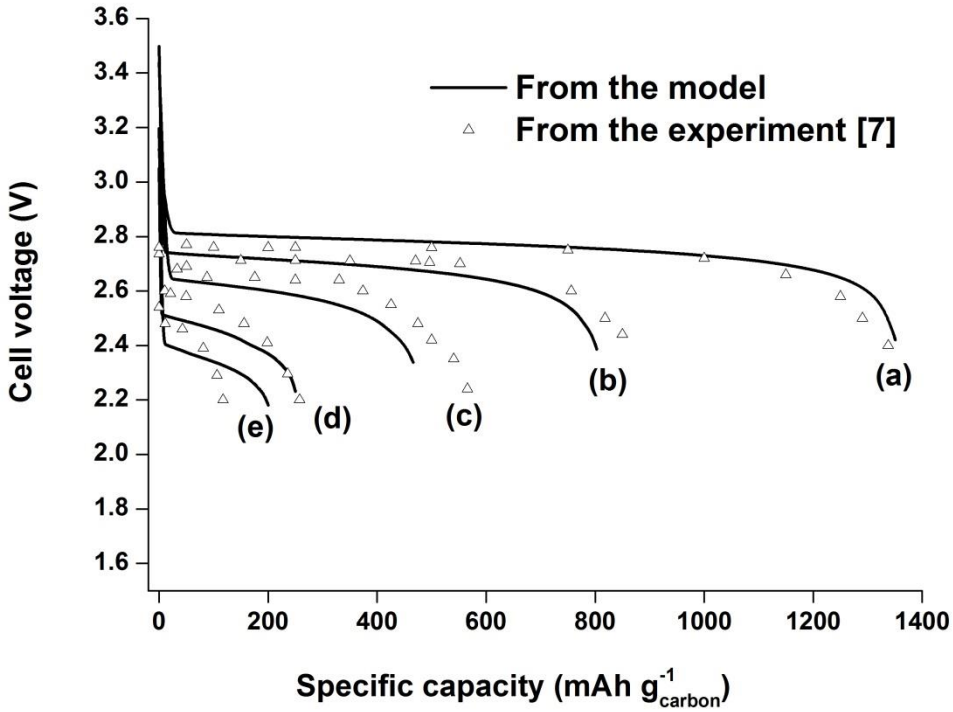

Figure 4-7: Comparison of the voltage-capacity curve between the model and experiment for a non-aqueous Li-air battery at different discharge rate (a) 0.05 mA cm^{-2}, (b) 0.1 mA cm^{-2}, (c) 0.2 mA cm^{-2}, (d) 0.5 mA cm^{-2}, and (e) 1.0 mA cm^{-2}. The other parameters used in the model are the same as described in Figure 4-2.

For a battery on charge, after the provided solid lithium peroxide ($\varepsilon_{Li_2O_2}$) has been produced during discharging, there will be a finite Li_2O_2 concentration ($c_{Li_2O_2}$)

dissolved in solution (saturation concentration). The rate of oxidation reaction (battery charging) would be constant and will only decrease when the solid Li_2O_2 is consumed or $c_{Li_2O_2}$ goes below the solubility limit (c_{max}). Therefore, the model assumption applied on charge is that the dissolution rate (r_{diss}) of solid peroxide is quick compared to electrochemical reaction and can be written in Eq. (4-22). The dissolution rate equation is included for $c_{Li_2O_2}$ species balance in Eq. (4-5) during battery on charge and the driving force term for this reaction is when the $c_{Li_2O_2}$ decreases below its solubility in the electrolyte (c_{max}). It can be expressed as follows:

$$r_{diss} = k_d \varepsilon_{Li_2O_2} (c_{max} - c_{Li_2O_2}) \tag{4-22}$$

where k_d is the dissolution rate constant for Li_2O_2 during charge which assumed very fast, and c_{max} is the solubility limit of Li_2O_2 dissolved in organic electrolyte.

In the charge process, the voltage increased sharply to reach a plateau at about 4.0 V as shown in Figure 4-2 and this is largely consistent with the published charge curve at the same charging rate with a slight difference [7]. The charge capacity is almost equal to its capacity when discharging (discharge and charge capacity 722 and 674 mAh g_{carbon}^{-1}, respectively). Hence, this model, in which the published parameters are applied, can be used to describe the Li-air battery behaviour as well as optimise the cell performance and will be compared later to the actual experimental data which was generated in our lab.

4.3.2 Effect of oxygen solubility

One of the major drawbacks of current Li-O_2/Li-air batteries is the low current densities at which the cell operates. The important factor that limits the performance of a Li-air battery is the solubility of oxygen in the electrolyte. It was summarised from the work of Read et al. (2002) that, to improve the performance of Li-air batteries, one should either increase the diffusion coefficient of oxygen or increase the oxygen solubility in the organic electrolyte to enhance the reaction rate of the cathode so that the solid Li_2O_2 efficiently fills in the entire pores [7, 11]. In this section, the solubility of oxygen is varied in the model to simulate the cell cycling behaviour. In practice, this parameter can be increased by using a solvent with a high capability to dissolve oxygen, such as a solvent based on perfluorinated solvents or ether-based electrolytes [24]. When the solubility of oxygen is increased from the base case of 3.22 mol m^{-3} to a high solubility

of oxygen concentration of 9.46 mol m^{-3}, the discharge specific capacity and specific energy of a Li-air cell increase as is shown in Figure 4-8. The battery capacity when discharged at a low current density 0.1 mA cm^{-2} increased from 722 mAh g_{carbon}^{-1} at the low oxygen solubility (oxygen concentration 3.22 mol m^{-3}) to 1400 mAh g_{carbon}^{-1} at the highest oxygen solubility (oxygen concentration 9.46 mol m^{-3}).

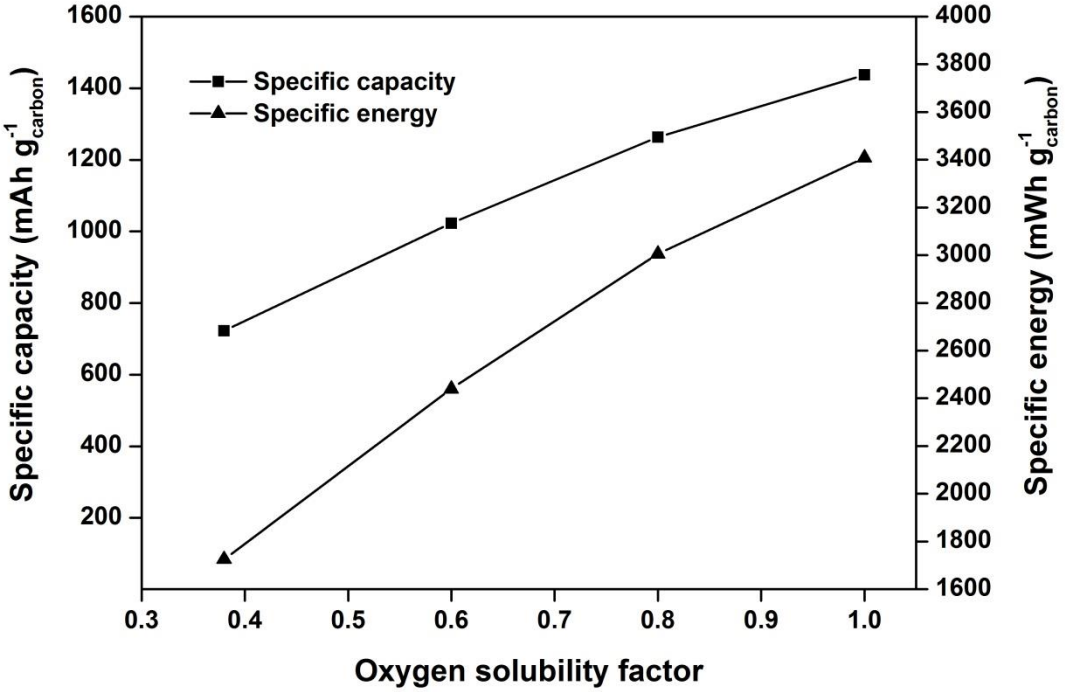

Figure 4-8: Effect of oxygen solubility at a rate of 0.1 mA cm^{-2} on the specific capacity and energy for a Li-air battery. The other parameters used in the model are the same as described in Figure 4-2.

Moreover, it can be seen from Figure 4-9 that the discharge potential of the Li-air battery also increases, from ca. 2.68 V to 2.80 V with the highly dissolved oxygen concentration in the electrolyte. The cell performance is enhanced because the oxygen can substantially diffuse further inside the porous structure when a solvent with a greater solubility of oxygen is used. For the battery cycling, it is apparent from the same figure that no significant difference can be seen from the charge potentials of Li-air battery at various oxygen solubilities, i.e. increasing dissolved oxygen will not affect the cell's performance significantly on the charging period as can be appreciated from the kinetic oxidation reaction.

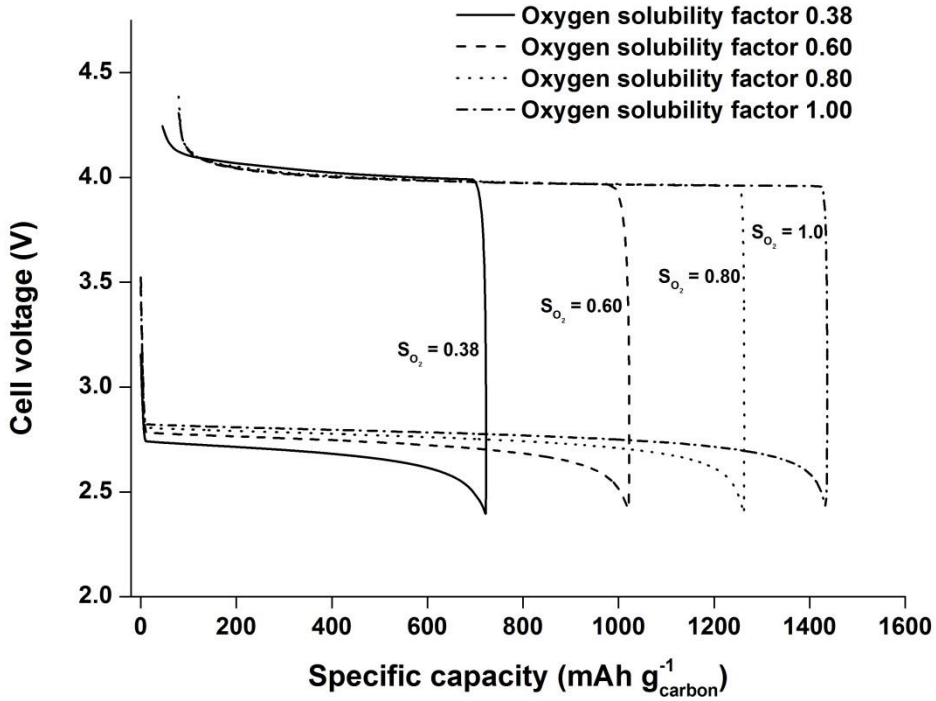

Figure 4-9: Effect of oxygen solubility at a rate of 0.1 mA cm^{-2} on the voltage-capacity curve on discharge then charge for the Li-air battery. The other parameters used in the model are the same as described in Figure 4-2.

It is interesting to note that the difference in discharge capacity among the works reported previously [7, 9, 18, 24] is largely as a result of the diverse properties of electrolytes to dissolve the distinct amount of soluble oxygen. A recent study by Lu et al. (2011) [24] showed that the high discharge capacity of Li-air battery can be attributed to higher oxygen solubility in the electrolyte with 1,2-dimethoxyethane (DME) used in his work than that oxygen solubility in the electrolyte with propylene carbonate (PC). From his work, the solubility of oxygen in the electrolyte with DME is around 8.76 mol m^{-3} providing the specific capacity 2,600 mAh g_{carbon}^{-1} at low discharge current density of 250 mA g_{carbon}^{-1} (which compares to approximately 0.1 mA cm^{-2} in our simulation). This capacity is higher than in our work (only 1,400 mAh g_{carbon}^{-1}) with the same solubility of oxygen concentration. Many possible explanations could account for this but one factor might be that the diffusion coefficient for oxygen in our model (7 x 10^{-10} m^2 s^{-1}) is lower than the one in electrolyte with DME (4 x 10^{-9} m^2 s^{-1}) and the transference numbers describing the fraction of the total current carried by Li^+ in a solution are different between the two electrolytes. However, if these parameters are applied in our model including the solubility of oxygen in DME (8.76 mol m^{-3}) at low

discharge current density of 0.1 mA cm^{-2}, the cell capacity from our simulation (2,400 mAh g_{carbon}^{-1}) almost equals the cell using DME electrolyte. Therefore, this developed model can be appropriately used to predict the behaviour of Li-air battery when changing detailed parameters.

4.3.3 Effect of lithium peroxide solubility

The discharged products of a Li-air battery, Li_2O and Li_2O_2, are not very soluble in a non-aqueous electrolyte and are also considered as one of the main reasons that limit the battery's performance. Therefore, introducing some additives or co-solvents to the electrolyte solution can partially enhance the solubility of the discharged products and improve the battery performance. It has been demonstrated that adding tris(pentafluorophenyl) borane (TPFPB) can substantially increase the solubility of Li_2O_2 in carbonate based solvent from very low amount of 0.19 mol m^{-3} to 190 mol m^{-3} [25]. Consequently, it is interesting to use the model to simulate the variation of Li_2O_2 solubility on performance.

On addition of the TPFPB additive, not only does the solubility of the lithium oxide increase but also both the Li^+ transference numbers and the electrolyte conductivities are enhanced for those electrolytes with added TPFPB complex [25]. Xie et al. (2008) reported that the addition of TPFPB increases the Li+ transference numbers (t_+) as high as 0.7 (t_+ equal to 0.26 applied in the model) [25]. The increase in both transference numbers and conductivity was not considered in our current model which is focused only the effect of Li_2O_2 solubility. From the data in Figure 4-10, it is apparent that increasing the solubility of Li_2O_2 in the electrolyte does not affect the discharge voltage and specific capacity of the Li-air cell's performance. However, there is a significant improvement in the charge cycling cell voltage, i.e. the magnitude of charge voltage decreased by approximately 400 mV at higher Li_2O_2 concentration dissolved in the electrolyte. The improvement in charge potential in the case of increasing the Li_2O_2 solubility is related to better surface oxidation reaction kinetics (Eq. (4-12).

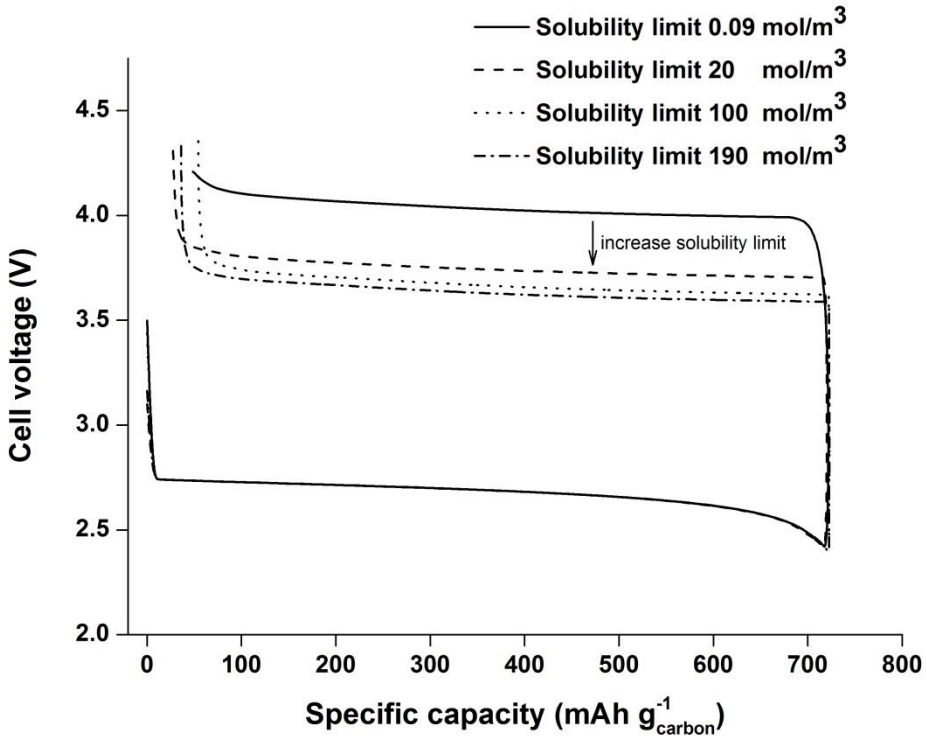

Figure 4-10: Effect of Li_2O_2 solubility factor at a rate of 0.1 mA cm^{-2} on the voltage-capacity curve on discharge on discharge then charge for the Li-air battery. The other parameters used in the model are the same as described in Figure 4-2

4.3.4 Effect of kinetic rate constant and porosity

As the cell's performance depends on the porous electrode, one option to improve the battery's operation is that the applied catalysts, such as metal oxide catalysts and noble metal catalysts, with carbon active materials can reduce the overpotential and thus increase the cell's efficiency. To investigate the effect of different catalysts on the battery's behaviour, the effect of cathodic rate constant (k_c) on the discharge voltage of the cell as a function of the specific capacity is shown in Figure 4-11. This rate coefficient is assumed to be constant and having a uniform distribution inside the cathode. As can be seen from the results in Figure 4-11, the discharge voltage plateau gradually increases with the high value of k_c due to the reduced overpotential of the cathode electrode. The value of 3.4×10^{-16} m^7 s^{-1} mol^{-2} of k_c demonstrated an onset voltage of about 2.85 V, and an average voltage plateau of 2.82 V (only 140 mV lower than estimated equilibrium potential of 2.96 V for Li_2O_2 formation). This can be attributed to the reasonably high reduction reaction activity at the carbon/catalyst interface with higher catalyst activity.

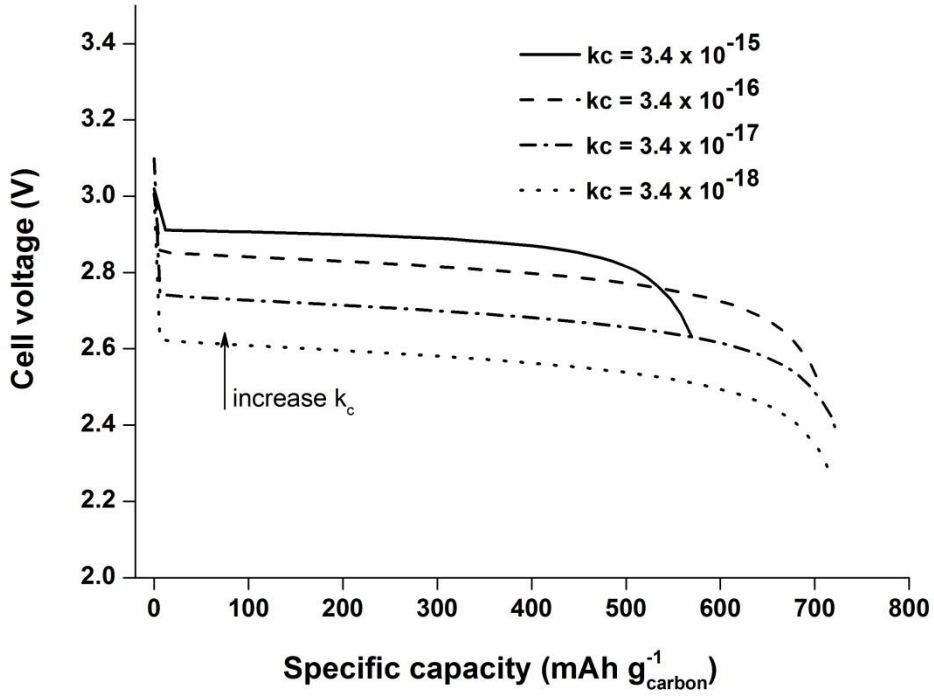

Figure 4-11: Effect of cathodic rate constant (k_c) at a rate of 0.1 mA cm^{-2} on the voltage-capacity curve on discharge. The other parameters used in the model are the same as described in Figure 4-2.

However, there was a relatively small increase in the specific capacity of the cathode at different rate constants. The results of this study do not support those of previous research [6, 18, 26] which demonstrate that the various catalysts can improve both the specific capacity and discharge voltage. A possible explanation for this might be that the carbon porosity is modified by the reaction with catalyst during the preparation [27]. As a result, some of the closed micro-pores are opened for the greater access of discharge products, and some open pores are widened. However, this effect which influences the battery capacity was not included in our model with applying the same cathode structure (carbon loading, thickness and porosity) in every case.

For the case of varying initial cathode porosity, the pore structure of a porous carbon cathode is a significant factor in the Li-air battery's performance. The large pore volume allows more spaces for the three-phase among carbon solid, liquid electrolyte and oxygen gas, able to facilitate the reaction in the electrode [22, 28]. The extra volume inside the cathode also provides more space for accommodating the solid discharge products. Thus, the model evaluated the effect of initial cathode porosity. When varying

the cathode porosity, the specific surface area of the cathode as described in Chapter 3 was also changed and considered in each case following the expression below:

$$a_0 = \frac{3\varepsilon_c}{r_s} = \frac{3(1-\varepsilon^0)}{r_s} \tag{4-23}$$

The variations in specific surface area with the cathode porosity obtained from the relation in Eq. (4-23) are presented in Table 4-3. It is apparent that the specific surface area reduces with the increasing porosity due to the decrease in active material.

Table 4-3: Specific surface and discharge capacity for different initial porosity

Initial porosity	**Specific surface area ($m^2\ m^{-3}$)**	**Discharge capacity ($mAh\ g_{carbon}^{-1}$)**
0.60	4.80×10^6	466.83
0.73	3.24×10^6	714.97
0.80	2.40×10^6	874.51
0.85	1.80×10^6	1000.68

As shown in Figure 4-12, the results show that the battery capacity increases with more space available to accommodate discharge products. The effect of porosity in the model can be referred to the pore structure of the cathode in practical Li-air batteries. If the carbon materials used to fabricate the cathode electrode have meso-pore or macro-pore structures, they are beneficial for accommodating discharge products, thus leading to a high discharge capacity [28, 29].

It is worth noting that the changing of porosity in the model only affects the specific surface area of the cathode as shown in Table 4-3. This has no effect on the quantity of carbon loading on the electrode. Hence, the discharge capacities are calculated on the same basis of gram carbon to consider the effect of varying porosity only as presented in Table 4-3 and Figure 4-12. Moreover, it is assumed in relation to the porosity applied in the model that there are no micro-pore channels which are not utilised by lithium oxides inside the porous cathode, i.e. all the pore spaces have been accommodated by the discharge products.

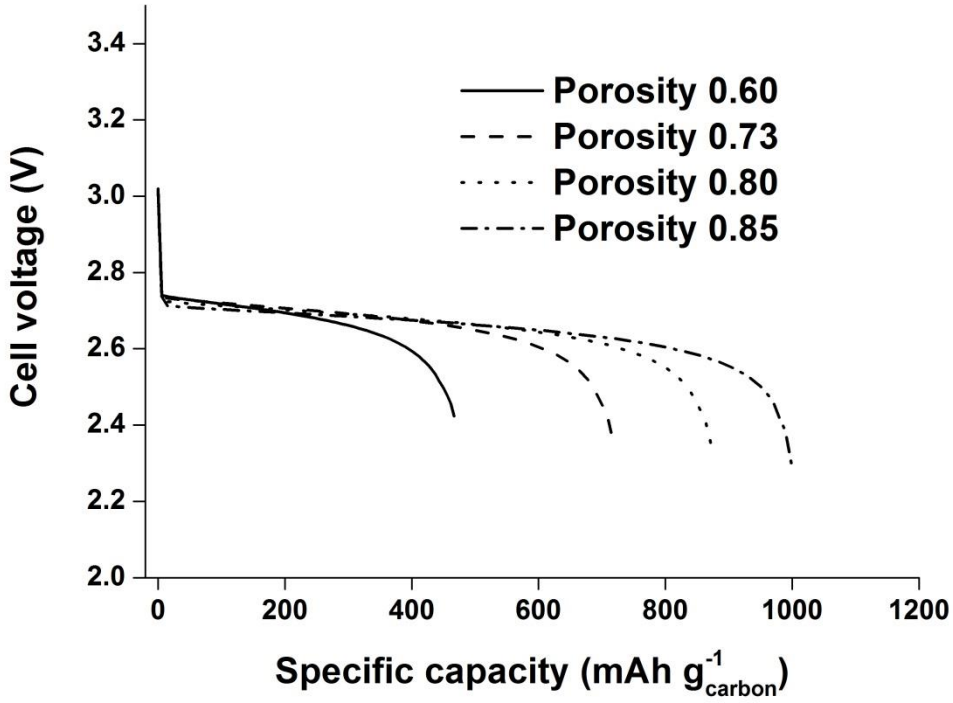

Figure 4-12: Effect of initial cathode porosity at a rate of 0.1 mA cm^{-2} on the voltage-capacity curve on discharge. The other parameters used in the model are the same as described in Figure 4-2.

4.3.5 Effect of cathode thickness

Besides concentrations and discharge conditions affecting the Li-air battery's behaviour, the thickness of the cathode electrodes also plays an important role in the electrochemical performance. Figure 4-13 shows the cell discharge voltage as a function of specific capacity for the different cathode thickness. Obviously, the thicker the electrode, the lower the cell's performance in term of specific capacity. This can be attributed to both the slow diffusion of oxygen dissolved in non-aqueous electrolyte and the long residence time moving through the thicker electrode. A number of experimental published works showed that the scanning electron microscopy (SEM) images of the cathode surface on the air side ($x = L$) of the fully discharged battery were almost filled in the space by solid lithium oxides deposition [10, 24, 30], but this behaviour did not appear on the separator side ($x = L_c$). To investigate the effect of cathode thickness, the dimensionless, Damköhler number, is introduced as shown in the equation below:

$$Da = \frac{j/nF}{D_{O_2,eff} \cdot c_{O_2}/L} \tag{4-24}$$

The Damköhler number defined in Eq. (4-24) expresses a ratio of current density of electrochemical reaction rate to oxygen diffusion rate, or it can be said to refer to the ratio of the characteristic time of oxygen diffusion to the reaction time. A unity of Damköhler number means an equal rate of surface electrochemical reaction and oxygen mass transport due to diffusion. From the Damköhler number (Da) for each cathode thickness in Figure 4-13, it indicates that all the numbers are greater than unity and the higher value (Da = 4.95) provides lower specific cell capacity (410 mAh g_{carbon}^{-1}) when discharging Li-air at the current density of 0.1 mA cm^{-2}.

When the Damköhler number is large (more than unity), the Li-air performance is controlled by the diffusion of oxygen which has a low diffusion coefficient in non-aqueous electrolyte and can also be affected by the tortuosity of the porous cathode. As a result, the cell demonstrated the small specific capacity as the thicker electrode and high value for the thinner electrode. To further calculate the Damköhler number, Table 4-4 compares this number in relation to different cathode thicknesses and discharge current densities. The Damköhler number for the cathode thickness of 750 μm at different discharge rates as shown in Table 4-4 corresponds to the voltage-capacity curve in Figure 4-7 which describes the better Li-air performance as the low Damköhler number at small discharge rate. This study has shown that, to meet the high cell performance (Damköhler number lower than unity), the cathode electrode should be on average at a thickness of around 500-750 μm and operating on the low current density (0.05 mA cm^{-2}). For the higher discharge rate or thicker cathode, the cell will suffer from the diffusion-controlled limitation which can overcome this problem using the electrolyte with high solubility and diffusivity of oxygen to reduce the Damköhler number.

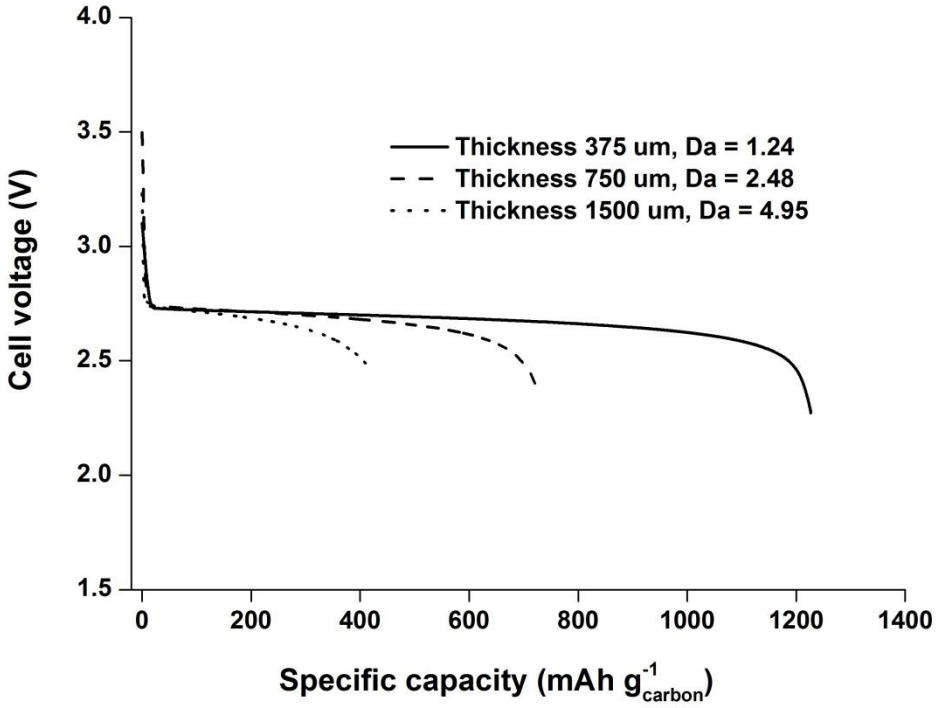

Figure 4-13: Effect of cathode thickness on different Damköhler numbers at a rate of 0.1 mA cm^{-2} on the voltage-capacity curve on discharge. The other parameters used in the model are the same as described in Figure 4-2.

Table 4-4: Comparison of Damköhler number in different cathode thickness and discharge current densities for oxygen diffusion coefficient ($D_{O_2} = 7 \times 10^{-10}$ m^2 s^{-1}).

Thickness	0.05 (mA cm^{-2})	0.1 (mA cm^{-2})	0.2 (mA cm^{-2})	0.5 (mA cm^{-2})
250	0.41	0.83	1.65	4.13
375	0.62	1.24	2.48	6.19
500	0.83	1.65	3.30	8.25
750	1.24	2.48	4.95	12.38
1000	1.65	3.30	6.60	16.51
1250	2.06	4.13	8.25	20.64
1500	2.48	4.95	9.91	24.76

4.3.6 Electrolyte with high solubility Li_2O_2 additive

One of the main issues during the operation of a Li-air battery is the build-up of the solid Li_2O_2 depositing and covering the active surface of the porous cathode. From the previous section, some amount of boron complex, e.g. tris (pentafluorophenyl) borane (TPFPB), can substantially increase the solubility of Li_2O_2 in a carbonate-based solvent within a limited concentration. Hence, it would be interesting to model the cell in the

absence of solid oxide formation in case the electrolytes have a high solubility of Li_2O_2. Without solid formation, the porosity and active surface area inside the cathode are assumed to be constant during the discharge operation. Then, the local concentration of Li_2O_2 increases continuously with time in the electrolyte. This may affect the density and viscosity of the electrolyte solution and the diffusivity of oxygen when high concentrations Li_2O_2 are encountered.

The data for the density of electrolytes depending on concentration of Li_2O_2 is not known, therefore, we have adopted the information of solution density which is dependent on $LiPF_6$ concentrations from [31]. The variation of electrolyte density is increased linearly with $LiPF_6$ concentrations. Changes et al. (2002) measured the electrolyte density depending on $LiPF_6$ concentrations between 0.2-1.5 molar at 25 °C [31] and this data is extrapolated to the desired concentration in the model as present in Table 4-5. The volume of the cell system is assumed to be constant during simulation. Similarly, the viscosity of the electrolyte solution also changes with salt concentration and this relation is applied in the model. Changes et al. (2002) [31] investigated the relative viscosity (μ_r) of a concentrated electrolyte solution by applying the Jones-Dole equation which was used to describe the viscosity of solutions when the salt concentration (c) is varied as in the following expression:

$$\mu_r = \mu/\mu_0 = 1 + Ac + Bc^2 \tag{4-25}$$

where μ and μ_0 (2.59×10^{-3} Pa s, in PC:DME solvent) are the viscosities of the solution and pure solvent respectively, and *A* and *B* are the coefficients which are 0.4 (M^{-1}) and 1.10 (M^{-2}), respectively. Moreover, the diffusivity coefficient of oxygen decreases with increasing viscosity of the electrolyte. To describe this behaviour, the relationship between viscosity and the diffusion coefficient of oxygen is given by the Stokes-Einstein equation as follows:

$$D_{O_2} = \frac{kT}{6\pi\mu a} \tag{4-26}$$

The definitions for each parameter in equation above are defined in Chapter 3 in the oxygen diffusion section. The variations of electrolyte density, viscosity, and diffusion coefficient of oxygen depending on the solution concentrations are summarised in Table 4-5. These variables are applied in the Li-air model only in this section to describe the effect of electrolyte with high solubility Li_2O_2 additive.

Table 4-5: Variations of electrolyte density, viscosity, and oxygen diffusion coefficient depending on solution concentration

Concentration (mol dm^{-3})	**Density (kg m^{-3})**	**Viscosity (Pa s)**	**Oxygen diffusion coefficient (m^2 s^{-1})**
0.2	1135	2.71×10^{-3}	6.65×10^{-10}
0.5	1163	2.59×10^{-3}	5.89×10^{-10}
1.0	1207	3.07×10^{-3}	4.41×10^{-10}
2.0	1306	4.09×10^{-3}	2.32×10^{-10}
3.0	1403	13.69×10^{-3}	1.32×10^{-10}
5.0	1595	32.09×10^{-3}	5.62×10^{-11}

The results of cell voltage discharge at 0.1 mA cm^{-2} obtained in the model with and without the solid lithium oxide formation is shown in Figure 4-14a. The specific capacity predicted by the model without the formation of solid (546 mAh g_{carbon}^{-1}) is lower than the model that includes the effect of the porosity change due to the Li_2O_2 solid formation. The former also demonstrates a slightly lower discharge voltage plateau compared to the latter. This effect may be the result of the high density and viscosity of the electrolyte solution when highly soluble salts are encountered.

As the salt concentration in electrolyte solution increased with time by the high-dissolved discharge product of Li_2O_2, the oxygen diffusion rate fell because of the high salt concentration and increasing solution viscosity. It can be seen from the oxygen transport inside the porous cathode in Figure 4-14b that the decrease in oxygen concentration with discharge time is greater than the case with the solid Li_2O_2 formation (Figure 4-5) and the diffusion is limited very close to the cathode/current collector interface owing to the high resistance of oxygen transport in a highly viscous solution.

The results of this study indicate that the high salt concentration which leads to an increase in the density and viscosity of the electrolyte severely deteriorates the Li-air performance at a higher rate than is the case with the solid Li_2O_2 formation. In order to use the electrolyte with high solubility of Li_2O_2, the discharged electrolyte needs to be replaced with the fresh one to maintain the performance of the Li-air battery. This mechanism with the circulating fresh electrolyte is presented in the next section in a Li-air flow battery.

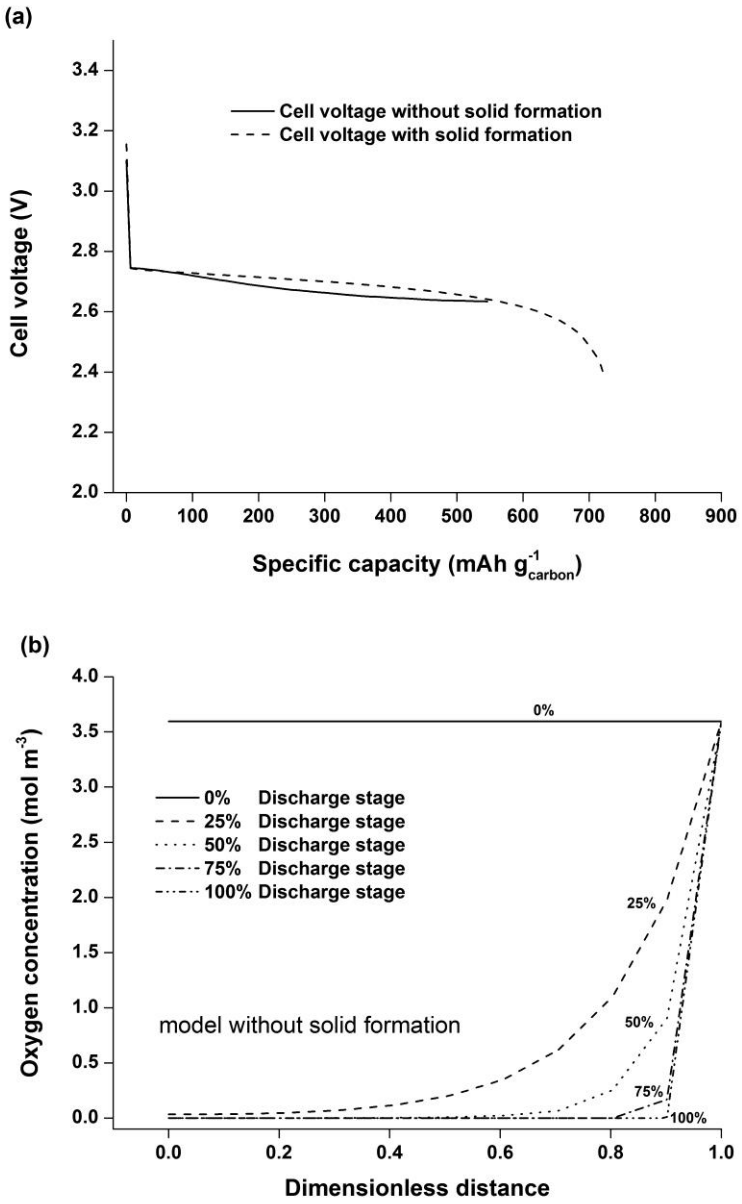

Figure 4-14: (a) Comparison of the Li-air cell discharge voltage at a rate 0.1 mA cm^{-2} between cell with and without solid Li_2O_2 formation. (b) Local concentrations of oxygen profile inside the Li-air cell without solid Li_2O_2 formation during discharge at a rate 0.1 mA cm^{-2} at different discharge state (0% = battery is fully charged).

4.4 A Li-air Flow Battery

As mentioned earlier, although Li-air batteries have a remarkably theoretical energy density they still suffer from major problems as follows: (1) the battery's discharge products (Li_2O_2/Li_2O) are not soluble in organic electrolytes leading to deposits mostly near the air side of the porous air electrode because of the high oxygen concentration on this side. This leads to inhomogeneous distribution of the solid products on the pores of

electrode and limit the usage of the cathode volume. This behaviour leads to a deterioration in the battery's performance on cycling as shown in Chapter 5; and (2) the low diffusion and solubility of oxygen in organic electrolyte limits the battery's ability to operate at the high current and power densities.

To overcome this problem, a new design structure of Li-air flow battery which consists of two functional units, an electrochemical reaction unit (ordinary Li-air battery) and an electrolyte recycling unit, was recently proposed [32-34]. In this system, a metallic lithium anode in an organic electrolyte and a porous cathode in an aqueous electrolyte are placed in the same compartment and separated by a lithium ionic conductor (LISICON) separator [32, 35]. Instead of using oxygen directly from the atmosphere, the electrolyte with saturated oxygen is circulated into the porous electrode of electrochemical reaction unit and thereafter it is replenished the oxygen concentration with an electrolyte recycling system as shown in Figure 4-15.

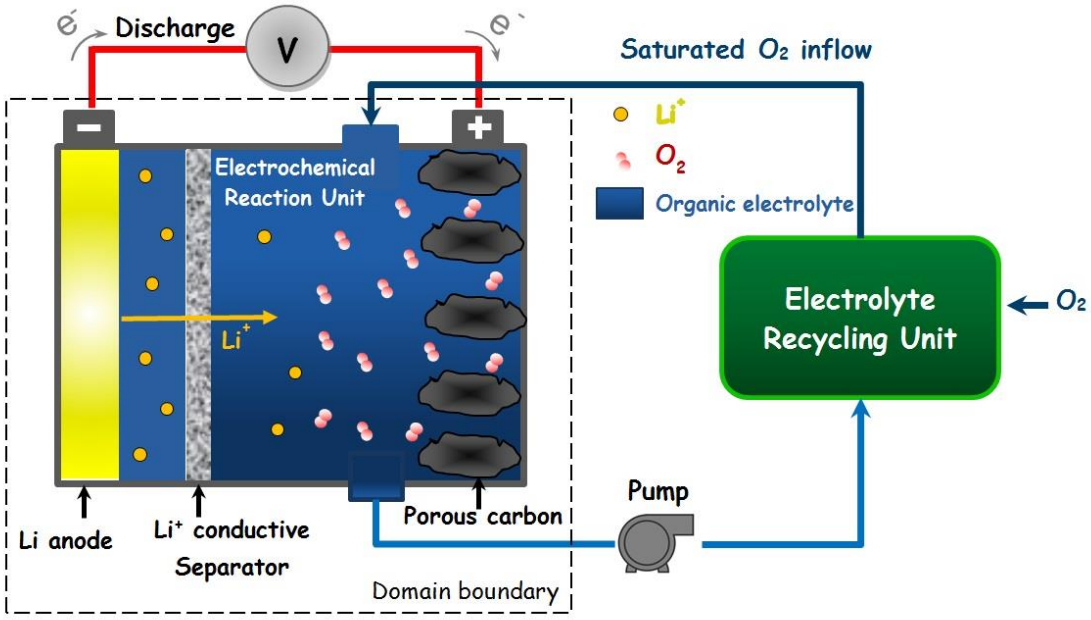

Figure 4-15: Schematic representation of the developed Li-air flow battery with electrochemical reaction unit and electrolyte recycling unit.

He et al. (2010) investigated a Li-air fuel cell with a flow design structure for discovering improved stability and performance in a battery [32]. The cell consists of two subunits: an energy conversion unit that performs the electrochemical reaction and a reaction-product recycling unit that collects/removes LiOH discharge product. The aqueous alkaline electrolyte was applied in this Li-air flow battery. However, the

oxygen in this system was still obtained from the atmosphere and not from the electrolyte recycling unit, which serves as the carrier medium to remove the discharge product (LiOH) and prevent corrosion under strong alkaline conditions. This new designed battery structure maintains galvanostatic discharge curve at 0.5 mA cm^{-2} for one week with a voltage plateau near 2.8 V and a high discharge capacity of about 19,000 mAh g^{-1} (mass including carbon, catalyst and binder).

A recent study by Chen et al. (2013) reported the first time of a high-rate rechargeable Li-air flow battery [34]. It consists of a lithium-ion conducting glass-ceramic membrane sandwiched by a lithium anode in an organic electrolyte and a carbon nanoform cathode through which oxygen-saturated aqueous electrolyte flows. The oxygen was bubbled separately in the electrolyte recycling unit to replenish its saturation before the electrolyte was circulated back to the electrochemical reaction unit to supply sufficient oxygen for high power output. The main advantage of the new design of Li-air flow batteries compared to conventional Li-air batteries is that oxygen is supplied from the aqueous electrolyte solution instead of diffusing from the window of the porous cathode. Hence, the battery performance is not limited by the oxygen's diffusion along the cathode thickness any more. A Li-air flow shows a high capacity of 5 mA cm^{-2} and gives a power density of 7.64 mW cm^{-2} at a constant discharge current density of 4 mA cm^{-2}.

Therefore, it is interesting to develop the cathode structure of the present Li-air battery model into a flow battery system. The domain boundary that considers the Li-air flow battery in the two-dimensional model is shown as the dotted line in Figure 4-15. Thus, the flow battery model was operated in a two-dimensional system. To enable the flow system, a mathematical model which includes the convection term of oxygen concentration has been proposed to develop a continuous flow into the porous cathode in the direction of the y-axis and flow out at the bottom of the porous cathode as shown in Figure 4-15. The model assumed that the flow of electrolyte affected only the oxygen species in the Li-air flow system.

Thus, the flow of saturated oxygen electrolyte maintains a uniform concentration of oxygen throughout the entry cathode electrode during the discharging battery. Therefore, the flux equation for oxygen mass transport expressed in Eq. (4-7) was modified to include the convection term as follows:

$$\boldsymbol{N_{O_2}} = -D_{O_2,eff}\nabla c_{O_2} + \boldsymbol{v}_y c_{O_2} \quad (4\text{-}27)$$

where v_y is the superficial velocity in y-axis direction which corresponds to superficial volume averages over a unit volume of the cathode electrode including both pores and matrix. This velocity is defined as volume flow rates per unit cross section of the electrode. Thus, to keep a constant oxygen concentration over the entire cell, the electrolyte was assumed to flow into the porous electrode on the y-axis direction at very low flow rate as 0.05 cm s^{-1}. As a result, the system can simply be assumed to have a laminar flow and an average constant concentration of oxygen.

Moreover, the circulated electrolyte in the flow battery model was used as the organic electrolyte in a way which was different from the published papers which used an aqueous electrolyte [32, 34]. This flow model also assumed that the discharge products were removed immediately after the oxygen reduction reaction with the flow of electrolyte, i.e. the concentration of discharge products was lower than their saturated concentration and thus there was no accumulation of the solid discharge products inside the pores of the cathode. To compare the battery's performance between the flooded electrode and flow battery, the same model parameters as presented in previous section were applied to the flow battery. The biggest difference is that the saturated oxygen was circulated in the direction of the y-axis instead of accessing it from the atmosphere.

With the same other parameters as presented in this chapter, the voltage-capacity curve on discharge at a rate of 0.1 mA cm^{-2} obtained from the Li-air model of the flooded electrode (without convection term) and the flow battery electrode can be compared in Figure 4-16. It is apparent that the flow electrode demonstrates a substantial increase in specific capacity for more than 1,000 mAh g_{carbon}^{-1} (discharged time equal to 19 days). Moreover, the discharge voltage plateau also increases for the new proposed type of electrode about 110 mV due to the steady distribution of oxygen concentration inside the cathode electrode compared to the diffusion-limited oxygen in flooded electrode (provided capacity only 722 mAh g_{carbon}^{-1}).

The solid discharge products (Li_2O_2 and Li_2CO_3) are the major factor that limits the discharge capacity of the Li-air with the flooded electrode. Without the accumulation of these products, the surface area of the cathode can repeatedly perform the electrochemical reaction, and there are no voltage and active surface losses from the

solid resistivity and passivation, respectively. As can be seen from the discharge curve of flooded electrode in Figure 4-16, the discharge voltage gradually drops from 2.73 V to 2.58 V during discharge and reaches the voltage of 2.4 at the end of discharge due to the mass transport limitation. In contrast to the flow electrode, the discharge curve remains steady due to no accumulation of solid inside the porous cathode. Moreover, it is apparent that the developed flow electrode battery can provide the everlasting discharge capacity as long as the continuous supply of the oxygen through the porous cathode.

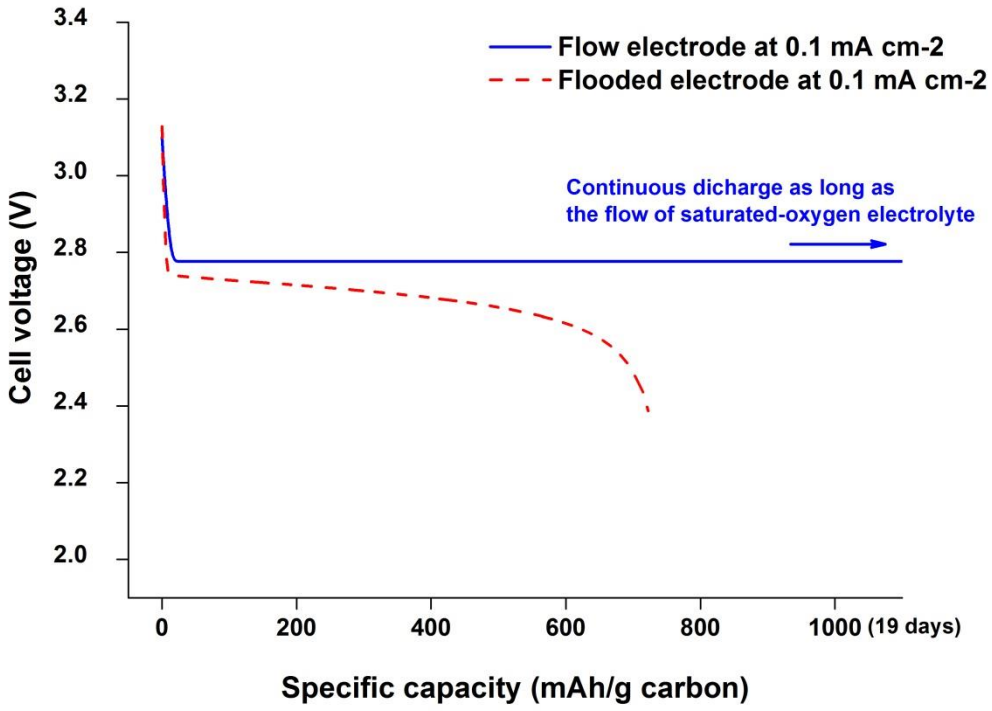

Figure 4-16: Voltage-capacity curve on discharge for a non-aqueous Li-air battery compared between the flow electrode and flooded electrode battery at a rate of 0.1 mA cm^{-2}. The electrolyte contains 1 M $LiPF_6$ dissolved in an organic solvent. The cathode electrode thickness is 750 μm with a porosity of 0.73.

The voltage-capacity curves on discharge at various discharge current densities obtained from the model of Li-air flow battery are presented in Figure 4-17. It is apparent that the flow battery can operate at a high current density and maintain the discharge performance for more than 17 days at all discharge rates. With the increase of applied current density, the discharge voltage linearly decreases. The operating voltage is maintained at 2.77 V at the low current density of 0.1 mA cm^{-2}, and even at the high current density of 4 mA cm^{-2}, the discharge voltage still keeps steady at 1.67 V. In

contrast to the case of a flooded electrode, the highest discharge current density was only 1 mA cm^{-2} with the discharge capacity at 200 mAh g_{carbon}^{-1}, as presented in Figure 4-7.

Figure 4-18 clearly presents a linear decrease in the discharge voltage with the growth of applied current densities, while the power density sharply increases with the current density. The performances of the Li-air flow battery model follow the same trend of Chen et al. (2013) [34]. In their work, the acid electrolyte was flowed into the cathode electrode and showed that the discharge voltage decreased from 3.2 V at a current density of 1 mA cm^{-2} to 1.5 V at a high current density of 5 mA cm^{-2}, and a Li-air flow battery provided the maximal power density of 7.46 mW cm^{-2} at the current density of 4 mA cm^{-2} [34]. The difference in the flow battery performances between this model and their work results from the different electrolytes supplied to the cathode electrode, leading to the difference in standard cell potential (2.96 V in organic electrolyte and 4.26 V in acid electrolyte).

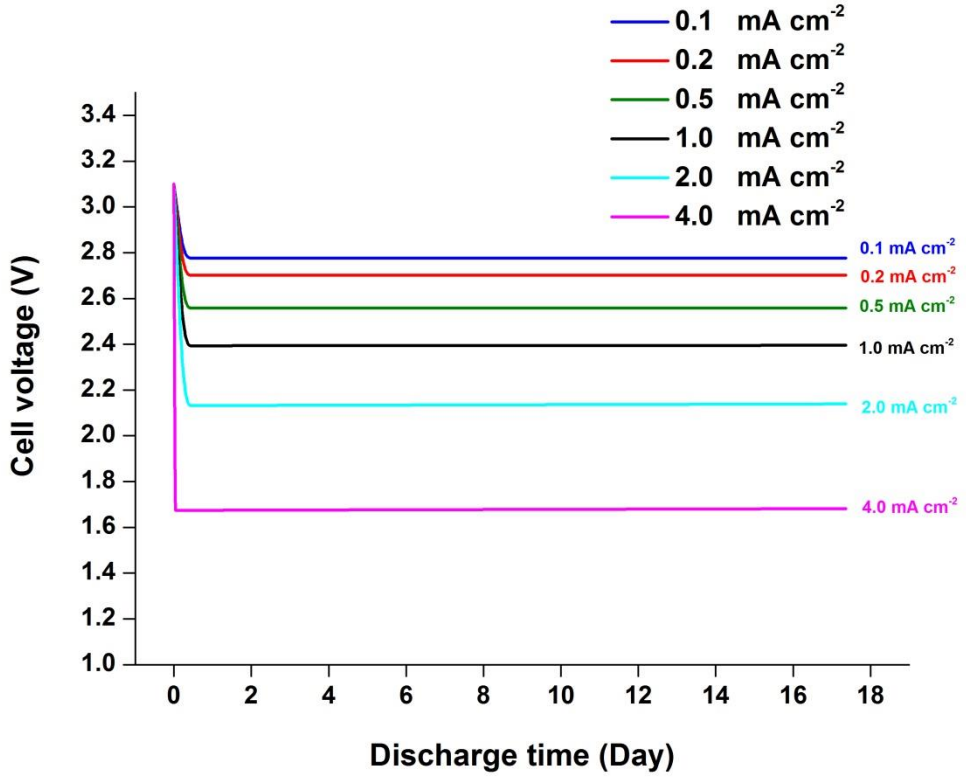

Figure 4-17: Comparison of the voltage-capacity curves on discharge for a non-aqueous Li-air flow battery at different current densities. The electrolyte contains 1 M $LiPF_6$ dissolved in organic solvent. The cathode electrode thickness is 750 μm with a porosity of 0.73.

This clearly shows that the new developed structure of the Li-air battery integrated with an electrochemical reaction unit and an electrolyte recycling unit provides a continuous reduction of inexhaustible oxygen supplied from the recycling unit. This design not only delivers a steady discharge voltage, but also allows the Li-air to operate at the high current densities. Meanwhile, the Li-air flow battery has the potential to deliver a high capacity and energy. In view of the model results, the developed Li-air flow battery could be a promising alternative battery structure for an energy source.

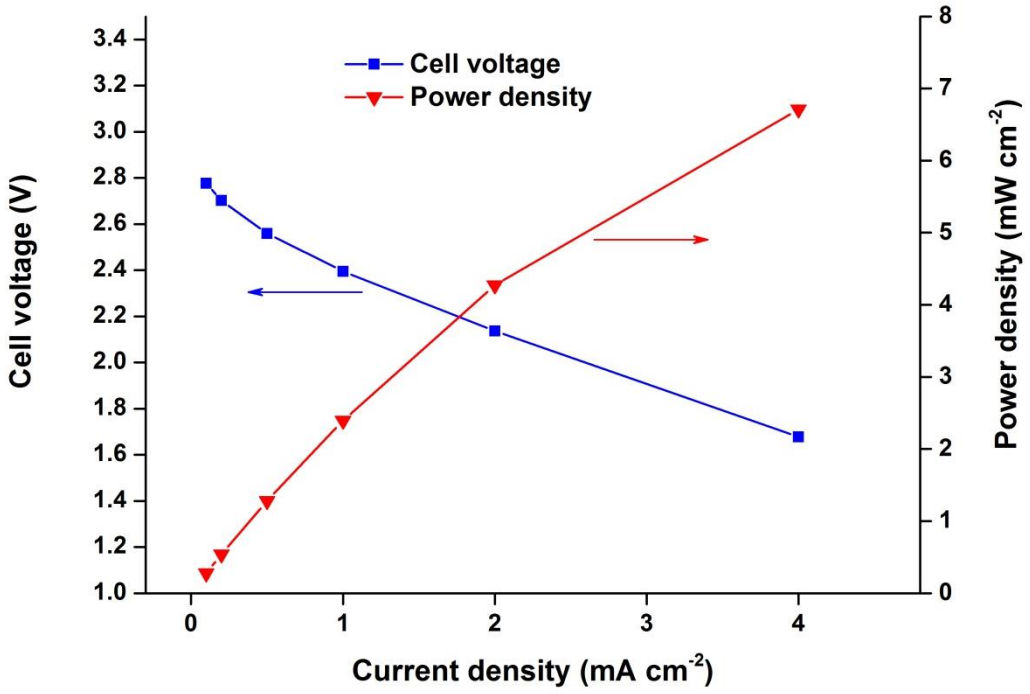

Figure 4-18: The power performance for a non-aqueous Li-air flow battery at different current densities. The electrolyte contains 1 M $LiPF_6$ dissolved in organic solvent. The cathode electrode thickness is 750 μm with a porosity of 0.73.

However, the flow battery model in this study was based on the simplistic assumptions without considering the practical behaviour. The Li-air flow model presented above only investigated the main mechanisms of the real Li-air flow system. The following aspects are not included in the flow model:

i. The metallic lithium is consumed during the continuous discharge and at the high current density. Its thickness could reduce with the battery's operation and this leads to the cell's termination.
ii. The ohmic resistance of the lithium ion separator, which is a lithium-ion conducting glass-ceramic membrane, was reported as the predominant resistance (90 Ω m^2) in the Li-air flow battery [34]. The flow battery system

needs the thick membrane to prevent the crossover of species and provide a stable separator.

iii. The electrolyte regeneration rate of oxygen should be balanced to the oxygen reduction rate at cathode electrode of the Li-air battery. In this case, the volume of the electrolyte storage unit could be varied according to the energy output requirements so that the recycling unit has enough time to replenish the oxygen concentration.

Clearly, the above aspects need to be investigated in the future for the development of the Li-air flow battery to create model results which are close to producing a practical Li-air flow system.

4.5 Conclusion

A micro-macro homogeneous one-dimensional model has been developed for the rechargeable Li-air battery using a concentrated binary electrolyte theory. The model successfully predicts the effects of an applied current density, solubility limits for both oxygen and Li_2O_2, a high degree of Li_2O_2 accumulation and the influence of the cathode structure. This model considers the time dependence and space dependence of the battery system and also includes the mass transport along the depth of the cell and the local mass transfer between Li_2O_2 layers and active surface morphology changing with the Li_2O_2 growth. The simulated cell potential for discharging is around 2.5-2.7 V and charging at around 4 V, which are in line with the experimental data. The nominal discharge capacity based on weight of carbon alone at 0.1 mA cm^{-2} is about 722 mAh g_{carbon}^{-1}, which is in agreement with the experimental observation. Increasing the solubility limit of oxygen enhances the discharge capacity and also increases the cell discharge potential, but does not affect the charge potential. Improving the solubility of Li_2O_2 in the electrolyte can reduce the charging voltage but has little effect on the cell capacity. The present model can predict the potential and capacity of the battery and correlates the battery performance to parameters of reaction species and cathode structures with reasonable accuracy.

Moreover, the new developed structure of a Li-air flow battery integrated with an electrochemical reaction unit and an electrolyte recycling unit can continuously deliver the discharge capacity from inexhaustible oxygen supplied from the recycling unit. This could be a promising alternative battery structure for the energy storage device.

4.6 References

1. Abraham, K.M. and Z. Jiang, *A polymer electrolyte-based rechargeable lithium/oxygen battery*. Journal of the Electrochemical Society, 1996. **143**(1): p. 1-5.
2. Ogasawara, T., A. Débart, M. Holzapfel, P. Novák and P.G. Bruce, *Rechargeable Li_2O_2 electrode for lithium batteries.* Journal of the American Chemical Society, 2006. **128**(4): p. 1390-1393.
3. Kuboki, T., T. Okuyama, T. Ohsaki and N. Takami, *Lithium-air batteries using hydrophobic room temperature ionic liquid electrolyte.* Journal of Power Sources, 2005. **146**(1-2): p. 766-769.
4. Zhang, J.G., D. Wang, W. Xu, J. Xiao and R.E. Williford, *Ambient operation of Li/Air batteries.* Journal of Power Sources, 2010. **195**(13): p. 4332-4337.
5. Laoire, C.O., S. Mukerjee, K.M. Abraham, E.J. Plichta and M.A. Hendrickson, *Influence of nonaqueous solvents on the electrochemistry of oxygen in the rechargeable lithium-air battery.* Journal of Physical Chemistry C, 2010. **114**(19): p. 9178-9186.
6. Cheng, H. and K. Scott, *Carbon-supported manganese oxide nanocatalysts for rechargeable lithium-air batteries.* Journal of Power Sources, 2010. **195**(5): p. 1370-1374.
7. Read, J., *Characterization of the lithium/oxygen organic electrolyte battery.* Journal of the Electrochemical Society, 2002. **149**(9): p. A1190-A1195.
8. Peng, Z., et al., *Oxygen reactions in a non-aqueous Li^+ electrolyte.* Angewandte Chemie - International Edition, 2011. **50**(28): p. 6351-6355.
9. Debart, A., A.J. Paterson, J. Bao and P.G. Bruce, *a-MnO_2 nanowires: A catalyst for the O_2 electrode in rechargeable lithium batteries.* Angewandte Chemie - International Edition, 2008. **47**(24): p. 4521-4524.
10. Zhang, S.S., D. Foster and J. Read, *Discharge characteristic of a non-aqueous electrolyte Li/O_2 battery.* Journal of Power Sources, 2010. **195**(4): p. 1235-1240.
11. Read, J., K. Mutolo, M. Ervin, W. Behl, J. Wolfenstine, A. Driedger and D. Foster, *Oxygen Transport Properties of Organic Electrolytes and Performance of Lithium/Oxygen Battery.* Journal of the Electrochemical Society, 2003. **150**(10): p. A1351-A1356.
12. Newman, J. and W. Tiedemann, *Porous-Electrode Theory with Battery Applications.* AIChE Journal, 1975. **21**(1): p. 25-41.

13. Wang, C.Y., W.B. Gu and B.Y. Liaw, *Micro-macroscopic coupled modeling of batteries and fuel cells: I. Model development.* Journal of the Electrochemical Society, 1998. **145**(10): p. 3407-3417.
14. Sandhu, S., J. Fellner and G. Brutchen, *Diffusion-limited model for a lithium/air battery with an organic electrolyte.* Journal of Power Sources, 2007. **164**(1): p. 365-371.
15. Andrei, P., J.P. Zheng, M. Hendrickson and E.J. Plichta, *Some possible approaches for improving the energy density of Li-air batteries.* Journal of the Electrochemical Society, 2010. **157**(12).
16. Albertus, P., G. Girishkumar, B. McCloskey, R.S. Sánchez-Carrera, B. Kozinsky, J. Christensen and A.C. Luntz, *Identifying capacity limitations in the Li/oxygen battery using experiments and modeling.* Journal of the Electrochemical Society, 2011. **158**(3): p. A343-A351.
17. Zhang, X., et al., *A simple method of making a Li-air battery with longevity.* International Journal of Electrochemical Science, 2012. **7**(11): p. 10562-10569.
18. Debart, A., J. Bao, G. Armstrong and P.G. Bruce, *An O_2 cathode for rechargeable lithium batteries: The effect of a catalyst.* Journal of Power Sources, 2007. **174**(2): p. 1177-1182.
19. Viswanathan, V., K.S. Thygesen, J.S. Hummelshøj, J.K. Nørskov, G. Girishkumar, B.D. McCloskey and A.C. Luntz, *Electrical conductivity in Li_2O_2 and its role in determining capacity limitations in non-aqueous Li-O_2 batteries.* The Journal of Chemical Physics, 2011. **135**(21): p. -.
20. McCloskey, B.D., A. Speidel, R. Scheffler, D.C. Miller, V. Viswanathan, J.S. Hummelshøj, J.K. Nørskov and A.C. Luntz, *Twin Problems of Interfacial Carbonate Formation in Nonaqueous Li–O_2 Batteries.* The Journal of Physical Chemistry Letters, 2012. **3**(8): p. 997-1001.
21. Cheng, H. and K. Scott, *Selection of oxygen reduction catalysts for rechargeable lithium-air batteries-Metal or oxide?* Applied Catalysis B: Environmental, 2011. **108-109**: p. 140-151.
22. Xiao, J., D. Wang, W. Xu, R.E. Williford, J. Liu and J.G. Zhang, *Optimization of air electrode for Li/air batteries.* Journal of the Electrochemical Society, 2010. **157**(4): p. A487-A492.
23. Zhang, S.S., K. Xu and J. Read, *A non-aqueous electrolyte for the operation of Li/air battery in ambient environment.* Journal of Power Sources, 2011. **196**(8): p. 3906-3910.

24. Lu, Y.-C., D.G. Kwabi, K.P.C. Yao, J.R. Harding, J. Zhou, L. Zuin and Y. Shao-Horn, *The discharge rate capability of rechargeable Li-O_2 batteries.* Energy & Environmental Science, 2011. **4**(8): p. 2999-3007.
25. Xie, B., H.S. Lee, H. Li, X.Q. Yang, J. McBreen and L.Q. Chen, *New electrolytes using Li_2O or Li_2O_2 oxides and tris(pentafluorophenyl) borane as boron based anion receptor for lithium batteries.* Electrochemistry Communications, 2008. **10**(8): p. 1195-1197.
26. Lu, Y.C., H.A. Gasteiger, M.C. Parent, V. Chiloyan and Y. Shao-Horn, *The influence of catalysts on discharge and charge voltages of rechargeable Li-oxygen batteries.* Electrochemical and Solid-State Letters, 2010. **13**(6): p. A69-A72.
27. Ominde, N., N. Bartlett, X.Q. Yang and D. Qu, *The effect of oxygen reduction on activated carbon electrodes loaded with manganese dioxide catalyst.* Journal of Power Sources, 2008. **185**(2): p. 747-753.
28. Tran, C., X.Q. Yang and D. Qu, *Investigation of the gas-diffusion-electrode used as lithium/air cathode in non-aqueous electrolyte and the importance of carbon material porosity.* Journal of Power Sources, 2010. **195**(7): p. 2057-2063.
29. Yang, X.h., P. He and Y.y. Xia, *Preparation of mesocellular carbon foam and its application for lithium/oxygen battery.* Electrochemistry Communications, 2009. **11**(6): p. 1127-1130.
30. Yang, X.H. and Y.Y. Xia, *The effect of oxygen pressures on the electrochemical profile of lithium/oxygen battery.* Journal of Solid State Electrochemistry, 2010. **14**(1): p. 109-114.
31. Chagnes, A., B. Carré, P. Willmann and D. Lemordant, *Modeling viscosity and conductivity of lithium salts in γ-butyrolactone.* Journal of Power Sources, 2002. **109**(1): p. 203-213.
32. He, P., Y. Wang and H. Zhou, *A Li-air fuel cell with recycle aqueous electrolyte for improved stability.* Electrochemistry Communications, 2010. **12**(12): p. 1686-1689.
33. Wang, Y., P. He and H. Zhou, *Li-Redox Flow Batteries Based on Hybrid Electrolytes: At the Cross Road between Li-ion and Redox Flow Batteries.* Advanced Energy Materials, 2012. **2**(7): p. 770-779.
34. Chen, X.J., A. Shellikeri, Q. Wu, J.P. Zheng, M. Hendrickson and E.J. Plichta, *A high-rate rechargeable Li-air flow battery.* Journal of the Electrochemical Society, 2013. **160**(10): p. A1619-A1623.

35. Wang, Y. and H. Zhou, *A lithium-air battery with a potential to continuously reduce O_2 from air for delivering energy*. Journal of Power Sources, 2010. **195**(1): p. 358-361.

Chapter 5: Modelling of Electrolyte Degradation and Cycling Behaviour in a Li-air Battery

In this Chapter, a micro-macro homogeneous model was developed to understand the continuous deterioration of cycle performance and energy efficiency related with non-aqueous rechargeable Li-air batteries. This includes the practical feature of Li_2CO_3 formation which occurs by electrolyte degradation during battery cycling. Discharge products such as Li_2O_2 and Li_2CO_3, formed in various non-aqueous electrolytes can limit the cyclability and passivate the surface of the porous cathode. This model followed the same structure of the micro-macro homogeneous model discussed in Chapter 4. The main differences were the addition of electrolyte degradation and product formation of Li_2CO_3. With this model it was possible to create a more practical computational model for Li-air batteries in organic solvents. This model can be used to describe the behaviour of Li-air batteries as well as to optimise the performance and structure of these battery electrodes.

5.1 Introduction

The advantages in using non-aqueous systems are to avoid the problem of H_2 evolution due to the reaction of lithium with water and prevent lithium metal corrosion [1]. For the non-aqueous system, the desired reactions during discharge process for Li-air batteries is the formation of lithium peroxide (Li_2O_2) from the oxygen reduction reaction with lithium ions (Li^+) from the oxidation reaction at the anode according to following reactions

Anode $$Li \rightleftharpoons Li^+ + e^- \qquad (E^0 = 0.00\, V_{Li}) \tag{5-1}$$

Cathode $$2Li^+ + O_2 + 2e^- \rightleftharpoons Li_2O_2 \qquad (E^0 = 2.96\, V_{Li}) \tag{5-2}$$

Previous studies have identified Li_2O_2 as the main reaction product in the pores of cathode after battery discharging, with the process being reversible on charge [2-6]. Up to now, there have been various proposed different mechanisms for oxygen reduction reaction (ORR) with Li^+ electrolytes depending on the type of electrolyte, catalyst and battery operating conditions.

A recent in-situ spectroscopic study of oxygen reaction in non-aqueous electrolyte by Peng et al. reported strong evidence that lithium superoxide (LiO_2) is indeed an intermediate species during oxygen reduction before disproportion to the final Li_2O_2 product [7]. On charge the Li_2O_2 is directly oxidised into oxygen and Li^+ without going through the intermediate LiO_2 route. However, the reversibility of Li-air batteries is still far for being ideal for use as energy storages because of the formation of many non-desired products in the porous cathode. It has been demonstrated that these different discharge products strongly depend on the kinetics of the oxygen reduction, which is affected by the presence of a catalyst as well [3, 8, 9], and also by the type of electrolytes and solvents used in the Li-air batteries [10-15]. Generally, the electrolytes frequently used in these Li-air batteries are based on organic carbonate-based solvent owing to their success in Li-ion batteries.

Organic carbonate-based electrolytes (e.g., $LiPF_6$ in propylene carbonate, (PC) or ethylene carbonate (EC)) have been widely used in Li-air batteries [3, 4, 6, 12, 16-18]. However, recently it has been demonstrated that the cycle life of Li-air battery using carbonate-based electrolyte is mainly limited by the electrolyte decomposition between oxygen and electrolyte. This mechanism forms irreversible organic and inorganic carbonate species, such as lithium alkylcarbonates and Li_2CO_3 during discharging, rather than the desired Li_2O_2 which can reversibly produce oxygen on charging [12, 15, 19-22]. Different characterization techniques have supported identification of these discharge by-products formed by reduction of carbonate-based solvent molecules that react with superoxide radical anions ($O_2^{\cdot-}$) generated from single-electron reduction of oxygen [12, 14]. Therefore, a more stable electrolyte that does not produce the irreversible by-product formation during the cell operation is required for a truly reversible Li-air battery.

Ether-based electrolytes are now attractive for the Li-air battery because of this compatibility with lithium anodes, more stable to oxidation potentials than organic carbonate solvent, safe and low volatility [11, 14]. Bruce and co-workers investigated the ether-based Li-air battery and demonstrated that the Li_2O_2 formed on first discharge and disappeared after 5 cycles [11]. However, they also found that even ether electrolytes decompose to give a mixture of Li_2CO_3, lithium formate (HCO_2Li), lithium

acetate (CH_3CO_2Li), CO_2 and H_2O, and these discharge by-products accumulate inside the electrode with further battery cycling. The stability test on the discharge products in Li-O_2 battery using the different types of organic solvents (e.g. glyme-based ether, carbonates, sulfoxides, phosphates, nitriles and ionic liquid) has been reported by Xu et al. [14]. By using various analyzed techniques, a large amount of Li_2O_2 was found in the discharged air electrode in glyme-based electrolytes (glymes are generally known as poly(ethylene glycol)dimethyl ethers)); however, Li_2CO_3 was also clearly detected in all the electrodes during discharge from all electrolytes studied with different solvents [14].

Moreover, a recent study by the same group [22] demonstrated that the formation of Li_2CO_3 on the active electrode surface cannot be reversed during the charging step up to 4.5 V which is higher than the reported charging voltage for Li-air battery (normal charge voltage up to 4.0 V). Therefore, Li_2CO_3 may be formed inside the porous cathode, regardless of most solvents used to date, and deteriorate the battery efficiency and short battery cycle life (i.e. Li-air battery cannot fully rechargeable for long cyclability).

In Chapter 4, a model of the cycling behaviour of Li-air batteries [23] did not take into account the electrolyte degradation behaviour. In this Chapter, a modified version for the Li-air model included the parasitic reactions, considering the irreversible Li_2CO_3 as the main by-product. The model predicted the time dependence of electrolyte concentration, non-uniform porosity and reaction rates. Although other by-products besides Li_2CO_3 are formed during electrolyte decomposition, their quantities may be considered as insignificant relative to the Li_2CO_3. During discharging, the desired Li_2O_2 and irreversible Li_2CO_3 form and coexist on the active surface of carbon electrode. The results from gases analysis by mass spectrometry showed that CO_2, which could be considered as the active material to cause the Li_2CO_3 formation, are generated on discharge for both carbonate and ether based solvents, as described by Bruce group [11, 12]. The mechanisms for Li_2CO_3 formation are presented in the next section.

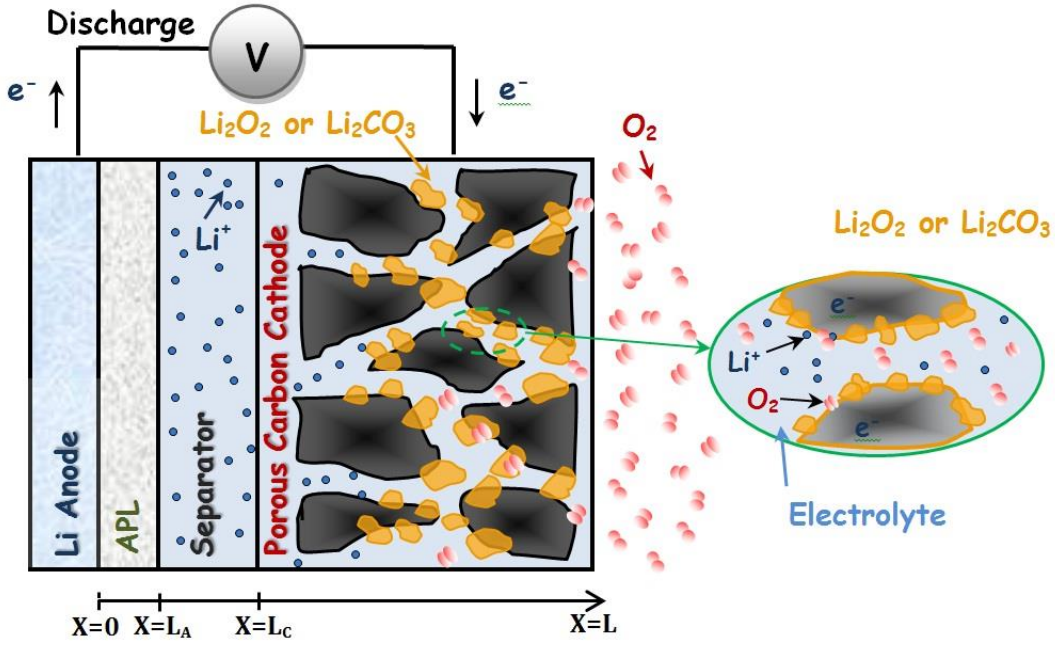

Figure 5-1 Schematic computation domain of a Li-air battery during discharge operation. The inset demonstrates the discharge products formation of Li_2O_2 and Li_2CO_3 covering on the porous carbon surface.

5.2 Theoretical Mechanism Analysis

The Li-air battery as shown in Figure 5-1 contains a metallic lithium anode, a separator containing electrolyte, and a porous carbon or catalyst-loaded carbon air electrode filled with an organic electrolyte comprising a dissolve lithium salt in an aprotic solvent. The Li^+ transport through the separator to the porous cathode. The produced electrons are conducted through the external circuit towards the active cathode, where the charge transfer reduction reaction takes place with the combination of Li^+ and oxygen to form lithium oxides or Li-based compounds depending on the types of electrolyte used and the electrochemical reaction occurred in the Li-air system. As mentioned earlier, the battery electrolytes play an important role in defining whether the cathode can provide the desired electrochemical products. However, to simplify our model simulation, Li_2O_2 is the main discharged product depositing inside the porous of Li-air battery following Eq. (5-2) when using several non-aqueous electrolytes, e.g. organic carbonate-based or ether-based solvent. Moreover, the Li_2CO_3 formation, formed during the electrolyte degradation, is also considered as the main by-product coexisting with Li_2O_2.

The exact detail of the reaction routes at the cathode can be complicated due to the formation of intermediates. It has been identified that the nucleophilic attack of

superoxide on the O-alkyl carbon group of the electrolyte is a usual starting mechanism for decomposition of organic carbonates, alkyl carboxylates, and alkyl esters of moderately strong inorganic acids [24]. Hence, it is possible to propose a mechanism to describe the formation reaction of Li_2CO_3. This can be divided into two reaction mechanisms: (1) Li_2CO_3 formation from the reaction of superoxide with carbon dioxide in mechanism 1, as described previously [11, 25, 26]; (2) the Li_2CO_3 occurs from the electrochemical reduction of CO_2, due to the electrolyte degradation with CO_2 as shown in mechanism 2, which was similar to the proposed salts formation in the solid electrolyte interface (SEI) film in Li-ion batteries [27, 28]

- ***Mechanism 1:***

$$2O_2 + 2e^- \xrightarrow{k1a} 2O_2^- \qquad (E^0 = 3.18\, V_{Li}) \qquad (5\text{-}3)$$

$$2O_2^- + 2CO_2 \xrightarrow{k1b} C_2O_6^{2-} + O_2 \qquad \text{RDS} \qquad (5\text{-}4)$$

$$C_2O_6^{2-} + 4Li^+ + 2O_2^- \rightarrow 2Li_2CO_3 + 2O_2 \qquad (5\text{-}5)$$

Overall $4Li^+ + 2CO_2 + 2O_2^- + 2e^- \rightarrow 2Li_2CO_3 + O_2 \qquad (E^0 = 7.19\, V_{Li}) \qquad (5\text{-}6)$

- ***Mechanism 2:***

$$CO_2 + e^- \xrightarrow{k2a} CO_2^- \qquad (5\text{-}7)$$

$$CO_2^- + CO_2 + e^- \xrightarrow{k2b} CO + {CO_3}^{2-} \qquad \text{RDS} \qquad (5\text{-}8)$$

$$2Li^+ + {CO_3}^{2-} \rightarrow Li_2CO_3 \qquad (5\text{-}9)$$

Overall $2Li^+ + 2CO_2 + 2e^- \rightarrow Li_2CO_3 + CO \qquad (E^0 = 2.49\, V_{Li}) \qquad (5\text{-}10)$

- ***Solvent degradation***

$$O_2 + e^- \xrightarrow{k1a} O_2^- \qquad (E^0 = 3.18\, V_{Li}) \qquad (5\text{-}11)$$

$$O_2^- + [Solvent] \rightarrow [Solvent]^- \qquad (5\text{-}12)$$

$$[Solvent]^- + O_2 \rightarrow CO_2 + H_2O + HCO_2Li + CH_3CO_2Li \qquad (5\text{-}13)$$

Overall $2O_2 + [Solvent] + e^- \rightarrow CO_2 + H_2O + HCO_2Li + CH_3CO_2Li \qquad (5\text{-}14)$

Mechanism 1 commences with oxygen reduction in the porous cathode to form O_2^- in Eq. (5-3) which can either react with CO_2 (produced from the solvent degradation with

O_2 described below) to generate the peroxydicarbonate anion $C_2O_6^{2-}$ and then Li_2CO_3 (Eq. (5-4) and (5-5)) or may react directly with solvent in both carbonate and ether based electrolyte, in turn, leading to the intermediate species of peroxoradical and the ether peroxide (combined together as $[Solvent]^-$ in Eq. (5-12)), respectively [11, 12]. These intermediate species can readily undergo, in the presence O_2, oxidative decomposition reactions (Eq. (5-13)), which are analogous to combustion reactions, leading to the formation of H_2O and CO_2 [29-31]. The oxidative decomposition also produces lithium formate and lithium acetate products (Eq. (5-14)) which are not considered here in the model.

Mechanism 2 deals with the reduction of CO_2 in non-aqueous solvents which has been extensively studied, because CO_2 has a greater solubility in non-aqueous media than in water and is used as material feed to produce more valuable organic compounds, such as methane, ethane, ethylene, methanol etc., [32]. The CO_2 reactant in this mechanism is also generated from the electrolyte degradation described above. There are many mechanism routes for reduction of CO_2 depending on cathode metals and solvents used [32]. However, one of the main reaction products are CO_3^{2-} and CO as described in Eq. (5-8) which can be created from the reduction of CO_2^- intermediate species [28, 32]. Hence, in the presence of Li^+, the $LiCO_3$ could be formed following the route in mechanism 2 which is considered in the model.

With the use of organic solvent for electrolyte, both Li_2O_2 and Li_2CO_3 can be produced as discharged products and are usually insoluble in the cell electrolyte. As a result, the repeated depositing film of different lithium salts over the carbon surface after each discharge and charge step prevents species transport and the electrochemical reaction, and diminishes the electronic conductivity of the air electrode and electrolyte concentration leading to cell voltage loss [20].

5.3 Model Development

5.3.1 Model description

In this Chapter, a schematic computation domain for a prismatic single cell of a Li-air battery was the same as in Chapter 4 as shown in Figure 5-1, which consists of a thin lithium sheet negative electrode, an anode protective layer (APL), a separator, and a porous carbon oxygen cathode filled with an organic electrolyte. Current collectors are

placed at the back of each electrode. The electrolytic solution was considered as a concentrated binary electrolyte to describe the motion for of each species in the systems.

The main difference in this model was the addition of electrolyte degradation effects to form Li_2CO_3 together with Li_2O_2 as the solid products inside the porous cathode. Hence, the governing equations and assumptions for the model in this Chapter are similar to that in Chapter 4 except the kinetic reactions and product formation. As in Chapter 3 the rate expression at the porous cathode was described only the formation of Li_2O_2, the kinetic expressions for the other reactions are explained in more details in section 5.3.5.

5.3.2 Model assumption

In the same way of the Li-air model in Chapter 4, in this particular model the following assumptions were used in this model

i. The Li-air cell is operated under isothermal conditions so that the thermal effects are not considered
ii. The lithium salts of Li_2O_2 and Li_2CO_3 are the main discharge products which only occur and deposit inside the porous cathode.
iii. The electrolytes used in Li-air batteries are assumed a binary monovalent electrolyte which consists of a single salt in a homogeneous organic solvent mixture.
iv. The electrolyte behaviour is based on concentrated solution theory to simulate the Li^+ diffusion.
v. The pores in the cathode are full of liquid phase electrolyte such as a solution of lithium hexafluorophosphate ($LiPF_6$) in a non-aqueous solvent.
vi. The oxygen is assumed to dissolve in the organic electrolyte with a saturated initial concentration.
vii. Convection for mass transport is negligible inside the cell.

Table 5-1 Governing equations used in the micro-macro homogeneous model with electrolyte degradation.

Equation description		
1. Transport of species		
Species material balance	$\frac{\partial(\varepsilon c_i)}{\partial t} = -\nabla \cdot \boldsymbol{N}_i + r_i$	(5-15)
Molar flux for Li^+	$\boldsymbol{N_{Li}} = -D_{Li,eff}\nabla c_{Li} + \frac{\boldsymbol{i}_2 t_+}{F}$	(5-16)
Molar flux for species	$\boldsymbol{N_i} = -D_{i,eff}\nabla c_i$	(5-17)
2. Conservation of charge		
Solid-phase current density	$\boldsymbol{i}_1 = -\sigma_{eff}\nabla\phi_1$	(5-18)
Liquid-phase current density	$\boldsymbol{i}_2 = -\kappa_{eff}\nabla\phi_2 - \frac{2RT\kappa_{eff}}{F}(t_+ - 1)\left(1 + \frac{\partial lnf}{\partial lnc_{Li}}\right)\nabla lnc_{Li}$	(5-19)
Charge conservation	$\nabla \cdot \boldsymbol{i}_1 + \nabla \cdot \boldsymbol{i}_2 = 0$	(5-20)
Charge transfer current density	$\nabla \cdot \boldsymbol{i}_2 = \sum_m a j_m$	(5-21)
3. Rate expression at cathode		
Butler-Volmer equation	$\frac{j_c}{nF} = k_a(c_{Li_2O_2})exp\left[\frac{(1-\beta)nF}{RT}\eta_c\right] - k_c(c_{Li^+})^2(c_{O_2})exp\left[\frac{-\beta nF}{RT}\eta_c\right]$	(5-22)
Mechanism 1, Mechanism 2 and Solvent degradation	Described in section 5.3.5	
4. Rate expression at anode		
Butler-Volmer equation	$j_a = i_0\left[exp\left(\frac{(1-\beta)nF}{RT}\eta_a\right) - exp\left(\frac{-\beta nF}{RT}\eta_a\right)\right]$	(5-23)

5.3.3 Governing equations

Having accounted for all assumptions the governing equations described in Chapter 3 could be simplified as presented in Table 5-1. The definitions and expressions of all parameters can be referred to Chapter 3. It is worth noting that the molar flux for species was replaced in Eq. (5-17) instead of oxygen due to many species (O_2, O_2^-, CO_2)

reacted inside the air electrode.

5.3.4 Boundary conditions

As there are no changes of battery geometry and operating conditions, the boundary conditions for the model with electrolyte degradation are the same as in Chapter 4 and presented in Table 5-2. The boundary conditions discussed in this section are referred to position in Figure 5-1. Apart from the initial values and parameters summarised in Table 3-4, this Chapter requires the additional parameters to solve the governing equation as presented in Table 5-3.

Table 5-2 Boundary conditions used in the micro-macro homogeneous model with electrolyte degradation.

Conservation of species	
Boundary condition are imposed for Li^+ and oxygen concentration, and for the solid and electrolyte current density $at\ x = L$:	
$c_{O_2} = S_{O_2} * c_{O_2,ext}$	(5-24)
$N_{Li} = 0$	(5-25)
$i_1 = I$	(5-26)
$i_2 = 0$	(5-27)
Boundary condition $at\ x = L_c$:	
$i_1 = 0$	(5-28)
Boundary condition $at\ x = 0$:	
$N_{O_2} = 0$	(5-29)
$c_{Li} = 1\ mol\ dm^{-3}$	(5-30)
The voltage of the cell is calculated by the difference between the electrode potential at cathode current collector and the electrolyte potential at the anode side	
$V_{cell} = \phi_1(x = L) - \phi_2(x = 0)$	(5-31)

Table 5-3 Additional parameters used in the Li-air model (SI unit)

Parameter	Value	Unit	symbol	Ref.
Electrolyte properties				
Superoxide diffusion coefficient	9 x 10^{-10}	$m^2\ s^{-1}$	$D_{O_2^-}$	[5]
Carbon dioxide diffusion coefficient	1 x 10^{-9}	$m^2\ s^{-1}$	D_{CO_2}	[26]
Kinetic parameters				
Reaction rate coefficient for $\mathbf{O_2^-}$ formation	8.1 x 10^{-15}	$m\ s^{-1}$	k_{1a}	Assumed
Reaction rate coefficient for Li_2CO_3	370	$m^3\ s^{-1}$	k_{1b}	[26]
Reaction rate constant of CO_2 reduction	1 x 10^{-23}	$m\ s^{-1}$	k_1	[28]
Reaction rate constant of CO_2 reduction	4.22 x 10^{-}	$m\ s^{-1}$	k_2	[28]
Reaction rate constant of CO_2 formation	5.9 x 10^{-15}	$m\ s^{-1}$	k_{VI}	[33]

5.3.5 Rate expressions at cathode

The actual reaction paths and mechanisms for the discharge products are not available and quite complex involving various intermediates. Hence to describe the electrochemical kinetic expression for the porous cathode the model adopts the kinetic expression based on Eq. (5-2) for Li_2O_2 formation and on Eq. (5-6) and Eq. (5-10) for Li_2CO_3 formation.

Li_2O_2 formation:

For electrochemical reaction of Li_2O_2 at the cathode, a modified version of the Butler-Volmer equation is applied in the model using two rate coefficients as described in Chapter 3. The reaction for Li_2O_2 formation presented in Eq. (4-2) also depends on the concentration of Li^+ and oxygen for discharge and the concentration of Li_2O_2 during charge as in the following equation

$$\frac{j_c}{2F} = k_a\left(c_{Li_2O_2}\right)exp\left[\frac{(1-\beta)nF}{RT}\eta_m\right] - k_c(c_{Li})^2\left(c_{O_2}\right)exp\left[\frac{-\beta nF}{RT}\eta_m\right] \tag{5-32}$$

$$\eta_m = \phi_1 - \phi_2 - \Delta\phi_{film} - E_m^0 \tag{5-33}$$

$$\Delta\phi_{film} = j_m R_{film}\varepsilon_s \tag{5-34}$$

where k_a and k_c are the anodic and cathodic rate constant, respectively, β is the symmetry factor equal to 0.5, η_m is surface or activated overpotential for individual reaction, m, at the cathode, $\Delta\phi_{film}$ and R_{film} are the voltage drop and the electrical

resistivity across Li_2O_2 film formation, respectively, ε_s is the volume fraction of solid formation of discharge products of Li_2O_2 and Li_2CO_3, and E_m^0 is the theoretical open-circuit potential for each reaction. In this Chapter, R_{film} is not constant as applied in Chapter 4 but the electrical resistivity of Li_2O_2 dynamically changed with Li_2O_2 growth instead ($R_{film}= l\ exp[c_1(l - c_2)]$ in Eq. (3-48) in Chapter 3).

Li_2CO_3 formation:

As explained before, the Li_2CO_3 formation is one of the discharge by-products coexisting with Li_2O_2. Thus, the decomposition of electrolyte, which initially forms CO_2 and finally generates Li_2CO_3 as described above, occurs during Li-air operation. Some of the elementary steps in the electrolyte degradation sequences that lead to these by-products may be irreversible and non-electrochemical, so that the overall kinetic expression is very complex. Therefore, we use the kinetics for Li_2CO_3 formation of both mechanism 1 and 2 above based on the published kinetic data.

For the mechanism 1, the superoxide radical anion that is initially formed (Eq. (5-3)) during Li-air discharge as evidenced in previous study [7], attacks CO_2 which is generated from solvent decomposition (from Eq. (5-14)) to finally form Li_2CO_3 with the presence of Li^+ as follow reaction

$$j_{c1} = Fk_{1a}\left(c_{O_2}\right)\left[-exp\left(\frac{-\beta nF}{RT}\eta_m\right)\right] \tag{5-35}$$

$$r_{c1} = k_{1b}(c_{O_2^-})(c_{CO_2}) \tag{5-36}$$

where k_{1a} and k_{1b} are the rate constant for the electrochemical reaction to form O_2^- and chemical reaction to generate Li_2CO_3, respectively. We use the Tafel form in Eq. (5-35) rather than the Butler-Volmer form because the large kinetic overpotential during cell discharge puts the reaction in the Tafel region and considers only discharge (irreversible for O_2^- formation. It has been demonstrated that the chemical reaction in Eq. (5-36) is found to be first-order with to respect to both O_2^- with CO_2 reactants and is the rate determining step (RDS). Hence, the other reaction is considered as equilibrium and the formation of Li_2CO_3 can be predicted by using Eq. (5-35) and Eq. (5-36) together.

For mechanism 2, the reduction of CO_2 in non-aqueous solvent is considered for the

Li_2CO_3 formation. The kinetic for the reaction in mechanism 2 was systematically proposed by Welford and coworkers [28] and adopted for this simulation as summarised in the follow reaction

$$r_{c2} = k_{eff}(c_{CO_2}) \tag{5-37}$$

in which

$$k_{eff} = \frac{k_1}{1 + K'} exp\left[\frac{-\alpha F}{RT}\eta_m\right] \tag{5-38}$$

where

$$K' = \frac{k_1}{k_2} exp\left[\frac{-\alpha F}{RT}\eta_m\right] \tag{5-39}$$

where k_1 and k_2 are the rate constant for the electrochemical reaction for the mechanism of the reduction of CO_2 and α is the transfer coefficient which is given the value as 0.43 [28]. However, preliminary simulated results showed that the discharge product of Li_2CO_3 mostly comes from the electrochemical reaction in mechanism 1 rather than from the reduction CO_2 in mechanism 2, as demonstrated in Figure 5-2. Figure 5-2 compared the Li_2CO_3 formation between the two mechanisms in different state of battery discharge. From this data we can see that the Li_2CO_3 from the mechanism 2 (inset graph) is significantly lower (5×10^{-5} at 100% discharge state) than that produced from mechanism 1 (0.026 at the same discharge state) during the battery discharging. Hence, the main contribution for the build-up of Li_2CO_3 in this model was from the electrochemical reaction of mechanism 1. However, both mechanisms were included in this study.

Solvent degradation:

The CO_2 generation can be created from the electrolyte degradation which is first attacked by the superoxide formation as described in Eq. (5-14). Apart from this decomposition, some reports demonstrate that side reactions to form CO_2 were observed at the cathode and were attributed to carbon decomposition during charge process [14, 34]. However, only the CO_2 generated from electrolyte degradation will be considered here. Addressing this kinetic expression, because a detailed mechanism is not available, the CO_2 formation based on the overall reaction in Eq. (5-14), which consider the solvent concentration as constant is

$$j_{c3} = Fk_{VI}(c_{O_2})\left[-exp\left(\frac{-\beta nF}{RT}\eta_m\right)\right] \quad (5\text{-}40)$$

where k_{IV} is the rate constant for the electrochemical reaction to form CO_2 and the others are the same as described above.

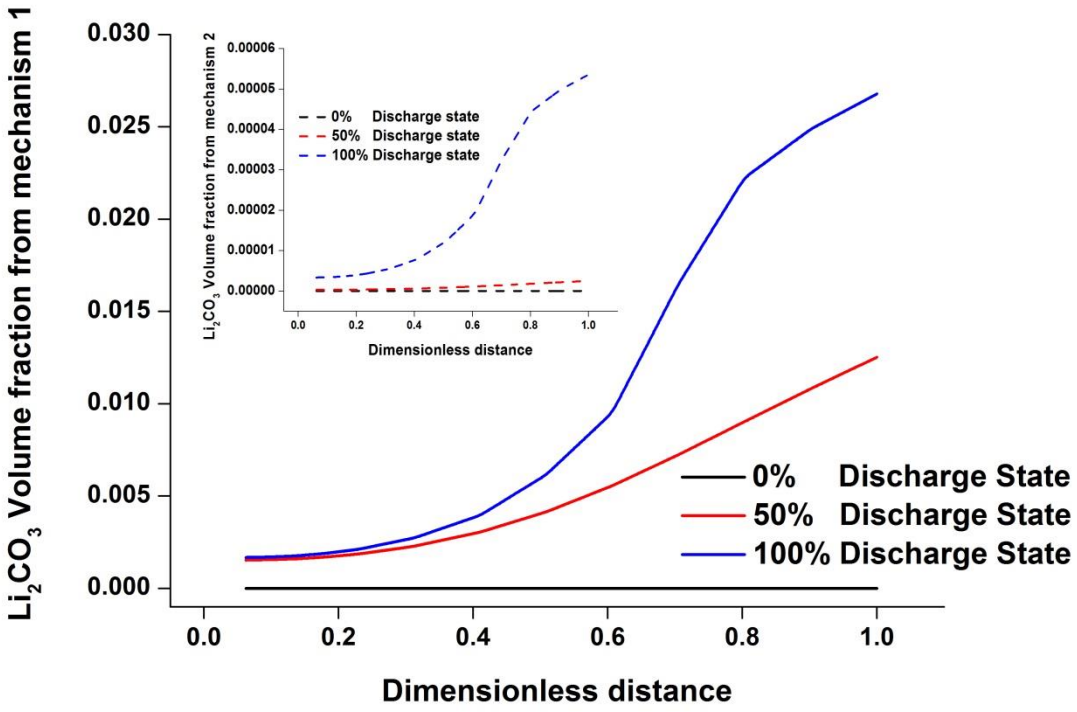

Figure 5-2 Compared the Li_2CO_3 formation from the two mechanisms. The inset shows the Li_2CO_3 volume fraction from the mechanism 2 (dotted line).

5.3.6 Solution technique

The conservation equations and the boundary conditions described above were discretized using a finite element method and solved in one-dimensional battery system by commercial software package COMSOL multiphysics version 4.3. The COMSOL software is designed to solve a set of coupled differential and algebraic equations and the battery simulation model is performed on a 32 bit Windows platform with 4 GB RAM, and Intel Core 2 Duo 2.93 GHz processor. The different transport equations and the electrochemical reactions were solved as time dependent until the cell voltage reached the stop condition. The solution were considered as converged solution when the difference between two results was less than 10^{-4} (relative tolerance) for all variables.

5.4 Results and Discussion

The one-dimensional Li-air cell model including parasitic reactions from electrolyte degradation was simulated and tested against the performance during battery cycling. As mentioned before, this model was based on previous work created in Chapter 4 and could be validated by using the experimental cycle performance obtained in our labs, due to sufficient rechargeable data. A comparison of the simulated and experimental Li-air battery cycling behaviour is shown in the next section. As can be seen from Figure 5-4, the discharge capacity from the experimental data and simulation results were in good agreement and the model predicted the typical trend of the Li_2CO_3 accumulation on cycling resulting in electrode passivation and capacity fading.

5.4.1 Cycling performance

To predict the variation of the capacity retention on cycling behaviour, the variation of voltage on discharge and charge curve for 10 cycles of a rechargeable Li-air battery in 1 M $LiPF_6$ dissolved in a non-aqueous solvent operating between 2.2 and 4.2 V vs Li/Li^+ at a rate of 0.1 mA cm^{-2} is shown in Figure 5-3. This cycling model was carried out at an operating temperature of 298.15 K in pure 1 atm of oxygen. It can be seen from the discharge and charge cycle that the cell potential began to fall steeply at the first discharge, from a voltage of 3.1 V to a plateau at around 2.7 V, and decreased continuously to 2.2 V at the end of discharge. The discharge potential during cycling was around 2.5-2.7 V which was the same as discharge voltage of Li-air batteries reported by previous research works for similar battery discharge in pure oxygen [9, 35].

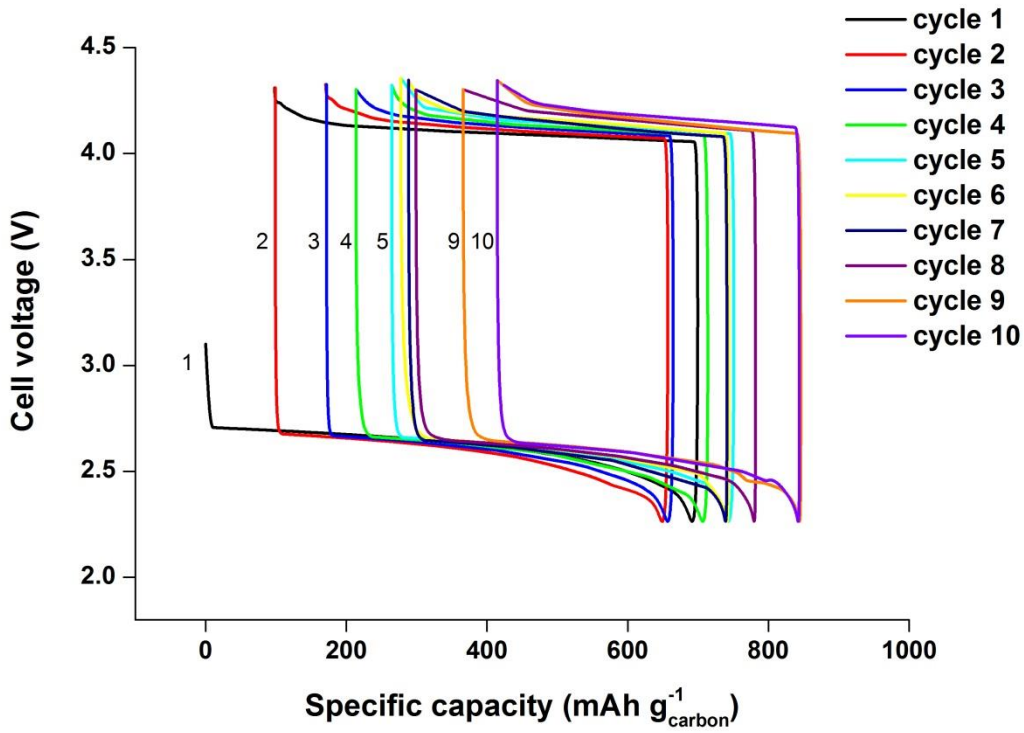

Figure 5-3 Variation of voltage-capacity curve in 10 cycles on discharge and then charge between 2.2 and 4.2 V versus Li/Li^+ for a non-aqueous Li-air battery at a rate of 0.1 mA cm^{-2}. The electrolyte contains 1 M $LiPF_6$ dissolved in acetronitrile under 1 atm of oxygen at operating temperature 298.15 Kelvin. The cathode electrode thickness is 750 μm with porosity of 0.73.

In contrast, the charge voltages increased with time around 4.0-4.25 V depending on a number of cycles. This increase in charging overpotential could be attributed to the loss of cathode active surface due to the repeated passivation from Li_2CO_3 occurred from the electrolyte degradation during discharge. It is apparent from Figure 5-3 that the reduction of capacity occurs mainly on charging, i.e. each cycle the charge capacity is lower than that during discharge step. This makes the charge/discharge efficiency less than 100% and causes the rapid capacity fading. From the data in Figure 5-3, the charge potentials move to values approximately 100-200 mV higher on cycling, whereas the average discharge potentials slightly decrease. In summary, the Li-air cell model including the Li_2CO_3 formation from electrolyte degradation exhibits the cycling ability and the continuously battery capacity fading on cycling.

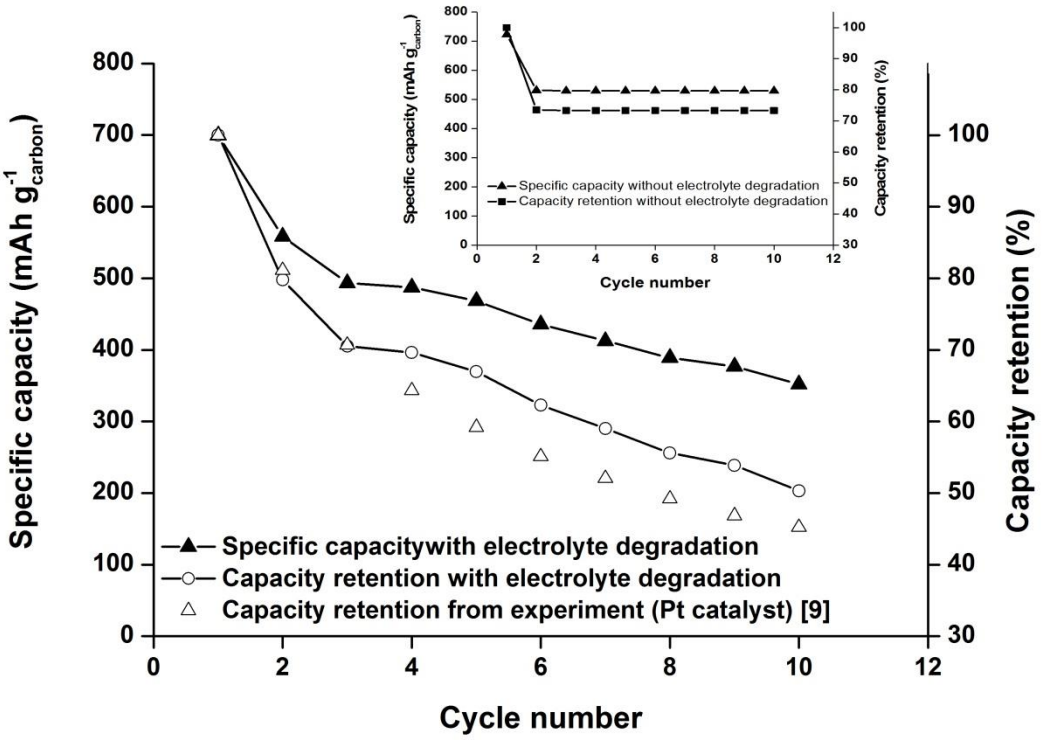

Figure 5-4 The cycle performance (discharge capacity and capacity retention against cycle number) of the 10-cycle rechargeable Li-air battery in the model that includes the Li_2CO_3 formation from the electrolyte degradation. Battery was cycled at a rate 0.1 mA cm^{-2}. The capacity retention from the model and our group experiment is also plotted for comparison. The inset shows the model without the effect of electrolyte decomposition. The other parameters used in the model are the same as described in Figure 5-3.

In practice, one of the most significant properties for battery other than its initial performance is stability which can be measured by retention of discharge capacity on cycling [2, 9, 18, 35]. Thus, for better clarity, the results obtained from the cycling behaviour of Figure 5-3 are presented in more details in term of the variation of specific capacity on discharge (capacities are expressed per gram of carbon in the electrode) and retention of capacity as shown in Figure 5-4. The discharge capacity on the first cycle using the parameters in Table 3-4 and Table 5-3 was about 700 mAh g_{carbon}^{-1}, based on the weight of carbon alone. However, on continuous discharging, the rechargeable Li-air battery is faced with performance deterioration on cycling.

The capacity of the battery fell constantly to a low value of 468 mAh g_{carbon}^{-1} after 5 cycles which can retain the capacity back to around 67%, corresponding to a capacity

retention of 13% per cycle. At the 10th cycle, the discharge capacity was even lower to 352 mAh g_{carbon}^{-1} with a capacity retention of 5% per cycle. At the 10th cycle, the discharge capacity was even lower to 352 mAh g_{carbon}^{-1} with a capacity retention of 50% (5% per cycle). The data in Figure 5-4 were summarised in Table 5-4 for better clarity. For comparison, Figure 5-4 has an inset that demonstrates the performance of a rechargeable Li-air model without any parasitic reaction form the electrolyte degradation. It can be seen that, without the side reaction, the Li-air battery can maintain its performance during cycling, but this is the ideal case for the Li-air battery and the researchers are still developing the batteries which remain stability on operation.

Table 5-4 The Li-air cycle performances on each cycle from the model including the electrolyte degradation.

Cycle No.	Specific capacity (mAh g^{-1})	Capacity retention (%)	Capacity retention per cycle (%)
1	700.00	100	100
2	558.27	79.79	40
3	493.32	70.51	23.5
4	487.26	69.64	17.5
5	468.48	66.96	13.4
6	435.79	62.28	10.4
7	412.74	58.99	8.4
8	389.02	55.60	7.0
9	376.88	53.86	6.0
10	352.04	50.31	5.0

To see if the parasitic model gave the similar results with the experimental measurements [9], the battery performance data obtained in our group experiment were plotted and compared with the model results as also shown in Figure 5-4. Because of the difference on discharge capacities acquired from the variety of Li-air cell configuration and materials (electrolyte and carbon properties), the data from the experiment could be normalised in term of the capacity retention for use as a comparison. As can be seen from Figure 5-4, the experimental results from Li-air with catalyst are similar to those from the simulation model. Both results followed the decreasing trend of capacity retention during the battery cycling. The capacity retention of a rechargeable Li-air battery with carbon-supported Pt catalyst demonstrated a

slightly lower value than the model results, with a difference of around 5% of retention. The lower capacity retention from the experiment than the simulation results can be attributed to the electrocatalyst used in the prepared carbon electrode in non-aqueous solvent (Pt catalyst), which promotes the electrolyte solvent decomposition rather than the desired ORR at the cathode [36]. McCloskey et al. concluded that the electrolyte solvent decomposition rather than Li_2O_2 formation was being catalysed by the heterogeneous electrocatalysts (Au, Pt, MnO_2) [36].

Moreover, the catalytic battery was probably confronted by performance deterioration by other factors which include degradation of carbon cathode materials as well as formation of other soluble (and insoluble) products and intermediates, which gradually decreased with the same trend as in the model results. Overall, from this study, the model results and experimental data seem to be in good agreement or at least, this model showed more reliability in predicting the cycling behaviour than that which excludes Li_2CO_3 accumulation from electrolyte degradation (inset of Figure 5-4). The model is potentially a promising tool to identify the Li-air cell degradation mechanisms and forecast the cell performance for new cell designs and scale-up.

5.4.2 Cathode Porosity change

To investigate the effect of electrolyte degradation on the porous electrode, Figure 5-5 compares the results for the porosity profiles inside the cathode obtained at the end of discharge in each battery cycle. The Li-air cell was cycled at a rate of 0.1 mA cm^{-2} between a discharge and charge potential of 2.2 and 4.3 V which was the same detail as presented in Figure 5-3. During each cycle, the discharge products preferentially deposit near the oxygen feed side (at $x = L$ in Figure 5-1) due to the slow diffusion and small solubility of oxygen preventing some of the active area of the cathode from taking part in the reaction. This behaviour is similar to that presented in Chapter 4.

On cycling, it is apparent from the graph that the available porosity of the rechargeable battery especially near the far side of electrode ($x = L$) continuously decreases at the end of each discharge cycle. The porosity in the cathode after the end of first cycle was about 0.28, cf. the initial value of 0.73. From this result, it is worth noting that the terminating discharge of Li-air battery was not the direct result of the clogging pore at the cathode surface being the limiting factor for discharge capacity, because there are

still some available pores for the access of reactant species. The termination of the cell discharge process could be attributed to the rapid build-up of the discharge products of both Li_2O_2 and Li_2CO_3 covering the active sites on the carbon active surface. This cell termination from product passivation is consistent with the conclusions from both the experimental work [37] and the Li-oxygen simulation model [33].

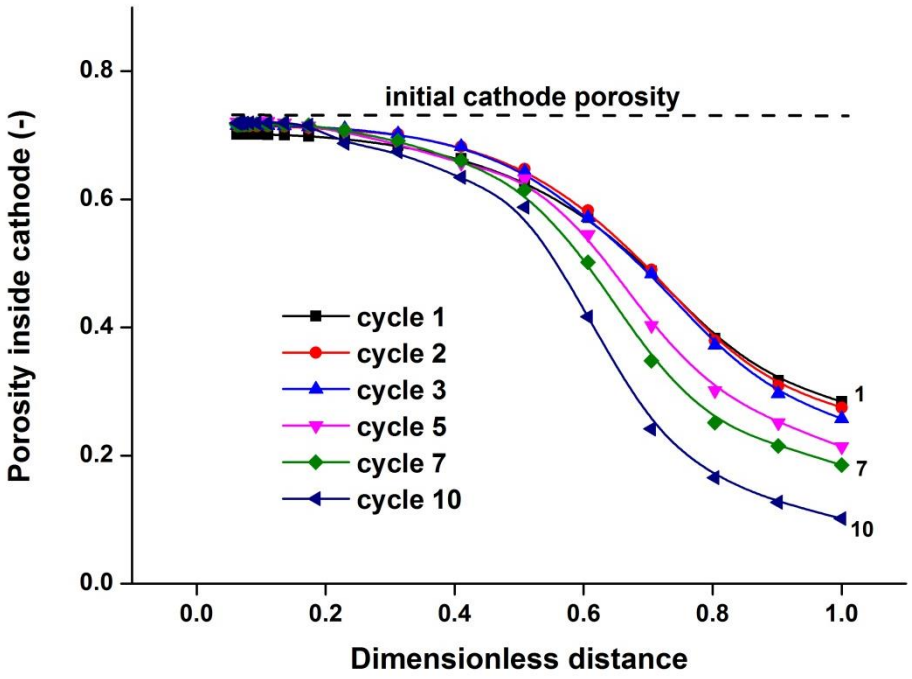

Figure 5-5 Local porosity profiles inside the Li-air cell collected at the end of each discharge cycles at a rate 0.1 mA cm^{-2}. The parameters used in the model are the same as described in Figure 5-3.

When the Li-air battery was repeatedly operated until the end of 10th cycle, the available porosity at the porous electrode/current collector interface fell to only 0.1 as shown in Figure 5-5. The result may be explained by the fact that the porosity of the discharge cathode is affected by the accumulation of Li_2CO_3 on cycling, formed during discharge [21]. Xu et al. studied the charging process of Li-O_2 batteries with organic carbonate electrolyte and found that after the cell was discharged to 2.0 V in an oxygen atmosphere and then recharged to 4.6 V, CO_2 was the dominant released gases from the oxidation of Li_2CO_3 [21]. Several studies have revealed the similar results for the oxidation of Li_2CO_3 during Li-air batteries charging [20, 34, 38]. These results confirm that Li_2CO_3 can be involved in oxidation reaction during the charging process only at high charging potential > 4.0 V, which is not considered in this simulation. As can be

seen in Figure 5-6, the volume fraction of Li_2CO_3 at electrode/current collector interface ($x = L$) steadily increases and gradually deposits inside the cathode with repeated cycling of the Li-air cell, from a volume fraction percentage about 3.7% on the first cycle to 24% in the final cycle.

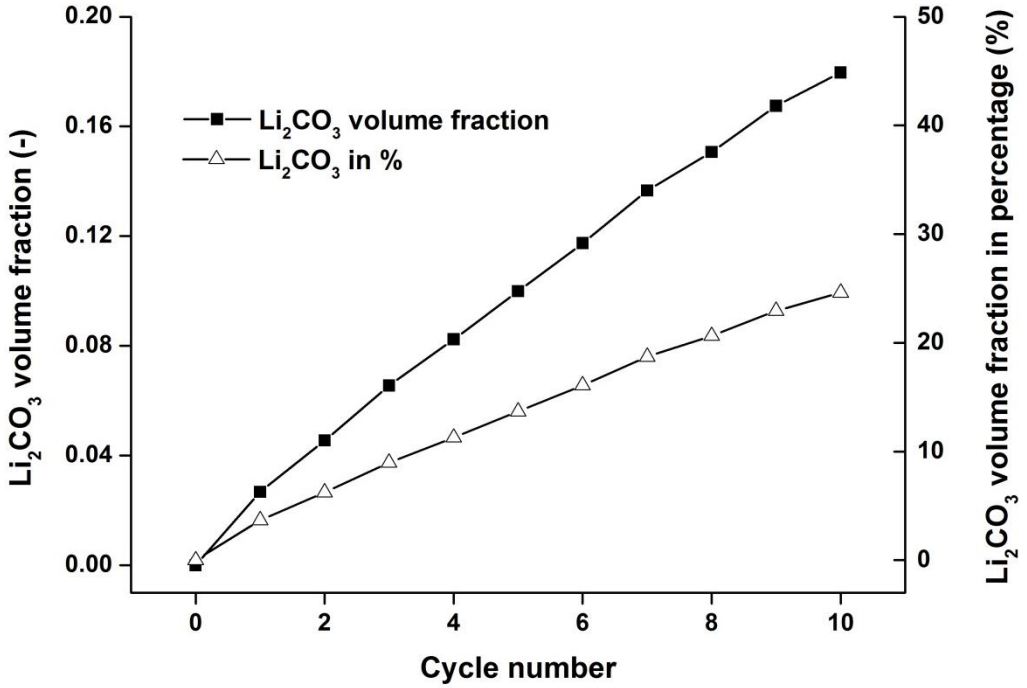

Figure 5-6 Volume fraction of Li_2CO_3 formation inside the the Li-air cell at the end of each discharge cycle. The Li_2CO_3 volume fraction in percentage is also plotted. The parameters used in the model are the same as described in Figure 5-3.

5.5 Conclusions

In this study, our previous micro-macro homogeneous model for a rechargeable Li-air battery has been developed to include the practical feature of Li_2CO_3 formation which normally occurs from electrolyte degradation during battery cycling. The modified model can successfully predict the Li-air cell cycling behaviour which starts from the first discharge to the cell potential of 2.2 V and charges until 4.2 V in 10 cycles. The cycle performance deterioration measured in term of retention of discharge capacity on cycling was predicted from the developed model which includes the effect of irreversible Li_2CO_3 discharge product. As a result, we obtain a good agreement between this cell cycling simulation and porous-electrode experiment data, thus creating a more reliable model for a rechargeable Li-air battery in non-aqueous electrolyte.

Consequently, the charging voltage slightly increases in each cycle during the recharging process. This result is partly due to the repeated passivation of discharge products on the porous carbon, which leads to decrease in electrochemical active area. The termination of the cell discharge is not from pore blockage by the depositing discharge products as there are some available pores at the end of each discharge cycle. The cathode porosity decreases overtime during cycling while the volume fraction of Li_2CO_3 gradually increases in a number of cycles. The present model developed here considers only Li_2O_2 as the main discharge product and Li_2CO_3 as the by-product coexisting during battery discharge process. Thus, the main conclusions of our modelling work are only applicable when the Li-air cell follows the formation of Li_2O_2 and Li_2CO_3 as the final discharge products.

5.6 References

1. Christensen, J., P. Albertus, R.S. Sanchez-Carrera, T. Lohmann, B. Kozinsky, R. Liedtke, J. Ahmed, and A. Kojic, *A critical review of Li/air batteries.* Journal of the Electrochemical Society, 2012. **159**(2): p. R1-R30.
2. Abraham, K.M. and Z. Jiang, *A polymer electrolyte-based rechargeable lithium/oxygen battery*. Journal of the Electrochemical Society, 1996. **143**(1): p. 1-5.
3. Debart, A., A.J. Paterson, J. Bao, and P.G. Bruce, *a-MnO_2 nanowires: A catalyst for the O_2 electrode in rechargeable lithium batteries.* Angewandte Chemie - International Edition, 2008. **47**(24): p. 4521-4524.
4. Read, J., *Characterization of the lithium/oxygen organic electrolyte battery.* Journal of the Electrochemical Society, 2002. **149**(9): p. A1190-A1195.
5. Laoire, C.O., S. Mukerjee, K.M. Abraham, E.J. Plichta, and M.A. Hendrickson, *Elucidating the mechanism of oxygen reduction for lithium-air battery applications.* Journal of Physical Chemistry C, 2009. **113**(46): p. 20127-20134.
6. Ogasawara, T., A. Débart, M. Holzapfel, P. Novák, and P.G. Bruce, *Rechargeable Li_2O_2 electrode for lithium batteries.* Journal of the American Chemical Society, 2006. **128**(4): p. 1390-1393.
7. Peng, Z., et al., *Oxygen reactions in a non-aqueous Li^+ electrolyte.* Angewandte Chemie - International Edition, 2011. **50**(28): p. 6351-6355.
8. Lu, Y.C., H.A. Gasteiger, M.C. Parent, V. Chiloyan, and Y. Shao-Horn, *The influence of catalysts on discharge and charge voltages of rechargeable Li-*

oxygen batteries. Electrochemical and Solid-State Letters, 2010. **13**(6): p. A69-A72.

9. Cheng, H. and K. Scott, *Selection of oxygen reduction catalysts for rechargeable lithium-air batteries-Metal or oxide?* Applied Catalysis B: Environmental, 2011. **108-109**: p. 140-151.
10. Laoire, C.O., S. Mukerjee, K.M. Abraham, E.J. Plichta, and M.A. Hendrickson, *Influence of nonaqueous solvents on the electrochemistry of oxygen in the rechargeable lithium-air battery.* Journal of Physical Chemistry C, 2010. **114**(19): p. 9178-9186.
11. Freunberger, S.A., Y. Chen, N.E. Drewett, L.J. Hardwick, F. Bardé, and P.G. Bruce, *The Lithium–Oxygen Battery with Ether-Based Electrolytes.* Angewandte Chemie International Edition, 2011. **50**(37): p. 8609-8613.
12. Freunberger, S.A., Y. Chen, Z. Peng, J.M. Griffin, L.J. Hardwick, F. Bardé, P. Novák, and P.G. Bruce, *Reactions in the rechargeable lithium-O_2 battery with alkyl carbonate electrolytes.* Journal of the American Chemical Society, 2011. **133**(20): p. 8040-8047.
13. Cecchetto, L., M. Salomon, B. Scrosati, and F. Croce, *Study of a Li-air battery having an electrolyte solution formed by a mixture of an ether-based aprotic solvent and an ionic liquid.* Journal of Power Sources, 2012. **213**(0): p. 233-238.
14. Xu, W., et al., *The stability of organic solvents and carbon electrode in nonaqueous Li-O_2 batteries.* Journal of Power Sources, 2012. **215**: p. 240-247.
15. McCloskey, B.D., D.S. Bethune, R.M. Shelby, G. Girishkumar, and A.C. Luntz, *Solvents critical role in nonaqueous Lithium-Oxygen battery electrochemistry.* Journal of Physical Chemistry Letters, 2011. **2**(10): p. 1161-1166.
16. Read, J., K. Mutolo, M. Ervin, W. Behl, J. Wolfenstine, A. Driedger, and D. Foster, *Oxygen Transport Properties of Organic Electrolytes and Performance of Lithium/Oxygen Battery.* Journal of the Electrochemical Society, 2003. **150**(10): p. A1351-A1356.
17. Beattie, S.D., D.M. Manolescu, and S.L. Blair, *High-capacity lithium-air cathodes.* Journal of the Electrochemical Society, 2009. **156**(1): p. A44-A47.
18. Cheng, H. and K. Scott, *Carbon-supported manganese oxide nanocatalysts for rechargeable lithium-air batteries.* Journal of Power Sources, 2010. **195**(5): p. 1370-1374.
19. Mizuno, F., S. Nakanishi, Y. Kotani, S. Yokoishi, and I. Hideki, *Rechargeable li-*

air batteries with carbonate-based liquid electrolytes. Electrochemistry, 2010. **78**(5): p. 403-405.

20. Xiao, J., J. Hu, D. Wang, D. Hu, W. Xu, G.L. Graff, Z. Nie, J. Liu, and J.G. Zhang, *Investigation of the rechargeability of Li-O_2 batteries in non-aqueous electrolyte.* Journal of Power Sources, 2011. **196**(13): p. 5674-5678.
21. Xu, W., V.V. Viswanathan, D. Wang, S.A. Towne, J. Xiao, Z. Nie, D. Hu, and J.-G. Zhang, *Investigation on the charging process of Li_2O_2-based air electrodes in Li-O_2 batteries with organic carbonate electrolytes.* Journal of Power Sources, 2011. **196**(8): p. 3894-3899.
22. Xu, W., et al., *Reaction mechanisms for the limited reversibility of Li-O_2 chemistry in organic carbonate electrolytes.* Journal of Power Sources, 2011. **196**(22): p. 9631-9639.
23. Sahapatsombut, U., H. Cheng, and K. Scott, *Modelling the micro–macro homogeneous cycling behaviour of a lithium–air battery.* Journal of Power Sources, 2013. **227**(0): p. 243-253.
24. Bryantsev, V.S., M. Blanco, and F. Faglioni, *Stability of Lithium Superoxide LiO_2 in the Gas Phase: Computational Study of Dimerization and Disproportionation Reactions.* The Journal of Physical Chemistry A, 2011. **114**(31): p. 8165-8169.
25. Roberts Jr, J.L., T.S. Calderwood, and D.T. Sawyer, *Nucleophilic oxygenation of carbon dioxide by superoxide ion in aprotic media to form the $C_2O_6^{2-}$ species.* Journal of the American Chemical Society, 1984. **106**(17): p. 4667-4670.
26. Wadhawan, J.D., P.J. Welford, E. Maisonhaute, V. Climent, N.S. Lawrence, R.G. Compton, H.B. McPeak, and C.E.W. Hahn, *Microelectrode studies of the reaction of superoxide with carbon dioxide in dimethyl sulfoxide.* Journal of Physical Chemistry B, 2001. **105**(43): p. 10659-10668.
27. Tasaki, K., A. Goldberg, J.J. Lian, M. Walker, A. Timmons, and S.J. Harris, *Solubility of lithium salts formed on the lithium-ion battery negative electrode surface in organic solvents.* Journal of the Electrochemical Society, 2009. **156**(12): p. A1019-A1027.
28. Welford, P.J., B.A. Brookes, J.D. Wadhawan, H.B. McPeak, C.E.W. Hahn, and R.G. Compton, *The Electro-reduction of Carbon Dioxide in Dimethyl Sulfoxide at Gold Microdisk Electrodes: Current | Voltage Waveshape Analysis.* The Journal of Physical Chemistry B, 2001. **105**(22): p. 5253-5261.
29. Atkinson, R., *Atmospheric reactions of alkoxy and β-hydroxyalkoxy radicals.*

International Journal of Chemical Kinetics, 1997. **29**(2): p. 99-111.

30. Curran, H.J., P. Gaffuri, W.J. Pitz, and C.K. Westbrook, *A comprehensive modeling study of n-heptane oxidation.* Combustion and Flame, 1998. **114**(1-2): p. 149-177.
31. Sinha, A. and M.J. Thomson, *The chemical structures of opposed flow diffusion flames of C3 oxygenated hydrocarbons (isopropanol, dimethoxy methane, and dimethyl carbonate) and their mixtures.* Combustion and Flame, 2004. **136**(4): p. 548-556.
32. Jitaru, M., D.A. Lowy, M. Toma, B.C. Toma, and L. Oniciu, *Electrochemical reduction of carbon dioxide on flat metallic cathodes.* Journal of Applied Electrochemistry, 1997. **27**(8): p. 875-889.
33. Albertus, P., G. Girishkumar, B. McCloskey, R.S. Sánchez-Carrera, B. Kozinsky, J. Christensen, and A.C. Luntz, *Identifying capacity limitations in the Li/oxygen battery using experiments and modeling.* Journal of the Electrochemical Society, 2011. **158**(3): p. A343-A351.
34. Ottakam Thotiyl, M.M., S.A. Freunberger, Z. Peng, and P.G. Bruce, *The Carbon Electrode in Nonaqueous Li-O_2 Cells.* Journal of the American Chemical Society, 2013. **135**(1): p. 494-500.
35. Debart, A., J. Bao, G. Armstrong, and P.G. Bruce, *An O_2 cathode for rechargeable lithium batteries: The effect of a catalyst.* Journal of Power Sources, 2007. **174**(2): p. 1177-1182.
36. McCloskey, B.D., R. Scheffler, A. Speidel, D.S. Bethune, R.M. Shelby, and A.C. Luntz, *On the efficacy of electrocatalysis in nonaqueous Li-O_2 batteries.* Journal of the American Chemical Society, 2011. **133**(45): p. 18038-18041.
37. Ren, X., S.S. Zhang, D.T. Tran, and J. Read, *Oxygen reduction reaction catalyst on lithium/air battery discharge performance.* Journal of Materials Chemistry, 2011. **21**(27): p. 10118-10125.
38. Liu, Y., R. Wang, Y. Lyu, H. Li, and L. Chen, *Rechargeable Li/CO_2-O_2 (2 : 1) battery and Li/CO_2 battery.* Energy & Environmental Science, 2014. **7**(2): p. 677-681.

Chapter 6: Modelling of Operation of a Lithium-air Battery with Ambient Air and Oxygen-Selective Membrane

In this chapter, a macro-homogeneous model taken from the previous chapters has been developed to evaluate the impact of replacing pure oxygen with ambient air on the performance of a rechargeable non-aqueous Lithium-air ("Li-air") battery. The operation of a Li-air battery in ambient air conditions is regarded as a critical problem to be solved before this battery can be used for practical application. All of the model features from the previous chapters (Li_2O_2 and Li_2CO_3 discharge products, cycling behaviour and electrolyte degradation) have been included in this chapter to investigate the relationship between Li-air battery and air conditions. In addition, the model was integrated with an oxygen-selective membrane to improve the Li-air battery's performance in term of discharge capacity. This model can be used to describe the behaviour of Li-air batteries in ambient air conditions as well as to optimise the performance and structure of these batteries.

6.1 Introduction

The rechargeable Li-air, which has specific energy levels several times higher than Li-ion batteries makes it a candidate for a new generation of energy storage devices [1-4]. Since the first report of a non-aqueous electrolyte Li-air battery in 1996 [5], especially after a breakthrough in the cycle life by Bruce's group [6], the rechargeable Li-air battery has been investigated intensively [6-11]. However, many scientific and technical challenges have to be overcome to realise the potential of this cutting-edge technology. A key area is to gain an insight into chemical/electrochemical processes that take place inside the Li-air battery via an effective mathematical model.

An aprotic Li-air battery contains a metal lithium anode, a solid separator and a porous air electrode filled with a non-aqueous Li^+ electrolyte. The fundamental electrochemical reactions are shown below:

Anode $\quad Li \rightleftharpoons Li^+ + e^- \quad (E^0 = 0.00\ V_{Li})$ (6-1)

Cathode $2Li^+ + O_2 + 2e^- \rightleftharpoons Li_2O_2 \quad (E^0 = 2.96\, V_{Li})$ (6-2)

Here, Eq. (6-2) is an ideal electrochemical reaction, desired to make a truly rechargeable Li-air battery [6, 12, 13]. In practice, there are other side reactions, forming detrimental products, such as Li_2CO_3 [6, 12, 13].

However, almost all of the current studies on Li-air batteries are run in pure oxygen and controlled dried atmosphere in a glove box to minimise the contaminated substances from the ambient air. Thus, this battery can perform according to a high rate capability, owing to high oxygen concentration, and maintain a long-term operation. Our recent model studies also simulated the Li-air battery including the electrolyte degradation and operation in pure oxygen [14, 15]. To succeed in making a Li-air battery for use in practical applications, one critical problem to be solved is operating Li-air batteries in an ambient air environment [16, 17]. There are several challenges when Li-air batteries are applied to air conditions compared to those of pure oxygen feeding. The first is the unavoidable moisture (about 1% in volume) in the surrounding air, which may penetrate into the cell system together with oxygen. The presence of moisture can corrode the metallic lithium anode due to the hydrolysis reaction with highly reactive lithium as shown in reaction (6-3) [17]. This results in the fast battery failure and causes serious safety issues.

$$2Li + 2H_2O \rightleftharpoons 2LiOH + H_2 \quad (6\text{-}3)$$

The second is the insufficient concentration of oxygen due to its low partial pressure in the atmosphere, leading to the limitation of Li-air batteries from high discharge rates because of the small oxygen solubility in the electrolyte. The third problem is that the small amount of carbon dioxide (CO_2) from air feeding may react with superoxide anions formed during the initial oxygen reduction on discharge process, to generate carbonate species, leading to the deposition of these by-products on the cathode surface [12, 18, 19]. It is worth noting that CO_2 could be considered as the active material to form the Li_2CO_3 and lithium alkyl carbonates instead of the desired produce Li_2O_2 [12, 19, 20]. Furthermore, these side reactions lead to a continuous and irreversible consumption of electrolytes and thus the Li-air batteries cannot maintain their sustainable ability during charge/discharge cycles.

To minimise the battery problem when using air, Li-air batteries under current research are mainly operated in pure oxygen [5-7, 9]. There is a small volume of published works demonstrating the behaviour of Li-air batteries with air feeding [11, 16, 17, 21]. These studies solved the contaminated gases problems by using an oxygen-selective water barrier membrane covering the outer surface of the cathode to prevent moisture and to selectively permeate oxygen into the porous cathode at the same time. Zhang et al. (2010) developed an oxygen-selective immobilised liquid membrane for a non-aqueous Li-air battery operated in ambient air with 20-30% relative humidity [17]. The membranes were easily prepared by soaking high viscosity silicone oil into porous metal or Teflon substrates. A Li-air battery integrated with these membranes can be operated in ambient air for 16.3 days with a specific capacity of 789 mAh g^{-1} and specific energy of 2,182 Wh kg^{-1} based on the weight of carbon. The same group also studied the hydrophobic zeolite membrane and polytetrafluoroethylene (PTFE) membrane as oxygen-selective water barriers [16]. The latter protected a Li-air cell against moisture and supplied oxygen for 21 days with a specific capacity of 1022 mAh g^{-1} and specific energy of 2,792 Wh kg^{-1} based on the weight of carbon.

Zhang et al. (2010) investigated the ambient operation of non-aqueous Li-air batteries integrated with a heat-sealable polymer membrane to serve as both an oxygen-diffusion membrane and moisture barrier [11]. The membrane could also reduce the evaporation of electrolytes during battery operation. The Li-air battery with this membrane demonstrated the discharge capability in ambient air for more than one month with a specific energy of 362 Wh kg^{-1} based on the total weight of the battery including its packaging. However, all of the research previously mentioned on ambient air only studied the performances of Li-air batteries on the discharge phase without showing those on the charging or cycling process, which could provide more important data for battery stability than only a single discharge.

In this chapter, the previous Li-air battery model with electrolyte degradation is modified to operate the Li-air battery in an ambient air environment [14, 15], which severely damages Li-air performance and is still a critical problem to be solved before the Li-air battery can be used for practical application. The two species in air; oxygen and CO_2 are considered in the model in air-feeding conditions with the exception of moisture or using dried air in the model. Although this model does not include all the

effects that could occur in the Li-air battery with an ambient air operation, the key mechanisms, covering the main impact of using air that directly affects the porous cathode behaviour during battery operation and leads to detrimental Li-air performance are considered. The effect of N_2 reacting with Li species is not considered.

Therefore, the mathematical model for a Li-air battery with air-feeding condition can be used to identify battery-limiting mechanisms and reduce the amount of time-consuming work compared to the experimental effort. Moreover, it also avoids the serious safety problems that could happen when the ingression of moisture reacts with the lithium metal anode. This model can be used to describe the behaviour of Li-air batteries in ambient air conditions as well as to optimise the performance and structure of these battery electrodes.

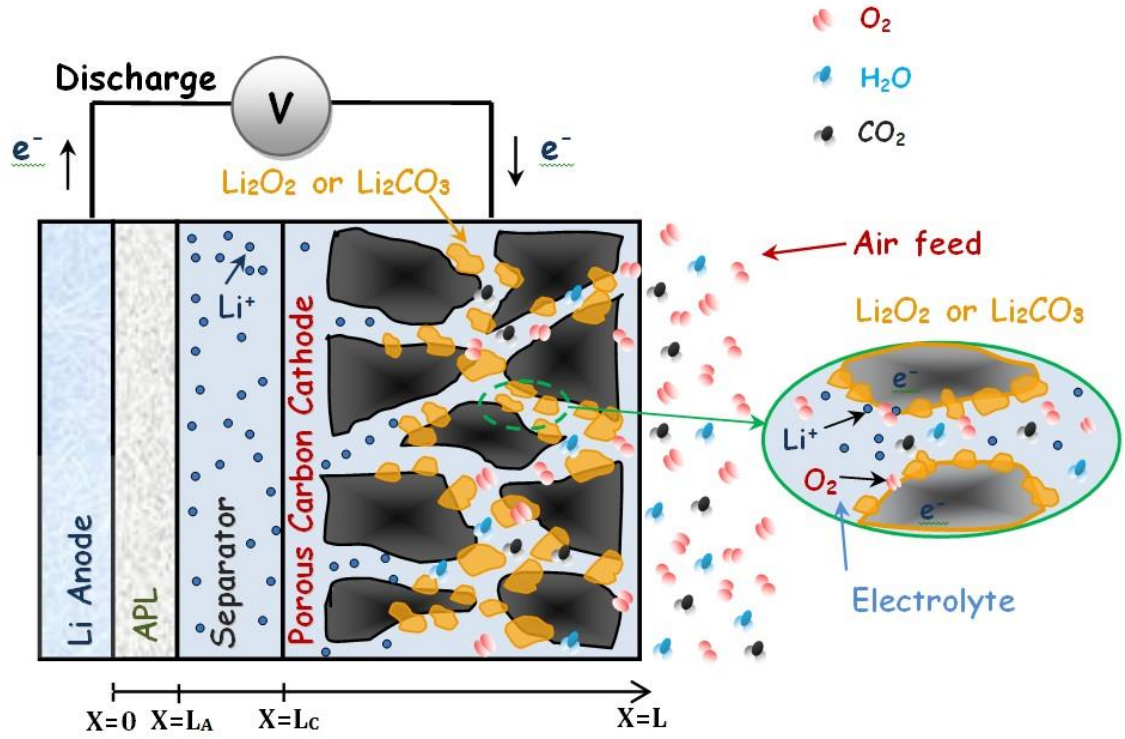

Figure 6-1: Schematic computation domain of a Li-air battery during discharge operation. A Li-air battery operated with ambient air-feeding and the inset demonstrates the formation of Li_2O_2 and Li_2CO_3 as discharge products covering the porous carbon surface.

6.2 Theoretical Mechanism Analysis

A typical Li-air battery, shown in Figure 6-1, contains a lithium metal anode, a separator containing electrolytes, and a porous carbon or catalyst-loaded carbon air

electrode filled with an organic electrolyte comprising a dissolved lithium salt in an aprotic solvent. During discharge, the lithium metal anode oxidises to Li^+ and electrons are conducted through the external circuit, while Li^+ is transported towards the porous cathode. Oxygen is reduced at the active surface with Li^+, thus leading to the desired discharge products of Li_2O_2 and the by-product of Li_2CO_3 or lithium alkyl carbonates resulting from the electrolyte decomposition [12, 13, 19]. These products influence the Li-air performance and cannot be completely removed during the battery cycling process. To simplify our simulation, the model assumed that Li_2O_2 was the main discharge product depositing inside the porous cathode (Eq. (6-2)) and the irreversible Li_2CO_3 by-product coexisting with Li_2O_2 when using non-aqueous electrolytes. This section describes the two main mechanisms that occur inside the Li-air battery and were applied to the model.

6.2.1 Effect of using ambient air condition

The critical problems when using air as a feeding reactant for Li-air batteries are the low oxygen solubility in the electrolyte and the CO_2 gas diffusing into the battery with oxygen. Although the amount of CO_2 in the atmosphere is small compared to oxygen, its solubility in non-aqueous solvents is much higher than oxygen, as shown in Table 6-1.

Table 6-1 Solubility of CO_2 in various solvents at 25° C [22]

Solvent	**CO_2 concentration (mol dm^{-3})**	**Oxygen concentration (mol dm^{-3})**
Water	0.033	0.00027
Methanol	0.06	-
Tetrahydrofuran (THF)	0.205 ± 0.008	-
Acetonitrile (AN)	0.279 ± 0.008	0.00211
Dimethylformamide (DMF)	0.199 ± 0.006	-
Dimethylsulphoxide (DMSO)	0.138 ± 0.003	-

To investigate these effects, the model was changed with the feed condition from pure oxygen to ambient air at the porous cathode entrance. Considering the amount of oxygen and CO_2 content in the atmosphere [23] (78% N_2, 21% O_2, 0.035% CO_2), the concentrations of oxygen and CO_2 in the electrolyte can be determined in term of Henry's law which states that:

$$c_g = H_g \bar{p}_g \tag{6-4}$$

where c_g is the concentration of gasses in the electrolyte, H_g is the Henry's law constant which depends on the electrolyte and temperature used in the Li-air battery, and $\bar{p}_g$ is the partial pressure of the gas which depends on mole fraction of each species in the atmosphere. Henry's law is correct to describe the solubility of gas for low concentrations and low partial pressures. The concentrations of oxygen and CO_2 calculated from Henry's law (Eq. (6-4)) can be compared to each other in Table 6-2. These concentrations are applied in the Li-air model as initial conditions to represent the air-feeding, unless otherwise specified. It can be seen that, although the CO_2 composition in the atmosphere is not very high, its Henry's law constant (4.59) is almost twice that of oxygen (2.95), i.e. the solubility of CO_2 in non-aqueous solvents is higher than oxygen [22]. This high solubility of CO_2 into the electrolyte could affect the Li-air performance due to the formation of Li_2CO_3.

Hence, unlike the previous model in Chapters 4 and 5 which used only pure oxygen as feeding condition, the present model applied the air condition to the low solubility of oxygen and CO_2 as contaminants. These concentrations in the porous cathode can affect the Li-air battery's performance during battery cycling. Nitrogen is also able to gain access through the cathode but has little or no effect with a lithium-based electrolyte on the Li-air battery performance [24].

Table 6-2 Henry's constant and calculated concentration in non-aqueous at 25° C

Species	**Henry's law constant (mol m^{-3} atm^{-1})**	**Concentration (mol m^{-3})**	**Ref.**
O_2	2.95	0.6182	calculated from [25]
CO_2	4.59	0.0043	[26]

6.2.2 Electrolyte degradation

In order to succeed in the application of non-aqueous Li-air batteries, the finding electrolytes with high stability during battery operation is a prerequisite for the long-cycled life of Li-air batteries, especially in an oxygen-rich environment and under catalytic conditions [27]. Since the Li-air batteries have been currently developed, there is still no proper electrolyte that can meet all of these requirements: 1) high stability [12, 18, 28, 29], 2) high boiling point (low evaporation), and 3) high oxygen solubility and diffusivity as well as less sensitive to moisture [30]. At present, various non-aqueous electrolytes have been widely examined and applied in Li-air batteries based on

different types of solvents, e.g. carbonates, ethers, sulfoxides, nitriles and ionic liquid [31]. However, Li_2CO_3 formation from the decomposition of electrolytes by Li-O_2 intermediates (O_2^-) and products was also clearly detected inside the electrode during discharge from all electrolytes which were dissolved in different solvents [31]. The electrolyte degradation mechanisms proposed in Chapter 5 and in our previous work [15] are also included in the present model and reinstated as described below. It is worth noting that the Li_2CO_3 formation from mechanism 2 in Chapter 5 demonstrated no significant contribution compared to mechanism 1. Therefore this chapter considers only Li_2CO_3 from mechanism 1 to minimise the computation resource.

Li_2CO_3 formation

$$2O_2 + 2e^- \xrightarrow{k1a} 2O_2^- \qquad (E^0 = 3.18\,V) \qquad (6\text{-}5)$$

$$2O_2^- + 2CO_2 \xrightarrow{k1b} C_2O_6^{2-} + O_2 \qquad \text{RDS} \qquad (6\text{-}6)$$

$$C_2O_6^{2-} + 4Li^+ + 2O_2^- \rightarrow 2Li_2CO_3 + 2O_2 \qquad (6\text{-}7)$$

Overall $4Li^+ + 2CO_2 + 2O_2^- + 2e^- \rightarrow 2Li_2CO_3 + O_2 \qquad (E^0 = 7.19\,V) \qquad (6\text{-}8)$

Solvent degradation

$$O_2 + e^- \xrightarrow{k1a} O_2^- \qquad (E^0 = 3.18\,V) \qquad (6\text{-}9)$$

$$O_2^- + [Solvent] \rightarrow [Solvent]^- \qquad (6\text{-}10)$$

$$[Solvent]^- + O_2 \rightarrow CO_2 + H_2O + HCO_2Li + CH_3CO_2Li \qquad (6\text{-}11)$$

Overall $2O_2 + [Solvent] + e^- \rightarrow CO_2 + H_2O + HCO_2Li + CH_3CO_2Li \qquad (6\text{-}12)$

It is worth noting that the exact details of the reaction routes for the electrolyte degradation to form Li_2CO_3 can be complicated regarding several intermediates during cell operation. Then, the proposed mechanisms above are a possibility to describe the formation reaction of Li_2CO_3 as reported previously [19, 32, 33].

With the use of air-feeding conditions instead of pure oxygen for the porous carbon cathode, the CO_2 in this model could be generated from two routes, one from solvent or electrolyte degradation (Eq. (6-12)) and the other from the atmospheric air. Both Li_2O_2 and Li_2CO_3 can be produced as discharged products and are usually insolubly in the cell

electrolyte. As a result, the repeated depositing film of different lithium salts over the carbon surface after each discharge and charge step could affect the reaction mechanisms at the active area/electrolyte interfaces, and the transport of species inside the pores leading to battery deterioration [34].

6.3 Model Development

6.3.1 Model description

In this chapter, a schematic computation domain for a prismatic single cell of a Li-air battery is the same as in previous chapters as shown in Figure 6-1. All of the model features from previous chapters (Li_2O_2 and Li_2CO_3 discharge products, cycling behaviour and electrolyte degradation) remained the same in this chapter. The main difference was the set of feed conditions applied to the dry air through the porous cathode electrode.

Hence, the governing equations and assumptions for the model in this chapter are similar to that in Chapter 5 excepting that the initial conditions are changed to the air condition. All the rate expressions at the porous cathode are the same as described in Chapter 3.

6.3.2 Model assumption

In addition to the general assumption discussed in Chapter 5, the following simplifications were adopted in this particular model:

i. The fed air through the porous cathode is dry without moisture.
ii. The air is dissolved into the electrolyte.
iii. No gas phase is formed in the porous electrode.

6.3.3 Governing equations

The governing equations used in the air feeding Li-air model are listed in Table 6-3. The equations for the conservation of species and charges as well as the kinetic expressions are the same ones used in the electrolyte degradation model in Chapter 5. The boundary conditions are only the difference in this chapter.

Table 6-3 Governing equations used in the air feeding Li-air battery model.

Equation description		
1. Transport of species		
Species material balance	$\frac{\partial(\varepsilon c_i)}{\partial t} = -\nabla \cdot \boldsymbol{N}_i + r_i$	(6-13)
Molar flux for Li^+	$\boldsymbol{N_{Li}} = -D_{Li,eff}\nabla c_{Li} + \frac{\boldsymbol{i}_2 t_+}{F}$	(6-14)
Molar flux for species	$\boldsymbol{N_i} = -D_{i,eff}\nabla c_i$	(6-15)
2. Conservation of charge		
Solid-phase current density	$\boldsymbol{i}_1 = -\sigma_{eff}\nabla\phi_1$	(6-16)
Liquid-phase current density	$\boldsymbol{i}_2 = -\kappa_{eff}\nabla\phi_2 - \frac{2RT\kappa_{eff}}{F}(t_+ - 1)\left(1 + \frac{\partial lnf}{\partial lnc_{Li}}\right)\nabla lnc_{Li}$	(6-17)
Charge conservation	$\nabla \cdot \boldsymbol{i}_1 + \nabla \cdot \boldsymbol{i}_2 = 0$	(6-18)
Charge transfer current density	$\nabla \cdot \boldsymbol{i}_2 = \sum_m a j_m$	(6-19)
3. Rate expression at cathode		
Butler-Volmer equation	$\frac{j_c}{nF} = k_a(c_{Li_2O_2})exp\left[\frac{(1-\beta)nF}{RT}\eta_c\right] - k_c(c_{Li^+})^2(c_{O_2})exp\left[\frac{-\beta nF}{RT}\eta_c\right]$	(6-20)
Li_2CO_3 (Mechanism 1)	$j_{c1} = Fk_{1a}(c_{O_2})\left[-exp\left(\frac{-\beta nF}{RT}\eta_m\right)\right]$	(6-21)
	$r_{1b} = k_{1b}(c_{O_2^-})(c_{CO_2})$	(6-22)
Solvent degradation	$j_{c3} = Fk_{VI}(c_{O_2})\left[-exp\left(\frac{-\beta nF}{RT}\eta_m\right)\right]$	(6-23)
4. Rate expression at anode		
Butler-Volmer equation	$j_a = i_0\left[exp\left(\frac{(1-\beta)nF}{RT}\eta_a\right) - exp\left(\frac{-\beta nF}{RT}\eta_a\right)\right]$	(6-24)

6.3.4 Boundary conditions

To operate the model with air feeding, the boundary condition for the species at the cathode/current collector interface ($x = L$) were applied in relation to the oxygen and CO_2 concentrations following Table 6-2. The other boundary conditions were the same as in Table 5-2.

6.3.5 Solution technique

The conservation equations and the boundary conditions described above were

discretized using a finite element method and solved using a one-dimensional battery system by commercial software package COMSOL multiphysics (version 4.3). The COMSOL software is designed to solve a set of coupled differential and algebraic equations. The battery simulation model is performed on a 32 bit Windows platform with 4 GB RAM, and Intel Core 2 Duo 2.93 GHz processor. The different transport equations and the electrochemical reactions were solved as time dependent until the cell voltage reached the stop condition. The solution was considered as a converged solution when the difference between two results was less than 10^{-4} (relative tolerance) for all variables.

6.4 Results and Discussion

The one-dimensional Li-air battery implemented with the model equations as presented in the previous section have been simulated and solved to analyse the impact of using ambient air condition which has a severe effect on Li-air batteries compared to the case of pure oxygen. The model was based on the previous chapter and could be validated by using the experimental cycle performance obtained in our labs, due to sufficient rechargeable data. In this section, first, the Li-air battery is considered in terms of the effects of using dried air compared to the effects of those without electrolyte degradation to distinguish between these two mechanisms. Then, the model combined the two effects together to investigate the cell's performance in term of discharge specific capacity and Li_2CO_3 accumulation on cycling resulting in electrode passivity and capacity fading.

6.4.1 Li-air performance with air-feeding

To compare the effect of using air in the Li-air battery, all parameters applied in the model are the same as in Chapters 4 and 5 (Table 3-3 and Table 5-3), and the oxygen and CO_2 concentrations in dry air are applied by following the atmospheric condition with low partial pressure as presented in Table 6-2. This model section excludes the effects from electrolyte degradation and considers the effect from air-feeding only. The voltage-capacity results on the 1st cycle obtained from the Li-air cell at different discharge rates are presented in Figure 6-2. It is apparent that, at the high discharge rate of 0.1 mA cm^{-2}, there is a significant decrease in cell discharge capacity which provided only 117 mAh g_{carbon}^{-1} when using air as the active reactant unlike the cell's performance in pure oxygen providing the first discharge capacity at around 722 mAh

g_{carbon}^{-1} at the same discharge rate. A large deterioration in discharge capacity can be attributed to the low oxygen solubility in electrolytes at partial pressure 0.21 atm (0.618 mol m^{-3} compared to pure oxygen of 3.264 mol m^{-3} at 1 atm) and high discharge rate resulted in limited oxygen diffusion in the porous cathode. The CO_2 concentration, which is even lower concentration than that of oxygen, could not much affect the cell capacity from Li_2CO_3 formation on the 1st cycle.

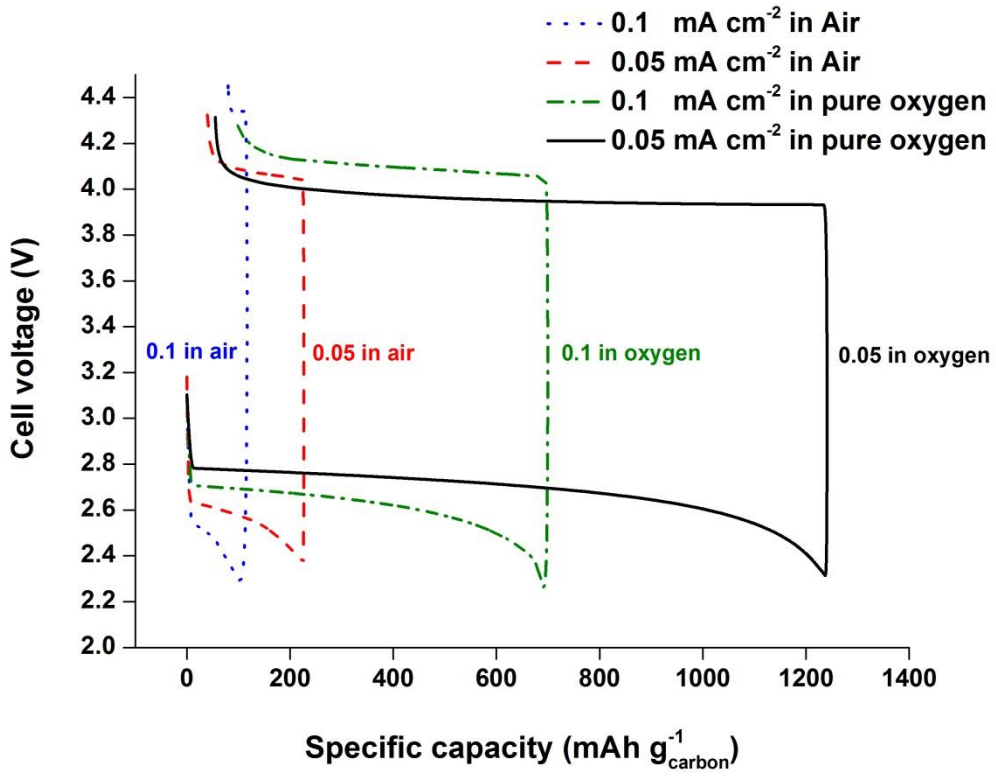

Figure 6-2: Comparison of the voltage-capacity curve for a non-aqueous Li-air battery model in different feeding conditions between pure oxygen and ambient air at two operating rates of 0.05 and 0.1 mA cm^{-2}. The electrolyte contains 1 M $LiPF_6$ dissolved in non-aqueous solvent. The cathode electrode thickness is 750 μm with porosity of 0.73. The cell cycle is simulated between 2.4 and 4.2 V versus Li/Li^+ in at operating temperature 298.15 K.

Because the cell's performance provided the limited capacity at a high discharge rate and could not determine the cell cycling behaviour, the discharge rate in the model was changed to a lower value as 0.05 mA cm^{-2} to investigate the air effect compared to the pure oxygen at the same cycling rate as that presented in Figure 6-2. It is apparent from the graph that, although the battery capacity increases on changing the discharge rate (from 117 to 226 mAh g_{carbon}^{-1}), there has been a clear reduction in the capacity from

1,240 (in pure oxygen) to 226 mAh g_{carbon}^{-1} when using ambient air as the feed. What is also interesting in this data is that the inlet air affected the cell's capacity and also the discharge voltage decreasing from 2.75 V in pure oxygen to 2.55 V in air at the same discharge rate.

The cell performance is poorer because of the lower oxygen diffusion and solubility further inside the porous structure when a Li-air battery is operated under ambient conditions. Moreover, the cycling profile of a Li-air battery in Figure 6-3 indicates that the discharge voltage slightly drops due to gradual Li_2CO_3 deposition when repeated cycles of the Li-air battery are conducted. Because the effect of electrolyte degradation is not included in this model section to clarify the effect of ambient air, the battery profile between the 2nd-8th cycles in Figure 6-3 shows a slight decrease in specific capacity due to Li_2CO_3 being generated from the low CO_2 concentrations in the air. The combined effects of air and electrolyte degradation will present in the next section.

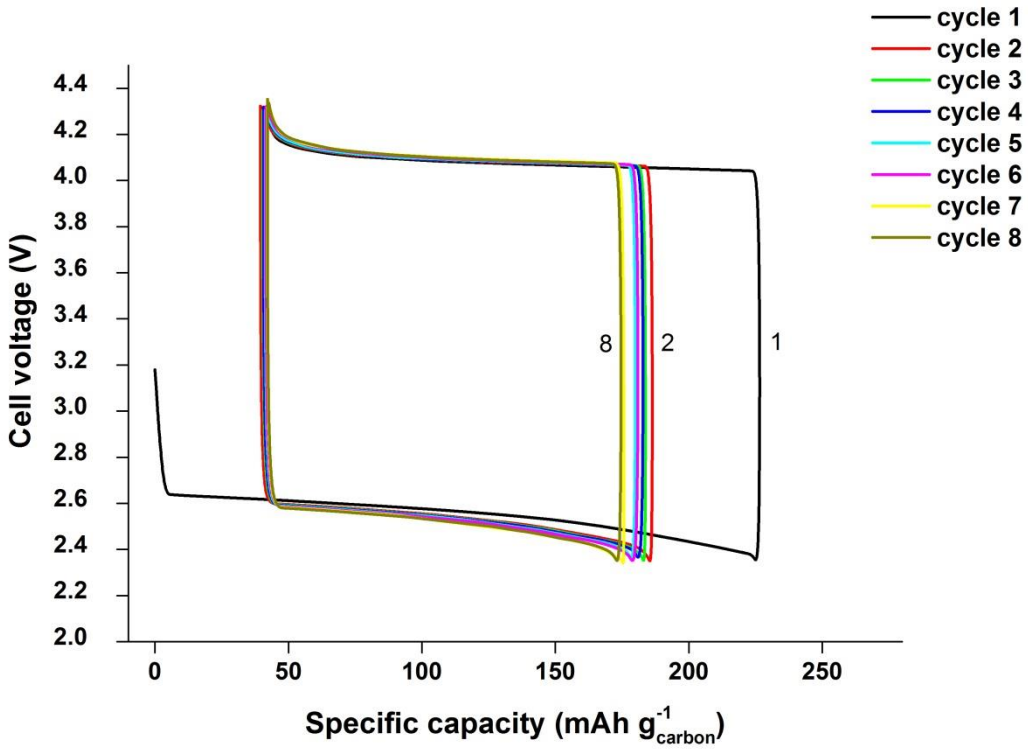

Figure 6-3: Variation of voltage-capacity curve for a non-aqueous Li-air battery using ambient air in 8 cycles on discharge and then charge between 2.2 and 4.2 V compared to Li/Li^+ at a rate of 0.05 mA cm^{-2}. The other parameters used in the model are the same as described in Figure 6-2.

The capacity retention of Li-air at a rate of 0.05 mA cm^{-2} is presented in Figure 6-4, when the cell is operated using an air inlet. The graph shows that the capacity retention gradually falls from 100% in the 1st cycle (cell discharge capacity of 226 mAh g_{carbon}^{-1}) to 65% in 2nd cycle and slightly decreases afterwards to 58% in the 8th cycle. The significant difference in capacity retention between the 1st and 2nd cycle is due to the incomplete reversible Li_2O_2 decomposition during the recharging cell after the 1st discharge. Thereafter, the cell is affected by the Li_2CO_3 formation (generated from Eq. (5-6)) and demonstrates a small decrease in the capacity retention during the cycling due to the fact that there is little contaminated CO_2. As can be seen from Table 6-4, the volume fraction of Li_2CO_3 collected at the cathode/current collector interface at the end of each discharge cycle slightly increases and gradually deposits inside the cathode with the repeated cycles of the Li-air battery.

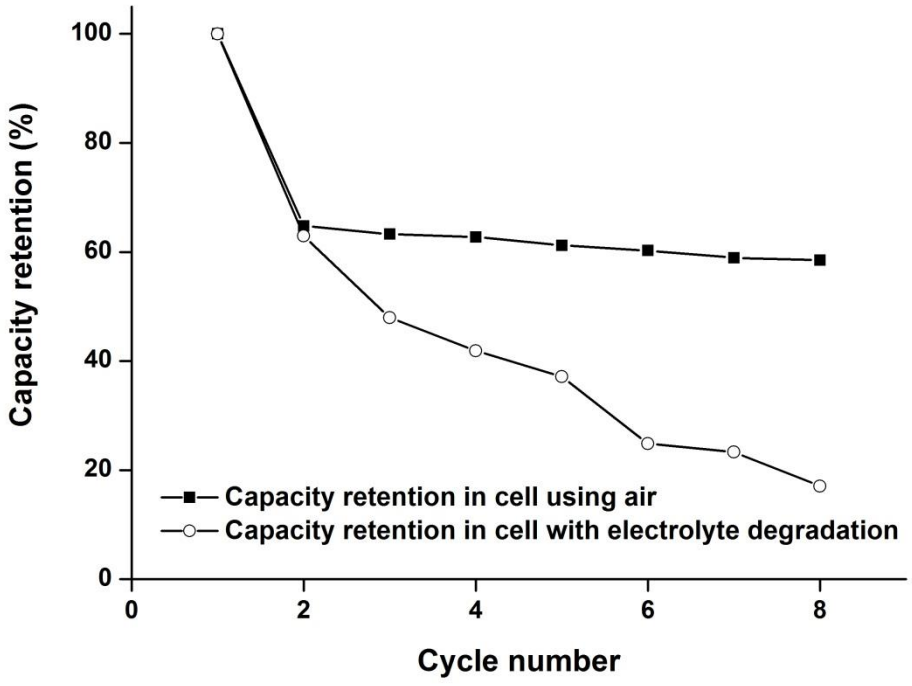

Figure 6-4: The cycle performance in term of capacity retention of an 8-cycle rechargeable Li-air battery in ambient air feeding with a comparison between the cells with stabilised electrolytes and those with the effects of electrolyte degradation. The battery was cycled at a rate 0.05 mA cm^{-2}. The other parameters used in the model are the same as described in Figure 6-2.

Table 6-4: Specific discharge capacity and Li_2CO_3 formation for a non-aqueous Li-air battery operated in ambient air in 8 cycles at a rate of 0.05 mA cm^{-2}. The data was examined with comparison made between the cell with stabilised electrolytes and those with the effects of electrolyte degradation.

cycle	Discharge capacity ($mAh\ g^{-1}_{carbon}$)		Capacity retention (%)		Li_2CO_3 volume fraction	
	Feeding air	With ED [a]	Feeding air	With ED [a]	Feeding air	With ED [a]
1	226.65	250.47	100.00	100.00	0.0031	0.0431
2	146.84	157.70	64.79	62.96	0.0072	0.0812
3	143.44	120.10	63.29	47.95	0.0108	0.1095
4	142.26	104.90	62.77	41.88	0.0143	0.1390
5	138.74	93.02	61.21	37.14	0.0178	0.1674
6	136.57	62.27	60.25	24.86	0.0212	0.1875
7	133.63	58.35	58.96	23.30	0.0245	0.2078
8	132.58	42.74	58.49	17.06	0.0277	0.2232

[a] Li-air battery performance combining the effect of feeding air and electrolyte degradation

This volume fraction is also plotted in Figure 6-5 but the value is unnoticeable due to the scale when compared to Li_2CO_3 formation from the Li-air model including electrolyte degradation effect, which will be described in the next section. Because the Li_2CO_3 formation tends to follow the straight line during the battery simulation of 8-repeated cycle, estimation of the cell can be made in terms of how many cycles will be achieved until the Li_2CO_3 deposition shows a significant impact on the Li-air cycling. Figure 6-5 also provides the predicted Li_2CO_3 volume fraction extended to the 80th cycle, corresponding to the value of 0.28. In other words, when the Li-air battery is operated using ambient air with stabilised electrolytes or without electrolyte degradation, discharge and charge can be repeated to about 60-65 cycles before Li_2CO_3 formation reaches the same value as a Li-air battery, compared to in Figure 6-5, which, when combined with electrolyte degradation, only gives 8 cycles.

The evidence from this study indicates that the air-feed affects the Li-air battery's performance in term of decreasing the discharge capacity due to low diffusion and solubility of oxygen, but this ambient air operation does not impact too much for the Li_2CO_3 generation during short-term cycles (8 cycles) due to the limited CO_2

contamination from the atmosphere.

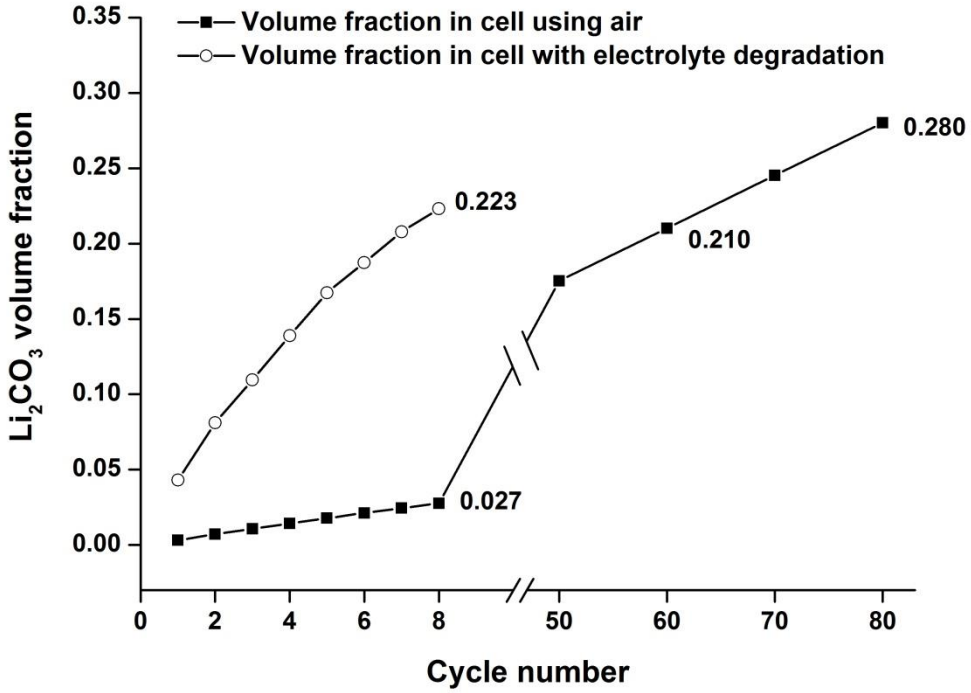

Figure 6-5: Volume fraction of Li_2CO_3 formation inside the the Li-air battery at the end of each discharge cycle compared to that between the cells with stabilised electrolytes and with electrolyte degradation effect. The parameters used in the model are the same as described in Figure 6-2.

6.4.2 Comparing the Li-air model with the experiment using air-feed

As the previous section demonstrates, the performance of the Li-air battery was explored at various discharge rates on ambient air-feeding, whereas the developed model in this section is now validated against our group's experimental data on the Li-air battery. The result of the 1st cycle obtained from the Li-air battery assembled in our lab is compared to the simulation as shown in Figure 6-6. The air electrode was prepared by loading 3.54 mg cm^{-2} of Super P (Timcal, surface area 61 m^2 g^{-1}) without using any catalyst. The electrolyte which was loaded in the electrochemical cell and applied to the simulation for this section was a 1 M lithium bis-trifluoromethansulfonyl imide (LiTFSI) in tetraethylene glycol dimethyl ether (TEGDME or tetraglyme).

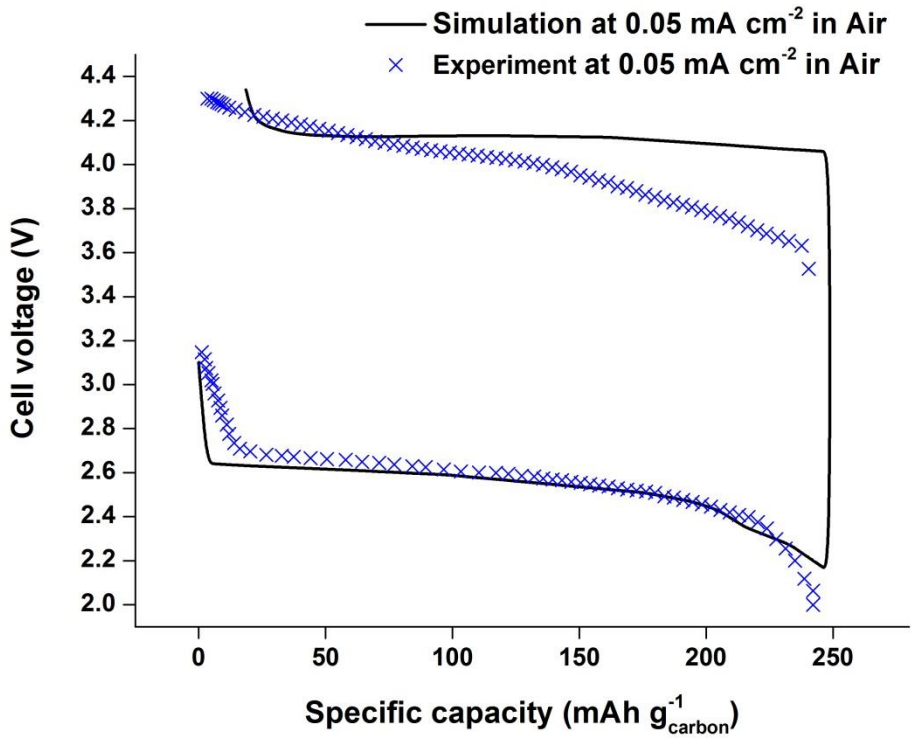

Figure 6-6: Voltage-capacity curve for a non-aqueous Li-air battery operated in ambient air feeding on the 1st cycle was validated against our group experiment at a rate of 0.05 mA cm^{-2}. The electrolyte contains 1 M LiTFSI dissolved in TEGDME. The cell cycle is simulated between 2.4 and 4.2 V versus Li/Li^+ and both results are tested at operating temperature 298.15 K.

It can be seen from the graph that the cell voltage-capacity curve at a rate of 0.05 mA cm^{-2} from the model matches the experimental data well during cell operation in 1 atm of dry atmospheric air. During discharge, the cell's potential fell steeply at the beginning, from a voltage of 3.1 V to a plateau at around 2.6 V which was well-matched to the Li-air test cell for a similar electrolyte and operating conditions. The Li-air model continuously discharged until reaching the cut-off voltage at 2.2 V corresponding to the discharge capacity based on the weight of carbon alone at 248 mAh g_{carbon}^{-1}, whereas the real system provided the discharge performance at 242 mAh g_{carbon}^{-1}. The validation of this study indicates that the developed Li-air model with the air feeding parameters can be used as a modelling tool to predict the Li-air battery performance in ambient conditions.

Contrary to expectations, the charging profile for the Li-air model did not match the experiment cell closely at the commencement of the charging process as demonstrated

in Figure 6-6. The former started to charge at 4.0 V and maintained at this potential until the end of charging step, while the latter begin at 3.6 V and gradually increased to the same cut-off charging voltage at 4.3 V. The most likely cause of different in charging potential between the two results is that the Li_2O_2 formed on the first discharge of the Li-air battery with tetraglyme based solvent coexists with a mixture of Li_2CO_3, HCO_2Li, CH_3CO_2Li, and esters, due to electrolyte decomposition [19]. These products were not included for charging process in the case of Li-air battery model which considered only the Li_2O_2 as the truly rechargeable product. Hence, the charging potential of experimental cell may vary according to the quantity of discharge products other than Li_2O_2. Moreover, the charge potential and capacity from both experiment and simulation were similar. This comparison confirms that the model results and experimental data show similarities and that the model is a promising tool to identify the Li-air battery mechanisms and forecast the cell's performance in ambient air.

6.4.3 Li-air performance combining the electrolyte degradation effect

In the previous section, the model demonstrates only the effect which the air-feeding has and allows us to study the impact of using air on the Li-air battery's performance. However, in practice, the challenge in non-aqueous electrolyte degradation still remains during the operation of the battery and the formation of Li_2CO_3 is unavoidable. Since the Li-air battery is still in its early development phase, there is no electrolyte that is perfectly compatible with the Li-air battery without some electrolyte degradation taking place. Hence, the model combines the effects of electrolyte degradation together with air operation.

As summarised in Table 6-4, the key results obtained from cycling Li-air battery with electrolyte degradation are compared with the cell using air-feeding and also plotted in Figure 6-4 and Figure 6-5 in term of capacity retention and Li_2CO_3 formation, respectively. It is apparent that the discharge capacity decreases dramatically during cell cycling from 250 mAh g_{carbon}^{-1} in the 1st cycle to very low value of 43 in the 8th cycle due to the high amount of irreversible Li_2CO_3 deposition as present in Figure 6-5. This cell performance falls faster than the Li-air with stable electrolyte as the latter can maintain the discharge capacity to 132 mAh g_{carbon}^{-1} at the same cycle (see Table 6-4). The capacity retention (decreasing to 17% in the 8th cycle) from the cell with electrolyte decomposition also follows the same trend of discharge capacity as shown in

Figure 6-4.

From this study, the electrolyte could be considered as a key component and one of the main issues which needs to be solved at present to sustain the rechargeability of non-aqueous Li-air batteries. It needs to be stable both in terms of oxygen rich electrochemical condition during Li-air operation and intermediate-reduced species as well as the lithium oxides (LiO_x) compounds which are formed on discharge. Fundamentally, the stable electrolyte determines a desired discharge product (Li_2O_2) and whether a truly rechargeable Li-air battery can be built or not, i.e., high coulombic efficiency during each cycle is close to 99% to maintain battery cycle life. It is worth noting that, although the electrolyte degradation in this model was not based on a detailed mechanism which includes complex elementary steps in the reaction sequence [12, 19], the generic Li_2CO_3 formation could be adequate to predict the Li-air deterioration during cycling.

6.5 Li-air battery performance with an oxygen-selective membrane

As the mechanism of Li_2CO_3 formation and the hydrolysis reaction with the metallic lithium anode results from the cathode exposed to CO_2 and H_2O respectively from ambient air, it is necessary to prevent these gases entering to the Li-air batteries. For example, the outer surface of the porous cathode could be covered with an oxygen diffusion membrane that may not only provide a much larger solubility of oxygen through the membrane but also block CO_2 and moisture content from the atmosphere [16, 17]. Moreover, the membrane could also minimise the evaporation of electrolyte from the Li-air battery.

In this section, the developed model considers the Li-air cell performance with the use of a membrane as an oxygen- selective medium to obtain a better discharge capacity and a CO_2 barrier to decrease the Li_2CO_3 formation. As shown in Figure 6-7, the porous cathode of a Li-air battery is protected by the oxygen selective membrane facing the atmosphere. As seen in the previous section, the Li-air battery including electrolyte decomposition effect tends to have higher Li_2CO_3 formation than the cell with the impact of CO_2 from the atmosphere alone. Hence, to distinguish these effects when the Li-air battery integrates a membrane barrier, the electrolyte degradation effect is excluded in this section.

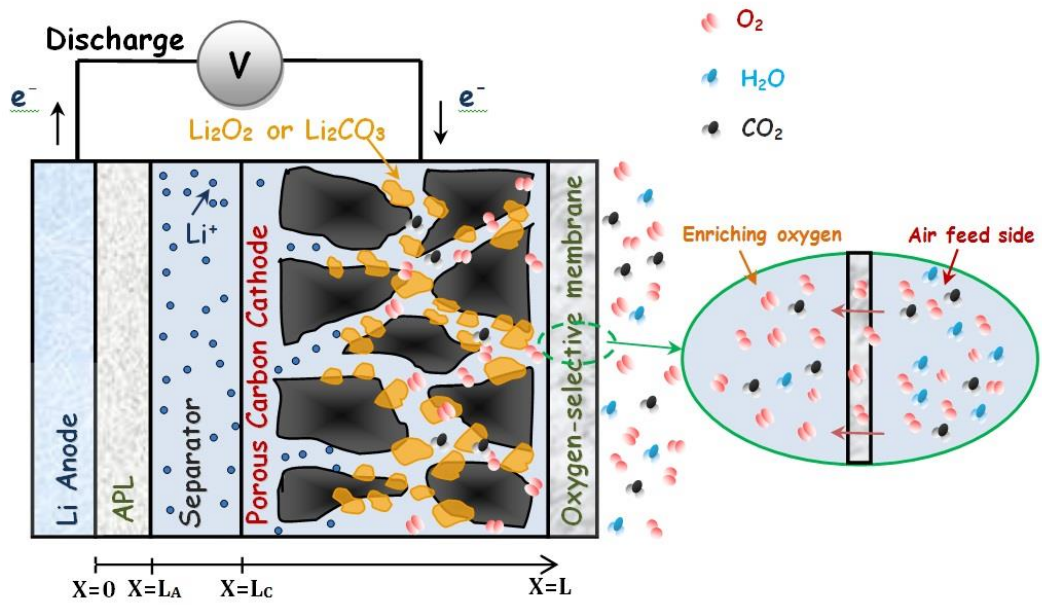

Figure 6-7: Schematic computation domain of a Li-air battery protected by an oxygen-selective membrane at the cathode.

A membrane could be simply considered as an interphase barrier covering the Li-air porous cathode and used for the separation of ambient air into oxygen-enriching steam diffusing through the Li-air battery. The separation for each gas in membranes occurs due to different physical properties in terms of permeability and solubility of the species flowing through the membrane. In this section, the Li-air model will be integrated with the silicone oil as an oxygen-selective liquid membrane for improving cell performance which is operated in ambient air. As mentioned early, the immobilized silicone oil membrane loaded in the various porous support films has been conducted in the Li-air batteries enabling them to operate in ambient air with a better performance [17].

To describe the mechanism of species in the membrane, a simplified development of the theory of gas transportation across a membrane is presented. For the single gas species, several assumptions will be made to simplify the model and the diffusion of gas through the membrane can be defined by Fick's first law:

$$N_{i,m} = -D_{i,m}\frac{dc_i}{dx} \tag{6-25}$$

where $N_{i,m}$ is the diffusion flux of gas through the membrane, $D_{i,m}$ is the diffusion coefficient in the membrane medium, and dc_i/dx is the concentration gradient of the gas across the membrane. If the diffusion flux does not change with time, a steady-state

condition exists. Hence, diffusion of gases exists through a membrane for which the concentrations of the diffusing species on both sides of a membrane are held constant. For a very thin membrane, if $D_{i,m}$ is assumed to be constant, Eq. (6-25) can be rearranged to:

$$N_{i,m} = D_{i,m} \frac{(c_i - c_{i,m})}{l} \tag{6-26}$$

where c_i and $c_{i,m}$ are the concentrations of the gas on upstream (air side) and downstream (after pass membrane), respectively, and l is the thickness of the membrane. For the membrane characterisation, the air or species permeation can be measured using the following equation:

$$P_i = \frac{\bar{F}_i}{A_m \Delta \bar{p}_{i,g}} = \frac{N_{i,m}}{\Delta \bar{p}_{i,g}} \tag{6-27}$$

where $\bar{F}_i$ is the permeation flow rate of gas *i* (mol s^{-1}), A_m is the membrane surface area (m^2), and $\Delta \bar{p}_{i,g}$ is the partial pressure differential of gas *i* (Pa). By combining Eq. (6-26) and Eq. (6-27) together, we can determine the concentration of gases after passing the membrane.

Table 6-5: The characterisation of the membrane and permeability of gases.

Membrane properties [a]	**Value**	**Ref.**
Thickness (m)	5×10^{-5}	[17]
Oxygen permeability (mol m^{-2} s^{-1} Pa^{-1})	2×10^{-7}	[35]
CO_2 permeability (mol m^{-2} s^{-1} Pa^{-1})	1.08×10^{-6}	[35]
Oxygen diffusion coefficient in membrane (m^2 s^{-1})	1.6×10^{-9}	[35]
CO_2 diffusion coefficient in membrane (m^2 s^{-1})	1.1×10^{-9}	[35]
Oxygen concentration after passing membrane (mol m^{-3})	2.18	Calculated
CO_2 concentration after passing membrane (mol m^{-3})	0.012	Calculated

[a] the membrane used in the model consists of silicone oil as the main material.

To date, various oxygen-selective membranes have been developed and laminated on the porous cathode to allow the unpressurised air to permeate through the membranes, i.e. no pressure is applied at the upstream side of the membrane. Several assumptions are made to simplify the calculation: 1) the different partial pressures of individual gases between the two side of the membrane covering the surface of the Li-air battery are not known unlike the membrane-testing cell that can be directly measured by the

pressure gauge; hence we assume that this value is as low as possible; 2) the diffusion coefficients of species in the thin membrane are assumed to be constant. The membrane characterisation and gases permeability for use in the Li-air battery with oxygen-selective membrane model are summarised in Table 6-5. The calculated concentrations of oxygen and CO_2 after passing the membrane are 2.18 and 0.012 mol m^{-3}, respectively.

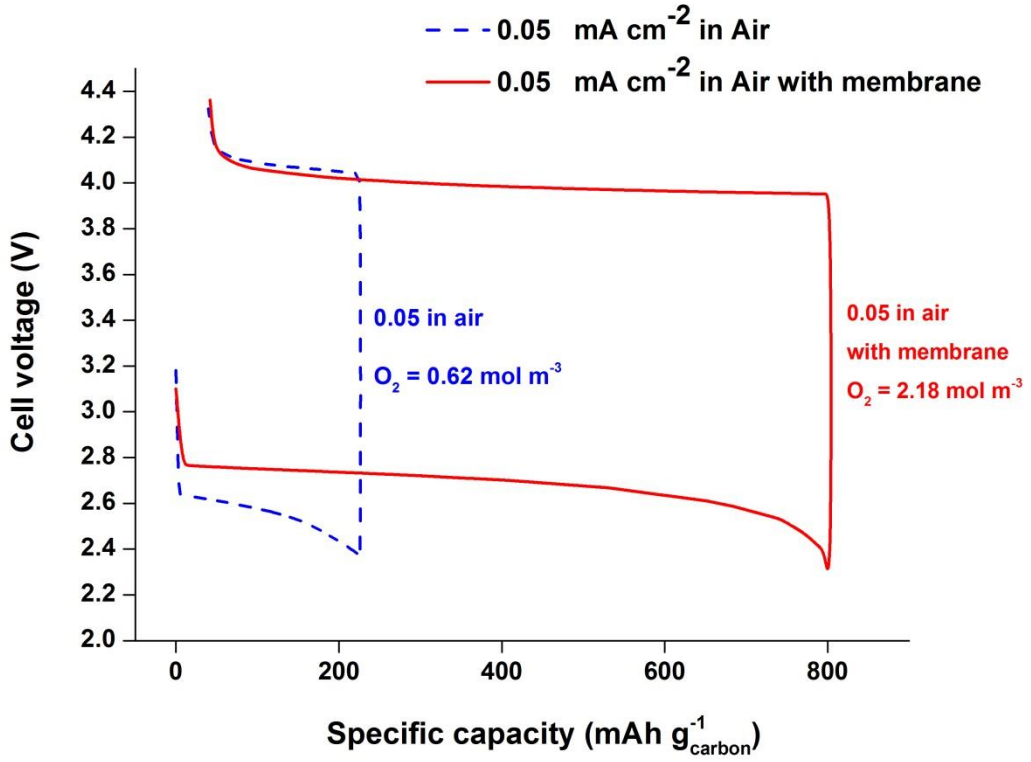

Figure 6-8: Comparison of the voltage-capacity curve for a non-aqueous Li-air battery model operated in ambient air in the case with and without oxygen-selective membrane at a rate of 0.05 mA cm^{-2}. The other parameters used in the model are the same as described in Figure 6-2.

The Li-air performance obtained from the air-feeding cell integrated with the 50 µm thickness of silicone oil membrane is compared to the absence one in Figure 6-8. Although, the membrane can enrich the oxygen concentration from 0.62 mol m^{-3} in air to 2.18 mol m^{-3} after passing the membrane, this is still not enough to operate the Li-air battery at high discharge rate. Hence, the low discharge rate at 0.05 mA cm^{-2} was applied in this section. As shown in Figure 6-8, the silicone oil membrane with a relatively high oxygen permeability of 2×10^{-7} mol m^{-2} s^{-1} Pa^{-1} (oxygen concentration 2.18 mol m^{-3}) at room temperature enabled the Li-air batteries to operate in ambient air with a specific capacity of 796 mAh g_{carbon}^{-1}, 3.5 times higher than the case without

using membrane due to higher oxygen concentration. This discharge capacity obtained from the model is similar to that obtained from the Li-air battery experiment using silicone oil liquid membrane for operation in ambient air, corresponding to a specific capacity of 789 mAh g_{carbon}^{-1} [17].

Moreover, it is apparent from the graph that the discharge cell voltages also increased, from ca. 2.60 V to 2.75 V with the high oxygen concentration in the Li-air cell protected with membrane but the charging voltage was not affected much due to the constant Li_2O_2 concentration which is assumed as the main product during battery charging. The CO_2 concentration also increased after permeation through the membrane owing to the higher permeability of CO_2 (1.08×10^{-6} mol m^{-2} s^{-1} Pa^{-1}) in silicone oil than oxygen (2×10^{-7} mol m^{-2} s^{-1} Pa^{-1} Table 6-5). However, the Li_2CO_3 generated from this increasing CO_2 did not notably influence the Li-air performance on the 1st cycle compared to the significant enhancement of specific capacity.

6.5.1 Membrane with high oxygen permeability

One of the most significant properties of the membrane for attainment in superior Li-air performance in term of high capacity and discharge rate is the high oxygen permeability. In this section, the effect of oxygen permeability at various ranges on maximum discharge capacity at different rates is presented for a 50μm thick membrane. The data was calculated using the equations as derived in the previous section. This assumes that the air window on the membrane and the cathode electrode have equal geometric areas.

The maximum specific discharge capacity at different rates for a Li-air battery obtained from an oxygen-selective membrane of any permeability can be compared in Figure 6-9. It is apparent from the graphs that the specific capacity enhances high oxygen permeability and it becomes smaller at higher discharge currents due to the limitation of the oxygen's ability to diffuse inside the cathode. However, even with the high oxygen-permeable membrane, the maximum discharge current to perform a Li-air battery is only 0.5 mA cm^{-2} with discharge capacity below 300 mAh g_{carbon}^{-1}. The results of this study indicate that, although the specific capacity of Li-air batteries is about two times higher than in conventional Li-ion batteries (150 mAh g_{carbon}^{-1}), the operating discharge currents are still not high enough for use in heavy-duty power devices or electric

vehicles which require higher discharge rate (> 2 mA cm^{-2}) [36].

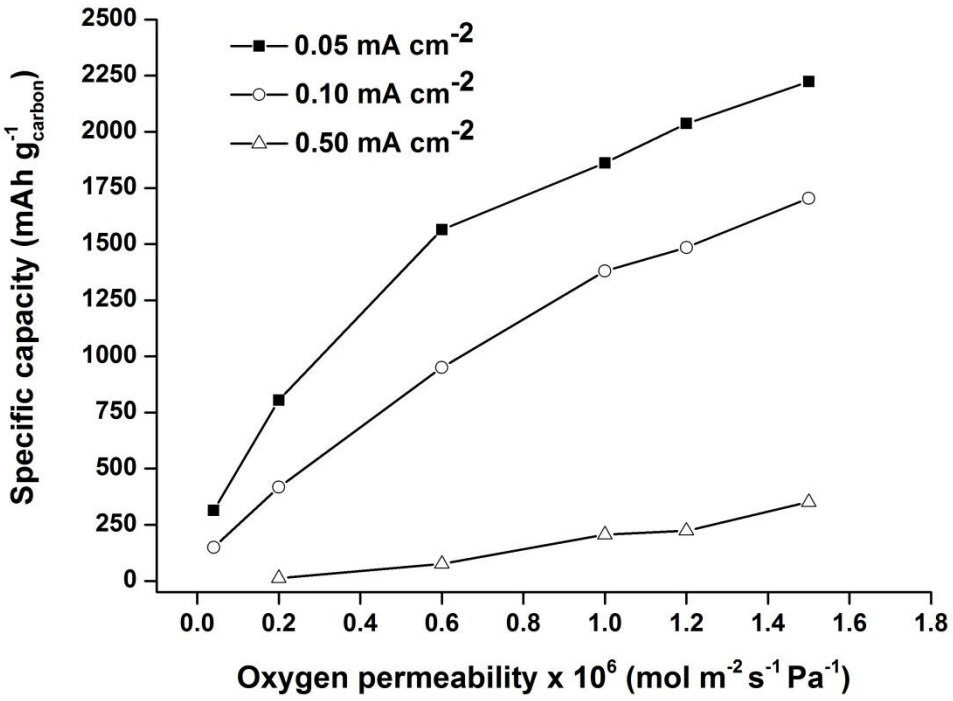

Figure 6-9: Effect of oxygen permeability on maximum specific discharge capacity at different discharge rates of a non-aqueous Li-air battery protected with a 50 μm thick oxygen-selective membrane. The other parameters used in the model are the same as described in Figure 6-2.

For CO_2 transport through most oxygen-selective membranes, its permeability is often comparable to oxygen, i.e. ratios of P_{O_2}/P_{CO_2} are generally less than unity [24]. CO_2 from atmosphere can react with the desired Li_2O_2 discharge product or electrolytes to form Li_2CO_3. The Li_2O_2 can be reversibly converted to evolve oxygen at about 4.0-4.5 V lower than the Li_2CO_3 which requires high potential more than 4.5 V to recharge [12, 37]. Hence, if the membrane is being used for a rechargeable Li-air battery, it must effectively separate the CO_2 from the air inlet for maintaining a long-life cycle of Li-air battery. This is a challenge because materials with high oxygen permeability also have high CO_2 permeability [35, 38]. However, the CO_2 impurity is not the problem in primary Li-air batteries due to the absence of charging process so the final discharge product does not matter. A recent study of a novel non-aqueous Na-air battery by Das et al. (2013) reported that a gas mixture of CO_2 (63%) and oxygen (37%) can increase the discharge capacity of Na-air battery in tetraglyme-based electrolyte from 1,390 in pure

oxygen to 2,882 mAh g_{carbon}^{-1}, an increase of 2.1 times [39]. Therefore, without any recharging, CO_2 can help the primary battery to increase the performance.

Nitrogen is an inert gas and has little or no effect with lithium-based electrolyte on the Li-air battery's performance [24]. Published studies exist which describe lithium nitride (Li_3N) formation generated from the direct reaction of nitrogen with lithium in Li-ion batteries at room temperature during charge-discharge cycles [40, 41]. The same behaviour could possibly occur on the surface of metallic lithium in Li-air battery. However, in this work, we focus on the porous cathode which contributes to the main part of Li-air battery. Moreover, the permeability ratios between oxygen and nitrogen (P_{O_2}/P_{N_2}) are normally higher than the unity, thus increasing the relative content of oxygen over nitrogen in the feeding steam.

6.6 Conclusions

A macro-homogeneous model was developed and used to analyse the capacity and cycling behaviour of the rechargeable Li-air battery operated under ambient air conditions. The model uses a set of governing equations which describe species transport, charge and reaction kinetics within the battery, taking into consideration of by-product formation, electrolyte decomposition and changes in surface area and porosity. The model can accurately predict the capacity feature and the detrimental effect of electrolyte decomposition and Li_2CO_3 formation on the capacity retention. The model forecasts a significant influence of using an oxygen-selective membrane, which could lead to an increment in specific capacity of up to 4 times. The simulated results are in a good agreement with the experimental data.

6.7 References

1. Bruce, P.G., S.A. Freunberger, L.J. Hardwick and J.M. Tarascon, *Li-O_2 and Li-S batteries with high energy storage.* Nature Materials, 2012. **11**(1): p. 19-29.
2. Christensen, J., P. Albertus, R.S. Sanchez-Carrera, T. Lohmann, B. Kozinsky, R. Liedtke, J. Ahmed and A. Kojic, *A critical review of Li/air batteries.* Journal of the Electrochemical Society, 2012. **159**(2): p. R1-R30.
3. Girishkumar, G., B. McCloskey, A.C. Luntz, S. Swanson and W. Wilcke, *Lithium-air battery: Promise and challenges.* Journal of Physical Chemistry Letters, 2010. **1**(14): p. 2193-2203.

4. Lee, J.S., S.T. Kim, R. Cao, N.S. Choi, M. Liu, K.T. Lee and J. Cho, *Metal-air batteries with high energy density: Li-air versus Zn-air.* Advanced Energy Materials, 2011. **1**(1): p. 34-50.
5. Abraham, K.M. and Z. Jiang, *A polymer electrolyte-based rechargeable lithium/oxygen battery.* Journal of the Electrochemical Society, 1996. **143**(1): p. 1-5.
6. Ogasawara, T., A. Débart, M. Holzapfel, P. Novák and P.G. Bruce, *Rechargeable Li_2O_2 electrode for lithium batteries.* Journal of the American Chemical Society, 2006. **128**(4): p. 1390-1393.
7. Read, J., *Characterization of the lithium/oxygen organic electrolyte battery.* Journal of the Electrochemical Society, 2002. **149**(9): p. A1190-A1195.
8. Kuboki, T., T. Okuyama, T. Ohsaki and N. Takami, *Lithium-air batteries using hydrophobic room temperature ionic liquid electrolyte.* Journal of Power Sources, 2005. **146**(1-2): p. 766-769.
9. Cheng, H. and K. Scott, *Carbon-supported manganese oxide nanocatalysts for rechargeable lithium-air batteries.* Journal of Power Sources, 2010. **195**(5): p. 1370-1374.
10. Laoire, C.O., S. Mukerjee, K.M. Abraham, E.J. Plichta and M.A. Hendrickson, *Influence of nonaqueous solvents on the electrochemistry of oxygen in the rechargeable lithium-air battery.* Journal of Physical Chemistry C, 2010. **114**(19): p. 9178-9186.
11. Zhang, J.G., D. Wang, W. Xu, J. Xiao and R.E. Williford, *Ambient operation of Li/Air batteries.* Journal of Power Sources, 2010. **195**(13): p. 4332-4337.
12. Freunberger, S.A., Y. Chen, Z. Peng, J.M. Griffin, L.J. Hardwick, F. Bardé, P. Novák and P.G. Bruce, *Reactions in the rechargeable lithium-O_2 battery with alkyl carbonate electrolytes.* Journal of the American Chemical Society, 2011. **133**(20): p. 8040-8047.
13. Xu, W., V.V. Viswanathan, D. Wang, S.A. Towne, J. Xiao, Z. Nie, D. Hu and J.-G. Zhang, *Investigation on the charging process of Li_2O_2-based air electrodes in Li-O_2 batteries with organic carbonate electrolytes.* Journal of Power Sources, 2011. **196**(8): p. 3894-3899.
14. Sahapatsombut, U., H. Cheng and K. Scott, *Modelling the micro–macro homogeneous cycling behaviour of a lithium–air battery.* Journal of Power Sources, 2013. **227**(0): p. 243-253.

15. Sahapatsombut, U., H. Cheng and K. Scott, *Modelling of electrolyte degradation and cycling behaviour in a lithium–air battery.* Journal of Power Sources, 2013. **243**(0): p. 409-418.
16. Zhang, J., W. Xu, X. Li and W. Liu, *Air dehydration membranes for nonaqueous lithium-air batteries.* Journal of the Electrochemical Society, 2010. **157**(8): p. A940-A946.
17. Zhang, J., W. Xu and W. Liu, *Oxygen-selective immobilized liquid membranes for operation of lithium-air batteries in ambient air.* Journal of Power Sources, 2010. **195**(21): p. 7438-7444.
18. Xu, W., et al., *Reaction mechanisms for the limited reversibility of Li-O_2 chemistry in organic carbonate electrolytes.* Journal of Power Sources, 2011. **196**(22): p. 9631-9639.
19. Freunberger, S.A., Y. Chen, N.E. Drewett, L.J. Hardwick, F. Bardé and P.G. Bruce, *The Lithium–Oxygen Battery with Ether-Based Electrolytes.* Angewandte Chemie International Edition, 2011. **50**(37): p. 8609-8613.
20. Takechi, K., T. Shiga and T. Asaoka, *A Li-O_2/CO_2 battery.* Chemical Communications, 2011. **47**(12): p. 3463-3465.
21. Zhang, D., R. Li, T. Huang and A. Yu, *Novel composite polymer electrolyte for lithium air batteries.* Journal of Power Sources, 2010. **195**(4): p. 1202-1206.
22. Jitaru, M., *Electrochemical carbon dioxide reduction - fundamental and applied topics (review).* Journal of the University of Chemical Technology and Metallurgy, 2007. **42**(4): p. 333-344.
23. MacKenzie, F.T., *Our Changing Planet: An Introduction to Earth System Science and Global Environmental Change*2010: Prentice Hall.
24. Crowther, O. and M. Salomon, *Oxygen selective membranes for Li-air (O_2) batteries.* Membranes, 2012. **2**(2): p. 216-227.
25. Read, J., K. Mutolo, M. Ervin, W. Behl, J. Wolfenstine, A. Driedger and D. Foster, *Oxygen Transport Properties of Organic Electrolytes and Performance of Lithium/Oxygen Battery.* Journal of the Electrochemical Society, 2003. **150**(10): p. A1351-A1356.
26. Gennaro, A., A.A. Isse and E. Vianello, *Solubility and electrochemical determination of CO_2 in some dipolar aprotic solvents.* Journal of Electroanalytical Chemistry and Interfacial Electrochemistry, 1990. **289**(1–2): p. 203-215.

27. Shao, Y., F. Ding, J. Xiao, J. Zhang, W. Xu, S. Park, J.G. Zhang, Y. Wang and J. Liu, *Making Li-air batteries rechargeable: Material challenges.* Advanced Functional Materials, 2013. **23**(8): p. 987-1004.
28. McCloskey, B.D., D.S. Bethune, R.M. Shelby, G. Girishkumar and A.C. Luntz, *Solvents critical role in nonaqueous Lithium-Oxygen battery electrochemistry.* Journal of Physical Chemistry Letters, 2011. **2**(10): p. 1161-1166.
29. Mizuno, F., S. Nakanishi, Y. Kotani, S. Yokoishi and I. Hideki, *Rechargeable li-air batteries with carbonate-based liquid electrolytes.* Electrochemistry, 2010. **78**(5): p. 403-405.
30. Wang, Y., D. Zheng, X.Q. Yang and D. Qu, *High rate oxygen reduction in non-aqueous electrolytes with the addition of perfluorinated additives.* Energy and Environmental Science, 2011. **4**(9): p. 3697-3702.
31. Xu, W., et al., *The stability of organic solvents and carbon electrode in nonaqueous Li-O_2 batteries.* Journal of Power Sources, 2012. **215**: p. 240-247.
32. Roberts Jr, J.L., T.S. Calderwood and D.T. Sawyer, *Nucleophilic oxygenation of carbon dioxide by superoxide ion in aprotic media to form the $C_2O_6^{2-}$ species.* Journal of the American Chemical Society, 1984. **106**(17): p. 4667-4670.
33. Wadhawan, J.D., P.J. Welford, E. Maisonhaute, V. Climent, N.S. Lawrence, R.G. Compton, H.B. McPeak and C.E.W. Hahn, *Microelectrode studies of the reaction of superoxide with carbon dioxide in dimethyl sulfoxide.* Journal of Physical Chemistry B, 2001. **105**(43): p. 10659-10668.
34. Xiao, J., J. Hu, D. Wang, D. Hu, W. Xu, G.L. Graff, Z. Nie, J. Liu and J.G. Zhang, *Investigation of the rechargeability of Li-O_2 batteries in non-aqueous electrolyte.* Journal of Power Sources, 2011. **196**(13): p. 5674-5678.
35. Robb, W.L., *Thin Silicone membranes-their permeation properties and some applications.* Annals of the New York Academy of Sciences, 1968. **146**(1): p. 119-137.
36. Liu, X.-M., Z.d. Huang, S.w. Oh, B. Zhang, P.-C. Ma, M.M.F. Yuen and J.-K. Kim, *Carbon nanotube (CNT)-based composites as electrode material for rechargeable Li-ion batteries: A review.* Composites Science and Technology, 2012. **72**(2): p. 121-144.
37. Zhang, T. and H. Zhou, *A reversible long-life lithium-air battery in ambient air.* Nature Communications, 2013. **4**.
38. Dias, A.M.A., M. Freire, J.A.P. Coutinho and I.M. Marrucho, *Solubility of oxygen*

in liquid perfluorocarbons. Fluid Phase Equilibria, 2004. **222-223**: p. 325-330.

39. Das, S.K., S. Xu and L.A. Archer, *Carbon dioxide assist for non-aqueous sodium-oxygen batteries.* Electrochemistry Communications, 2013. **27**: p. 59-62.
40. Wang, H., W.-D. Zhang, Z.-Q. Deng and M.-C. Chen, *Interaction of nitrogen with lithium in lithium ion batteries.* Solid State Ionics, 2009. **180**(2–3): p. 212-215.
41. David, D.J., M.H. Froning, T.N. Wittberg and W.E. Moddeman, *Surface reactions of lithium with the environment.* Applications of Surface Science, 1981. **7**(3): p. 185-195.

Chapter 7: Modelling of Na-air Battery with Porous Gas Diffusion Electrode

In this chapter, a macro-homogeneous model to evaluate the impact of replacing a conventional flooded electrode with a gas diffusion electrode on the performance of a non-aqueous Na-air battery is presented. The Na-air batteries have recently been considered by researchers as an advanced rechargeable battery which replaces the lithium anode with cheap and abundant sodium metal for environmental and sustainable development. This novel battery should provide the similar performance to Li-air batteries to fulfil the growing energy storage demands for the electrical vehicles and stationary applications. This model used the micro-macro homogeneous system as discussed in Chapter 4 and the electrolyte degradation effect in Chapter 5. The biggest difference is that the cathode structure was applied a gas diffusion electrode instead of being flooded. Moreover, the loss of electrolyte volume fraction due to the degradation during battery cycling was also considered.

7.1 Introduction

Over recent decades many studies have devoted much effort to rechargeable lithium-oxygen/air batteries (Li-air) for advanced energy storage and new electrochemical technology with high theoretical specific energy [1-3]. In contrast to commercial lithium-ion battery systems, the Li-air battery merges the advantage of fuel cells and batteries in that one of the active materials (oxygen) comes from the atmospheric air. Assuming lithium peroxide (Li_2O_2) as a solid product, the cell system ideally operates at up to a potential of 2.96 V and exhibits a theoretical specific energy of 11,640 Wh kg^{-1}, several times higher than that of conventional lithium-ion batteries generally applied in commercial electronic devices and electric vehicles. However, a major problem with this kind of application is the large overpotentials in practical cells, on discharge ($\eta_{dis} \approx$ 300 mV) and on charge (η_{chg} > 1000 mV), resulting in low round-trip efficiency during battery cycling. Therefore, effort has been made to search for suitable catalysts to increase Li-air performance.

Despite the Li-air batteries safety and efficiency issues, some early results reveal more

complex cell reactions [4-6]. There is strong evidence that the non-aqueous electrolytes applied in Li-air batteries using both carbonate and ether-based solvents tended to react with the intermediate reactive superoxide radical product and decompose irreversibly during battery discharge and charge cycles [7-9]. Recent research found that the Li-air operated in ether-based electrolyte can form the desired discharge product of Li_2O_2, but it still suffers from electrolyte degradation and results in large overpotentials [10-12]. Moreover, there is increasing concern that the cost of lithium may rise as demand for battery materials increases [13]. Hence, substitution of lithium by sodium metal, which provides very suitable redox potential almost as high as lithium ($E^0_{(Na^+/Na)} = -2.71$ compared to $E^0_{(Li^+/Li)} = -3.05$ versus standard hydrogen electrode (SHE)), may offer promising rechargeable metal-air batteries for energy storage application.

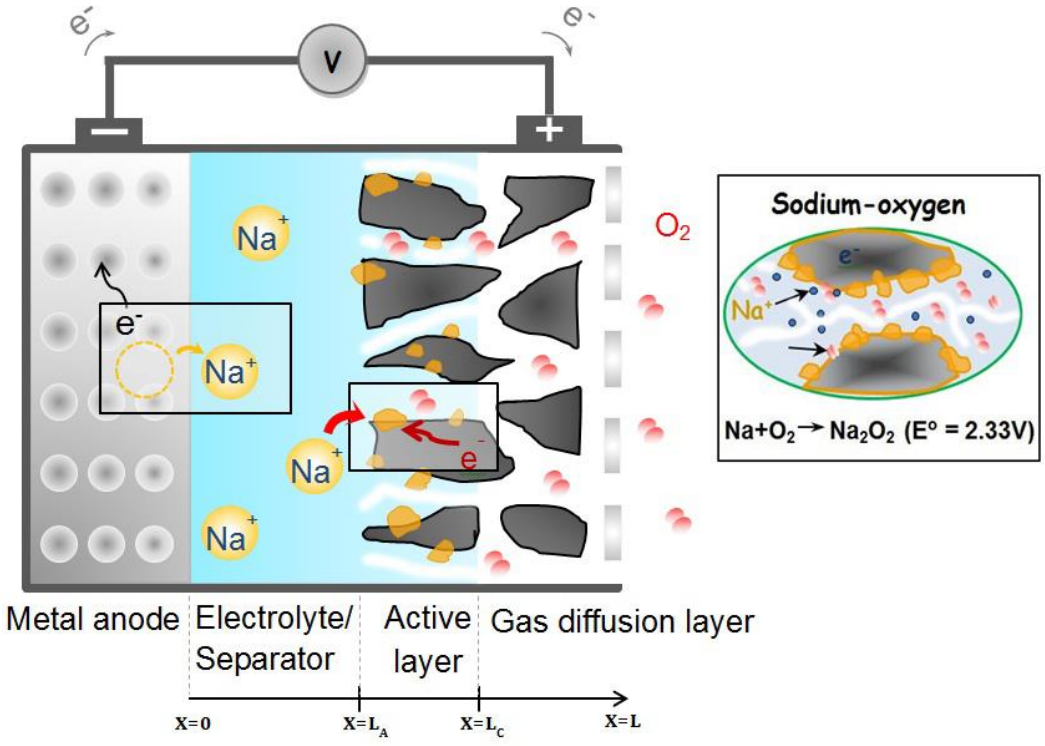

Figure 7-1 Schematic computation domain of a Na-air battery with gas diffusion electrode during discharge operation. The inset demonstrates the discharge products formation of Na_2O_2 covering on the porous carbon surface.

The Na-oxygen/air cell has a high specific energy depending on the discharge products, i.e. Na_2O_2 provides 1,605 Wh kg^{-1} with a standard cell potential $E^0 = 2.33\,V$. Furthermore, sodium is placed right below lithium in the periodic table and it is expected that their chemical properties could be similar. The working principle of both

lithium and sodium oxygen battery systems is similar in concept as shown in Figure 7-1. For a non-aqueous electrolyte system, the possible cell reactions during discharge process for Na-air battery are the formation of different sodium oxide products by the reduction reaction with oxygen according to following reactions

Cathode $Na^+ + O_2 + e^- \rightarrow NaO_2 \quad (E^0 = 2.27\ V\ vs\ Na)$ (7-1)

$2Na^+ + O_2 + 2e^- \rightarrow Na_2O_2 \quad (E^0 = 2.33\ V\ vs\ Na)$ (7-2)

$4Na^+ + O_2 + 4e^- \rightarrow 2Na_2O \quad (E^0 = 1.95\ V\ vs\ Na)$ (7-3)

There are several studies of Na-air batteries. The different types of discharge products (sodium oxides) have been reported depending on the solvent used in the system as summarised in the Table 7-1.

Table 7-1 Different discharge products from the studies of Na-air batteries.

Cathode	**Electrolyte**	**Reactant**	**Main product**	**Ref.**
GNS	0.25M $NaPF_6$/DME	Dried air	Na_2O_2	[14]
GNS	0.25M $NaClO_4$/DME	Dried air	Na_2O_2	[14]
Thin film carbon	0.25M $NaPF_6$/DME	Dried air	Na_2O_2	[14]
Carbon-fibre	0.25M $NaPF_6$/DME	Dried air	Na_2O_2	[14]
Diamond-like carbon (DLC)	1M $NaPF_6$/EC:DMC	Dried air	Na_2O_2/ Na_2CO_3	[15]
Super P/PVDF	0.75 M $NaCF_3SO_3$/ionic liquid	Pure O_2	$Na_2C_2O_4$	[16]
Super P/PVDF	1M $NaClO_4$/TEGDME	Pure O_2	Na_2CO_3	[16]
Carbon-fibre gas diffusion layer	0.5M $NaCF_3SO_3$/DEGDME	Pure O_2	NaO_2	[17]
Ketjet Black/NMP	1M $NaClO_4$/PC	Pure O_2	Na_2CO_3	[18]
Ketjet Black/NMP	1M $NaClO_4$/TEGDME	Pure O_2	Na_2O_2	[18]

GNS = Graphene nano sheet, NMP= N-methyl-2-pyrrolidone (binder)

Na-air batteries are also regarded as another promising alternative energy storage system and several attempts have been made to build Na-air batteries [13, 19]. The feasibility of a liquid-sodium-oxygen cell with polymer electrolytes has been reported and operated at high temperature up to 100 ºC to eliminate the sodium dendrite formation at the anode [20]. However, liquid sodium is well known as highly corrosive and the high operating temperatures are challenging for practical applications.

Sun *et al*. have investigated a rechargeable Na-air battery working at room temperature with a carbonate-based electrolyte using dry-air and found that both crystallised sodium peroxide (Na_2O_2) and amorphous sodium carbonate (Na_2CO_3) coexist as the discharge products but disappear during charging [15]. The thin film electrode based on the weight of carbon film provided an initial discharge capacity of 1884 mAh g_{carbon}^{-1} at a discharge voltage plateau of 2.3 V. For the initial charge process, this thin film air electrode had sluggish diffusion and reaction kinetics during charging with a starting charging potential of 3.5 V, ending at 3.9 V [15]. Thus, this system also suffers from similar high overpotential and low energy efficiencies to the Li-air battery with a carbonate-based electrolyte.

Hartmann *et al*. have recently studied a reversible Na-O_2 cell using an ether-based electrolyte showing that the main discharge product was sodium superoxide (NaO_2) deposited on a carbon-fibre gas diffusion layer. The cell performance gave a very low overpotential during the discharge/charge cycle (< 200 mV) at current densities of 0.2 mA cm^{-2} [17]. The charging process at low current densities (0.12 mA cm^{-2}) showed a voltage plateau between 2.3 and 2.4 V, which is close to the potential for the decomposition of NaO_2 (Eq. (7-1)) to form Na^+ and oxygen [17].

Recently, Kim *et al.* investigated the electrochemical reaction mechanisms of Na-O_2 batteries in alkyl-carbonated and ether based electrolytes showing a clear distinction between discharge products with the two types of electrolytes [18]. It was found that the rechargeable cell with carbonate-based electrolyte was based on the formation and decomposition of sodium carbonate (Na_2CO_3), while the ether-based cell was cycled from the main product of hydrated sodium peroxides ($Na_2O_2.H_2O$).

Overall the report literature has shown the feasibility of Na-air batteries as candidates for a new energy storage device. However, little attention has been paid to the Na-air battery modelling. Unlike the previous Li-air models, which considered the cathode as a flooded porous electrode [21, 22], this model studied the cycling behaviour of a Na-air battery based on macro homogeneous model using a gas diffusion electrode (GDE) in contact with a liquid electrolyte. This model accounts for mass transfer in the gas diffusion layer and active layer with the set of equations for material balances and electrochemical kinetics. The model also included the electrolyte degradation effect to

form Na_2CO_3 by-product and predicts the time dependence of species concentrations, non-uniform porosity and cell performance in different discharging rates and initial parameters. The gradual loss of electrolyte from the electrolyte decomposition was considered in this chapter. Although other byproducts besides Na_2CO_3 are formed during electrolyte decomposition, their quantities may be considered as insignificant relative to both the main discharge products of Na_2O_2 and Na_2CO_3, which are considered in this study. This model can be used to describe the behaviour of Na-air batteries as well as to optimise the performance and structure of these battery electrodes.

7.2 Theoretical mechanism analysis

GDE, which consist of a very complicated structure of small porosity, are the key feature in fuel cells and batteries. Recently, they have been increasingly applied in metal-air battery systems to enhance their performance [2, 17]. The mathematical model of Na-air presented in this study was one-dimensional and considered the battery as consisting of a gas diffusion layer (GDL), a cathode active layer comprising partially dissolved sodium salt in an aprotic solvent and a separator containing electrolyte, as presented in Figure 7-1. During discharge, the oxidation reaction of sodium metal occurs at the sodium-electrolyte interface is as follows

Anode $$Na\,(metal) \rightarrow Na^+ + e^- \qquad (E_{ref} = 0\ V\ vs\ Na) \qquad (7\text{-}4)$$

There are three phases in GDE: the gas phase of the reactants (oxygen or air), the solid phase of electrically conductive material (carbon and catalyst), and the liquid phase of electrolyte solution. The transport and electrochemical processes taking place in GDE are as follow

i. The reactant gas (oxygen or air) transports from the atmosphere to the surface of GDE.
ii. The reactant diffuses through the porous GDL, which contains conductive material.
iii. The reactant gas dissolves at the gas-liquid interphase into the porous active layer.
iv. The reactant in the liquid phase transports to the active site via liquid phase diffusion.

v. The ionic reactant (Na^+) is generated by the oxidation reaction at the anode and transports by diffusion and migration through the separator and the active layer.
vi. At the partially-wetted pore formed by liquid electrolyte in active layer, there takes place the electrochemical reaction between oxygen and Na^+.
vii. The electrons are transported in the solid matrix by electrical conduction to or from the current collector and conducted towards the active area, where the charge transfer reduction takes place between Na^+ and oxygen to form the sodium oxide products depends on the types of electrolytes used and electrochemical reaction.

Due to reaction at the Na-air cathode involving oxygen reduction in non-aqueous electrolytes containing sodium salts, it is believed that, like Li-air battery systems, the discharge product of Na_2O_2 could be formed in Na-air batteries [15], and this reaction includes a two-step reaction consisting of the electrochemical formation of sodium superoxide (NaO_2) and then chemical decomposition of NaO_2 to form Na_2O_2 [23, 24]. As this battery system is analogous to the Li-air battery model [21, 22], the mechanisms considered in this Na-air model are the reduction reaction of oxygen to form the desired product of Na_2O_2 during battery discharging and by-product Na_2CO_3 generated from the electrolyte solvent degradation [18].

7.2.1 Electrolyte degradation

Analogous to the Li-air battery, finding suitable electrolytes with high stability during cell operation is a key to obtaining long-term Na-air battery cyclability, especially in an oxygen-rich environment and catalytic conditions [25]. Since Na-air batteries have been developed, various non-aqueous electrolytes have been examined. Kim *et al.* proposed the reaction mechanism for Na-air batteries with both alkyl-carbonate and ether based electrolytes and found that these two electrolytes also decomposed during the battery discharging and charging processes [18]. Hence, the electrolyte degradation mechanisms proposed in chapter 6 were also included in this model as described below

Na_2CO_3 formation

$$2O_2 + 2e^- \xrightarrow{k1a} 2O_2^- \qquad (E^0 = 2.84\, V_{Na}) \qquad (7\text{-}5)$$

$$2O_2^- + 2CO_2 \xrightarrow{k1b} C_2O_6^{2-} + O_2 \qquad \text{RDS} \qquad (7\text{-}6)$$

$$C_2O_6^{2-} + 4Li^+ + 2O_2^- \rightarrow 2Na_2CO_3 + 2O_2 \quad (7\text{-}7)$$

Overall $4Na^+ + 2CO_2 + 2O_2^- + 2e^- \rightarrow 2Na_2CO_3 + O_2 \quad (E^0 = 6.85\, V_{Na}) \quad (7\text{-}8)$

Solvent degradation

$$O_2 + e^- \overset{k1a}{\longrightarrow} O_2^- \quad (E^0 = 2.84\, V_{Na}) \quad (7\text{-}9)$$

$$O_2^- + [Solvent] \rightarrow [Solvent]^- \quad (7\text{-}10)$$

$$[Solvent]^- + O_2 \rightarrow CO_2 + H_2O + HCO_2Li + CH_3CO_2Li \quad (7\text{-}11)$$

Overall $2O_2 + [Solvent] + e^- \rightarrow CO_2 + H_2O + HCO_2Li + CH_3CO_2Li \quad (7\text{-}12)$

It is worth noting that the exact detail of the reaction routes for the electrolyte degradation to form Na_2CO_3 are complicated involving several intermediates during cell operation. Moreover, the loss of electrolyte volume by degradation during the battery operation is considered and explained in the model section.

7.2.2 Charging process

For the Na-air battery, different discharged products have been reported during the battery operation as mentioned previously and summarised in Table 7-1. The model assumes that Na_2O_2, which is the desired product, is oxidised to Na^+ and oxygen during charging (reverse of Eq. (7-2)). Therefore, the charging process for Na-air battery applied in this model is similar to the Li-air battery model described in chapter 3.

7.3 Model Development

7.3.1 Model description

This chapter investigated the various parameters on the performance of Na-air battery by using a macroscopic one-dimensional model of a gas diffusion electrode in contact with a non-aqueous electrolyte. The mathematical model for a prismatic single cell of a Na-air battery consists of three domain regions, which are: a separator, an active layer and a GDL, as shown in Figure 7-1. The reaction in the cathode and anode were followed Eq. (7-2) and Eq. (7-4), respectively and also included the electrolyte degradation as described above.

7.3.2 Model assumption

As the Na-air battery system is complex with the various reactions and mass transport species into two phases (gas and liquid), the build-up of Na_2O_2 and Na_2CO_3, the electrolyte loss by degradation, and the dynamic change of porosity and interfacial surface area, several model assumptions were adopted to support the calculation as follow

viii. The Na-air battery is operated in isothermal conditions so that the thermal effects are not considered.
ix. Ideal gas behaviour is applied in the cell due to low operating pressure.
x. The solid salts of Na_2O_2 and Na_2CO_3 are the main discharge products which only occur and deposit inside the active layer of GDE.
xi. The electrolytes used in Na-air batteries are assumed a binary monovalent electrolyte which consists of a single salt in a homogeneous organic solvent mixture.
xii. The pores in the active layer consist of a three-phase system: gas from the reactant species, liquid from the non-aqueous electrolyte, and solid from active carbon and discharge products.
xiii. The separator is impermeable to oxygen gas.

The model of the Na-air battery using GDE as the cathode electrode is similar to that of fuel cell systems excepting that there is no flow channel in the former (reactant gas is packed inside the battery system), then the boundary conditions between the bulk reactant gas and GDL are taken as the feed gas compositions.

7.3.3 Mass transport for reactant gas

In the Na-air battery, the oxidant (air or pure oxygen) flows from the gas reservoir (bulk gas) through porous gas diffusion media, in which no electrolyte is present, and moves through the porous active layer, which is partially wetted with non-aqueous electrolyte to form a 3-phase interfacial area, before dissolving and transporting in electrolyte to react with Na^+ at the reaction surface of active carbon. To achieve a high efficiency of GDE, a continuous supply of reactant gas has to reach the thin electrolyte film covering on the surface of the porous active layer. In this model, only transport processes for reactant gas in the porous media were considered with two transport phenomena of diffusion and convection.

For the dynamic one-dimensional Na-air battery model, the conservation of mass of gas can be expressed as

$$\rho \frac{\partial w_i}{\partial t} + \nabla \cdot \boldsymbol{N_{i,mass}} = S_{mass} \tag{7-13}$$

where w_i is the mass fraction of species i, ρ is the density of the gas mixture, and S_{mass} is the mass source term from any reactions. The total mass flux $\boldsymbol{N_{i,mass}}$ for the transport of gas species i, due to diffusion and convection, is given by

$$\boldsymbol{N_{i,mass}} = \boldsymbol{J_i} + \rho \boldsymbol{u} w_i \tag{7-14}$$

where $\boldsymbol{J_i}$ is the diffusion flux and $\rho \boldsymbol{u} w_i$ is the convective flux, i.e. the product of density and velocity.

As the models were developed to cover the variety of feeding reactant gases (i.e. oxygen or air mixture), the Stefan-Maxwell equation and Darcy's law were adopted to model the mass transport processes in the gas channel of the GDE. The Stefan-Maxwell equation was used to account for the effect of interactions between species during mass transport and the velocity of species inside the porous media was calculated from Darcy's law (defined in Eq. (7-22)). To include the Stefan-Maxwell equation for mass transport, the mass balance in Eq. (7-13) can be modified in the following form

$$\rho \frac{\partial w_i}{\partial t} + \nabla \cdot \left[\rho \boldsymbol{u} \cdot w_i - \rho w_i \sum_j \widetilde{D}_{ij} \left\{ \nabla x_j + (x_j - w_j) \frac{\nabla p}{p} \right\} \right] = S_{mass} \tag{7-15}$$

where x_j is the mole fraction of species j, p is the pressure inlet to the system, and $\widetilde{D}_{ij}$ are the binary symmetric diffusivities of the species pair i-j. The second term $\rho \boldsymbol{u} \cdot w_i$ is the convection term. The velocity vector $\boldsymbol{u}$ can be calculated from Darcy's law. The third term in the form of Stefan-Maxwell equation describes the effect of diffusion.

The binary symmetric diffusivities in Eq. (7-15) take into account molecular interactions in the gas mixture. These values depend on species concentration and diffusivity for a binary mixture, and can be calculated from the effective Stefan-Maxwell diffusivities

$$\widetilde{D}_{11} = \frac{\frac{(w_2 + w_3)^2}{x_1 D_{23}^{eff}} + \frac{w_2^2}{x_2 D_{13}^{eff}} + \frac{w_3^2}{x_3 D_{12}^{eff}}}{\frac{x_1}{D_{12}^{eff} D_{13}^{eff}} + \frac{x_2}{D_{12}^{eff} D_{23}^{eff}} + \frac{x_3}{D_{13}^{eff} D_{23}^{eff}}} \tag{7-16}$$

$$\widetilde{D}_{12} = \frac{\frac{w_1(w_2 + w_3)}{x_1 D_{23}^{eff}} + \frac{w_2(w_1 + w_3)}{x_2 D_{13}^{eff}} + \frac{w_3^2}{x_3 D_{12}^{eff}}}{\frac{x_1}{D_{12}^{eff} D_{13}^{eff}} + \frac{x_2}{D_{12}^{eff} D_{23}^{eff}} + \frac{x_3}{D_{13}^{eff} D_{23}^{eff}}} \tag{7-17}$$

The Stefan-Maxwell binary diffusivities D_{ij} are determined from an equation based on the kinetics of monoatomic gases theory at low density [26]

$$D_{ij} = \frac{0.0143 \times T^{1.75}}{p(v_i^{1/3} + v_j^{1/3})^2} \left[\frac{1}{M_i} + \frac{1}{M_j}\right]^{1/2} \tag{7-18}$$

where v_i are the molar diffusion volume for each component as summarised in Table 7-2, M_i is the molar mass of species i, and T is the system temperature, respectively.

Table 7-2 Molar diffusion volume for each component

	H_2	**O_2**	**N_2**	**H_2O**	**He**	**CO**	**CO_2**
v_i	6.12	16.3	18.5	13.1	2.67	18.0	26.9

Due to the gas transport passing through a porous structure of GDE, the diffusion coefficient of gas species is accounted for the tortuosity of the pore following a Bruggeman correlation [27]

$$D_{ij}^{eff} = D_{ij} \varepsilon_k^{1.5} \tag{7-19}$$

where D_{ij}^{eff} is the effective Stefan-Maxwell diffusivity and ε_k, is the porosity or void fraction (defined as the ratio of the void pore volume to the total sample volume). The subscription k means the porosity in different layers, e.g. separator, active layer, and GDL.

The expression described in Eq. (7-19) is not valid if the layer consists of two phase components, just like water production in the porous cathode of fuel cells. For a Na-air battery with GDE, the two-phase components occur in the active layer where the

amount of liquid electrolyte presents in the void space of gas diffusion pathway. Consequently, the effective Stefan-Maxwell diffusivity accounting for two-phase components should be modified as

$$D_{ij}^{eff} = D_{ij}\varepsilon_k^{1.5}(1-S)^{1.5} \tag{7-20}$$

where S is the liquid electrolyte fraction remaining inside the porous of active layer (defined as the ratio of liquid electrolyte volume to the total pore volume).

The source terms in Eq. (7-13) are coupled with the reactions at the porous active layer of GDE and only the oxygen reactant is involved given by

$$S_{mass} = \begin{cases} \dfrac{s_{O_2,k} M_{O_2} \sum J_{c,k}}{n_k F} & (at\ active\ layer) \\ \\ 0 & (elsewhere) \end{cases} \tag{7-21}$$

where $s_{O_2,k}$ is the stoichiometric number of oxygen and $J_{c,k}$ is the volumetric current density (A m^{-3}) of electrochemical reaction k occurred at the active layer of cathode.

Darcy's law is applied to model the convection within the porous media by relating the velocity vector with the pressure gradient, the fluid viscosity, and the permeability of porous structure, as described in following expression

$$\boldsymbol{u} = -\frac{\tilde{\kappa}}{\mu_i}\nabla p \tag{7-22}$$

where $\tilde{\kappa}$ is the permeability of the porous media, and μ_i is the pore-fluid viscosity of gas i in GDE. The Darcy's and Stefan-Maxwell equations are coupled via the velocity vector $\boldsymbol{u}$ and gas mixture density, ρ, which is calculated from

$$\rho = \frac{\sum M_i w_i}{RT} p \tag{7-23}$$

The viscosity of the cathode gas for air μ_{air} is given by [26]

$$\mu_{air} = 1.094 \times 10^{-5}(T/298)^{1.02} \tag{7-24}$$

The viscosity of the cathode gas for oxygen μ_{O_2} is given by the Chapman-Enskog theory of a pure monatomic gas [28]

$$\mu_{O_2} = 2.6693 \times 10^{-6}(0.1972 \times T)^{0.5} \tag{7-25}$$

7.3.4 Transport of oxygen through thin film electrolyte

The macro-homogeneous model for the active layer, which consists of three phases together, assumes that the active layer is a 'volume average' of the solid electrode and the electrolyte. Thus, the effective conductance of the active layer is the weighted volume average of respective conductance to account for the tortuosity of the porous electrode. The diffusion coefficients and film thickness are similarly averaged in the active layer.

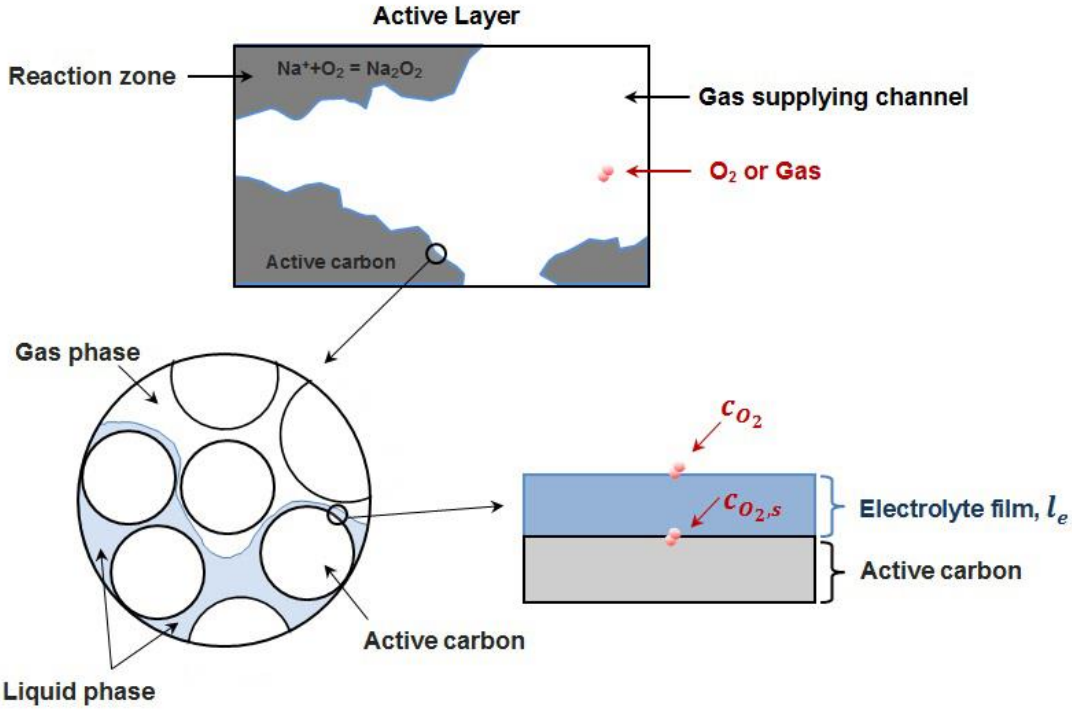

Figure 7-2 Schematic diagram of oxygen from the gas phase transporting through thin electrolyte film in the active layer.

Oxygen transport from the porous media to the active surface area occurs through a thin film of a non-aqueous electrolyte covering the carbon active material as presented in Figure 7-2. The film provides ion conductive paths from the separator to the active site. The average film thickness l_e can be estimated using the following equation [22, 29]

$$l_e = \left[\left(\frac{\varepsilon_e + \varepsilon_c}{\varepsilon_c}\right)^{1/3} - 1\right] r_s \tag{7-26}$$

where ε_e and ε_c are the volume fraction of liquid electrolyte and active material of cathode electrode (active carbon and binder), and r_s refers to the particle radius in the electrode.

It is worth noting that in this time-dependent model the electrolyte degradation is considered during battery cycling. Hence, ε_e continuously falls from the pore due to the effect of Na_2CO_3 formation.

To determine the oxygen concentration at the active surface ($c_{O_2,s}$), Fick's law for diffusion is used and coupled with the electrochemical reaction in which oxygen species is consumed at the active electrode surface as follow

$$-\frac{as_i}{nF} j_c = \frac{aD_{O_2,eff}(c_{O_2} - c_{O_2,s})}{l_e} \tag{7-27}$$

where $D_{O_2,eff}$ is the effective diffusion coefficient of oxygen across the electrolyte film, j_c is the local transfer current density at active layer that relates to the oxygen species, c_{O_2} is the dissolved oxygen concentration at gas/electrolyte interface, which can be determined by using Henry's law for solubility

$$c_{O_2} = H_{O_2} \bar{p}_{O_2} \tag{7-28}$$

where H_{O_2} is the Henry's law constant of oxygen which depends on the electrolyte and temperature used in the Na-air battery ($H_{O_2} = 2.95$ mol m^{-3} atm^{-1} as same as Chapter 6), and $\bar{p}_{O_2}$ is the partial pressure of oxygen which can be defined by Darcy's law [30].

7.3.5 Transport of species in electrolyte

As the previous section described the gas transport in the GDE which covered only the two domains of active and gas diffusion layer, this section provides the governing equations which describe conservation of species transport through the liquid electrolyte phase in the active layer and separator domains to clarify the mechanism inside the Na-air battery mentioned above.

The model used in this study is based on the macroscopic theory of porous electrode, which considers the electrolyte solution and solid matrix as a superimposed continuum [31, 32]. Then, a material balance equation for species i transport in the Na-air electrolyte can be expressed as

$$\frac{\partial(Sc_i)}{\partial t} = -\nabla \cdot \boldsymbol{N_i} + r_i \tag{7-29}$$

where c_i is the bulk concentration of species i in the solution phase which is averaged

over the volume of the solution in the pores, S is electrolyte fraction in the porosity of the electrode as defined in Eq. (7-48), $\boldsymbol{N_i}$ is the molar flux of species i in the porous solution averaged over the cross sectional area of the electrode, and r_i is the volumetric production rate of species i from the solid phase (electrode material) to solution phase (partial electrolyte in the porous) within the porous electrode.

The concentration of sodium salt electrolyte is the same as concentration of Na^+ due to the binary electrolyte assumption. Only the diffusion and migration transport of species are considered in liquid electrolyte without convection. Due to the ion movement, the flux equation for mass transport of Na^+ includes both migration and diffusion, and other species involve only the latter transport in porous cathode

$$\boldsymbol{N_{Na}} = -D_{Na,eff}\nabla c_{Na} + \frac{\boldsymbol{i_2} t_+}{F} \tag{7-30}$$

$$\boldsymbol{N_i} = -D_{i,eff}\nabla c_i \tag{7-31}$$

where t_+ is the transference number of Na^+, F is Faraday's constant which is equal to 96,485 C mol^{-1}, and $\boldsymbol{i}_2$ is the current density in the solution phase or electrolyte current density. The effective diffusion coefficient of species ($D_{i,eff}$) needs to be corrected to account for the effect of porosity and electrolyte volume fraction in the active layer, based on the Bruggeman correction

$$D_{i,eff} = (S\varepsilon)^{1.5} D_i \tag{7-32}$$

where D_i is the diffusion coefficient for each species in bulk electrolyte.

7.3.6 Conservation of charge

For the porous electrode theory, the charge conservation for the electrode matrix and solution phases would require the divergence of the total current density to be zero defined by

$$\nabla \cdot \boldsymbol{i}_1 + \nabla \cdot \boldsymbol{i}_2 = 0 \tag{7-33}$$

This expression is used to relate the current density in the conductive solid phase (carbon) to the current in the electrolyte phase in the active layer. In the one-dimensional description this equation derives as

$$i_1 + i_2 = -I \tag{7-34}$$

where I is the operating current density and is given to be negative during operation at a cathode in a Na-air battery.

7.3.7 Current density in electrode phase

In the Na-air battery, there are two regions containing carbon materials: active layer and GDL. Then, the movement of electrons in the solid matrix phase is governed by Ohm's law, which evaluates the electric potential variation or potential of electron, ϕ_1, as follows

$$\boldsymbol{i}_1 = -\sigma_{eff}\nabla\phi_1 \tag{7-35}$$

where σ_{eff} is the effective conductivity of the electron for each material region. This parameter is affected by the volume fraction of solid electrode inside the porous cathode.

7.3.8 Current density in electrolyte phase

In the active layer the current density in the solution phase or electrolyte current density which can be defined by the gradient of the potential in a 1:1 binary concentrated electrolyte solution as [32, 33]

$$\boldsymbol{i}_2 = -\kappa_{eff}\nabla\phi_2 - \frac{2RT\kappa_{eff}}{F}(t_+ - 1)\left(1 + \frac{\partial lnf}{\partial lnc_{Li}}\right)\nabla lnc_{Na} \tag{7-36}$$

where κ_{eff} is the effective conductivity of the electrolyte, ϕ_2 is the electrolyte potential (electric potential of Na^+), R is the universal gas constant which is equal to 8.3143 J mol^{-1} K^{-1}, T is the cell temperature in Kelvin, and f is the activity coefficient of $NaPF_6$ salt. In this equation, Bruggeman's correlation was also used to calculate the ionic conductivity

$$\kappa_{eff} = (S\varepsilon)^{1.5}\kappa \tag{7-37}$$

7.3.9 Charge transfer reaction

During discharge or charge, the electrochemical reactions occurring at the electrode/electrolyte interface (charges transfer reaction) are expressed for individual reactions according to the conventionally general formula of the form

$$\sum s_i M_i^{z_i} \rightarrow ne^- \tag{7-38}$$

The charge transfer from solid phase to electrolyte phase per unit volume of electrode ($\nabla \cdot \boldsymbol{i}_2$) is related to the individual average transfer current density occurred at the cathode given by

$$\nabla \cdot \boldsymbol{i}_2 = \sum_m a j_m \tag{7-39}$$

This equation states that the transfer current per unit electrode volume is equivalent to the electrode chemical reaction rate where the M_i is a species symbol participating in the electrochemical reaction, z_i and s_i are the charge number and the stoichiometric coefficient of the species i, n is the number of electron transferred in the reaction, a is the specific interfacial area of the pore per unit volume of the total electrode as described in chapter 3, and j_m is local transfer current density between electrode and electrolyte interface of each reaction at the cathode. The value of s_i, z_i, and n can be defined by matching with an individual electrode reaction using the general form of Eq. (7-38), for example, the value of s_{Na}, z_{Na}, and n of Na^+ from Eq. (7-2) are -2, 1, and 2, respectively.

In practical Na-air batteries, the precise reaction routes can be complicated regarding several intermediates as proposed in the previous reports [18]. Hence, both electrochemical reactions of Na_2O_2 and Na_2CO_3 formation inside porous electrode are considered in the present work. The superficial production rate of each species (referred to Eq. (7-29)) from solid phase to pore solution in the individual reactions *m* is given by Faraday's law

$$r_i = -\sum_m \frac{a s_{im}}{nF} j_m \tag{7-40}$$

7.3.10 Kinetic expressions at cathode

Since there is no report on the details of kinetic reaction for Na-air battery, the electrochemical reactions inside the active layer are analogous to that used in Li-air battery from previous chapters. The actual reaction paths and mechanisms for the discharge products are not available and quite complex involving various intermediate species. Hence to describe the electrochemical kinetic expressions in the porous active layer the model adopts the kinetic expression based on Eq. (7-2) for Na_2O_2 formation and on Eq. (7-8) and Eq. (7-12) for Na_2CO_3 formation.

Na_2O_2 formation

For electrochemical reaction of Na_2O_2 at the cathode, a modified version of the Butler-Volmer equation is applied in the model using two rate coefficients as the same kinetic equation for Li_2O_2 formation described in chapter 3 due to the similarity between these two discharge products. The reaction for Na_2O_2 formation depends on the concentration of Na^+ and oxygen for discharge and the concentration of Na_2O_2 during charge as in the following equation

$$\frac{j_c}{2F} = Sk_a\left(c_{Na_2O_2}\right)exp\left[\frac{(1-\beta)nF}{RT}\eta_m\right] - Sk_c(c_{Na})^2\left(c_{O_2,s}\right)exp\left[\frac{-\beta nF}{RT}\eta_m\right] \quad (7\text{-}41)$$

$$\eta_m = \phi_1 - \phi_2 - \Delta\phi_{film} - E_m^0 \quad (7\text{-}42)$$

$$\Delta\phi_{film} = j_c R_{film}\varepsilon_s \quad (7\text{-}43)$$

where k_a and k_c are the anodic and cathodic rate constant, respectively, β is the symmetry factor equal to 0.5, η_m is surface or activated overpotential for individual reaction, m, at the cathode, $\Delta\phi_{film}$ and R_{film} are the voltage drop and the electrical resistivity across Na_2O_2 film formation, respectively, ε_s is the volume fraction of solid formation of discharge products of Na_2O_2 and Na_2CO_3, and E_m^0 is the theoretical open-circuit potential for each reaction. As the reaction takes place in liquid electrolyte, the kinetics account for the amount of electrolyte (volume fraction, S) in the active layer.

Na_2CO_3 formation

As the Na-air battery used the same organic electrolyte like the case of Li-air battery, the formation of carbonate product could form in the same reaction of electrode degradation as presented in chapter 5. Hence, the Na_2CO_3 formation used the same kinetic equations as Li_2CO_3 formation due to the similarity in electrolyte used in both the Na-air and Li-air systems.

As explained before, the Na_2CO_3 formation is one of the discharge by-products coexisting with Na_2O_2. Thus, the decomposition of electrolyte, which initially forms CO_2 and finally generates Na_2CO_3 as described above, occurs during Na-air operation. Some of the elementary steps in the electrolyte degradation sequences that lead to these by-products may be irreversible and non-electrochemical, so that the overall kinetic expression is very complex. Therefore, we use the kinetics for Na_2CO_3 formation on Eq.

(7-8) above based on the published kinetic data.

First the superoxide radical anion that is initially formed (Eq. (7-5)) during Na-air discharge as evidenced in previous study [24], attacks CO_2 which is generated from solvent decomposition (from Eq. (7-12)) to finally form Na_2CO_3 with the presence of Na^+ as in the following reaction

$$j_{c1} = Fk_{1a}(c_{O_2})\left[-exp\left(\frac{-\beta nF}{RT}\eta_m\right)\right] \tag{7-44}$$

$$r_{c1} = k_{1b}(c_{O_2^-})(c_{CO_2}) \tag{7-45}$$

where k_{1a} and k_{1b} are the rate constant for the electrochemical reaction to form O_2^- and chemical reaction to generate Na_2CO_3, respectively. We use the Tafel form in Eq. (7-44) rather than the Butler-Volmer form because the large kinetic overpotential during cell discharge puts the reaction in the Tafel region and considers only discharge (irreversible for O_2^- formation. It has been demonstrated that the chemical reaction in Eq. (7-45) is found to be first-order with to respect to both O_2^- with CO_2 reactants and is the rate determining step (RDS) [24]. Hence, the other reaction is considered as equilibrium and the formation of Na_2CO_3 can be predicted by using Eq. (7-44) and Eq. (7-45) together.

Solvent degradation

The solvent degradation reaction uses the same expression as described in chapter 5 and is presented as follows

$$j_{c3} = Fk_{VI}(c_{O_2})\left[-exp\left(\frac{-\beta nF}{RT}\eta_m\right)\right] \tag{7-46}$$

where k_{IV} is the rate constant for the electrochemical reaction to form CO_2 and the others are the same as described above.

7.3.11 Rate expressions at anode and specific surface area

The electrochemical reaction rate for the anode includes the oxidation of sodium metal to soluble Na^+. It is described by a general Butler-Volmer equation as follow

$$j_a = i_0\left[exp\left(\frac{(1-\beta)nF}{RT}\eta_a\right) - exp\left(\frac{-\beta nF}{RT}\eta_a\right)\right] \tag{7-47}$$

where i_0 is exchange current density for anode, η_a is surface or activated overpotential for reaction at anode, and the other parameter are as described above.

7.3.12 Porosity change and electrolyte degradation

In this model, the porosity of GDL is composed of a single phase of reactant gas diffusing through the void space, whereas the porous media in the active layer is occupied by two phases of electrolyte and reactant gas. The bulk porosity (ε) in this layer, which is dynamically changed during charge and discharge, is divided between the liquid electrolyte (ε_l) and gas (ε_g) volume fractions. The liquid electrolyte (S) is the volume occupied by the liquid ε_l divided by the open pore volume ε. The phase balance can be depicted in Eq. (7-48)

$$\begin{aligned} \varepsilon_c + \varepsilon_l + \varepsilon_g &= 1 \\ \varepsilon_l + \varepsilon_g &= \varepsilon \\ S &= \frac{\varepsilon_l}{\varepsilon} \end{aligned} \tag{7-48}$$

The porosity volume change of the active layer will be decreased due to the formation of insoluble solid products covering the active particles as described in Eq. (7-49). The void space for gas transport is replaced by these solid particles. Thus, the effective diffusivity for gas species inside the active layer is used to describe how the pores are influenced by Na_2O_2 and Na_2CO_3 formation; this can be described by the Bruggeman relationship (referred to Eq. (7-19) and Eq. (7-20)). Because the solid distributions in the model are Na_2O_2 and Na_2CO_3, we use the properties of these solids for all of the discharge products formed

$$\frac{\partial \varepsilon}{\partial t} = \sum_{solid\ phase\ m} a j_m \frac{M_m}{nF\rho_m} \tag{7-49}$$

During battery cycling, the electrolyte is consumed or degraded by the Na_2CO_3 formation reaction as described in Eq. (7-12). Consequently, the electrolyte volume fraction also follows the same manner of porosity change in Eq. (7-50) and decreases following the charge transfer reaction of electrolyte degradation (j_{c3}) as

$$\frac{\partial \varepsilon_l}{\partial t} = a j_{c3} \frac{M_e}{nF\rho_e} \tag{7-50}$$

The volume fraction of the discharge solid formation can be determined from the cathode volume balance as

$$\varepsilon_s = 1 - \varepsilon - \varepsilon_c \tag{7-51}$$

where M_m, M_e and ρ_m, ρ_e are the molecular weight and the mass density of solid discharge products and electrolyte, respectively.

7.3.13 Boundary conditions

From Figure 7-1, a schematic view of the model cell consists of four boundaries and three domain regions. The boundary dimensions discussed in this section are referred to in this figure.

Table 7-3 Boundary conditions used in Na-air battery with gas diffusion electrode

Conservation of species	
As the pure oxygen gas was continuously supplied from the bulk reservoir, the specie mass fraction was set for cathode:	
$w_{O_2} = 1$ at $x = L$	(7-52)
As the separator was assumed impermeable to oxygen gas, the oxygen flux was zero. The flux of electrolyte was also zero at GDL/active layer interface:	
$N_{O_2} = 0$ at $x = L_a$	(7-53)
$N_{Na} = 0$ at $x = L_c$	(7-54)
At the inlet the operation pressure was set:	
p = 1 atm	(7-55)
Conservation of charge	
For conservation of charge the current density in the solid phase was set equal to the applied current density on gas diffusion layer. At the GDE/separator interface the current density in the solid phase was zero:	
$i_1 = I$ and $i_2 = 0$ at $x = L$	(7-56)
$i_1 = 0$ and $i_2 = I$ at $x = L_a$	(7-57)
The cell voltage was calculated by the difference between the electrode potential at cathode current collector and the electrolyte potential at the anode side:	
$V_{cell} = \phi_1(x = L) - \phi_2(x = 0)$	(7-58)

7.3.14 Solution technique

The conservation equations and the boundary conditions described above were discretized using a finite element method and solved in one-dimensional battery system by commercial software package COMSOL multiphysics version 4.3. The COMSOL software is designed to solve a set of coupled differential and algebraic equations and the battery simulation model is performed on a 32 bit Windows platform with 4 GB

RAM, and Intel Core 2 Duo 2.93 GHz processor. The different transport equations and the electrochemical reactions were solved as time dependent until the cell voltage reached the stop condition during discharge and charge. The solutions were considered as converged solutions when the difference between two results was less than 10^{-4} (relative tolerance) for all variables.

Table 7-4 Parameters used in the Na-air with gas diffusion electrode (SI unit)

Parameters	**Value**	**Unit**	**Symbol**	**Ref.**
Cell properties				
Thickness of separator	5×10^{-5}	m	L_A	[34]
Thickness of active layer	1.1×10^{-4}	m	L_C	[17]
Thickness of gas diffusion layer	1×10^{-4}	m	L	[17]
Porosity	0.80	-	ε^o	[17]
Specific interfacial area of cathode	3.75×10^{6}	$m^2\ m^{-3}$	a	Calculated
Electrical resistivity of Na_2O_2 formation	Eq. (3-48)	$\Omega\ m^2$	R_{film}	[29]
Electrolyte properties				
Electrolyte concentration	1000	$mol\ m^{-3}$	$c_{Na,0}$	[15]
Pure gas of oxygen	100%	-	$w_{O_2,0}$	
Henry's constant for oxygen in electrolyte	2.95	$mol\ m^{-3}\ atm^{-1}$		[35]
Solubility limit of Na_2O_2 in electrolyte	0.09	$mol\ m^{-3}$	c_{max}	[36]
Liquid electrolyte fraction	0.3	-	S	
Kinetic parameters				
Rate constant for anodic current	1.3×10^{-6}	$m\ s^{-1}$	k_a	Assumed
Rate constant for cathodic current	4.5×10^{-15}	$m^7\ s^{-1}\ mol^{-2}$	k_c	Assumed
Rate constant for O_2^- formation	8.1×10^{-15}	$m\ s^{-1}$	k_{1a}	Assumed
Rate constant for Na_2CO_3 formation	370	$m^3\ s^{-1}$	k_{1b}	[37]
Rate constant of CO_2 formation	5.9×10^{-15}	$m\ s^{-1}$	k_{VI}	[29]
Exchange current density for anode	1	$A\ m^{-2}$	i_0	Assumed
General parameters				
Mass density of Sodium peroxide (Na_2O_2)	2800	$kg\ m^{-3}$	$\rho_{Na_2O_2}$	[38]
Mass density of Sodium carbonate (Na_2CO_3)	2540	$kg\ m^{-3}$	$\rho_{Na_2CO_3}$	[38]
Operating temperature	298.15	K	T	

7.3.15 Summarised parameters

The parameters described in this chapter are summarised in Table 7-4. The electrolyte properties are the same as that used in Li-air battery model due to the lack of

information for $NaPF_6$ in non-aqueous electrolyte and referred to Table 3-4 in chapter 3. These basic parameters are applied in the Na-air model with gas diffusion electrode.

7.4 Results and Discussion

The dynamic one-dimensional Na-air battery model including parasitic reactions from electrolyte degradation was simulated and tested against the performance during battery cycling. The air cathode structure of the GDE replaced the flooded battery electrode used in the Li-air battery models [21, 22]. The GDE model was also considered the electrolyte volume loss from the reaction with intermediate species, O_2^-, to form Na_2CO_3 by-product as described in Eq. (7-8) and Eq. (7-12). Our cell simulation comprised a metallic sodium anode, a separator soaked with a 1 M solution of $NaPF_6$ in carbonate-based solvent, and a porous carbon gas diffusion electrode as the air cathode. Hartmann *et al*. fabricated the GDE with the thickness of 210 μm and no catalyst was used [17]. The porosity of the material (a binder-free GDL Freundenberg H2315, Quintech) was estimated to be around 80% [17]. These parameters were applied to our Na-air battery model with the GDE.

7.4.1 Battery performance

The performances of the rechargeable Na-air batteries with the GDE and the flooded electrode structure were compared. Both electrodes were considered the solid Na_2O_2 formation as the major discharged product with $E^0 = 2.33$ V (Eq. (7-2)). To predict the battery performances on 1st cycling behaviour for both types of electrode, the voltage-capacity profiles on discharge and charge operating between 1.8 and 3 V (vs Na/Na^+ as the reference electrode) at a discharge/charge rate of 0.1 mA cm^{-2} are compared as shown in Figure 7-3. Excepting the cathode structure, both GDE and flooded electrode structures of Na-air model were simulated with the same physical parameters, e.g. thickness, kinetic reactions, diffusivities and conductivities, and at an operating temperature of 298.15 K in pure oxygen. As can be seen from the voltage-capacity profile in Figure 7-3, the GDE shows a significant improvement in discharge capacity characteristics which provides a 47% increase in initial discharge capacity (over 1551 mAh g_{carbon}^{-1} at a rate of 0.1 mA cm^{-2}). It is worthwhile to note that the unit of "mAh g_{carbon}^{-1}" was chosen to report the battery capacity because, in most cases, the battery performances (capacity and energy) are directly related to amount of carbon as active material in porous cathode. Here the unit of "g_{carbon}" includes all carbon materials of

cathode, i.e. carbon in both active layer and GDL for GDE or carbon in porous cathode for flooded electrode.

It can be seen from the discharge and charge cycle that the cell potential of GDE began to fall steeply at the first discharge, from a voltage of 2.4 V to a plateau at around 2.2 V, and decreased continuously to 1.8 V. The discharge characteristic of Na-air with the GDE is comparable, but slightly lower than that of the lithium-air battery, giving around 2.6-2.7 V [2, 21]. The voltage difference correlates well to the difference in the standard electrode potentials between lithium ($E^0_{(Li^+/Li)} = -3.05$ V) and sodium ($E^0_{(Na^+/Na)} = -2.71$ V) [38]. At a low current density of 0.1 mA cm^{-2}, a wide voltage plateau of about 2.2 V, corresponding to discharge overpotential (η_{dis}) < 100 mV, is observed for the GDE, which is lower than the case of Li-air batteries (η_{dis} > 300 mV). The discharge capacities remain constant with the increase of the discharge rates, i.e. the discharge capacity is around 1551 mAh g_{carbon}^{-1} for 0.2 and 0.5 mA cm^{-2}. This behaviour is different from the case of the flooded electrode in that the capacity decreases with the high discharging rates due to the oxygen mass transport limitation as shown in chapter 4. In contrast, the oxygen supply in the case of GDE, is not limited by mass transport but the cell limitation is due to the solid product deposition inside the pores. Moreover, the discharge voltage for the GDE continuously decreases with the high current densities (2.13 V for 0.2 mA cm^{-2} and 2.01 V for 0.5 mA cm^{-2}) due to expected kinetic limitation at high currents with large overpotential.

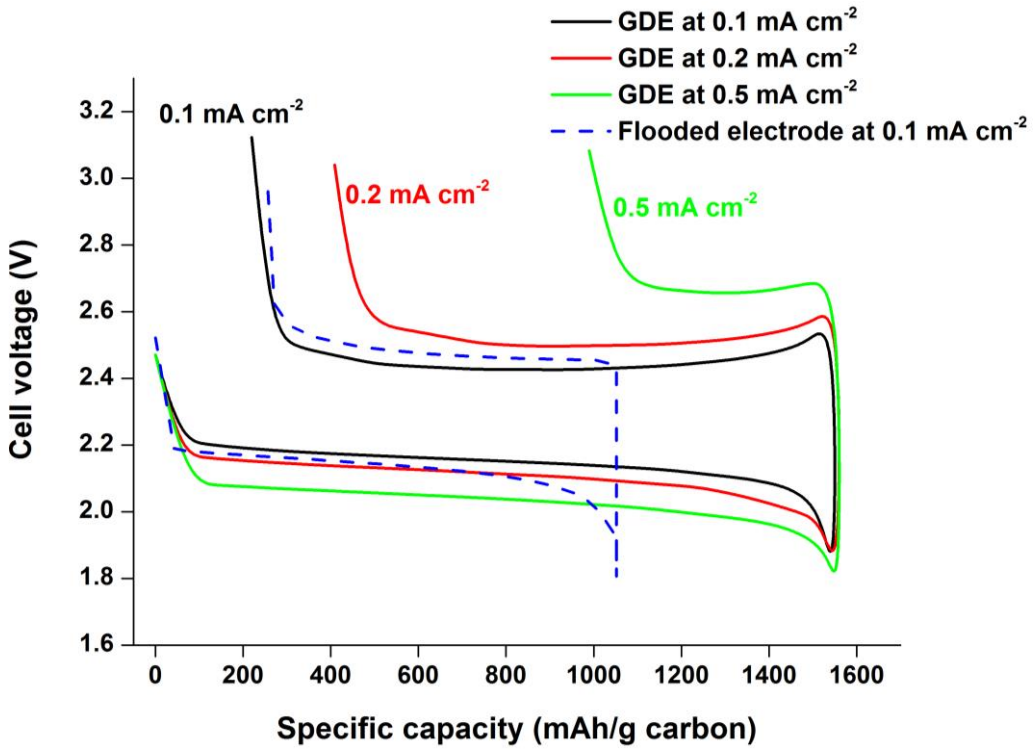

Figure 7-3 The Na-air performances on 1st cycle are compared between GDE and flooded electrode structure at room temperature 298.15 K. The cathode electrode thickness is 210 μm with porosity of 0.80. Both electrodes were operated between 1.8 and 3 V vs Na/Na^+ as reference electrode at a discharge/charge rate of 0.1 mA cm^{-2} under 1 atm of oxygen in 1 M $NaPF_6$ dissolved in carbonate-based solvent.

During the subsequent charge process at the low current density (0.1 mA cm^{-2}), the charge performance for GDE showed a voltage plateau between 2.4-2.5 V, which is close to the potential for the decomposition of Na_2O_2 to form Na and oxygen ($E^0 = 2.33\ V$). In contrast to the case of GDE, the flooded electrode not only demonstrates limited discharge capacity (1051 mAh g_{carbon}^{-1}) but also provides a slightly lower discharge voltage plateau < 2.2 V and a higher charge voltage than the case of the GDE (~ 2.51 V cf. 2.42 V in GDE). These results clearly demonstrated the advantage of the GDE over the flooded electrode in term of battery performance on the 1st cycle.

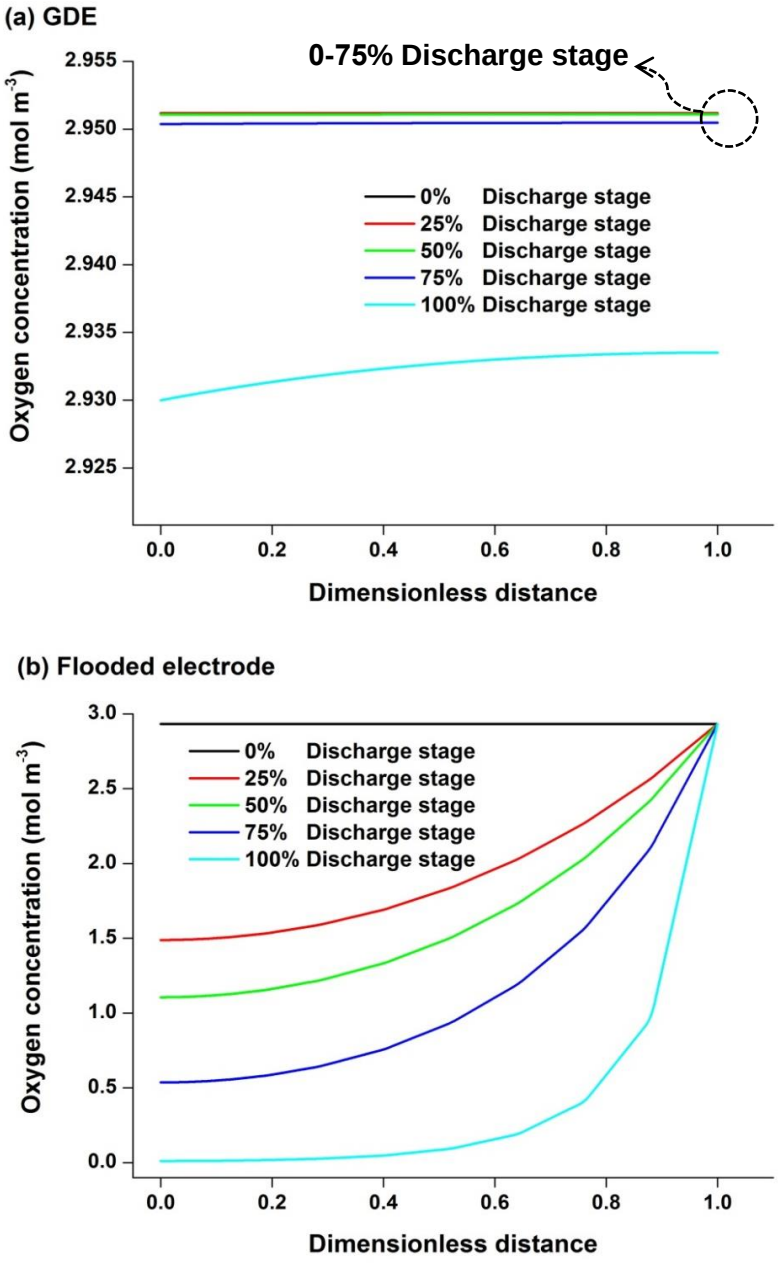

Figure 7-4 The comparison of oxygen profile inside the porous cathode of Na-air battery at a discharge rate 0.1 mA cm^{-2} on different discharge stages (100% means the end of discharge) between two cathode structures: (a) oxygen profile in active layer of GDE, (b) flooded electrode.

It is well known that the cathode structure of GDE has been widely used in Metals-air and fuel cell systems due to its unique functional porous structure. The high battery performance from the GDE battery could be attributed to an efficient 3-phase interface and porous structure (Figure 7-2), which not only enable a highly accessible electrochemical reaction, but also a large path for the reactant mass transport. Figure 7-4 compares the oxygen concentration profile along the cathode thickness during the 1st

battery discharge at various discharge states (current density 0.1 mA cm^{-2}) between the GDE and flooded electrode. The oxygen profile in GDE slightly decreased from the initial concentration of 2.95 mol m^{-3} to 2.50 mol m^{-3} at the end of the 1st discharge. Moreover, the oxygen concentrations were relatively uniform throughout the active layer of GDE at all discharge states. The nearly constant concentration results from the pore structure of GDE, which provides good gas-diffusion in the electrode.

A recent study from our group [2] also studied the GDE a more open structure and larger total pore volume than the conventional electrode used in Li-air batteries. Thus, the GDE as the cathode is not limited by mass transfer of the reactive species as long as there are pores available for the gas phase to move inside the GDE structure. In contrast, the oxygen concentration profile for the flooded electrode (as shown in Figure 7-4b) continuously decreases from the pore entrance (gas feeding) inside the electrode due to the accumulation of discharge products reducing the pore space. The solubility of oxygen in non-aqueous liquid electrolytes is normally very low. Hence, the kinetics of electrochemical reaction of a gas in a completely flooded or immersed electrode is limited by the mass transfer rate of reactant gas to the reaction site.

Another reason for the GDE giving high battery capacity could be the uniform depositing of discharge products covering the active surface and replacing the void space of the electrode. As shown in Figure 7-5, both electrodes show a steady decrease of void space in each discharge state but in a different manners. In GDE the decreasing trend of porosity is uniform throughout the entire active layer (Figure 7-5a) whereas the porosity reduces noticeably only at the oxygen feed side in the case of the flooded electrode (Figure 7-5b). However, these results are not surprising because the decreasing porosity resulting from the discharge products corresponded well with the oxygen concentration pattern in Figure 7-4.

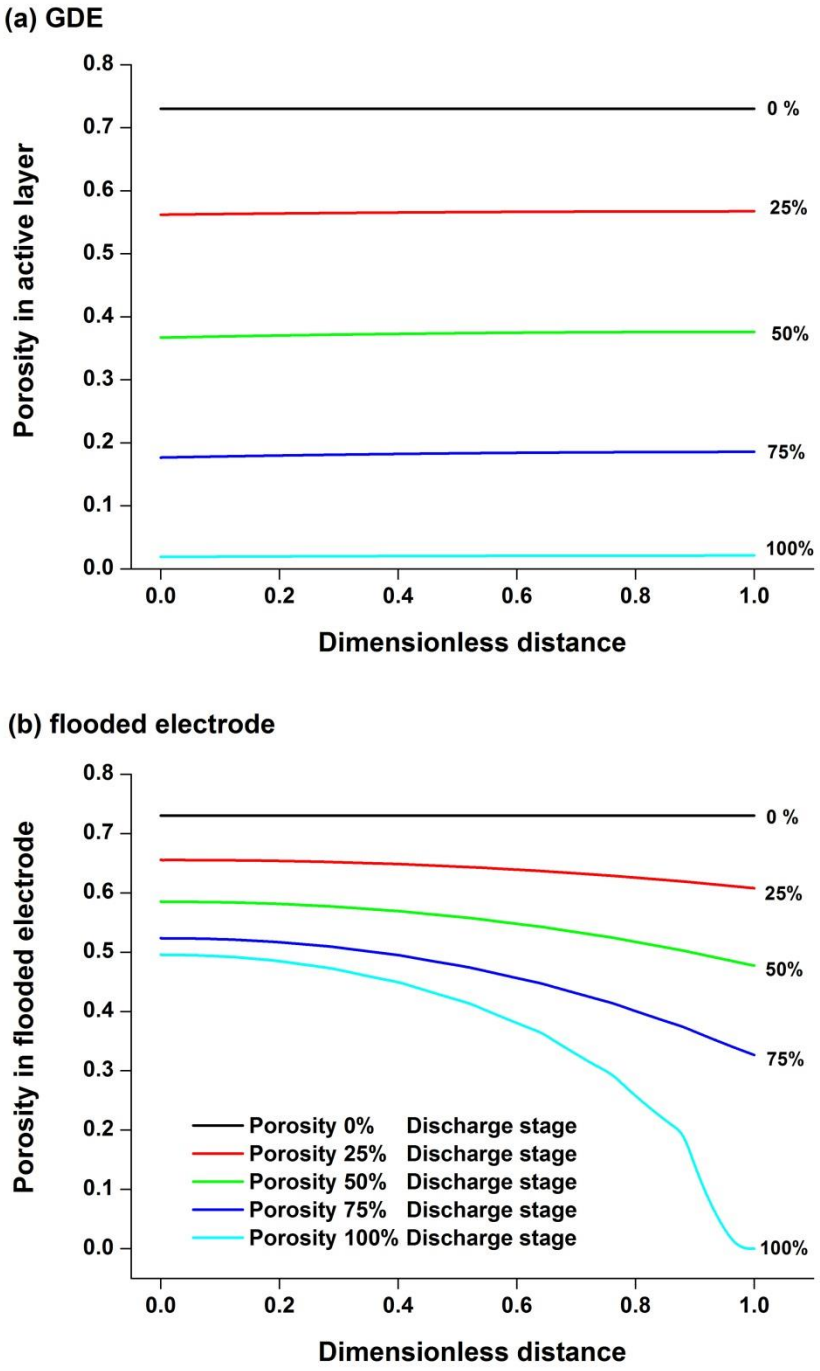

Figure 7-5 The comparison of porosity profile inside the porous cathode of Na-air battery at a discharge rate 0.1 mA cm^{-2} on different discharge stages (100% means the end of discharge) between two cathode structures: (a) porosity profile in active layer of GDE, (b) flooded electrode.

All of the results from the study indicate that the GDE shows better cathode performances for a rechargeable Na-air battery than that of the flooded electrode, delivering larger discharge capacities and higher discharge potential. The unique structure of the GDE plays a key role in promoting the formation of 3-phase contact,

resulting in a shorter diffusion distance for reactive species, as well as better discharge products distribution inside the active layer. Thus, the GDE could be a promising air cathode to replace the flooded-type electrode which is currently used in both lithium and sodium air batteries.

7.4.2 Cycling behaviour with electrolyte degradation

In practice, the battery stability, which can be measured by retention of discharge capacity during battery discharge/charge cycles, is more significant than its first discharge cycle. This issue of maintaining battery capacity is also the most challenging problem for Li-air batteries [39-42]. Hence, Na-air batteries could meet with the same problem. In this section, the cycling performance including electrolyte degradation to form Na_2CO_3 in Na-air battery using GDE is investigated.

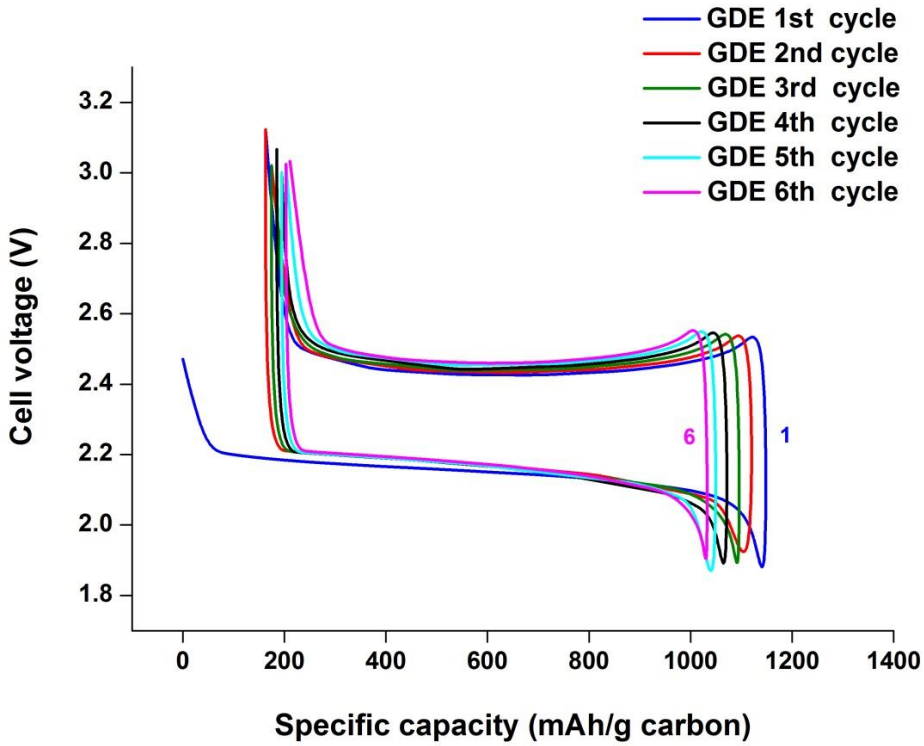

Figure 7-6 Variation of voltage-capacity curve in 6 cycles on discharge and then charge between 1.8 and 3 V versus Na/Na^+ for a non-aqueous Na-air battery using GDE at a rate of 0.1 mA cm^{-2}. The electrolyte contains 1 M $NaPF_6$ dissolved in carbonate-based solvent under 1 atm of oxygen at operating temperature 278.15 K. The other parameters used in the model are the same as described in Figure 7-3.

To predict the capacity retention on cycling, the variation of voltage on discharge and charge for 6 cycles of a rechargeable Na-air battery operating between 1.8 and 3.0 V at

a rate of 0.1 mA cm^{-2} is shown in Figure 7-6. This cycling was carried out at an operating temperature of 298.15 K in pure 1 atmosphere of oxygen gas. It can be seen from the discharge and charge cycle that the cell potential falls steeply at the first discharge, from a voltage of 2.4 V to a plateau at around 2.2 V, and decreases continuously to a final discharge potential at 1.8 V. At a low current density of 0.1 mA cm^{-2}, a wide voltage potential plateau for discharge during cycling was around 2.1-2.2 V, which was the same as the discharge voltage of Na-air batteries reported by previous research work for similar batteries operating in pure oxygen [17, 18]. The discharge voltage corresponded to an overpotential (η_{dis}) < 130 mV for the case of Na_2O_2 as the possible reaction product. This overpotential is lower than that of the Li-air batteries in chapter 4 and our published works with flooded electrode [21], demonstrating a discharge overpotential (η_{dis}) for Li-air batteries about 300 mV.

On charging for the Na-air battery (Figure 7-6), the voltage slightly rose to around 2.40-2.45 V ($\eta_{chg} \approx 100$ mV), which is close to the equilibrium potential ($E^0 = 2.33$ V) for the decomposition of Na_2O_2 to from Na^+ and oxygen as presented in Eq. (7-2). After the Na-air battery had continuously cycled, the charge voltage gradually increased overtime between 2.40-2.50 V depending on the number of cycles. This increase in charging overpotential could be attributed to the loss of cathode active surface due to the repeated deposition of Na_2CO_3 resulting from the electrolyte degradation during discharge as shown in Figure 7-7. It can be seen that Na_2CO_3 formation in the active layer is uniform following the oxygen concentration for the GDE (Figure 7-4a) and gradually accumulates with continuous cycling. The cycling performances and volume fractions of Na_2CO_3 at the end of each discharge cycle are also summarised in Table 7-5. This solid Na_2CO_3 requires a high charging potential (> 4 V) to be completely removed it from the electrode [18] and accumulates inside the active layer. Moreover, it is apparent from the Figure 7-6 that the reduction of battery capacity occurs mainly on charging, i.e. in each cycle the charge capacity is lower than that during the discharge step. This makes the charge/discharge efficiency less than 100% and causes rapid capacity fading.

As mentioned above, the most significant property for a battery is the stability to maintain the discharge capacity during battery cycling. Thus, for better clarity, the results obtained from the battery cycling in Figure 7-6 are presented in more detail in terms of the specific capacity (capacities are expressed per gram of carbon in the electrode) and retention of capacity on each discharge cycle as compared in Table 7-5.

The discharge capacity on the first cycle was about 1150 mAh g_{carbon}^{-1}, based on the weight of carbon alone. For the following cycles, the performance of a rechargeable Na-air battery deteriorated by the Na_2CO_3 from electrolyte degradation on cycling. The battery capacity gradually decreased to a value of 922 mAh g_{carbon}^{-1} after 3 cycles which corresponds to a capacity retention of 27% per cycle. At the final cycle, the discharge capacity was even lower to 829 mAh g_{carbon}^{-1} with a capacity retention of 72% (12% per cycle).

In summary, the Na-air battery model using GDE as the cathode for reactant gas transport exhibits a better battery performance than the flooded electrode normally used in metal-air batteries. However, the Na-air batteries with non-aqueous electrolyte still suffers from solid by-product Na_2CO_3 formation accumulating during battery cycling, just like the Li-air batteries.

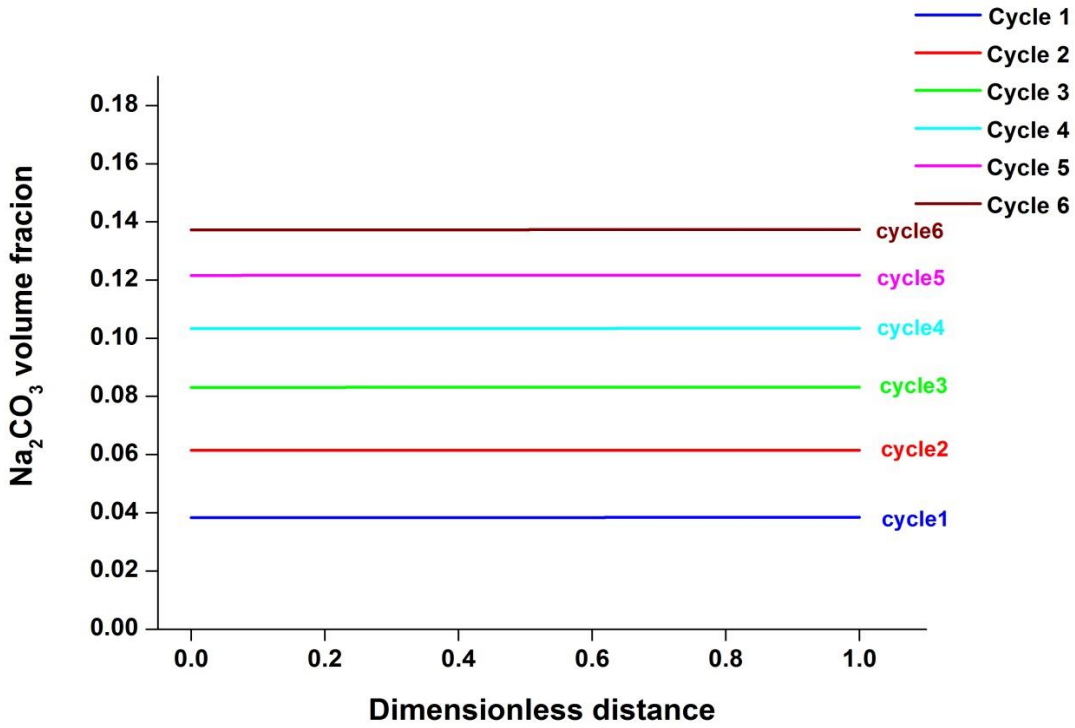

Figure 7-7 The volume fraction of Na_2CO_3 formation inside the active layer of the Na-air battery at the end of each discharge cycle. The parameters used in the model are the same as described in Figure 7-6. This of course assumes Na_2CO_3 is not oxidised to Na^+ and CO_2

Table 7-5 Specific discharge capacity and Na_2CO_3 formation for a nonaqueous Na-air battery using GDE operated in pure oxygen in 6 cycles at a rate of 0.1 mA cm^{-2}.

Cycle	Discharge capacity (mAh g^{-1})	Capacity retention (%)	Capacity retention per cycle (%)	Na_2CO_3 volume fraction
1	1149.47	100.00	100.00	0.038
2	959.04	83.43	41.71	0.061
3	922.14	80.22	26.74	0.083
4	887.65	77.22	19.30	0.103
5	856.11	74.48	15.00	0.121
6	829.63	72.17	12.03	0.137

7.4.3 Electrolyte loss during battery cycling

Figure 7-8 shows the electrolyte volume fraction (*S*) profile inside the active layer of GDE at the end of the battery discharging step in each cycle. It is apparent that the electrolyte volume fraction continuously decreased from the initial value of 0.30 in the 1st cycle to 0.21 in the 6th cycle. The loss of electrolyte occurred in a uniform pattern due to the uniform distribution of oxygen through the gas pores of the GDE, i.e. the electrolyte consumption took place whenever oxygen exists during discharge, and corresponded well with the Na_2CO_3 formation as shown in Figure 7-7.

Electrolyte depletion could affect the Na-air performance, mainly by the following aspects: (i) the reaction zones for the reduction of oxygen are decreased due to the loss of gas-electrolyte-carbon three-phase-interface. (ii) The active layer of electrode which is partially "dried" of electrolyte could not be utilised to accommodate discharge products. (iii) The ionic conductivity of Na^+ and the diffusion of oxygen and species in the electrolyte phase could be reduced following a Bruggeman correlation for the diffusion coefficient (Eq. (7-32)) and the conductivity (Eq. (7-37)), respectively. Thus, the overall battery performance on cycling of the Na-air battery could suffer from both irreversible Na_2CO_3 depositing on the active area of electrode and electrolyte depletion on repeated battery cycles. However, the former could affect deterioration in the discharge capacity more than the latter, as shown in previous sections of battery cycling behaviour.

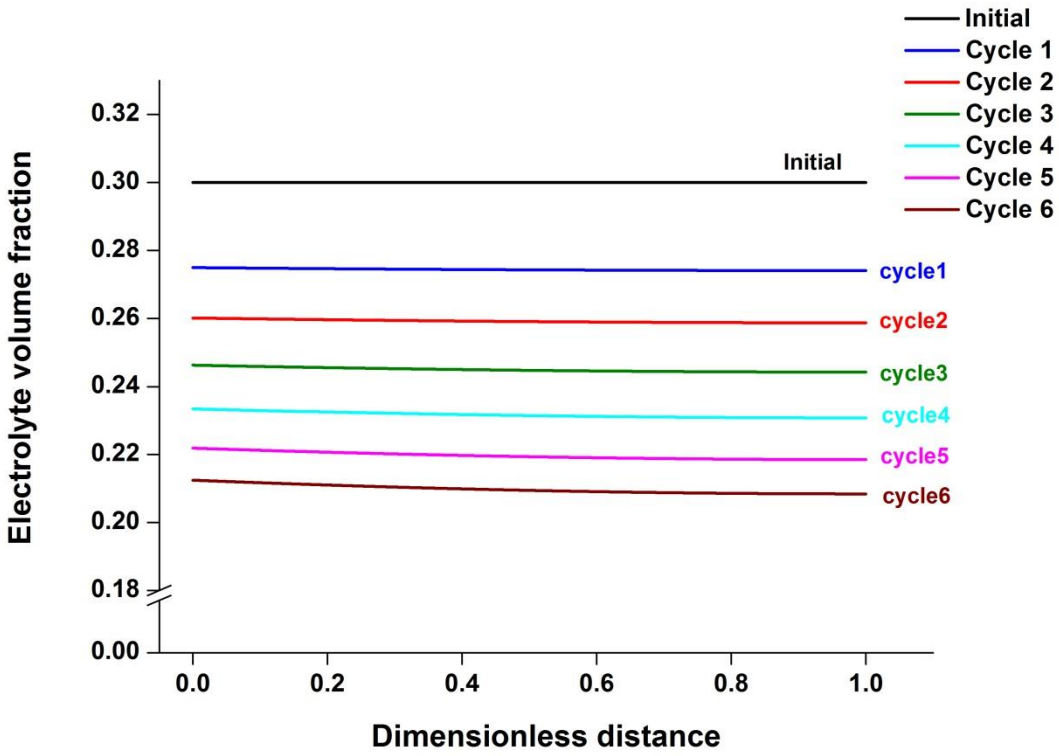

Figure 7-8 Volume fraction of electrolyte inside the active layer of the Na-air battery at the end of each discharge cycle. The parameters used in the model are the same as described in Figure 7-6.

7.4.4 Effect of electrolyte volume fraction

In the electrochemical reaction zones of a battery system, the introduction of liquid electrolyte as an ionic bridge between the active carbon particles is an important factor in achieving satisfactory battery performance. The ionic and electron conductivities in the active layer of GDE were influenced by the volume fractions of electrolyte in the pores of the electrode and active carbon particles formed on the electrode structure, respectively. As the ionic conductivity in a non-aqueous electrolyte (~ 0.4-0.9 S m^{-1}) is two or three order of magnitude lower than the electronic conductivity (~ 10-100 S m^{-1}) depending on the types of electrolytes and carbon materials [43], this factor is important on the Na-air performance. Therefore, the electrolyte volume fraction (S) was varied to investigate the 1st cycle of Na-air battery performance. This parameter influences the ionic conductivity and diffusivity of species dissolved in electrolyte as well as the effective surface for electrochemical reactions, i.e. the electrolyte/carbon interface. However, it will not affect the other volume fractions, such as carbon and porosity inside the active layer, because the definition of S is the ratio of electrolyte-filled volume to the total pore volume, i.e. the percentage of electrolyte to fully fill the pore

space (referred to Eq. (7-48)). Hence, the other volume fractions other than electrolyte were considered as constant values.

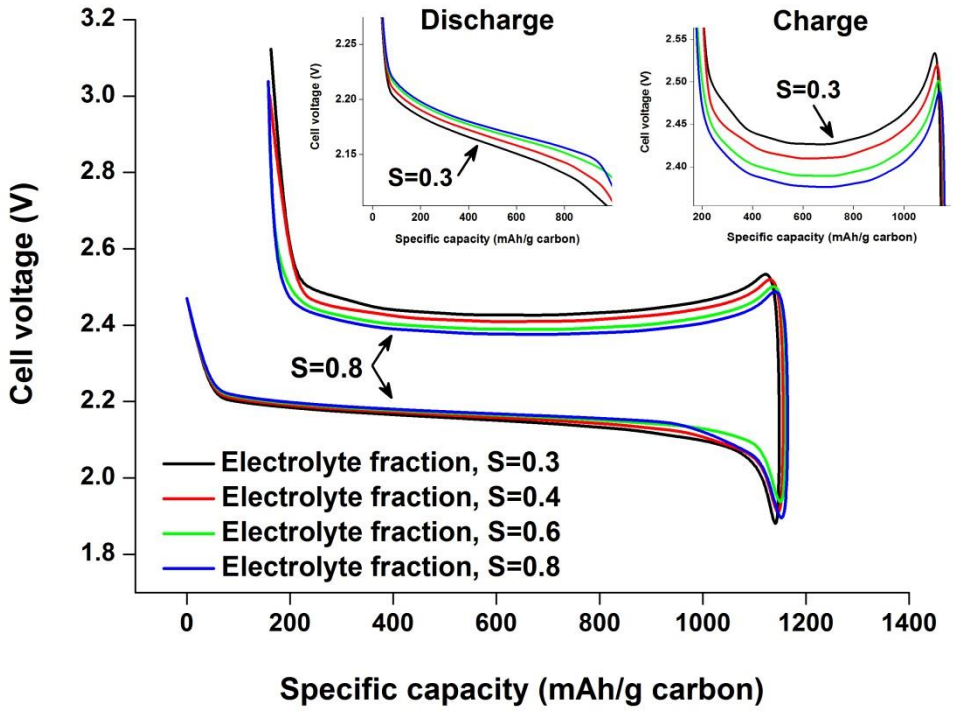

Figure 7-9 Voltage-capacity curve on the 1st cycle at the rate 0.1 mA cm^{-2} under 1 atm of oxygen for a non-aqueous Na-air battery at the different initial volume fraction of electrolyte in the active layer of GDE. The other parameters used in the model are the same as described in Figure 7-3.

Figure 7-9 shows the effect of electrolyte volume fraction on the 1st cycle of Na-air battery voltages and discharge capacities. It is apparent from the graphs that the highest discharge potential and lowest charge potential curve were achieved with the electrolyte volume fraction of 80% (S = 0.8), i.e. the highest roundtrip efficiency on the 1st battery cycle was obtained at 80% electrolyte loading. Because the main battery cycling results show no difference on the high cell voltage scale (in y-axis), Figure 7-9 also presents as insets the enlarged discharge and charge potentials ranges for better clarity. The battery discharge potential, when operated at a current density 0.1 mA cm^{-2}, increases from 2.15 V at the low electrolyte fraction of 30% to a marginal improvement of 2.17 V at the highest 80% electrolyte loading. The charging behaviour also showed a similar behaviour as discharge process, with the lowest charge voltage (2.38 V) at a 80% electrolyte volume fraction. However, there were no significant differences between the discharge capacities with the loading of electrolyte volume fractions. At high electrolyte

volume fraction, the battery system benefits from the mass transport of oxygen and the increasing reaction zones, where the oxygen gas-carbon-electrolyte interfaces co-exist, thus leading to higher performance especially for charge and discharge potentials.

Therefore, the amount of electrolyte inside the electrode affects the battery performance in term of discharge and charge potentials (the higher electrolyte volume fraction the better discharge and charge potentials). Of course, this high loading of electrolyte increased the electrolyte film thickness for dissolving oxygen diffusion to the active surface of carbon. However, this effect was counteracted by the greater reaction zones and better mass transport due to the increasing liquid electrolyte volume. Thus, the model provided a means of predicting electrolyte loading for Na-air performance in a particular set of operating conditions.

7.5 Conclusions

A macro-homogeneous model for gas diffusion electrode was developed and used to analyse the capacity and cycling behaviour of a rechargeable Na-air battery operated with pure oxygen. The model uses a set of governing equations which describe species transport, charge and reaction kinetics within the battery, taking into consideration the battery main features of by-product formation, electrolyte decomposition and loss during cycling, and changes in surface area and porosity. The gas diffusion electrode model predicted better cathode performances for a rechargeable Na-air battery than the batteries using a flooded electrode, delivering larger discharge capacities and higher discharge potentials. The model can accurately predict the capacity feature and the detrimental effect of electrolyte decomposition and Na_2CO_3 formation on the capacity retention. The model can be potentially used to optimise electrode structure and electrolyte loading in the active layer, leading to improved battery performances.

7.6 References

1. Girishkumar, G., B. McCloskey, A.C. Luntz, S. Swanson and W. Wilcke, *Lithium-air battery: Promise and challenges.* Journal of Physical Chemistry Letters, 2010. **1**(14): p. 2193-2203.
2. Cheng, H. and K. Scott, *Nano-structured gas diffusion electrode – A high power and stable cathode material for rechargeable Li-air batteries.* Journal of Power Sources, 2013. **235**(0): p. 226-233.

3. Bruce, P.G., S.A. Freunberger, L.J. Hardwick and J.M. Tarascon, *Li-O_2 and Li-S batteries with high energy storage.* Nature Materials, 2012. **11**(1): p. 19-29.
4. Read, J., *Characterization of the lithium/oxygen organic electrolyte battery.* Journal of the Electrochemical Society, 2002. **149**(9): p. A1190-A1195.
5. Sawyer, D.T. and J.S. Valentine, *How super is superoxide?* Accounts of Chemical Research, 1981. **14**(12): p. 393-400.
6. Aurbach, D., M. Daroux, P. Faguy and E. Yeager, *The electrochemistry of noble metal electrodes in aprotic organic solvents containing lithium salts.* Journal of Electroanalytical Chemistry, 1991. **297**(1): p. 225-244.
7. Freunberger, S.A., Y. Chen, Z. Peng, J.M. Griffin, L.J. Hardwick, F. Bardé, P. Novák and P.G. Bruce, *Reactions in the rechargeable lithium-O_2 battery with alkyl carbonate electrolytes.* Journal of the American Chemical Society, 2011. **133**(20): p. 8040-8047.
8. Mizuno, F., S. Nakanishi, Y. Kotani, S. Yokoishi and I. Hideki, *Rechargeable li-air batteries with carbonate-based liquid electrolytes.* Electrochemistry, 2010. **78**(5): p. 403-405.
9. Black, R., S.H. Oh, J.H. Lee, T. Yim, B. Adams and L.F. Nazar, *Screening for superoxide reactivity in Li-O_2 batteries: Effect on Li_2O_2/LiOH crystallization.* Journal of the American Chemical Society, 2012. **134**(6): p. 2902-2905.
10. Lu, Y.C., D.G. Kwabi, K.P.C. Yao, J.R. Harding, J. Zhou, L. Zuin and Y. Shao-Horn, *The discharge rate capability of rechargeable Li-O_2 batteries.* Energy and Environmental Science, 2011. **4**(8): p. 2999-3007.
11. Zhang, Z., et al., *Increased stability toward oxygen reduction products for lithium-air batteries with oligoether-functionalized silane electrolytes.* Journal of Physical Chemistry C, 2011. **115**(51): p. 25535-25542.
12. Laoire, C.Ó., S. Mukerjee, E.J. Plichta, M.A. Hendrickson and K.M. Abraham, *Rechargeable lithium/TEGDME-$LiPF_6$/O_2 battery.* Journal of the Electrochemical Society, 2011. **158**(3): p. A302-A308.
13. Kim, S.W., D.H. Seo, X. Ma, G. Ceder and K. Kang, *Electrode materials for rechargeable sodium-ion batteries: Potential alternatives to current lithium-ion batteries.* Advanced Energy Materials, 2012. **2**(7): p. 710-721.
14. Liu, W., Q. Sun, Y. Yang, J.Y. Xie and Z.W. Fu, *An enhanced electrochemical performance of a sodium-air battery with graphene nanosheets as air electrode catalysts.* Chemical Communications, 2013. **49**(19): p. 1951-1953.
15. Sun, Q., Y. Yang and Z.W. Fu, *Electrochemical properties of room temperature*

sodium-air batteries with non-aqueous electrolyte. Electrochemistry Communications, 2012. **16**(1): p. 22-25.

16. Das, S.K., S. Xu and L.A. Archer, *Carbon dioxide assist for non-aqueous sodium-oxygen batteries.* Electrochemistry Communications, 2013. **27**: p. 59-62.
17. Hartmann, P., C.L. Bender, M. Vračar, A.K. Dürr, A. Garsuch, J. Janek and P. Adelhelm, *A rechargeable room-temperature sodium superoxide (NaO_2) battery.* Nature Materials, 2013. **12**(3): p. 228-232.
18. Kim, J., H.D. Lim, H. Gwon and K. Kang, *Sodium-oxygen batteries with alkyl-carbonate and ether based electrolytes.* Physical Chemistry Chemical Physics, 2013. **15**(10): p. 3623-3629.
19. Ellis, B.L. and L.F. Nazar, *Sodium and sodium-ion energy storage batteries.* Current Opinion in Solid State and Materials Science, 2012. **16**(4): p. 168-177.
20. Peled, E., D. Golodnitsky, H. Mazor, M. Goor and S. Avshalomov, *Parameter analysis of a practical lithium- and sodium-air electric vehicle battery.* Journal of Power Sources, 2011. **196**(16): p. 6835-6840.
21. Sahapatsombut, U., H. Cheng and K. Scott, *Modelling of electrolyte degradation and cycling behaviour in a lithium–air battery.* Journal of Power Sources, 2013. **243**(0): p. 409-418.
22. Sahapatsombut, U., H. Cheng and K. Scott, *Modelling the micro–macro homogeneous cycling behaviour of a lithium–air battery.* Journal of Power Sources, 2013. **227**(0): p. 243-253.
23. Laoire, C.O., S. Mukerjee, K.M. Abraham, E.J. Plichta and M.A. Hendrickson, *Elucidating the mechanism of oxygen reduction for lithium-air battery applications.* Journal of Physical Chemistry C, 2009. **113**(46): p. 20127-20134.
24. Peng, Z., et al., *Oxygen reactions in a non-aqueous Li^+ electrolyte.* Angewandte Chemie - International Edition, 2011. **50**(28): p. 6351-6355.
25. Shao, Y., F. Ding, J. Xiao, J. Zhang, W. Xu, S. Park, J.G. Zhang, Y. Wang and J. Liu, *Making Li-air batteries rechargeable: Material challenges.* Advanced Functional Materials, 2013. **23**(8): p. 987-1004.
26. Poling, B.E., J.M. Prausnitz and J.P. O'Connell, *The Properties of Gases and Liquids*. Fifth ed2001, New York: McGRAW-HILL.
27. Bruggeman, D.A.G., *The calculation of various physical constants of heterogeneous substances.* Ann. Phys. (Leipzig), 1935. **24**: p. 636-679.
28. Hellemans, J.M., J. Kestin and S.T. Ro, *The viscosity of oxygen and of some of its mixtures with other gases.* Physica, 1973. **65**(2): p. 362-375.

29. Albertus, P., G. Girishkumar, B. McCloskey, R.S. Sánchez-Carrera, B. Kozinsky, J. Christensen and A.C. Luntz, *Identifying capacity limitations in the Li/oxygen battery using experiments and modeling.* Journal of the Electrochemical Society, 2011. **158**(3): p. A343-A351.
30. Scott, K., S. Pilditch and M. Mamlouk, *Modelling and experimental validation of a high temperature polymer electrolyte fuel cell.* Journal of Applied Electrochemistry, 2007. **37**(11): p. 1245-1259.
31. Newman, J. and W. Tiedemann, *Porous-Electrode Theory with Battery Applications.* AIChE Journal, 1975. **21**(1): p. 25-41.
32. Newman, J. and K.E. Thomas-Alyea, *Electrochemical Systems*. 3 ed2004, New York: John Wiley & Sons.
33. Schalkwijk, W.A.v. and B. Scrosati, *Advances in Lithium-Ion Batteries*2002, New York: Kluwer Academic/Plenum Publishers.
34. Zhang, J.G., D. Wang, W. Xu, J. Xiao and R.E. Williford, *Ambient operation of Li/Air batteries.* Journal of Power Sources, 2010. **195**(13): p. 4332-4337.
35. Read, J., K. Mutolo, M. Ervin, W. Behl, J. Wolfenstine, A. Driedger and D. Foster, *Oxygen Transport Properties of Organic Electrolytes and Performance of Lithium/Oxygen Battery.* Journal of the Electrochemical Society, 2003. **150**(10): p. A1351-A1356.
36. Tasaki, K., A. Goldberg, J.J. Lian, M. Walker, A. Timmons and S.J. Harris, *Solubility of lithium salts formed on the lithium-ion battery negative electrode surface in organic solvents.* Journal of the Electrochemical Society, 2009. **156**(12): p. A1019-A1027.
37. Wadhawan, J.D., P.J. Welford, E. Maisonhaute, V. Climent, N.S. Lawrence, R.G. Compton, H.B. McPeak and C.E.W. Hahn, *Microelectrode studies of the reaction of superoxide with carbon dioxide in dimethyl sulfoxide.* Journal of Physical Chemistry B, 2001. **105**(43): p. 10659-10668.
38. Lide, D.R., *CRC Handbook of Chemistry and Physics*. 87 ed2007, Boca Raton, Florida: Taylor & Francis.
39. Abraham, K.M. and Z. Jiang, *A polymer electrolyte-based rechargeable lithium/oxygen battery*. Journal of the Electrochemical Society, 1996. **143**(1): p. 1-5.
40. Cheng, H. and K. Scott, *Carbon-supported manganese oxide nanocatalysts for rechargeable lithium-air batteries.* Journal of Power Sources, 2010. **195**(5): p. 1370-1374.

41. Cheng, H. and K. Scott, *Selection of oxygen reduction catalysts for rechargeable lithium-air batteries-Metal or oxide?* Applied Catalysis B: Environmental, 2011. **108-109**: p. 140-151.
42. Debart, A., J. Bao, G. Armstrong and P.G. Bruce, *An O_2 cathode for rechargeable lithium batteries: The effect of a catalyst.* Journal of Power Sources, 2007. **174**(2): p. 1177-1182.
43. Sánchez-González, J., A. Macías-García, M.F. Alexandre-Franco and V. Gómez-Serrano, *Electrical conductivity of carbon blacks under compression.* Carbon, 2005. **43**(4): p. 741-747.

Chapter 8: Conclusions and Future Work

8.1 Conclusions

Although non-aqueous electrolyte Li-air batteries demonstrate great promise in high performance and much progress has been made, significant problems still remain for their practical applications; such as poor solubility and diffusion of oxygen, sluggish electrochemical kinetics, electrolyte degradation and insoluble discharge products covering on the surface of porous cathode as well as probably block the pathway of the reactive species. All of above problems are mostly due to the interfacial reactions of oxygen and the pore structure in the cathode electrode.

Following this research a computational model was developed to simulate the behaviour of non-aqueous electrolyte Li-air battery. This mathematical model of Li-air battery could be used as an important tool during battery design and development.

The developed model was a mechanistic system, i.e. all phenomena in the Li-air battery were described by differential and algebraic equations which were based on the physical and chemical behaviours of the species and battery processes. In order to solve these equations a commercial PDE solver software package, "COMSOL Multiphysics", was used to analyse the battery system through the finite element method. All the transport processes were taken into account in the Li-air battery porous cathode. As a result of these features, the model could be used to perform several tests at different operation conditions and could be also used to describe the behaviour of Li-air batteries as well as to optimise the performance and structure of these battery electrodes. In this study, four different versions of the one-dimensional model were developed. Each version included more complicated mechanisms occurring in the Li-air batteries to create a model that was closer to a practical battery system.

A micro-macro homogeneous mathematical model was developed for a non-aqueous rechargeable Li-air battery using a concentrated binary electrolyte theory. The model was able to predict the voltage-capacity profile (polarization performance) for discharging around 2.50-2.70 V and charging at around 4 V, and it showed a good

agreement with experimental data for the particular operating condition considered in this work. The model successfully predicted the effects of applied current density, solubility limits for both oxygen and Li_2O_2, high degree of Li_2O_2 accumulation and the influence of the cathode structure. The main features of this model were the considerations of the time and space dependence of the battery system during charge and discharge process, the microscopic behaviours of the local mass transport through the discharge products (Li_2O_2) layers and the potential loss from the resistivity of lithium oxides film, and the dynamic change of the active surface area and the porosity with the Li_2O_2 growth. The influence of solid products formed during the battery discharging was demonstrated to significantly affect the mass transport resistance inside the porous cathode electrode. As the continuous growth of these products, the oxygen species from the atmosphere steeply decreased near the oxygen feeding side of the cathode and the concentration was limited deep further inside the electrode. The active surface area for the electrochemical reaction site also reduced from the passivation of the discharge products.

The model was also used to evaluate the effect of active species concentrations. Increasing the solubility limit of oxygen enhanced the discharge capacity and also increased the cell discharge potential, but does not affect the charge potential. Improving the solubility of Li_2O_2 in the electrolyte can decrease the charging voltage but showed little effect on the cell capacity. Moreover, the promising structure of Li-air flow battery demonstrated the continuous discharge capacity from the inexhaustible oxygen supplied from the external electrolyte recycling unit.

A micro-macro homogeneous model for a rechargeable Li-air battery was further developed to include the practical feature of Li_2CO_3 formation which normally occurs from electrolyte degradation during battery cycling. The modified model successfully predicted the Li-air battery cycling behaviour which starts from the first discharge to the cell potential of 2.2 V and charges until 4.2 V in 10 cycles. The cycle performance deterioration measured in term of retention of discharge capacity on cycling was predicted from the developed model which includes the effect of irreversible Li_2CO_3 discharge product. As a result, the model showed a good agreement between this cell cycling simulation and porous-electrode experiment data, thus creating a more reliable model for a rechargeable Li-air battery in non-aqueous electrolyte. Consequently, the charging voltage slightly increased in each cycle during the recharging process. This

result was partly due to the repeated passivation of discharge products on the porous carbon, which lead to decrease in electrochemical active area.

It was observed that the termination of the cell discharge is not from pore blockage by the depositing discharge products as there are some available pores at the end of each discharge cycle. The battery termination was due to the electronic resistivity of the discharge products (both Li_2O_2 and Li_2CO_3) passivation on the active surface of porous cathode. The cathode porosity decreases overtime during cycling while the volume fraction of Li_2CO_3 gradually increases in a number of cycles.

A macro-homogeneous model was developed and used to analyse the capacity and cycling behaviour of the rechargeable Li-air battery operated under ambient air conditions which severely damages Li-air performance and is still a critical problem to be solved before the Li-air battery can be used for practical application. This model was based on the macro-homogeneous model with electrolyte degradation behaviour developed previously, but accounted for the air feeding effect. The model can accurately predict the capacity feature and the detrimental effect of electrolyte decomposition and Li_2CO_3 formation on the capacity retention. The simulating results were in a good agreement with the experimental data.

The performance of Li-air battery with air feeding significantly decreased in discharge capacity and this battery was limited to operate at very low discharge current density less than 0.05 mA cm^{-2}. Moreover, the cycling profile of Li-air battery indicated that the discharge voltage slightly drops due to gradual Li_2CO_3 deposition when repeatedly cycles the Li-air battery. This Li_2CO_3 was generated from the low CO_2 concentration accessing from the atmosphere. When the developed model included both the electrolyte degradation and air feeding effects, the Li-air performance indicated a dramatic decrease of discharge capacity. This result showed that the electrolyte could be considered as a key component and one of the main issues to be solved at present to sustain the rechargeability of non-aqueous Li-air batteries.

It was observed that when the Li-air battery was integrated with an oxygen-selective membrane, the model forecasted a significant influence of using this membrane, which could lead to up to 4 time increment in specific capacity higher than the case of Li-air battery without using membrane.

A macro-homogeneous model for gas diffusion electrode was developed and used to analyse the capacity and cycling behaviour of the rechargeable Na-air battery operated under pure gas of oxygen. Na-air battery, which is analogous to Li-air battery, still maintain an energy storage system with a high specific energy depending on the discharge products but the anode electrode is replaced by abundant and inexpensive sodium metal. The same principles of macro-homogeneous model were applied to analyse the Na-air battery. This confirmed that the model developed in this study can be used as the simulation tool in any metal-air batteries which demonstrates the similar physical and chemical mechanisms.

The gas-diffusion electrode in contact with liquid electrolytes was developed to account for mass transport in the gas layer and in the flooded layer with a set of model equations for material balances and electrochemical kinetics. The oxygen concentration profile in the gas diffusion electrode demonstrated a constant distribution due to the continuously-supplying oxygen from the gas channel. As this result, the gas diffusion electrode model showed the better cathode performance for a rechargeable Na-air battery than the conventional flooded electrode, delivering large discharge capacities and higher discharge potential. This model also included the continuous loss of electrolyte volume fraction due to the electrolyte degradation during the battery cycling.

8.2 Recommendations for future work

In summary, this thesis contributed to a better understanding of the major physical and electrochemical phenomena which occurred within a rechargeable Li-air battery (or other similar metal-air battery) in a non-aqueous electrolyte. The model proved to be potentially useful tools to predict the battery performance and all transport processes, and can be used to optimise the electrode structure as well. With this thesis a gap in Li-air battery modelling was filled; however, further work could be done in several areas such as;

1. The air cathode could be improved as asymmetric structure in which the porosity is not uniform distribution. With this feature the diffusion of species could depend on the space inside the porous cathode, i.e. diffusion coefficients are the function of x-axis.

2. The model could include carbon corrosion as presented in reaction (8-1). The CO_2 generated from the carbon corrosion during battery charging could contribute in the Li_2CO_3 formation, leading to the battery deterioration.

$$C + H_2O \rightarrow CO_2 + 4H^+ + 4e^- \qquad (E^0 = 0.207\ V\ vs\ SHE) \qquad (8\text{-}1)$$

3. As the Li-air flow battery model presented previously in Chapter 4 was simulated based on the simplistic assumptions, the full details of a new design structure for Li-air flow battery model, such as anode thickness and fluid flow dynamics, could be worth tracking next due to its high discharge capacity from the continuous reduction of inexhaustible oxygen supplied from the recycling unit. However, to perform this kind of simulations the computational resource must be substantially increased.
4. A non-isothermal model, which predicts the changing battery temperatures during charging and discharging, should be addressed. This behaviour could affect many physical and chemical parameters for the non-aqueous electrolyte as well as the battery performance.
5. A two-dimensional model can be further developed by considering a cylindrical cell (instead of 1D prismatic cell) in order to improve the surface area of electrochemical reaction as well as the battery performance.
6. The Na_2CO_3 discharge product in Na-air battery with carbonate-based electrolyte should be included on charge to decompose to CO_2 and Na^+. Further improvements include the more details of degradation kinetics on both electrolyte and electrode.

Appendix A: List of Publications

A.1 Scientific journals

1. Sahapatsombut, U., H. Cheng, and K. Scott, *Modelling of Operation of a Lithium-Air Battery with Ambient Air and Oxygen-Selective Membrane*. Journal of Power Sources, 2014. **249**: p. 418-430.

2. Sahapatsombut, U., H. Cheng, and K. Scott, *Modelling of electrolyte degradation and cycling behaviour in a lithium–air battery*. Journal of Power Sources, 2013. **243**: p. 409-418.

3. Sahapatsombut, U., H. Cheng, and K. Scott, *Modelling the micro–macro homogeneous cycling behaviour of a lithium–air battery*. Journal of Power Sources, 2013. **227**: p. 243-253.

A.2 Oral presentations

1. Sahapatsombut, U. and K. Scott, *Some possible approaches for improving the performance of rechargeable non-aqueous lithium-air batteries*. CEAM Postgraduate Research Conference 2013, Newcastle University, United Kingdom, 20-21 March 2013.

2. Sahapatsombut, U. and K. Scott, *Modelling the micro-macro homogeneous cycling behaviour of a lithium-air battery*. 9th Symposium on Fuel Cell and Battery Modelling and Experimental Validation (ModVal 9), Paul Scherrer Institut, CAMPUS Sursee, Switzerland, 2-4 April 2012.

3. Sahapatsombut, U. and K. Scott, *One-dimensional model for positive oxygen electrode for lithium-air battery*. CEAM Postgraduate Research Conference 2012, Newcastle University, United Kingdom, 20-21 March 2012.

A.3 Poster presentations

1. Sahapatsombut, U. and K. Scott, *Micro-macro homogeneous model for a lithium-air battery*. Industrial Advisory Board 2011 (IAB2011), Copthorne Hotel, Newcastle upon Tyne, United Kingdom, 1-2 December 2011.